EXPERIMENTAL AND NUMERICAL INVESTIGATION OF SYSTEM PERFORMANCE OF LATENT HEAT STORAGE UNIT INTEGRATED WITH SOLAR ASSISTED HEAT PUMP

A THESIS SUBMITTED TO
GRADUATE SCHOOL OF NATURAL AND APPLIED SCIENCES
OF
KOCAELİ UNIVERSITY

BY

ÇAĞATAY YILDIZ

IN PARTIAL FULFILLMENT OF THE REQIREMENTS
FOR
THE DEGREE OF DOCTOR OF PHILOSOPHY
IN
MECHANICAL ENGINEERING

KOCAELİ 2024

EXPERIMENTAL AND NUMERICAL INVESTIGATION OF SYSTEM PERFORMANCE OF LATENT HEAT STORAGE UNIT INTEGRATED WITH SOLAR ASSISTED HEAT PUMP

A THESIS SUBMITTED TO

GRADUATE SCHOOL OF NATURAL AND APPLIED SCIENCES

OF

KOCAELİ UNIVERSITY

BY

ÇAĞATAY YILDIZ

IN PARTIAL FULFILLMENT OF THE REQIREMENTS
FOR
THE DEGREE OF DOCTOR OF PHILOSOPHY
IN
MECHANICAL ENGINEERING

Prof. Dr. Müslüm ARICI **Supervisor, Kocaeli University**	………………………
Prof. Dr. Hasan KARABAY **Jury member, Kocaeli University**	………………………
Associate Prof. Dr. Mehmet Selçuk MERT **Jury member, Yalova University**	………………………
Prof. Dr. Sandro NIŽETIĆ **Jury member, University of Split**	………………………
Prof. Dr. Dong LI **Jury member, Northeast Petroleum University**	………………………
Dr. Mustafa SEÇİLMİŞ **Co-advisor, Kocaeli University**	**Appointed as the co-supervisor at the meeting of the Institute Board dated 26/04/2023 and numbered 2023/18.**

Thesis Defense Date: 02.07.2024

ETHICAL STATEMENT AND RESEARCH FUND SUPPORT

In this thesis/project study, which I prepared in accordance with the thesis writing rules of Kocaeli University Graduate School of Natural and Applied Sciences,

I declare that,

- This thesis/project is my own and an original work,
- I act in accordance with scientific ethical principles and rules at all stages of my study, including preparation, data collection, analysis, and presentation of information,
- I have cited all data and information obtained within the scope of this study and that I have included these sources in the bibliography,
- This study complies with the similarity criteria determined by the Graduate School of Natural and Applied Sciences of Kocaeli University in terms of the plagiarism software to which Kocaeli University is subscribed,
- I have not done any falsification of the data used,
- I have not submitted any part of this thesis/project as another thesis/project work at this university or another university.

☒ Any stage of this thesis/project work has not been provided any financial/infrastructural support by any institution/organization.

☐ The data and information produced within the scope of this thesis/project work were carried out by …...................................... with the financial/infrastructure support within the scope of the project no ….. .

I declare that I accept all the moral and legal consequences at any time that may arise regarding my work in the event of situation contrary to this statement.

Çağatay YILDIZ

PUBLISHING AND INTELLECTUAL PROPERTY RIGHTS

I declare that I have given Kocaeli University the permission to archive all, or any part of my graduate thesis/project approved by the Graduate School of Natural and Applied Sciences, in printed and electronic format, and make it available for use at the conditions specified as follows. Within this permission, all intellectual property rights except for the usage rights granted by Kocaeli University will remain with me and the usage rights of all or a part of my thesis/project in future studies such as articles, books, communiqués, licenses, patents is my own on condition both that the name of my advisor is reserved and within the knowledge of both parties. I declare and undertake that the thesis/project is my own original work, that I have not violated the rights of others and that I am the only authorized owner of my thesis/project. I undertake to use the copyrighted texts in my thesis, which must be used with written permission from their owners, with written permission, and to submit copies of them to the University when requested.

Within the scope of the ***"Directive on Collecting, Organizing and Making Access to Graduate Theses in Electronic Environment"*** published by the Council of Higher Education (CoHE), my thesis is made available in the CoHE National Thesis Center / Kocaeli University Libraries Open Access System, except for the conditions stated below.

[ ] With the decision of the institute board of directors, the opening of my thesis/project to access has been postponed for 2 years from the date of graduation.

[ ] With the reasoned decision of the institute board of directors, the opening of my thesis/project to access has been postponed for 6 months from the date of graduation.

[X] No confidentiality decision has been made regarding my thesis/project.

Çağatay YILDIZ

PREFACE AND ACKNOWLEDGEMENTS

The completion of this thesis holds great significance for my academic journey, offering profound insights into this discipline and providing invaluable experience in the academia. I would like to express my sincere appreciation to my supervisor Prof. Dr. Müslüm ARICI who provided a continuous support and guidance with all his generosity and patience during this long period. His deep knowledge and expertise in the field has significantly contributed to my development in many aspects. As my co-advisor, I would like to present my thankfulness to Dr. Mustafa SEÇİLMİŞ who never hesitated to share his deep experience in the field and contribute to my growth in this process. Besides, I am thankful to Prof. Dr. Hasan KARABAY and Assoc. Prof. Dr. Mehmet Selçuk MERT for their valuable and critical feedback that reflect a deep insight to the field, which significantly improved the quality of the work.

I am deeply grateful to my colleagues and friends at Kocaeli University for their support. Special thanks to Res. Asst. Ekrem TUNÇBİLEK for his precious assistance and motivation during this challenging period. Also, I would like to express my gratitude to my institution and workplace, Kocaeli University, for all infrastructure and great working environment they provided to me.

Finally, I would like to thank my mother Dr. Ayla YILDIZ, my father Dr. Ahmet YILDIZ, and my brother Burak Çağrı YILDIZ for their unwavering encouragement and motivation. Last but not least, I extend my heartfelt gratitude to my wife Selda YILDIZ for her continuous support with patience and faith in my capabilities. Deep inside, I am grateful to my daughter, Ayla, hoping that she will understand the reason for the time I took from her in the future.

June – 2024 Çağatay YILDIZ

CONTENTS

LIST OF FIGURES

LIST OF TABLES

INDEX OF SYMBOLS AND ABBREVIATIONS

A_{sc}	: Solar collector area (m^2)
A_{surf}	: Surface area (m^2)
a, b, c	: Dimensions of the fluid domain (m)
α	: Absorptivity
β	: Thermal expansion coefficient (1/K)
C	: Cost (TRY)
C_p	: Specific heat capacity (J/(kgK))
ε	: Turbulence dissipation rate (m^2/s^3)
f	: Liquid fraction
$\vec{F}$	: Body forces (N/m^3)
F_R	: Heat removal factor
$\vec{g}$	: Gravitational acceleration (m/s^2)
G_β	: Solar radiation incident on tilted surface (W/m^2)
h	: Convective heat transfer coefficient ($W/(m^2K)$)
H	: Enthalpy (J)
I	: Unit tensor
k	: Thermal conductivity (W/(mK))
k_{eff}	: Effective thermal conductivity (W/(mK))
$k*$	: Turbulent kinetic energy (m^2/s^2)
L_H	: Latent heat capacity (J/kg)
m	: Mass (kg)
$\dot{m}$	: Mass flow rate (kg/s)
μ	: Dynamic viscosity (Pa·s)
μ_t	: Turbulent viscosity (Pa·s)
p	: Pressure (Pa)
P	: Electrical power (W)
ρ	: Density (kg/m^3)
$\dot{Q}_C$	: Condenser load (W)
Q_C	: Thermal energy rejected from condenser (J, kWh)
$\dot{Q}_E$	: Evaporator load (W)
$\dot{Q}_{load}$	: Heating load of the space (W)
$\dot{Q}_{sc}$	: Useful heat gain of solar collector (W)
r	: Distance in radial direction (m)
$\vec{S}$	: Source term in momentum equation (N/m^3)
T	: Temperature (°C, K)
T_{amb}	: Ambient temperature (°C)
T_{st}	: Storage temperature (°C)
$T_{cond,i}$	: Temperature at condenser inlet (°C)
$T_{cond,o}$	: Temperature at condenser outlet (°C)
$T_{r=R}$	: Temperature at the last node of PCM in the tubes (°C)
T_{ref}	: Reference temperature (°C, K)
T_{TES}	: Water temperature in the TES tank (°C)
T_0	: Reference temperature for Boussinesq term (K)
t	: Time (s)
τ	: Transmittance

U_L : Overall heat transfer coefficient for heat loss (W/(m^{2}K))
V : Velocity (m/s)
$\dot{V}$: Volume flow rate (L/h)
W : Electrical energy (J, kWh)
$x_{i,j}$: Distances in Cartesian coordinates (m)

Abbreviations

ASHP : Air-Source Heat Pump
CAT : Cold Accumulation Tank
COP : Coefficient of Performance
COTR : Compression Operation Time Ratio
DSC : Differential Scanning Calorimetry
GSHP : Ground-Source Heat Pump
HAT : Hot Accumulation Tank
HP : Heat Pump
IEA : International Energy Agency
LSI : Load Shifting Index
PCI : Peak Clipping Index
PCM : Phase Change Material
SAWSHP : Solar-Assisted Water-Source Heat Pump
SCT : Solar Collector Tank
TES : Thermal Energy Storage
TGA : Thermogravimetric Analysis
WSHP : Water-Source Heat Pump

EXPERIMENTAL AND NUMERICAL INVESTIGATION OF SYSTEM PERFORMANCE OF LATENT HEAT STORAGE UNIT INTEGRATED WITH SOLAR ASSISTED HEAT PUMP

ABSTRACT

In this thesis work, integration of a thermal energy storage (TES) unit to the evaporator of a solar-assisted heat pump (SAHP) and condenser to an air-source heat pump (ASHP) were investigated, separately, in order to evaluate thermal behavior of the TES unit and heat pump (HP) performance from various aspects. In the first system (System-1), the TES unit was utilized as a heat source for the HP to attain longer operation times and peak clipping potential. In the second system (System-2), the TES unit was used as a heat sink for the HP to be able to use the stored thermal energy during on-peak times and attain load shifting. Thermal behavior and system performance were evaluated by the experiments for both systems considering phase change material (PCM) utilization. Regarding the experimental data, two different mathematical models were established for each system, and the thermal behavior and system performances were investigated for different PCMs in various conditions. As a result, it was found in the experiments that integration of PCM to the System-1 significantly enhanced total heating time by 30.6% at low storage temperatures, while it showed an adverse effect at high storage temperatures. In System-2, inclusion of PCM attained a higher HP performance and load shifting, however, using PCM resulted in lower discharging time, due to incomplete solidification. By elaborating the thermal performance of the systems numerically, it was concluded that using PCM brings a remarkable potential to energy efficiency and flexibility as well as heating time extension; however, their effective thermal conductivity must be improved to benefit these materials for enhanced energy efficiency, energy storage capacity and energy flexibility in heat pump systems.

Keywords: Energy Efficiency, Energy Flexibility, Heat Pump, Phase Change Material, Thermal Energy Storage.

GÜNEŞ ENERJİLİ ISI POMPASINA ENTEGRE GİZLİ ISI DEPOLAMA ÜNİTESİNİN SİSTEM PERFORMANSININ DENEYSEL VE SAYISAL İNCELENMESİ

ÖZET

Bu tez çalışmasında, bir ısıl enerji depolama (IED) ünitesinin güneş enerjisi destekli bir ısı pompasının buharlaştırıcı tarafına (Sistem-1), hava kaynaklı bir ısı pompasının ise yoğuşturucu tarafına entegrasyonu (Sistem-2) iki sistemin farklı koşullardaki davranışlarını belirlemek adına ayrı ayrı incelenmiştir. Birinci sistemde, IED ısı pompası için bir ısı kaynağı olarak kullanılarak sistemin çalışma süresinin artırılması ve pik enerji tüketiminin azaltılması hedeflenmiştir. İkinci sistemde ise IED’nin ısı pompasından aldığı ısıyı depolaması ve sonrasında pik zamanlarda bu enerjiyi kullanarak pik enerji yüklerini kaydırması ve esneklik sağlaması amaçlanmıştır. İki farklı sistemin ısıl davranışları, faz değiştiren malzeme (FDM) kullanımının etkisi dikkate alınarak bir dizi deneylerle belirlenmiştir. Sonrasında her bir sistem için birer matematik model geliştirilerek farklı şartlar ve farklı FDM kullanımları dikkate alınarak değerlendirmeler yapılmıştır. Deneyler sonucunda Sistem-1 kapsamında FDM kullanımının özellikle düşük ısıl depolama sıcaklıklarında toplam ısıtma süresini %30,6’ya kadar artırdığı gözlenmiş ancak yüksek depolama sıcaklıklarında ters etki yarattığı görülmüştür. Sistem-2’de ise FDM kullanımının ısı pompası performansını ve enerji esnekliğini olumlu etkilediği görülürken depolanan ısının deşarjı sırasında FDM’nin katılaşma sürecini tamamlayamadığı için ısıtma süresinde düşüş tespit edilmiştir. Matematik model üzerinde yapılan sayısal incelemeler FDM’nin enerji depolama ve enerji esnekliğini iyileştirme hususunda ciddi bir potansiyele sahip olduğunu ortaya koymuştur. Ancak bu potansiyelin söz konusu sistemler için değerlendirilebilmesi için mutlaka FDM içerisindeki ısı transferinin iyileştirilerek etkin ısıl iletkenliğin artırılması gerekmektedir.

Anahtar Kelimeler: Enerji Verimliliği, Enerji Esnekliği, Isı Pompası, Faz Değiştiren Malzeme, Termal Enerji Depolama.

GÜNEŞ ENERJİLİ ISI POMPASINA ENTEGRE GİZLİ ISI DEPOLAMA ÜNİTESİNİN SİSTEM PERFORMANSININ DENEYSEL VE SAYISAL İNCELENMESİ

GENİŞLETİLMİŞ TÜRKÇE ÖZET

Isıl enerji depolama sistemleri ısı pompalarına entegre edilerek enerji verimliliğinin artırılması, ısıtma süresinin uzatılması, depolanan enerjinin arz-talep dengesine göre esnek bir şekilde kullanılarak elektrik şebekelerindeki pik yüklerin azaltılması gibi çeşitli amaçlarla kullanılabilmektedir. Yakın gelecekteki ısıtma sistemlerinin elektrifikasyonu ve dekarbonizasyonu gibi noktalarda enerjinin esnek ve kontrollü bir biçimde kullanılması büyük önem taşımaktadır ve ısıl enerji depolama sistemleri bu amaca etkin bir şekilde hizmet edebilmektedir. Bu kapsamda ısıl enerji depolama sistemleri ısı pompalarının buharlaştırıcı veya yoğuşturucu taraflarına entegre edilebilir ve söz konusu amaçlar için farklı stratejiler altında kullanılabilmektedir. Bu tez çalışmasında, ısıl enerji depolama sistemlerinin ısı pompalarına iki farklı şekilde sağlanan entegrasyonu deneysel ve sayısal olarak incelenmiştir. Bu amaçla buharlaştırıcı tarafına entegre edilecek ısıl enerji depolama (IED) ünitesi için güneş enerjisi destekli bir ısı pompası göz önüne alınmışken (Sistem-1) yoğuşturucu tarafına entegrasyonu için hava kaynaklı bir ısı pompası dikkate alınmıştır (Sistem-2).

Öncelikle bir ısıl enerji depolama (IED) tankının güneş enerjisi destekli ısı pompaları dikkate alınarak su kaynaklı bir ısı pompası test düzeneğinin evaporatör tarafına entegrasyonu dikkate alınmıştır. Deneyler sırasında güneş kolektörleri kullanılmayıp verilen ısı bir elektrikli ısıtıcı yardımıyla simüle edilmiştir. Bu kapsamda yapılan testler için ısıl depolama tankının üç farklı depolama sıcaklığına erişmesi (T_{st}=35°C, 45°C ve 55°C) dikkate alınmıştır. Söz konusu ısıl depolama tankı içerisine faz değiştiren malzeme (FDM) dahil edilmesi için 32 adet çelik tüp modüler olarak yerleştirilmiştir. Tank içerisinde bu tüplerin dışında ısı transfer akışkanı ve aynı zamanda ısı depolama ortamı olarak su bulunmaktadır ve dolayısıyla hibrit bir ısı depolama ünitesi olarak tasarlanmıştır. Her bir sıcaklıkta yapılan testler için IED ünitesi öncelikle elektrikli ısıtıcı yardımıyla şarj edilmiş, sonrasında su kaynaklı ısı pompası aktif hale getirilerek depolanan enerjiyi tank içerisindeki su sıcaklığı referans olarak belirlenen T_{ref}=20°C'ye düşünceye kadar bir ısı kaynağı olarak kullanmıştır. Bu noktada ısı pompasının yoğuşturucu tarafına bağlı olan sıcaklık kontrollü bir soğutma grubu vasıtasıyla ısı pompasından alınan ısı, ısı transfer akışkanının gidiş ve dönüş sıcaklıkları sırasıyla 35°C-30°C dolaylarında olması kaydıyla 1,4 kW ile 3,8 kW arasında değişen ve ilgili ısı transfer akışkanının beş farklı debisiyle ayarlanan ($\dot{V}$=400, 600, 800, 1000, 1200 L/h) 5 farklı ısı yükünde çekilerek dur/kalk yöntemiyle çalışan ısı pompasının farklı şartlardaki performansı ortaya çıkarılmıştır. Ayrıca, IED tankı içerisindeki su ve FDM'nin ısıl davranışları da sıcaklık ölçümleriyle ortaya çıkarılmıştır. Testler, modüler tüpler içerisinde su ve FDM bulunması durumları için ayrı ayrı gerçekleştirilmiştir. Faz değişim sıcaklığı, gizli ısı depolama kapasitesi ve stabil faz değişim davranışı göstermesi gibi sebeplerden dolayı bu sistemde (Sistem-1) tüplerin içerisine ticari bir FDM olan Rubitherm RT26 kullanılmıştır. Deneyde elde edilen performans verilerinden yararlanılarak sistemin çalışması matematiksel olarak modellenmiş ve sonrasında farklı FDM'ler için sistem performansı ve ısı depolama malzemelerinin (su ve FDM) ısıl davranışları sayısal olarak elde edilmiştir. Bununla beraber matematiksel modele bir

güneş kolektörü de eklenerek sistemin ısıtma periyodu boyunca farklı hava koşullarındaki dinamik analizi gerçekleştirilmiştir. Ayrıca Sistem-1 kapsamında FDM kullanımının toplam ısıtma süreleri, enerji tüketimi ve pik yüklerin azaltılması hususundaki esneklikleri detaylandırılmıştır. Deneysel çalışmalar sonucunda FDM kullanımının özellikle düşük depolama sıcaklıklarında (T_{st}=35°C) ısıtma süresini %30,6'ya kadar artırabildiği tespit edilmiştir. Ayrıca FDM kullanımıyla kompresörün dur/kalk sayısında %10 civarında azalma ve böylece enerji tüketiminde %8'e varan azalma kaydedilmiştir. Ancak gizli ısının tümüyle kullanılamaması ve FDM'lerin duyulur ısı kapasitesinin suya göre oldukça düşük olması sebebiyle ısıtma tesir katsayıları özellikle düşük ısı yükünün dikkate alındığı durumlarda suya kıyasla düşük bulunmuştur. Öte yandan yapılan sayısal çalışmalarda, FDM kullanımının özellikle Aralık ve Ocak gibi güneş radyasyonunun düşük olduğu aylarda ısı depolama kapasitesini önemli ölçüde iyileştirme potansiyelinin olduğu ortaya çıkarılmıştır. Ancak düşük ısıl iletkenlikleri bu durumun önündeki en büyük bariyer olarak ortaya çıkmaktadır. Bu sistemlerde etkin ısıl iletkenliğin yaklaşık 4 kat artırılmasıyla FDM, ısı depolama malzemesi olarak su kullanılan duruma göre yaklaşık 2 kat daha fazla enerji depolayabilmekte ve sonrasında depoladığı gizli ısısını tamamen salabilmektedir.

İncelenen diğer sistemde (Sistem-2) ise IED ünitesinin pik dışı zamanlarda hava kaynaklı ısı pompasının sürekli çalışmasıyla şarj edilerek elektrik kullanımının pik yaptığı süreçlerde ısıtma işleminin tamamen veya kısmen IED ünitesi içerisine depolanan enerjiden sağlanması ve böylece pik yüklerin kaydırılması amaçlanmıştır. Bu sistemde referans sıcaklık, yerden ısıtma yapılabilecek limit sıcaklıklar dikkate alınarak T_{ref}=35°C olarak alınmış ve IED içerisindeki su sıcaklığı T_{st}=55°C'ye gelinceye kadar şarj işlemi devam etmiştir. Depolanan ısıl enerji, soğutma grubu yardımıyla 3,1 kW, 4,4 kW, 5,4 kW ve 12 kW olmak üzere dört farklı ısı yükünde çekilmiş ve sistemde FDM olması ve olmaması durumlarında enerjinin ne kadar süre sağlanabildiği izlenmiştir. Ayrıca IED tankı içerisinde su ve FDM'nin de sıcaklık değişimleri gözlenmiştir. Deneylerden elde edilen verilere dayalı olarak sistemin matematiksel modeli çıkarılmış ve sistemin ısıl şarj ve deşarj süreçlerindeki davranışı ve enerji esnekliği potansiyeli farklı FDM'ler için kıyaslamalı olarak incelenmiştir. Laurik asit kullanılarak gerçekleştirilen testlerde, ısı depolama malzemesi olarak su kullanılan durumun, laurik asit kullanılan duruma göre özellikle yüksek ısı yüklerinde daha uzun süre enerji sağlayabildiği görülmüştür. Sıcaklık değişimleri incelendiğinde, laurik asitin depoladığı enerjiyi deşarj süreci boyunca tamamen salamadığı ve hatta katılaşma sıcaklığının altında dahi faz değişimini tamamlayamadığı gözlenmiştir. Ancak ısı pompası ile şarj süresince yoğuşturucu tarafındaki sıcaklığı daha stabil bir halde tutarak daha yüksek ısıtma tesir katsayısı ile süreci tamamlaması itibariyle %3,2'ye kadar daha yüksek bir yük kaydırma endeksi (enerji esnekliği) sağlamıştır. Gece tarifesinde IED'nin şarj edilmesi ve FDM kullanılması durumunda elektrik giderlerinde en yüksek tasarruf sağlanmıştır ve bu tasarruf deşarj sırasındaki ısı yüküne bağlı olarak %14,8 ile %53,3 arasında değişmiştir. Kurulan matematik model ile elde edilen sayısal sonuçlar, Sistem-1'deki duruma benzer şekilde kullanılan FDM'nin ve etkin ısıl iletkenliğin önemini göstermiştir. FDM'nin etkin kullanılabilmesi için uygun faz değişim sıcaklığına, yüksek gizli ısı depolama kapasitesine ve standart parafin bazlı FDM'lere kıyasla yaklaşık 6 kat daha yüksek bir etkin ısıl iletkenliğe sahip olması gerekmektedir. Bu sayede yapılan incelemede gizli ısı kullanımı %66'dan %100'e kadar artırılabilmiş %68,9 olan yük kaydırma endeksi %82,3'e yükselebilmektedir.

Sonuç olarak incelenen her iki sistemde de FDM kullanımı, dar bir çalışma sıcaklığı aralığında suya göre daha yüksek enerji depolama ve salma kapasitesine sahip olabilmektedir. Ancak, yanlış faz değişim sıcaklığı seçimi, düşük gizli ısı kapasitesi gibi etkenlerden daha önemli olarak bu potansiyelin kullanımının önündeki en büyük engel FDM'lerin düşük ısıl iletkenliğe sahip olmasıdır. Bu nedenle ısı depolama sistemlerinde FDM kullanımı planlanırken ısı transferini iyileştirici tekniklerle birlikte kullanılması önerilmekte olup aksi durumda FDM kullanımının su kullanımına göre herhangi bir iyileştirici etki sağlayamayacağı görülmüştür. Güneşli gün sayısının ve güneşlenme süresinin uzun olduğu bölgeler için Sistem-1 daha verimli bir ısıtma sistemi olabilirken güneş radyasyonunun daha az olduğu ve buna bağlı olarak elektrikli ısıtmanın yaygın olduğu bölgelerde Sistem-2'nin kullanımı enerji verimliliği ve esnekliğine katkı sağlayabilecektir.

1. INTRODUCTION

Challenging the nature of the world for centuries, energy consumption for building heating has become a significant issue for society since the need for shelter has always been a vital issue in human life to provide safety and security, which will also undoubtedly continue in the future. Considering that modern human being cannot adapt themselves to the severe climatic conditions, especially sharp cold weather, the requirement of warmth becomes one of the essential needs along with other physiological requirements, as also indicated by Maslow's hierarchy of needs in the bottom level. This evidently indicates that the other high-level needs of society cannot be fulfilled unless heating issue of buildings where people exist is somehow resolved.

Buildings are the spaces where the majority of a human lifetime is spent. Therefore, proper heating of these structures is utmost important for people to feel themselves in a comfortable place. In order to meet the heating requirement in buildings, various heating systems and techniques have been developed over a long period, and these have been gradually developed and enhanced. In addition to that, different energy sources have been utilized for building heating, including fossil fuels such as coal, oil, and natural gas, as well as renewable energy sources such as solar and wind energy. Nevertheless, these developments could not yet satisfactorily reduce the high energy consumption in building heating applications, nor the high carbon emissions. Therefore, more efforts are needed for progressing in the field. One of the most effective ways to achieve the targeted points in this field is to develop and improve novel heating systems with higher efficiency and mitigated pollution. In the last decades for this purpose, heat pumps (HP) have been popular for being significantly efficient and applicable systems not to mention their high capability of using clean energy, even though partly. Heat pump systems withdraw part of the heating energy from a natural source such as air, water, ground, and solar energy. This energy is combined with the compression work to produce a few more times of heating energy which is supplied to the demand side. Hence, their coefficient of performance (*COP*) becomes larger than unity, which indicates that several times more heating energy can be obtained compared to the electrical energy supplied to the compressor in the heat pump cycle.

Electrification of heating systems is crucial, and it also sounds noticeably clean. Yet, there are other challenges such as the production process of electricity, i.e., whether it is produced using fossil fuels or not, the load on the electricity grids due to supplying a large amount of energy required for heating, and the efficiency of such heating techniques. Therefore, taking into account that each engineering improvement may bring up new challenges, these issues should be addressed by implementation of new techniques or technologies.

Thermal energy storage (TES) systems have been widely used in various engineering applications and became more popular than ever in the last decades due to the increasing importance of careful utilization of energy. Storing thermal energy in a proper way can ensure an effective utilization of energy since the utilization period of the stored energy can be controlled regarding its demand. For instance, solar thermal energy can be stored during diurnal periods where it is abundant, and this thermal energy can be used in nocturnal times where there is no renewable heat source from solar energy. Scaling this from daily basis up to a seasonal basis, solar energy stored in TES units in summer and spring times can be utilized in heating and domestic hot water applications in fall and winter times, considering Northern Hemisphere. While the thermal energy can be stored in various media as sensible heat, such as water tanks, aquifers, ponds, building structures, ground, or even rock beds, there are other techniques such as TES by latent heat or thermochemical reactions. Among them, latent heat storage using phase change materials (PCM) is noticeably popular as they have a large energy storage density at a nearly isothermal condition, which ensures a smaller storage volume for a given amount of energy and storing or releasing this energy in a small temperature interval which is usually more suitable for practical applications as being at suitable working conditions of system.

Combining the aforementioned two technologies, i.e., heat pumps and thermal energy storage units, is a remarkably effective way to provide an efficient and clean heating, together with effective and flexible use of energy by managing it regarding supply or demand sides as well as increasing the share of renewable sources in such applications. Integrating TES units into heat pumps can be mainly considered in two different layouts. A thermal energy storage unit can be either integrated to evaporator of the heat pump, especially if the HP is a water or ground source one, or it can be interrelated with the condenser of HP. In the first layout, an enhancement in the HP efficiency, compared to conventional air-source heat pumps or water-source heat pumps using a pond or lake as a heat source, is most likely expected due to the relatively augmented evaporator temperatures. At the same time, the share of using renewable energy can be increased, and the stored thermal energy can be used as the heat source of the HP in a high-demand period, which can additionally reduce costs, carbon emissions, as well as enhance energy flexibility. Here, renewable energy sources are suitable for thermal charge of the TES unit. In the second layout, an air-source heat pump (ASHP) is usually considered to thermally charge the TES unit that is used as the heat sink of the HP. Thus, thermal energy is preserved during the off-peak periods where the heating demand is low, and the electricity costs are relatively lower due to reduced grid loads at that time. Thereafter, the stored thermal energy can be used during peak periods, hence, a significant energy flexibility can be ensured, and the grid load and costs can be mitigated.

Even though these two systems, heat pumps and thermal energy storage units, are intensely investigated by researchers separately, the studies involving their coupling are rather fewer. As the significance of efficient energy use in heating, mitigation of carbon emissions as well as energy flexibility is increased in the last years, researchers started to focus on these topics as well. Nonetheless, there are still significant research potential in this field since the developed and developing countries try to convert their heating systems into the aforementioned heat pump and TES systems, and since each system and location has its own specifications that need to be examined individually. Furthermore, the processes involving TES with sensible and/or latent heat storage (using PCMs) have many other parameters such as TES medium or PCM used, the suitability to application, and demanded priorities, which bring the requirement of attentive investigation of each system. In addition to that, the relevant literature studies, which will be discussed in detail in the upcoming section, focus on a single system with a specific application or matching a specific need, by integrating TES either to evaporator or to condenser side of a HP, and there is no study to the best knowledge of author that includes a comprehensive experimental and numerical investigation that explores the performance of these two different TES-HP layouts from multiple perspectives, such as thermal behavior of the TES unit, system performance, and energy flexibility potential. Therefore, this thesis work proposes the investigation of two different TES-HP combinations for different point of view of application, in order to comprehensively elaborate the thermal behavior and system performance considering two different integration way of TES unit to a heat pump system. For this purpose, first, a TES unit was designed and integrated to the evaporator of the HP test rig to explore the system behavior for solar-assisted water-source heat pumps (SAWSHP), and the impact of sensible and latent heat on the system performance and peak load clipping potential was examined. In the second part, the TES unit was integrated to the condenser of the HP by modifying the experimental setup. In this layout, the system performance was also evaluated while the energy flexibility, i.e., load shifting, potential of the system was assessed. For both layouts, the effect of PCM existence on the system performance and flexible energy usage was explored by conducting the tests with and without PCM. Moreover, two different mathematical models were established in regard to the obtained experimental data, and the two systems were investigated in a more comprehensive way, considering different weather conditions and different PCM utilization. It is hoped that this thesis work, which includes a comprehensive investigation for both system layouts having their own benefits and challenges regarding the application area and user demand, can be a guidance for researchers and engineers working in the field.

2. BACKGROUND AND STATE-OF-THE-ART

Rapid development of industrial and residential sectors along with increasing world population in the last decades inevitably has brought together a significant augmentation in the energy consumption. Furthermore, this intense energy consumption trend causes hazardous changes in the climate affecting the human life. Thus, efficient use of energy becomes more important than ever as it is not only a matter of cost but also a matter of life-threatening future of human. Being one of the most energy-consumer sectors, buildings are responsible for approximately 40% of the end-use energy consumption. Residential and industrial buildings along with the relevant construction sectors for various building types are within this share (Lakhdari et al., 2020).

Among various energy consumption applications in buildings, such as space heating, domestic water heating, space cooling, appliances, cooking, and lighting, the space heating applications are by far the most energy consumer aspect in the regions located especially in temperate and continental climates. Considering all these applications in a residential building, the share of space heating comes to the top by 48%, whereas domestic water heating accounts for 22%, making the share of heating operations up to 70%, as seen from Figure 2.1 (Bouckaert et al., 2021; UN Environment Programme, 2019).

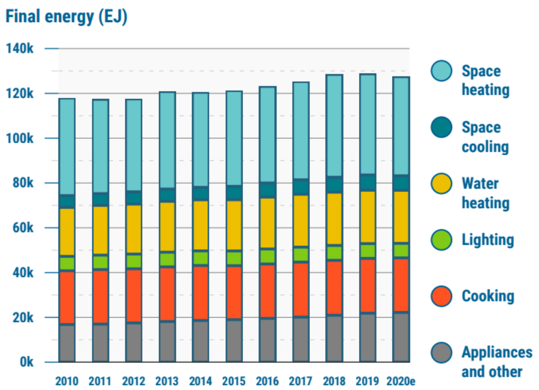

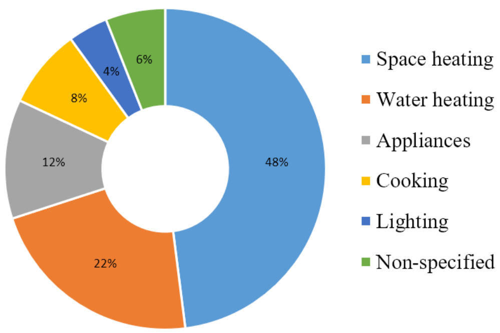

Figure 2.1. Global final energy consumption in EJ in recent ten years (left) and share of different applications in energy consumption (right)

This situation brings an important requirement for space heating applications, which should be energy-efficient and environment-friendly. Hence, efficient devices using completely or partly clean energy sources as well as having relevant operation strategies are in the scope of researchers to address the aforementioned issue, rather than using conventional methods such as using fossil fuels and direct electric heating. At this point, heat pumps come forth for efficient heating applications as well as using clean energy and attaining energy flexibility (Bampoulas et al., 2021; Ren et al., 2021). State of the art of heat pumps and details about their applications along with benefits and drawbacks are presented in the following subsection.

2.1. Heat Pumps – Significance, State of the Art, and Development

Continuously preserving their significance throughout the last few decades, heat pumps have recently ascended to a pivotal position for building heating applications due to its superiorities in the modern era where the dependence on fossil fuels for energy production is desired to be abandoned. Divided into two major categories basically as vapor-compression (mechanically driven) and sorption (thermally driven), heat pumps attain an efficient heat transfer from a low-temperature medium to a high-temperature medium. At this point, although the sorption-based heat pumps require significantly lower energy input, vapor compression heat pumps ensure a higher energy performance with low cost and low CO_2 emissions, as studies show (Miglioli et al., 2023). Vapor compression heat pumps are simple heating devices that use electrical energy in its compressor to transfer thermal energy from a cold to hot environment regarding the thermodynamic principle of vapor compression refrigeration cycle, as schematically shown in Figure 2.2 (Zhang et al., 2018).

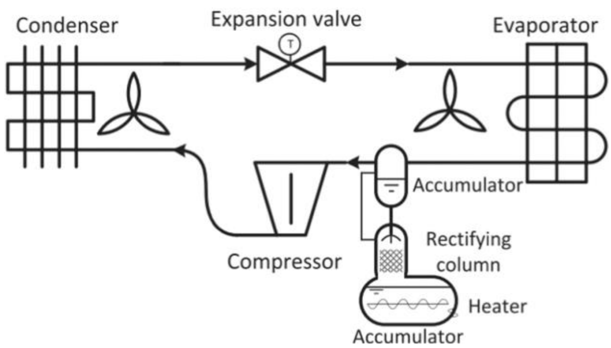

Figure 2.2. Schematic view of a simple air-to-air heat pump system based on vapor compression refrigeration cycle

In this cyclic operation, a refrigerant ideally in saturated vapor state is compressed in the compressor to the superheated vapor phase, and it passes through a heat exchanger named condenser where it releases the thermal energy into the environment or to a heat transfer fluid (HTF), during condensation. Thereafter, the refrigerant passes through an expansion device where it encounters a sudden pressure drop, and it enters the evaporator in liquid or liquid-vapor mixture phase in a lower pressure, which can be appropriate for rejection of heat from the environment or HTF and evaporate. Lastly, it completes the cycle by entering the compressor through the suction line. Thanks to this working principle, heat pumps meet the requirement of heating energy partly from electricity, in order to operate the compressor in the cycle, and partly from an environment the evaporator interacts with (Mohanraj et al., 2018). This environment can be a natural low-temperature heat source, such as air, water, or ground. Furthermore, as a renewable and abundant source, solar energy can be utilized to evaporate the refrigerant, and it can also help improving the efficiency and flexibility, which are evaluated in forthcoming sections. Heat pumps can be named by the energy source they benefit from, i.e., a heat pump rejecting heat from the air, water, or ground can be respectively named as air-source heat pump (ASHP), water-source heat pump (WSHP) and ground-source heat pump (GSHP) (Utlu et al., 2014). Should the solar energy accompany the evaporation process, the heat pump can be named as solar-assisted heat pump (SAHP) (Nouri et al., 2019).

Types of heat pumps regarding their heat source can be categorized as shown in Figure 2.3. Utilization of air-, water-, or ground-source heat pumps depends on a few aspects such as application, heating requirement, availability of source, and space. Nevertheless, they may have their own benefits and drawbacks, compared to each other. Air-source heat pumps have a relatively simpler structure due to rejecting heat from ambient air via a heat exchanger with fan (Yu et al., 2021a). It is easy for assembly and operation since it does not require a specific requirement for the installation. Besides, it also does not require a large space and can be installed in a compact way. Nonetheless, it has relatively lower efficiency compared to WSHP and GSHPs, and its utilization is challenging at the ambient temperatures close to the freezing point of water vapor as this may lead to frosting phenomenon on the evaporator (Yu et al., 2021b). Even though this challenge can be solved by defrosting operations, they require some amount of energy, reducing the heat pump efficiency as well as resulting in an intermittency in the operation (Qu et al., 2012; Xi et al., 2021). On the other hand, WSHPs and GSHPs have relatively higher efficiency as they directly reject heat from water or ground using a borehole structure or a horizontally arranged piping system where the HTF circulates (Benli and Durmuş, 2009).

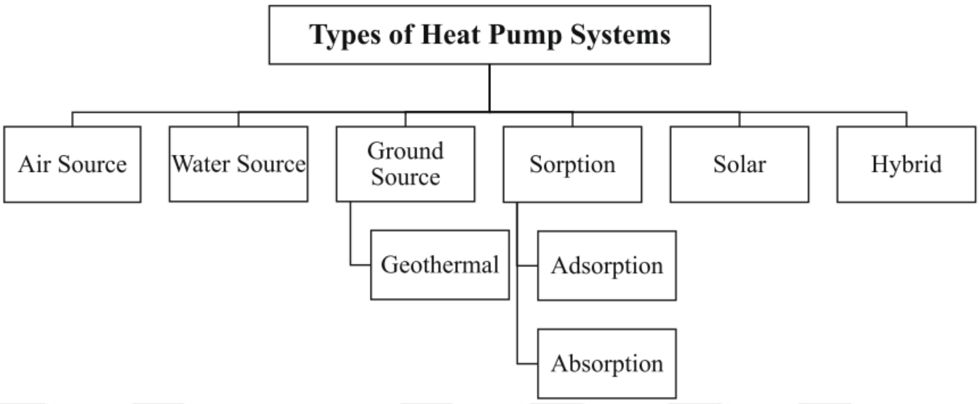

Figure 2.3. Categorization of heat pumps with respect to heat source

Not surprisingly, a water source such as a pond or lake for WSHP; and a ground space for GSHP is required to be present nearby to be able to reject the thermal energy for the evaporation process of the refrigerant in the heat pump cycle (Schibuola and Scarpa, 2016). Furthermore, the installation may require additional efforts and material, which makes these systems more complicated compared to ASHPs. This complication brings a benefit in terms of efficiency and stability, together with the advantage of non-requirement of defrosting. In addition to the heat pump types mentioned above, integration of solar energy utilization in heat pump systems is an effective way to take benefits of renewable energy sources in heating applications (Chu and Cruickshank, 2014). SAHPs take benefit of solar energy in various ways. Thermal energy taken from solar panels can be used to achieve higher evaporation temperatures in the heat pump cycle, which attains a higher thermal performance together with lower energy consumption resulting in lower CO_2 emissions (Miglioli et al., 2023). Besides, a storage tank can be utilized to store thermal energy into a medium such as water, which makes the system not only efficient but also more compact and cost-effective, compared to WSHP or GSHP mentioned above. Additionally, photovoltaic (PV) or photovoltaic/thermal (PV/T) panels are integrated to heat pumps in order to exploit solar energy and convert it into electrical energy to support the compressor and match the demand of hot water for direct use or any other process (Bisengimana et al., 2022;

Yang et al., 2018). This type of heat pumps is divided into two main categories with respect to the assembly of PV/Ts or solar collectors to the cycle, namely direct and indirect expansion SAHPs. Direct expansion solar-assisted heat pumps use the solar collector or PV/T system directly in the heat pump cycle where the refrigerant is evaporated by absorbing solar energy while passing through the PV/T panels. On the other hand, a heat transfer fluid is considered within the cycle where it absorbs heat from the solar collectors or PV/Ts, and then the heat transfer fluid aids the evaporation of the refrigerant flowing through an external heat exchanger, namely the evaporator (Brahim and Jemni, 2017). Nevertheless, utilization of solar energy in the nocturnal time becomes almost impossible although it is an abundant and clean energy source for many applications. At this point, it should be noted that storage of thermal energy becomes crucial to be able to use it as per needs and demands in an engineering application, and the storage of thermal energy can be ensured in various ways, which are presented in detail in Section 2.2. The air, water, ground sourced heat pumps together with solar assisted heat pumps are schematically shown in Figure 2.4 to illustrate their basic operation principles (Dawe, 2022; Niessink, 2019; Ninikas et al., 2014; Osterman and Stritih, 2021).

a)

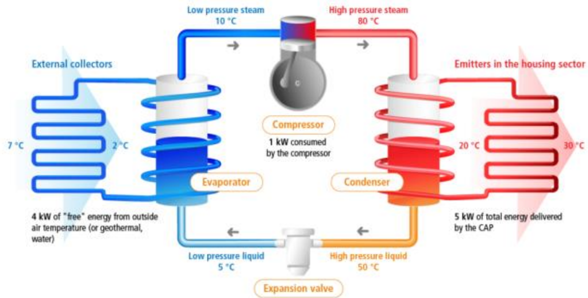

b)

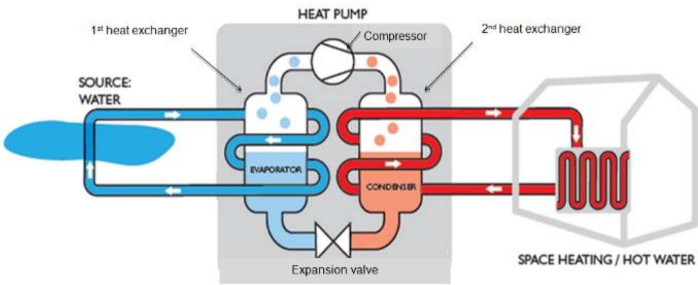

Figure 2.4. Schematic view of a) ASHP, b) WSHP, c) GSHP, and d) SAHP

c)

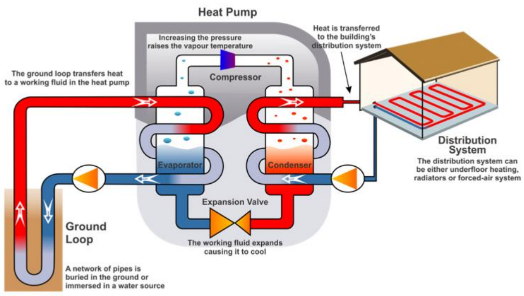

d)

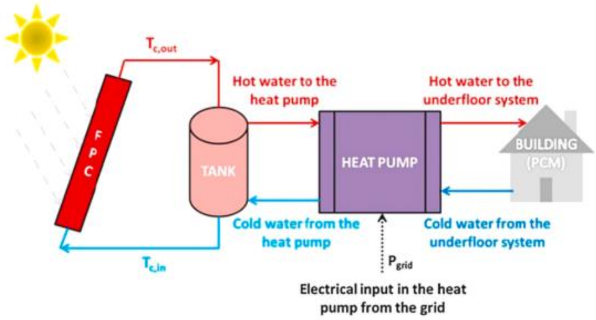

Figure 2.4. (Continued) Schematic view of a) ASHP, b) WSHP, c) GSHP, and d) SAHP

Space heating applications are still highly dependent on fossil fuels all around the world, regardless of the development level of countries. Considering the instability in the fossil fuel supplies relying on various factors around the world such as conflicts between countries and indefinite supply-demand relation resulting in instable costs, not to mention the global pollution they bring. Thus, numerous countries around the world, especially the United States, China, Japan, and the countries in the European Union, put a significant effort to electrify space heating applications through dense investments to the field (IEA, 2020). Although a question may arise concerning the source of the electric since the electricity is also mostly produced by fossil fuels, it can be emphasized here that there are on-going studies around the world focusing on the electricity generation from renewable energy sources. Hence, the remarkable potential of heat pumps for the aforementioned purposes is incontrovertible, and this potential is reflected by many research studies as well as applications and investments. According to a recent International Energy Agency (IEA) report on heat pumps (IEA, 2021), 2021 has been a record-year for heat pump sales in Europe with 2.2 million units, and the growth rate of the number of air-to-water heat pumps in Europe reached almost 50% in 2022 (see Figure 2.5).

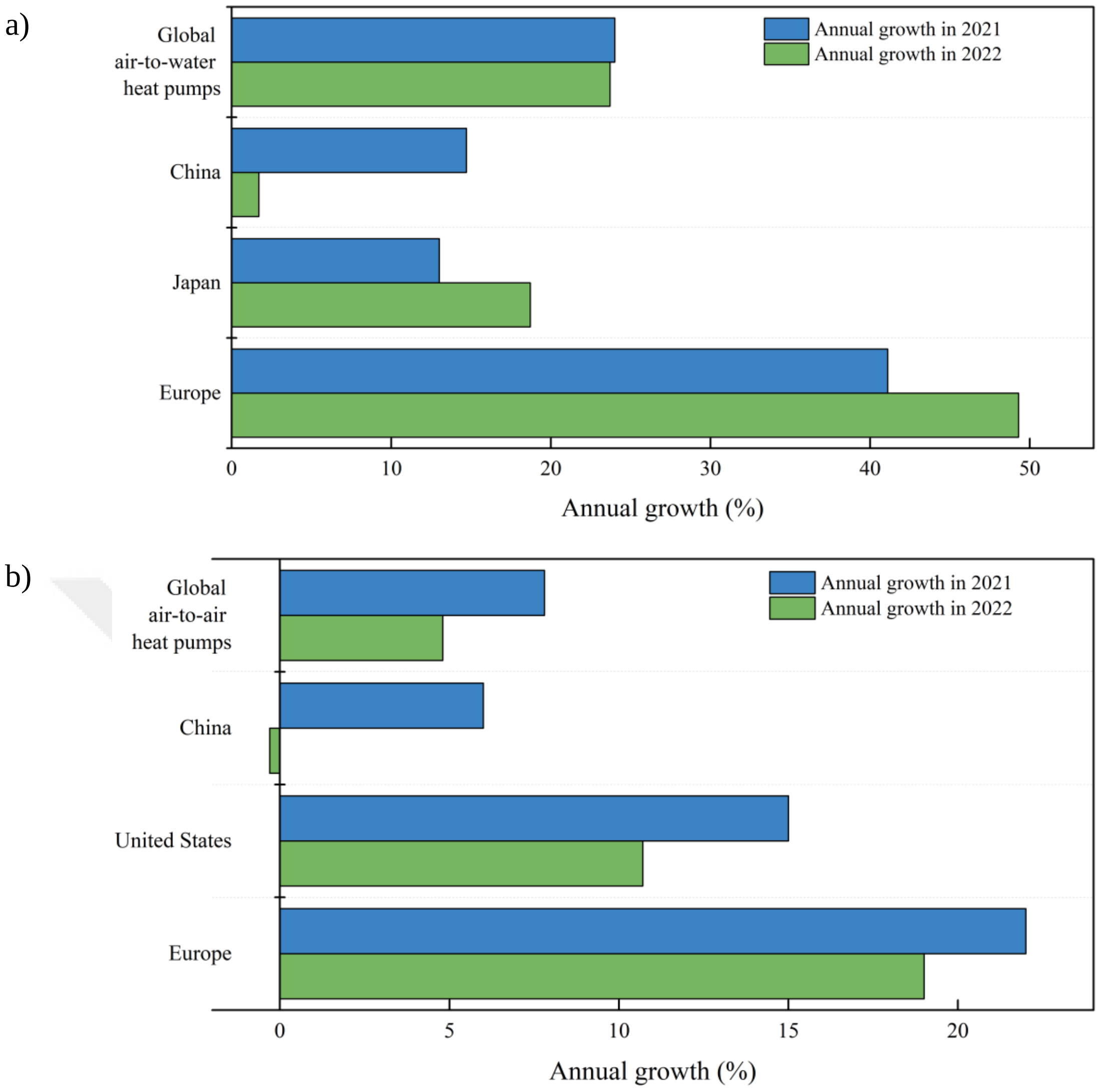

Figure 2.5. Annual growth of a) air-to-water and b) air-to-air heat pumps in 2022

Significant effort is made to reduce the dependence on fossil fuels in various sectors including building heating that consequently leads to decarbonization. Therefore, some countries accelerated their investment on electricity-driven environment friendly heating systems, which mainly covers heat pumps (Walker et al., 2022). Quantitative reports show that the share of heat pumps in global heating applications, which was 9% in year 2021, is expected to increase up to 18% in 2030, and the capacity of heat pumps is expected to increase significantly, particularly in developed countries, as shown in Figure 2.6.

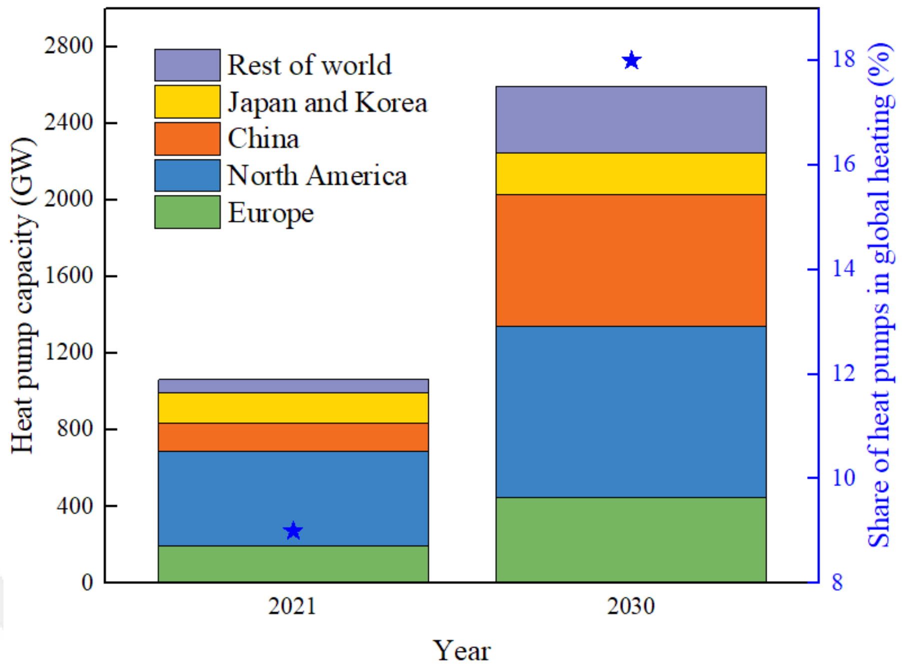

Figure 2.6. Heat pump installed capacity expectation in selected regions (black), and share of heat pumps in global heating (blue)

Aforementioned IEA Heat Pump Report foresees that installation of 600 million heat pump units will be required globally to achieve 20% of building heating needs in 2030, and 50% of heating demand will be met by heat pumps in 2050. Serious amount of installations are completed in European Union (EU) as well, where the air-to-air, air-to-water, and ground-source heat pumps are the most considered types, according to the latest report of European Heat Pump Association (Nowak, 2023). Türkiye also makes investments to increase its heat pump capacity as well. According to the national news agency of Türkiye, Mitsubishi Electric invests 113 Million USD in heat pump production in Türkiye, which includes 50% increase in the air-to-water heat pump manufacturing (Topcu, 2022). In addition to the investments in consideration with reduction of energy consumption and fossil fuel dependence, integration of heat pumps with renewable energy sources is taken into account as a significant target to be achieved, i.e., approaching net-zero energy building (NZEB) concept. Therefore, utilization of renewables in heat pumps as well as various heating applications is crucial, and the share of renewable electricity in heat pumps significantly increased from 2010 to 2021, and expected to grow further by 2030, as shown in Figure 2.7 (Bouckaert et al., 2021; IEA, 2021).

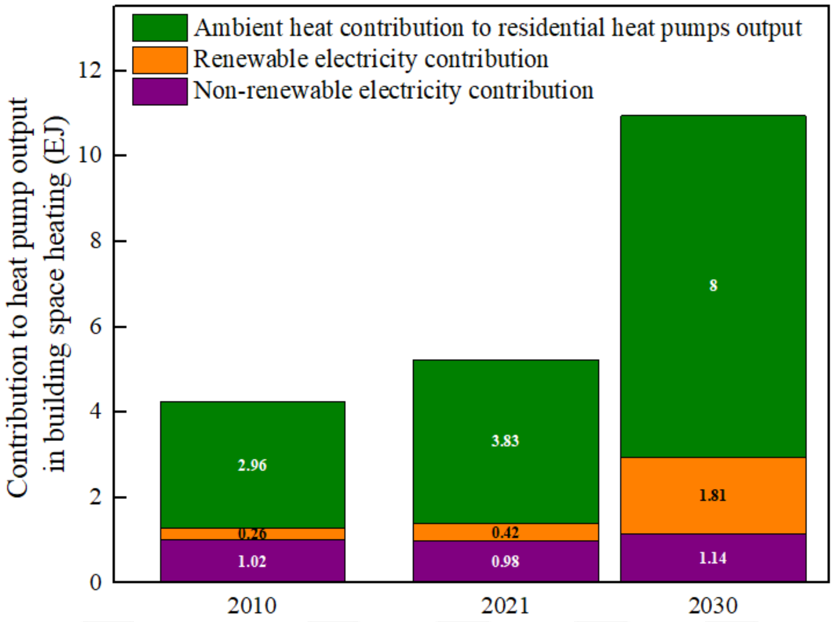

Figure 2.7. Contribution of ambient heat, renewable and non-renewable electricity to the heat pump output and future expectation

Despite ensuring highly efficient and clean heating applications for residential and industrial sectors, electrification of heating system in an intense way using heat pumps may lead to excessive loads in the electricity grid, which results in issues such as insufficient or instable electricity power in the grid and mismatch between supply and demand. To prevent this occurrence, effective and flexible use of energy should be taken into consideration. Furthermore, integration of renewable energy into the heating systems with heat pumps may require an adjustment of energy flexibility, namely the organization of supply and demand sides, due to the fact that renewable energy sources such as solar or wind energy are intermittent even though their presence is abundant (Reynders et al., 2013; Zhu et al., 2021). An effective way to reduce such instabilities and enhance energy flexibility as well as to mitigate the mismatch between supply and demand in heat pump heating systems is to use thermal energy storage systems along with them, which is popularly in scope of researchers in last years (Gu et al., 2023; Y. Li et al., 2021). Besides, according to the studies of which the results are reflected to Figure 2.8 (Shi et al., 2019), the developed and developing countries, including U.S.A., China, Türkiye, Canada, Spain, Australia, etc., attach a considerable importance to heat pump research and development dedicated to renewable energy utilization such as solar energy.

Figure 2.8. Main countries conducting research and development on heat pump systems coupled with renewable energy

2.2. Thermal Energy Storage: Overview and General Aspects

Controlling energy utilization is as crucial as its efficiency and cleanness since an uncontrolled and disorganized use of energy obviously leads to inefficiencies and overconsumption of produced energy. Therefore, produced energy should be held appropriately, and it should be used effectively. This can be achieved by using energy storage techniques. Similar to the batteries used to store electrical energy, thermal energy can be stored in various ways as well. Basically, TES means a process where the heat is accumulated into a medium that can maintain this energy to be used at a later time when it is demanded. Considering a heating application, this process is named as thermal charging, while releasing the stored thermal energy for use is called thermal discharging (Sterner and Stadler, 2019). Nevertheless, in cooling, air-conditioning, or chilling applications, the thermal charge and discharge terms can be used inversely since the term “cold storage” is the focus point in such applications (Sterner and Stadler, 2019).

Thermal energy storage techniques are usually categorized into three major phenomena depending on the physical or chemical structure of the charge or discharge process. As shown in Figure 2.9, TES encompasses sensible heat storage (SHS), latent heat storage (LHS), and thermochemical energy storage are the main techniques for TES. These techniques have obvious advantages and drawbacks over each other. One of the most evident differences between these methods is the volumetric energy storage capacity, meaning that the amount of energy that can be stored in a unit volume of material or medium. As seen in Figure 2.10, the required volume in order to store a given amount of thermal energy is the lowest in thermochemical storage, while it is the largest when SHS is considered using water with a temperature difference of 70 K (Arteconi et al., 2012). In the upcoming subsections, aforementioned types of thermal energy storage are presented in detail.

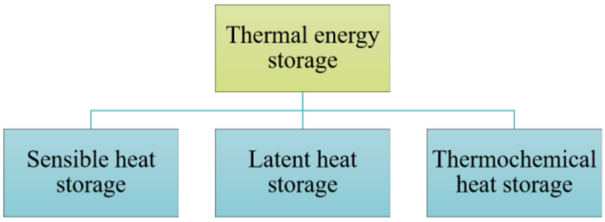

Figure 2.9. Major branches of thermal energy storage

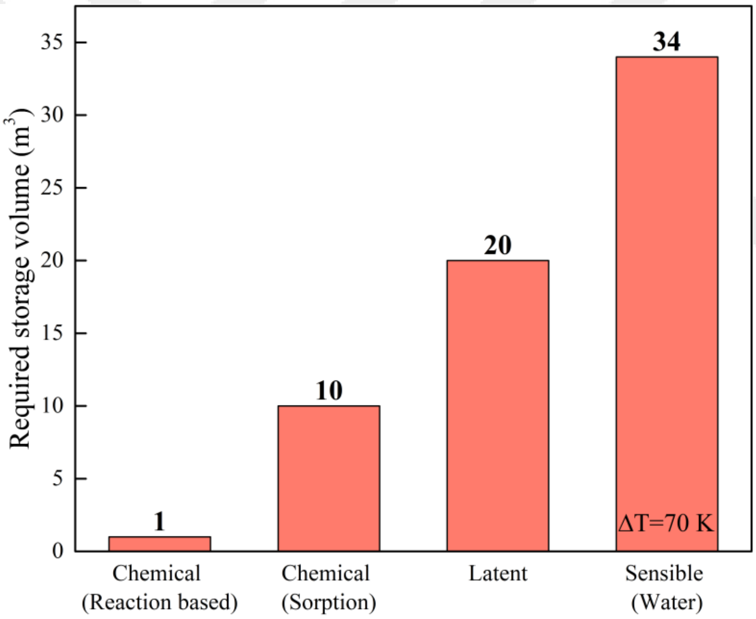

Figure 2.10. Comparison of required storage volumes for different TES techniques

2.2.1. Sensible Heat Storage

Increasing temperature of a material or medium by applying an energy input results in sensible heat storage (SHS). Thus, the physical state of material is preserved in this technique, while the energy storage or release is related to a remarkable temperature variation. Therefore, a wide range of materials or medium can be used in thermal energy storage applications as long as their specific heat capacity and other thermophysical properties are adequate. This aspect makes sensible heat storage a simple and inexpensive option for many engineering applications. Water tanks, ground, aquifers, rocks, and building structural mass are well-known examples of sensible heat storage media for applications dealing with building energy saving, space heating and cooling (Tunçbilek et al., 2023).

Having a significantly large specific heat capacity of around 4.187 kJ/(kg·K) and being abundant, water is one of the most popular sensible heat storage materials frequently used in various applications in residential and industrial sectors, such as domestic hot water (DHW) production and storage, solar energy harvesting, heating, ventilation, and air-conditioning (HVAC) (Pinel et al., 2011). The range of temperature in water storage tanks used for space heating and DHW is usually between 25°C and 80°C (Li, 2016). Besides, a phenomenon named temperature stratification may occur in water tanks depending on its design and working conditions, and the high-temperature portion of water is accumulated at the top, while the cooler one is sunk due to having higher density. The moderate temperature portion between these hot and cold portions is called thermocline (Rendall et al., 2020). Tank geometry, inlet and outlet positions, and natural or forced mixing effects are some of the factors that play an important role in thermal stratification. Water tanks considered for only SHS is desired to have a high level of stratification as well as a sufficient insulation, which increases thermal energy storage and release performance, affecting energy efficiency (Lugolole et al., 2019).

Ground soil and rock beds can be used as thermal energy storage media depending on their adequacy to an application. This type of media is usually suitable for long-term thermal energy storage since the thermal mass is large and the temperature fluctuations occur in a relatively longer period compared to water tanks or similar. Despite their nature of long term thermal charge and discharge, ground soil and rock beds do not require any separate site and they have a large mass to be used for energy storage (Xu et al., 2014). Furthermore, with its high heat capacity and density that are respectively around 920 J/(kg·K) and 1800 kg/m^3, ground soil has a high potential of thermal energy storage for building heating applications as well as flexible use of energy (Givoni, 1977). In order to charge and discharge thermal energy to/from ground soil or rock beds in building heating applications, borehole heat exchangers having U-shaped piping or horizontal serpentine structure (see Figure 2.11) are favorably used (Gustafsson et al., 2010; Rodrigo-ilarri et al., 2010). In case of storing heat at low temperatures, e.g., between 0°C and 40°C, heat pumps can be used to extract and beneficially use the stored energy. Otherwise, the thermal energy can be directly used via circulation pumps when the storage temperature is relatively high, such as 40°C – 80°C. The thermal storage efficiency of soil is generally around 70%, depending on soil type, because of its low thermal conductivity and inevitable heat losses (Reuss et al., 1997).

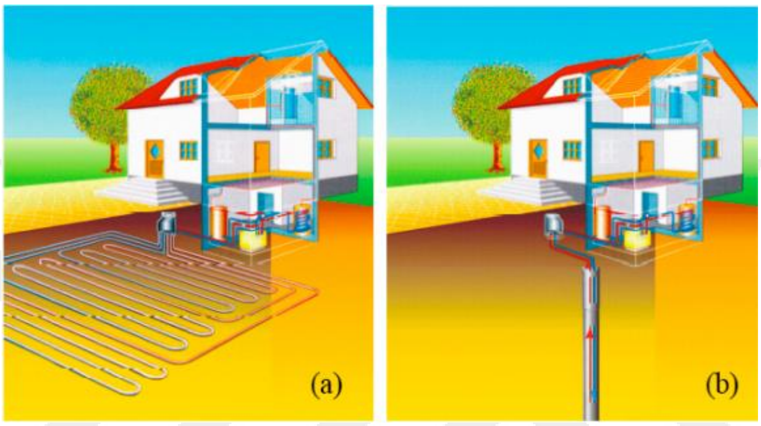

Figure 2.11. a) Horizontal ground heat exchanger, b) vertical ground heat exchanger (Rodrigo-ilarri et al., 2010)

Aquifers, which are rocky or sedimented geological bodies holding groundwater, are another natural form of thermal energy storage media. These structures are usually large, containing a large mass of water, which makes them suitable for long-term thermal energy storage via sensible heat, similar to the ground soil mentioned above, together with their low-cost usage possibility (Dincer et al., 1997). Thermal energy is stored in aquifers via solar energy in summer times, and it can be utilized in colder seasons as a heat source. An inverse operation is also possible for cooling applications. A heat pump can be used to take benefits of this naturally stored thermal energy; however, it is not an obligatory, and the energy can be directly used by the circulation through the space to be heated or cooled (Lee, 2010). Utilization of thermal energy from an aquifer is schematically illustrated in Figure 2.12 for bringing a visual understanding to the concept (Lee, 2010). As seen from the figure, a continuous or cyclic regime can be considered using TES from aquifers depending on thermal energy storage situation and groundwater conditions.

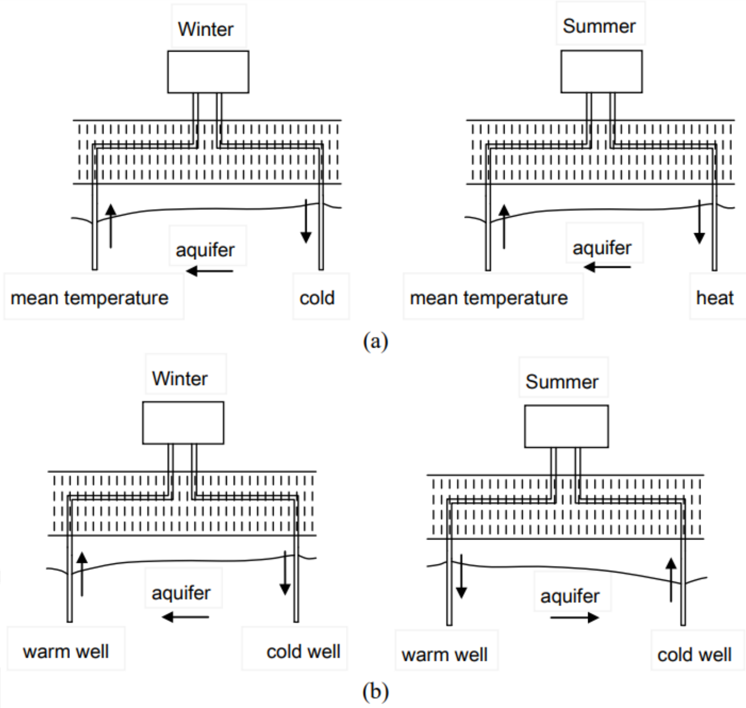

Figure 2.12. Illustration of thermal energy utilization via aquifers for a) continuous regime and b) cyclic regime (Lee, 2010)

In buildings, structural components have a significant mass, and some of these components, i.e., construction materials, are appropriate for storing and releasing thermal energy via sensible heat. Considering the capability of heat storage and release of these materials, the heating and cooling times of a building can remarkably vary. Relatedly, temperature fluctuations inside the building vary with respect to the structural thermal mass the building has. For instance, construction materials having heavy physical material content such as masonry have usually higher thermal mass compared to the lightweight materials such as fiber-supported timber or construction steel (Kendrick et al., 2012). As building construction materials are carefully selected taking into account the required structural thermal mass, thermal energy storage through these building components brings no additional installation costs or maintenance requirement, which makes this technique a favorable one for building energy regulations as well as energy flexibility (Wolisz et al., 2020). Yet, advanced control strategies may be required to fully take benefits of TES into structural thermal mass (Reynders et al., 2017). By using this technique for sensible heat storage in buildings, significant energy savings can be attained by regulating temperature fluctuations, which results in a more comfortable space for inhabitants and reduced costs and CO_2 emissions (Romero Rodríguez et al., 2018; Zilberberg et al., 2021).

2.2.2. Latent Heat Storage

Latent heat storage or release is a phenomenon, which usually takes place by the change of physical phase of a material, such as from solid to liquid, liquid to gas, solid to gas, or reverse forms of these processes. Some materials can also store and release thermal energy by solid-solid phase change with the variations in their physical structures reflected by crystallization (Nazir et al., 2019). As a general concept, these materials are called phase change materials (PCM), and they usually have remarkably high latent heat capacity, which means that they can store or release considerably high amount of thermal energy at a nearly constant temperature during phase change (Khan et al., 2016). Owing to their superiorities in latent heat capacity and a wide range of phase change temperatures, PCMs play an important role in applications where thermal energy storage and/or thermal energy management is of great importance, e.g., solar energy systems, cooling of electronic components, building heating/cooling and domestic hot water production, waste heat recovery, etc. (Qaiser et al., 2021).

Compared to sensible heat storage systems, usually a smaller volume is required to store a given amount of thermal energy via latent heat storage, which provides a higher energy storage density and makes this technique favorable for applications where the volume or space area is a constraint for the design (Sharma et al., 2023). Furthermore, as discussed previously, a significant temperature variation occurs in sensible heat storage systems, while almost an isothermal process occurs during latent heat storage, i.e., throughout the phase-change process of PCM (Li et al., 2023). Hence, applications such as TES integrated heat pumps, thermal management of electronics, and HVAC, where the storage temperature should be remained around a specific value, generally require latent heat utilization attained by various PCMs (Ali, 2019; Shahjalal et al., 2021). For a typical PCM which exhibits a solid to liquid phase change process, the temperature variation with respect to energy storage is shown in Figure 2.13. As illustrated, a significant amount of thermal energy is stored during phase change, namely latent heat, without any notable temperature variation.

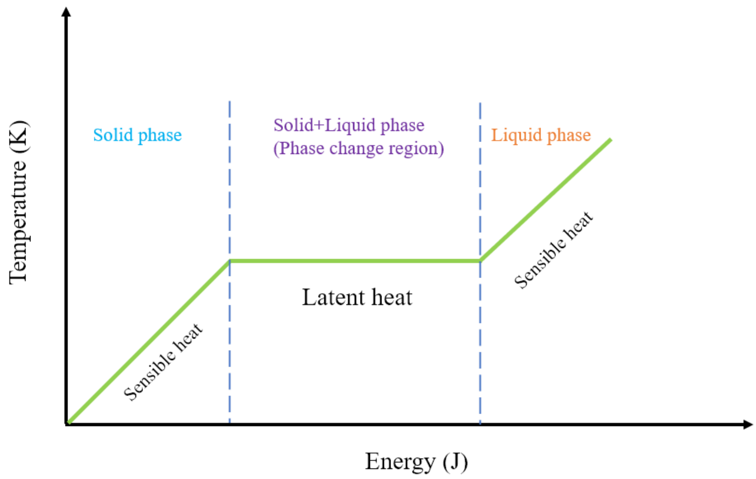

Figure 2.13. Illustration of temperature variation with respect to stored energy for a typical solid-liquid phase change material

Phase change materials used in latent heat storage systems can be categorized into several types depending on their physical structure and the phase change process they follow in order to absorb or release thermal energy (Sharma and Chauhan, 2022). As shown in Figure 2.14, PCMs can be classified regarding the physical phases changed in applications during heat absorption and release. Solid-Solid PCMs change their physical structure via crystallization during thermal energy storage, and they do not exhibit any liquid form (Fallahi et al., 2017). Furthermore, they have high latent heat capacity (Venkitaraj and Suresh, 2019) as well as advantages such as having no leakage problems (Feng et al., 2019). Liquid-Gas PCMs store and release a high amount of latent heat during boiling and condensation processes, and a typical application area of these materials is heat pipes (Fang et al., 2020).

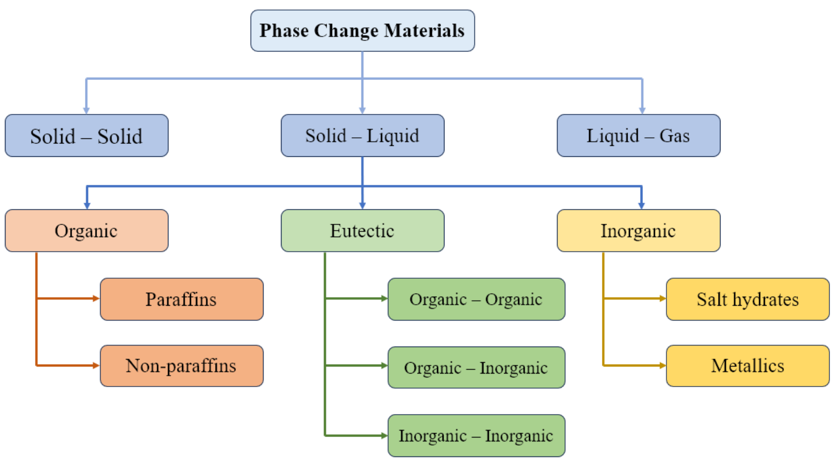

Figure 2.14. Classification of phase change materials

Apart from these two types of PCMs, the solid-liquid phase change materials are frequently used in thermal engineering applications because of their remarkable latent heat capacity, simplicity, and suitability for a wide range of applications requiring different thermal storage temperatures, as solid-liquid PCMs can be found with different melting temperatures (Khan et al., 2016). As a frequently used PCM type in thermal energy storage applications, solid-liquid PCMs have different types regarding their chemical and physical structure, namely the organic, inorganic, and eutectic ones. Organic PCMs consist of paraffins and fatty acids, which have carbon atoms in their chemical compounds. These materials are chemically stable in general and suitable for many TES applications as they have a consistent phase change temperature range together with sufficient latent heat storage capacity (Akeiber et al., 2016). Along with their desirable features, there are some crucial drawbacks of organic PCMs. They usually have a low thermal conductivity between the range of 0.1 W/m·K and 0.7 W/m·K, which is their greatest handicap in TES applications (Pereira da Cunha and Eames, 2016). Therefore, in practical applications, it is likely to employ thermal conductivity enhancement techniques to the organic PCMs in order to accelerate their melting and solidification rate, which helps exploiting the latent heat at a higher rate (Teggar et al., 2021; Yıldız et al., 2023). Using extended surfaces on PCM containers (Wu et al., 2022), inclusion of nanoparticles (Boumaza et al., 2023), utilization of porous media such as metal foams (V R and Chanda, 2023), and using multiple PCMs regarding their phase change temperatures (Mahdi et al., 2020) are some popular examples for heat transfer enhancement techniques implemented to PCMs. Another drawback of organic PCMs is that they are usually flammable and exhibit a considerable amount of volume expansion, as well as they are relatively expensive (D. Li et al., 2020).

On the other hand, inorganic PCMs, such as salt hydrates and nitrates, have relatively higher thermal conductivity compared to organic PCMs. In addition to that, they are regarded as low-cost materials for TES (Imran Khan et al., 2023). Nevertheless, chemical structure of some inorganic PCMs such as salt hydrates is not suitable to be conserved in metallic containers or capsules since they may exhibit a chemical reaction, which results in corrosion and deformations leading to leakage problems and ineffective operation of latent heat storage (Akeiber et al., 2016). Besides, occurrence of supercooling phenomenon and phase segregation are the major drawbacks of inorganic PCMs together with corrosiveness (Shen et al., 2020).

Eutectic PCMs are produced by mixing different types of PCMs to achieve desired PCM properties taking benefit of different single PCMs and prevent the aforementioned drawbacks (Kalidasan et al., 2023). In order to obtain an eutectic PCM, an organic-organic (Sharma et al., 2015), inorganic-inorganic (Risueño et al., 2017), and organic-inorganic mixtures (Karaipekli et al., 2016) can be considered.

Selection of appropriate PCM is crucial for thermal energy storage applications since the suitable phase change temperature to the considered application should be attentively determined in order to fully exploit the latent heat storage capability of the material. Otherwise, the latent heat can be utilized partly, or it can even not be exploited at all, leading to ineffective heat transfer as well as unnecessary cost increase. Along with the suitable phase change temperature, the PCM should have a sufficient amount of latent heat capacity. The melting-solidification temperatures and latent heat of fusion of PCMs noticeably vary depending on the PCM type. As seen in Figure 2.15, paraffins have a wide range of phase transition temperatures varying roughly between 0 and 100°C, while their latent heat capacity has a relatively narrower range, approximately between 150 and 200 kJ/L. Conversely, salt hydrates have narrower alternatives of phase change temperature compared to paraffins; however, they have a variety of latent heat capacity. Sugar alcohols, nitrates, hydroxides, chlorides, carbonates, etc., have a wider range of phase change temperatures and fusion heat values, nonetheless, their phase transition temperatures are higher than 100°C. Thus, paraffins and salt hydrates are more suitable for practical engineering applications such as solar energy systems, thermal management of electronics, thermal energy storage for heat pumps and building heating/cooling. As seen from the aforementioned figure, especially paraffins and fatty acids are available at the desired phase change temperatures for such applications. For instance, PCMs to be used in the latent heat storage applications together with heat pumps can be considered with a phase change temperature of around 0°C to 30°C for evaporator side and approximately 40°C to 80°C for condenser side integration in the vapor-compression cycle-based heat pumps.

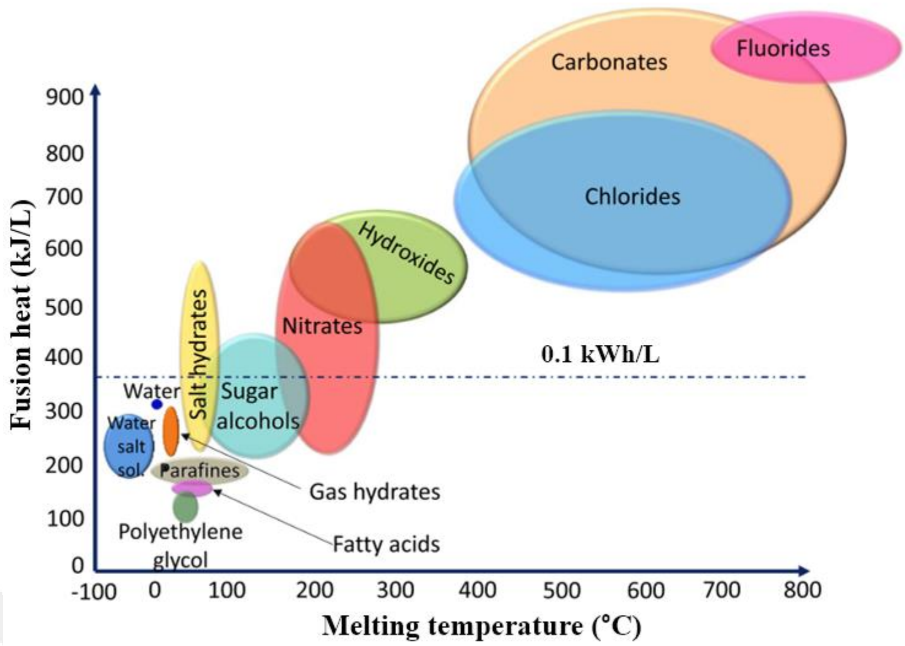

Figure 2.15. Ranges of melting temperature and fusion heat for some well-known PCM types (Imran Khan et al., 2023)

2.2.3. Thermochemical Energy Storage

Despite being in its early stage of development and requirement of significant amount of time and effort, thermochemical energy storage is a promising technology for TES applications because of its remarkably high energy storage density. As illustrated previously, two to twenty-times higher thermal energy can be stored or released using thermochemical energy storage techniques (Pardo et al., 2014).

Sorption-based and reaction-based thermochemical energy storage are two main phenomena in this type of TES. In sorption-based thermochemical energy storage, the energy is stored by a surface mechanism breaking the physical and chemical bonds between the sorbent and sorbate where the two major processes are absorption and adsorption. On the other hand, in reaction-based storage, the thermal energy is stored or released via reversible chemical reactions without sorption. The reaction based thermochemical energy storage has a significantly higher energy density and wider operation temperature range compared to sorption-based methods (Desai et al., 2021).

As thermochemical energy storage is based on composition and decomposition of atomic and molecular bonds of relevant materials, there is no heat loss during thermal charging and discharging processes in this technique (Sunku Prasad et al., 2019). Hence, the stored energy can be maintained for an unlimited period of time, theoretically, and thus, this technique becomes perfectly suitable for seasonal thermal energy storage applications (Desai et al., 2021; Solé et al., 2015a). In addition to that, a significant amount of thermal energy can be stored in small containers since the energy storage density of thermochemical systems is remarkably high (Pardo et al., 2014). Nevertheless, there are some challenges needed to be addressed, such as corrosiveness of some thermochemical materials with metallic containers and the requirement of an external additional energy to initiate the discharging (Solé et al., 2015b).

2.3. Integration of Thermal Energy Storage Systems to Heat Pumps

Considering the state-of-the-art of the heat pump technology together with its future prospects and potentials in building heating systems discussed in Section 2.1, coupling heat pumps with thermal energy storage systems is an indispensable necessity for effective and efficient energy use as well as managing the balance between supply and demand sides, which helps reducing the excessive loads in the grid and CO_2 emissions (Péan et al., 2019). From another point of view, using thermal energy storage systems coupled with heat pumps can increase the share of renewable energy utilization where the solar-assisted heat pumps constitute a practical implementation in this aspect (Lazzarin, 2020). For these purposes, various thermal energy storage techniques are taken into account in order to achieve an efficient and flexible use of energy. As mentioned in previous section, latent heat energy storage is a favorable option for thermal energy storage due to its high volumetric energy density and energy storage capability at a nearly isothermal process. Also, sensible heat storage techniques are suitable for heat pumps in a simpler way where water is frequently used for this purpose thanks to its remarkably high specific heat capacity (Qu et al., 2015). Nonetheless, thermochemical energy storage technology is not readily available for this purpose because of its complexity and cost. To conclude, sensible heat storage systems, such as water tanks, aquifers, ground, and rock beds, latent heat storage systems involving various phase change materials, and combination of sensible and latent heat storage systems are all suitable and promising methods for the integration of TES and heat pumps (Trinkl et al., 2009).

Integration of latent heat thermal energy storage systems into heat pumps can be accomplished using thermal energy storage tanks or units as a convenient technique. In heating and cooling systems with heat pumps, such tanks or units may contain PCM only, in order to consider latent heat storage and release via a heat transfer fluid passing through (Agyenim and Hewitt, 2010; Moreno et al., 2014a), as shown in Figure 2.16. Alternatively, a combination of sensible and latent heat storage can be acquired, e.g., using a water tank containing PCM modules inside, which is also called hybrid thermal energy storage unit (see Figure 2.17). Thereby, PCM and water can exchange thermal energy during charging and discharging processes, while water itself can store and release sensible heat as well (Kelly et al., 2014).

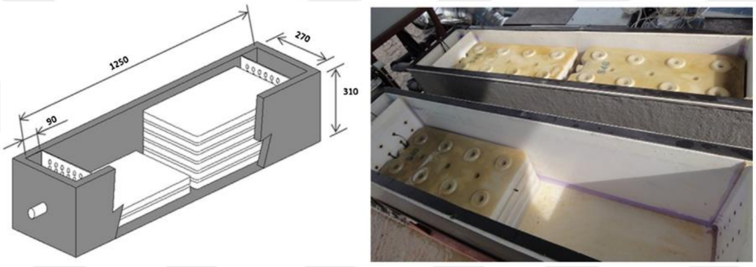

Figure 2.16. Latent heat thermal energy storage tanks used for HVAC applications (Moreno, Castell, et al., 2014)

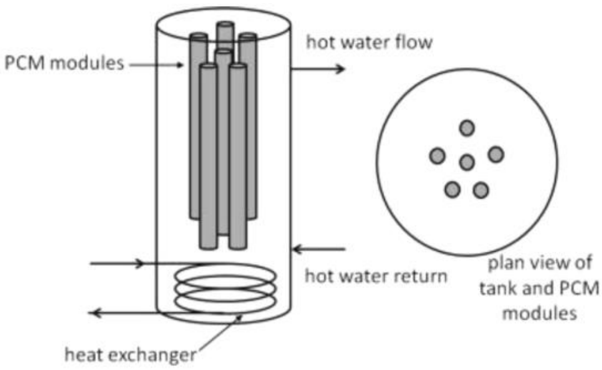

Figure 2.17. Schematic view of a thermal energy storage tank including water and PCM modules (Kelly et al., 2014)

Various factors including the type of heat pump, purpose and aim of thermal energy storage, and utilization period affect the system layout for the thermal energy storage unit integration to heat pumps. Therefore, thermal energy storage unit and heat pump coupling can be categorized as seasonal and short-term storage depending on the user requirements and type of heat pump which can be an air-source heat pump, water/ground-source heat pump, and solar-assisted heat pump (Pardiñas et al., 2017; Pinamonti et al., 2021). Relatedly, the assembly of the thermal energy storage system, i.e., to the evaporator or condenser of the heat pump, varies with respect to the design considerations along with the focused purpose of TES integration, such as energy efficiency, energy flexibility, or increasing the share of renewable energy utilization (Gu et al., 2023). Certainly, these objectives of benefit can be achieved at the same time. For example, a TES system integrated to a heat pump can achieve energy efficiency together with providing a more flexible energy usage. Nevertheless, the focus point of the design may be different, and the TES integration does not necessarily increase the energy efficiency while increasing energy flexibility or regulating supply-demand mismatch (Hirmiz et al., 2019). Alternatively stated, this relation is dependent on the system design and performance.

2.3.1. Energy Flexibility in Buildings: An Overview Related to Thermal Energy Storage and Heat Pumps

Energy flexibility is a wide-meaning term and covers a variety of applications and points of view, hence, there is no single definition of this concept. Depending on focus point, energy flexibility can refer to the flexibility of grid and electrical energy, flexible use of thermal energy in building heating and cooling, or both targets (Luc et al., 2019; Reynders et al., 2018). Yet, energy flexibility measures can be implemented to both electrical systems and thermal systems, even though its implementation is still limited in thermal systems compared to electrical ones (Luc et al., 2019). According to the Annex 67 of IEA, energy flexibility in buildings is regarded as a solution to the imbalance between the supply and demand caused by increasing utilization of renewable energy sources -which are intermittent energy sources- in electricity and thermal energy generation, without jeopardizing the occupant comfort (Jensen et al., 2017). Thus, controlling the energy generation and consumption through an effective way becomes a focal point for future energy systems in buildings.

In buildings, energy flexibility can be implemented at different levels depending on the scope in consideration, such as system-, building-, district-, and even sector-level, as seen in Figure 2.18. Furthermore, these levels can have different phases such as operation and design. Additionally, according to the purpose of the implementation, e.g., evaluation of system potential, control strategy, and energy management, different methods are studied (H. Li et al., 2021).

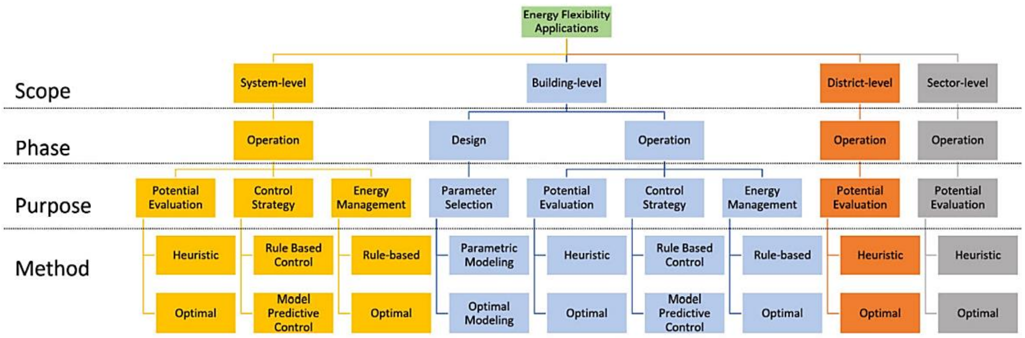

Figure 2.18. Hierarchical diagram for various energy flexibility applications (H. Li et al., 2021)

As a simpler perspective, the energy flexibility at a level of building heating/cooling systems can be defined as the ability of the system to react changes in supply and demand. Hence, it is divided into two main categories as supply and demand side where the studies focused on each of them or both of them in combination. As shown in Figure 2.19, supply side management and demand side management can be implemented using various methods from different perspectives with respect to the system design and user requirements (Luc et al., 2019).

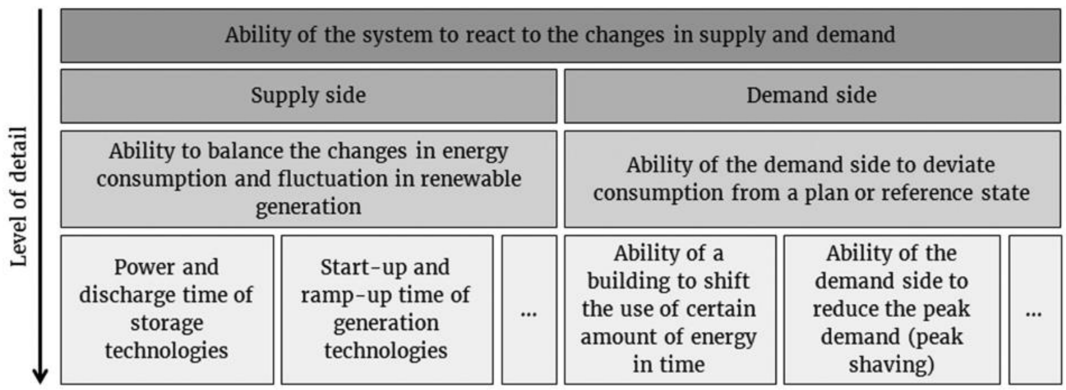

Figure 2.19. Level of details for supply side and demand side management activities (Luc et al., 2019)

Considering the number of literature studies separately searched by the keywords "Demand Side Management" and "Supply Side Management" in Scopus index, it is noticed that demand side management is notably more often studied compared to supply side management. As illustrated in Figure 2.20, various activities are considered for demand side management (DSM), which include load shifting, peak clipping, valley filling, strategic load growth/conservation, and flexible load shape (Hirmiz et al., 2019). Load shifting activities include shifting the load from on-peak to off-peak times by preventing the increase in energy consumption during peak times; hence, the same amount of energy is consumed in a distributed way during a certain period without violating grid capacity during on-peak periods. Peak clipping is a similar activity where the reduction of energy usage during on-peak times is aimed, while valley filling considers a systematic increase of loads in off-peak periods to utilize energy more effectively. Strategic load growth involves the increase in total energy consumption taking into account relative prices of different fuels in electricity generation, and the strategic conservation focuses on reducing the consumption during on-peak and off-peak periods (Gelazanskas and Gamage, 2014; Sharda et al., 2021). Out of these demand side management activities, load shifting and peak clipping are the most considered ones for focusing on energy efficiency and flexibility (Sharda et al., 2021).

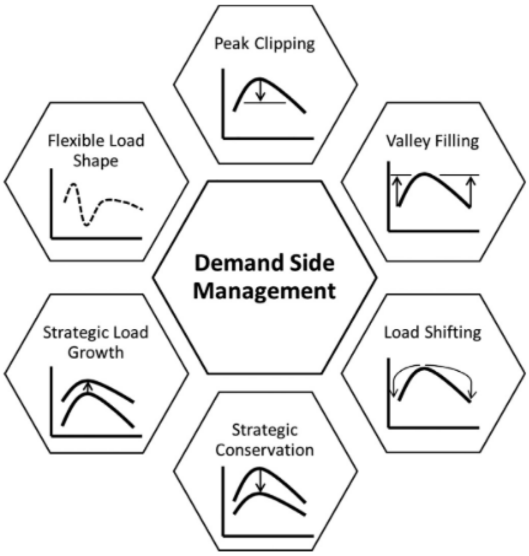

Figure 2.20. Different objectives for demand side management (Hirmiz et al., 2019)

Thermal energy storage systems integrated with heat pumps is an appropriate way to help organizing load shifting and peak clipping actions (Date et al., 2021). For this purpose, different thermal energy storage strategies can be considered with respect to the storage period, depending on the storage medium, energy source, and application, and these can be divided into two main parts, namely seasonal storage, and short-term storage. Seasonal thermal energy storage, also named as long-term storage, covers a long period ranging from weeks to years, whereas the short-term thermal energy storage is considered in a range between a couple of hours to a few days (Olsthoorn et al., 2016; Sartor and Dewallef, 2017). In addition to the options for thermal energy storage period, there are two major alternatives for the integration of a TES system to a heat pump, regarding the layout of the system, which are the assembly of TES to the evaporator of a heat pump and to the condenser of a heat pump (Pardiñas et al., 2017). As this thesis work focuses on the aforementioned two system layouts for TES integration to heat pumps, following subsections include the explanation of these two different ways of integration of TES to heat pumps.

2.3.2. Integration of Thermal Energy Storage Unit to Heat Pump Evaporator

When integrated to evaporator of a heat pump (HP), thermal energy storage systems act as a heat source medium with its stored energy, and it provides thermal energy for the evaporation of refrigerant. Hence, this type of an integration is likely to be seen in water-source and solar-assisted heat pump systems as well as ground-coupled solar-assisted heat pumps, namely hybrid source heat pumps (Han et al., 2008; Niu et al., 2013). For this type of applications, there could be two advantages: i) higher evaporation temperatures because of the stored heat at a relatively higher temperature can boost up the heat pump efficiency, i.e., the coefficient of performance (*COP*), and ii) the load shifting, or peak clipping, and augmentation in the share of renewable energy utilization can be attained (Pardiñas et al., 2017). Furthermore, utilization of latent heat storage systems with PCM helps obtaining temperature stability at the heat source of the HP (Zhou et al., 2023).

Stable heat source temperature and/or higher thermal efficiency for the HP can be achieved by integrating various thermal energy storage units in seasonal or short-term periods. Besides, the utilized thermal energy storage system may be benefiting the sensible heat, latent heat, or both in the same unit. For instance, thanks to the large thermal mass they own, aquifers and ground are good examples for seasonal (long-term) thermal energy storage media to be used as a heat source for a HP (Lee, 2010; Xu et al., 2014). In addition to that, it is possible to consider a large water tank partly or fully buried into the ground, rock bed, or concrete to store thermal energy within a heat exchange between the water tank and the surrounding medium (Dahash et al., 2019).

For example, Lottner et al. (2000) investigated the potential of seasonal TES along with Schematic illustrations of such systems having large storage tanks for seasonal thermal energy storage are given in Figure 2.21 (Hesaraki et al., 2015; Lottner et al., 2000), and it should be also noted that these systems are suitable to be utilized with solar energy systems (Hesaraki et al., 2015). Considering that these systems are able to store sensible heat, it is also possible to integrate PCM to these systems in order to further enhance the heat storage capacity. Recent studies involve latent heat storage materials to improve energy storage density as well as to aim at reducing the required storage tank volume.

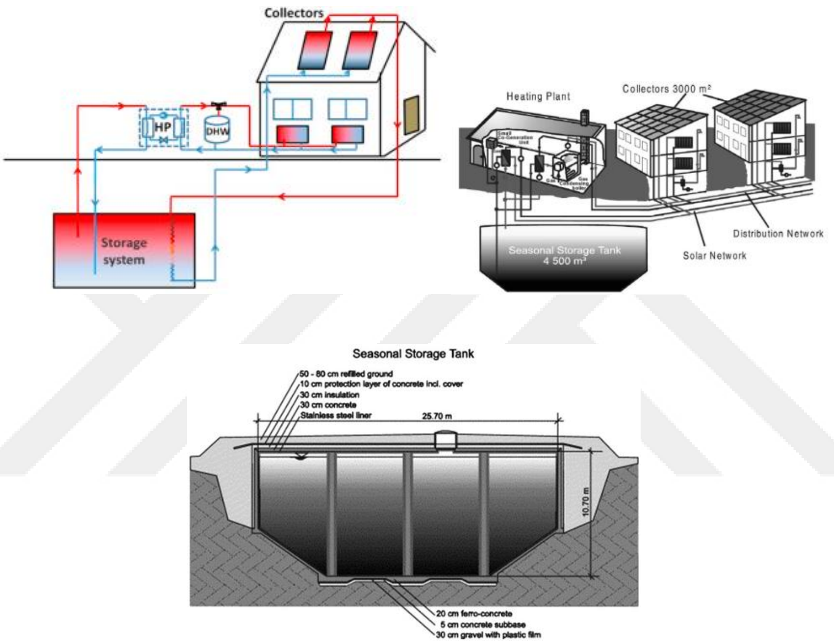

Figure 2.21. Schematic view of a SAHP system with seasonal TES tank connected to the heat source of the HP (left), a solar-assisted district heating system with 4500 m^3 seasonal storage tank buried into ground in Hamburg-Bramfeld (right), and the close-up schematic

In SAHPs, the solar energy can be collected in the periods when it is abundant, and then it can be used as heat source of the HP when the heating demand is high. This operation helps achieving multiple targets such as enhancing flexibility in energy utilization by demand side management, extending the operation time of the heat pump, increasing renewable energy utilization share, stable operation, and augmenting energy efficiency by the higher evaporation temperature (Plytaria et al., 2018; Sezen et al., 2021). Both in seasonal energy storage (Wang et al., 2010) and short-term energy storage (Moreno et al., 2014b), sensible and latent heat storage units can be used at the evaporator of solar-assisted heat pumps. In seasonal consideration, the solar energy is collected in the summer seasons (considering Northern Hemisphere), and it is stored in seasonal TES units. Then, the stored energy is used in the winter times when the heating demand is high. Considering that the storage temperature may be relatively low, this energy may not be adequate for direct heating, hence, it can be used in the evaporator of the heat pump. Thereby, the solar energy abundant in summer is used in winter, and the SAHP can be even coupled with ground heat sources as well (Wang et al., 2010). As a second option, solar energy can be stored in short-term, i.e., daily or every couple of days, during diurnal periods where the solar energy is abundant and the heating demand in the building is relatively low. Thereafter, the stored energy is used as the heat source for the HP in nocturnal time, and thereby, the share of renewable energy utilization in heating can be increased, and load shifting can be also achieved (Belmonte et al., 2022). Furthermore, depending on the system design, direct heating is another option for short-term TES when high storage temperatures can be reached (Chu and Cruickshank, 2014; Lazzarin, 2020). Compared to the seasonal storage systems, the thermal energy storage tanks of the short-term SAHP systems are relatively smaller and less complex, as expected, and a schematic view from the numerical study of Belmonte et al. (2022) is illustrated in Figure 2.22. Using PCMs can enhance the volumetric storage capacity of TES integrated to SAHP, as mentioned previously. One of the most important contribution of this utilization is that it can balance the mismatch between the supply and demand, and the service time of the HP system is increased while the operation of the compressor is shortened (Gómez et al., 2018).

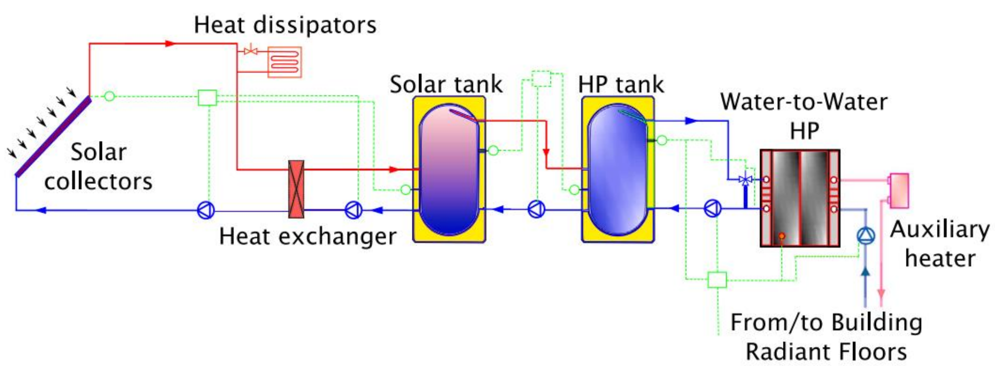

Figure 2.22. Schematic illustration of a SAHP system with short-term thermal energy storage unit integrated to evaporator

2.3.3. Integration of Thermal Energy Storage Unit to Heat Pump Condenser

Thermal energy storage units are used at the condenser of heat pumps in various applications. In this configuration, thermal energy storage unit takes a role of a heat sink, rather than heat source, as mentioned for evaporator. In the designs where the TES unit takes place at the condenser, the heat pump is used to charge the TES unit by sensible and/or latent heat. Thereafter, the accumulated heat is used for space heating, domestic hot water, or any other process requiring heat (Y. Li et al., 2020; Zou et al., 2017). Here, the operation period of the heat pump plays a significant role since it is determinative for the order of energy consumption of compressors as the electricity tariff varies throughout a day depending on policy of supply authorities, and this variation is usually adjusted regarding the load in the electricity grid (Bampoulas et al., 2021; Niu et al., 2013). Thus, as the key point here, integration of TES to HP condenser can help accumulating thermal energy in the off-peak periods, which is a time interval where the electricity consumption is lower, e.g., nocturnal times, and the stored thermal energy can be used in the on-peak periods without consuming high amount of electrical energy due to the partly or completely inactive compressor during this period (Shi et al., 2019). Similar to the previously mentioned HP systems with TES integrated to their evaporator, these systems can be designed to benefit sensible heat, or sensible and latent heat in combination, namely a hybrid system, as schematically illustrated in Figure 2.23. As seen from the figure, the system may contain a water tank to store thermal energy, and it can also include PCM modules, which can be in different shapes or properties, to improve its energy storage capacity.

Integration of TES systems to HP condensers helps ensuring the load on the grid to spread over different periods of the day, instead of accumulating into a specific time interval, resulting in excessive demand, which is an effective demand side management technique, namely the load shifting, to prevent wasting energy and attain an effective energy utilization (Luc et al., 2019). In addition, the electrical energy produced is more efficiently used this way, and it is not wasted in nocturnal periods. Moreover, authorities encourage society using electricity in off-peak periods by adjusting the prices within different tariffs. As depicted in Figure 2.24, Xu et al. (2021) showed the electricity tariff in Sweden along with the action of shifting the load from on-peak to off-peak periods.

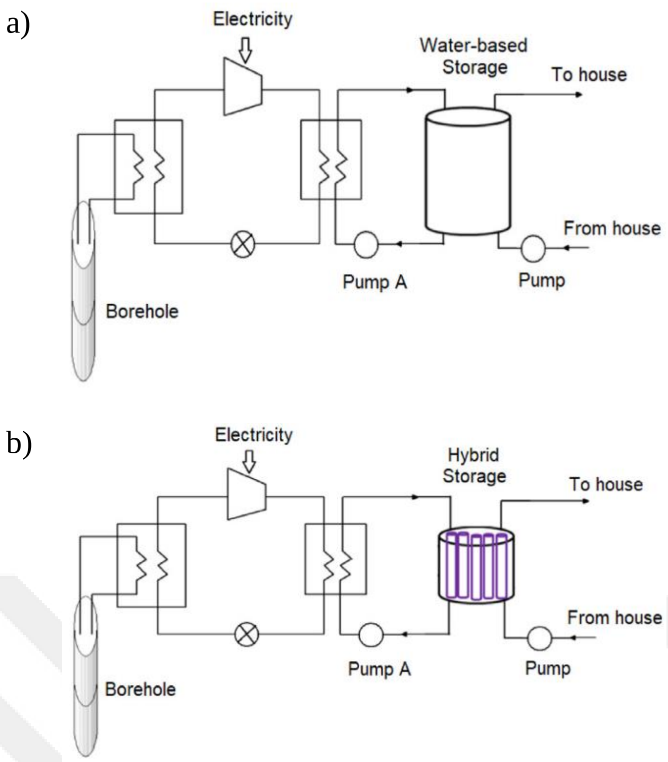

Figure 2.23. Schematic illustration of a a) water-based storage integrated and b) hybrid water-PCM storage integrated GSHP system

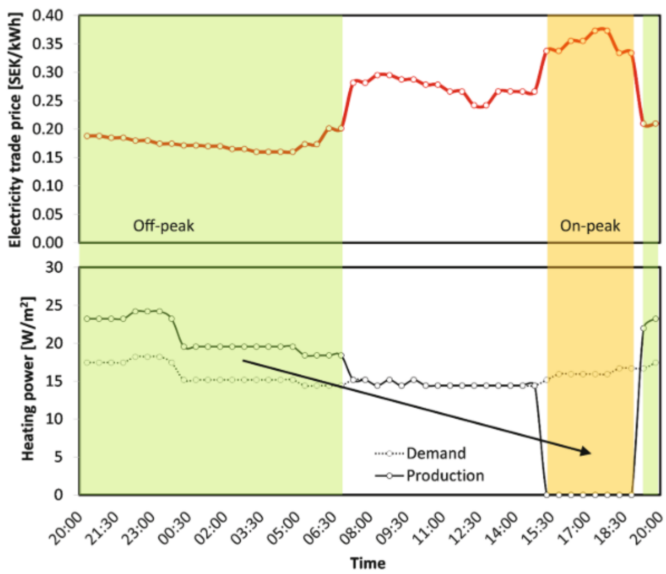

Figure 2.24. Variation of electricity prices depending on time of day and the load shifting activity carried out

As another example, the effect of TES utilization on the energy consumption along the time of day is well illustrated by Hirmiz et al. (2019) in Figure 2.25. It should be also stressed here that utilization of heat pumps, especially together with thermal energy storage systems, has a significant potential for decarbonization of building heating due to their ability of enhancing energy flexibility by the means of load shifting and peak clipping (Nair et al., 2022).

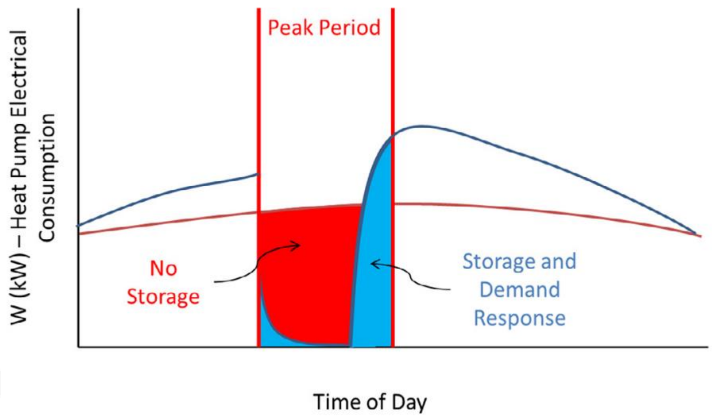

Figure 2.25. Representation of electricity utilization integral with and without TES integration to a heat pump

Coupling the condenser of heat pumps with thermal energy storage units is usually considered by air source heat pumps, i.e., air-to-water heat pumps in this case, because of their simplicity for the objective. Nevertheless, thermal energy storage with the heating load of a heat pump is improved using ground-source heat pumps, water-source heat pumps, and even solar system assistance. Thereby, load shifting activity can be evolved to an efficient way for short or long term storage as well as for domestic and district heating purposes (Abdur Rehman et al., 2021; Gaur et al., 2021; Xu et al., 2021).

2.4. Literature Survey

As the trend of electrification and decarbonization of heating systems has been rapidly increasing in numerous countries and there is a related necessity for the energy flexibility in order to achieve the requirements of this action, significant investments are considered on the heat pumps and thermal energy storage systems. Therefore, researchers accelerate their studies in this field in order to reduce the dependence on fossil fuels as well as international energy sources that rely on policies among governments. At this point, studies are clustered in different points of views, depending on the connection of thermal energy storage unit to the heat pump, i.e., condenser or evaporator, and the consideration the period of thermal energy storage, i.e., short-term, or seasonal. Regarding the relevant keywords, which are considered to be “heat pump”, “thermal energy storage”, “phase change materials” and “energy flexibility”, the number of studies in the last eleven years indexed by Scopus database is shown in Figure 2.26. As seen from the figure, an acceleratingly increasing number of studies indicates that the significance of the topic is increasing, due to the aforementioned reasons. Yet, it is also noticed from the figure that the number of studies become lower when the thermal energy storage is considered with PCMs specifically, and the decrement is even more prominent when energy flexibility is taken into account, which evidently indicate the needs for studies in these fields.

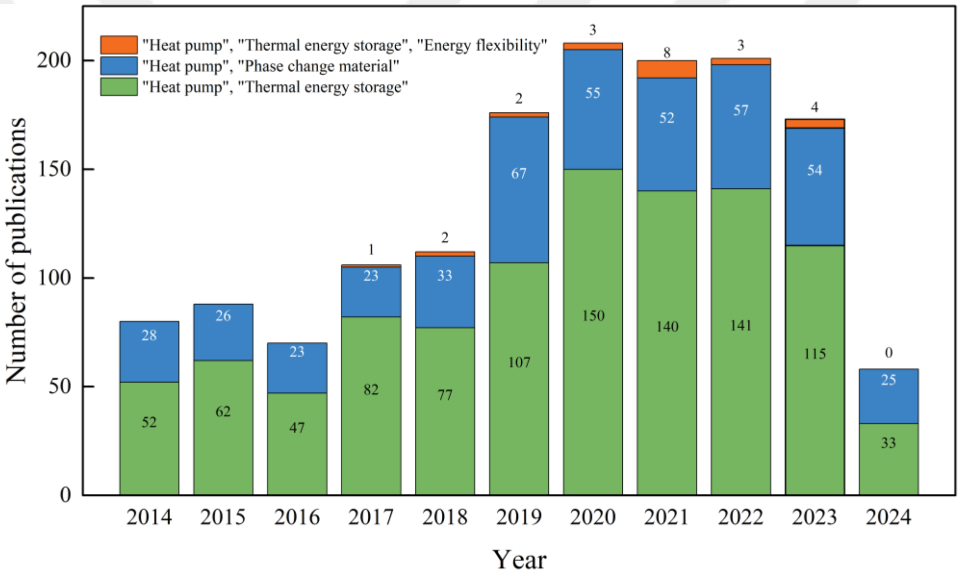

Figure 2.26. Number of studies in the field regarding Scopus database last updated in March 2024

Considering the literature works that deal with thermal energy storage integration to heat pump evaporators, it is noticed that the solar assisted heat pumps are more favorably studied because of their suitability of integration with renewable energy sources. Badescu (2003) conducted a numerical work to investigate the impact of sensible heat storage unit on the performance of a solar-assisted heat pump. The researcher focused on the length of the TES unit together with the number of pipes inside the unit. The results showed that the *COP* and exergetic efficiency values decrease when longer TES units are utilized. It was also stated that smaller TES units bring more efficient utilization but in a shorter time, while larger TES units are less efficient, but they provide energy for a longer period. Yumrutaş and Kaşka (2004) carried out an experimental work on a solar-assisted heat pump experimental setup that is integrated with thermal energy storage tank where water was used as the storage medium making the tank a sensible heat storage unit. Daily and monthly measurements were taken during the experimental work. They reported that the 650 L sensible heat storage tank was sufficient for residential heating purposes. Besides, higher storage temperatures were achieved during sunny days, and thus, the heat pump efficiency was significantly increased in sunny days, compared to cloudy days, where the heat pump *COP* values were 3.5 and 2.5, respectively.

Han et al. (2008) combined the solar assistance and ground heat source for the evaporator of heat pump in their numerical study. A water-to-water heat pump was considered for their numerical computations, and a TES unit was also integrated with solar collectors to store and release renewable thermal energy. Eight different operation modes were simulated by the authors regarding the operational design of the system. The numerical computations were carried out for a long-term, ranging from 146 to 1017 hours. The researchers made some assumptions to simplify the model, which include the neglection of temperature stratification effects on the charge and discharge, temperature-independent thermophysical properties of PCM inside the storage tank, isothermal phase change of PCM, simplified U-tube model, and neglected internal heat gains. Depending on different heating modes, such as direct heating, using individual or hybrid heat sources of ground and solar, the researchers reported total-energy-based average system *COP* in a range of 2.51 to 10.5. Furthermore, the authors highlighted that latent heat storage utilization significantly improved efficiency, which is reflected by an increase of 12.3% in system *COP*, compared to the SAHP without latent heat storage. In addition, they indicated that the system flexibility and stability was enhanced. A similar simulation study was conducted by Qi et al. (2008) where the researchers underlined that it is the first study that considers water and PCM in a seasonal thermal energy storage unit integrated to a solar-assisted heat pump. The authors considered $CaCl_2 \cdot 6H_2O$ as PCM inside the tank, which has a phase change temperature of about 29°C, hence, an appropriate thermal energy storage material for the heat source of SAHP applications. A storage tank of 456 m^3 having 2520 storage units was taken into account in the numerical simulations, and the abundant solar energy in summer was considered to be stored in the TES unit, which is then used as a heat source in winter conditions. It was reported in the study that the average heating *COP* during the heating period was computed as 4.2, and it was emphasized that this value is significantly higher than that of air-source heat pumps. With the seasonal latent heat thermal energy storage system, the solar collector efficiency was increased, the energy losses from the storage tank were reduced, and the size of the storage tank was considerably decreased compared to a central heating system using only water as a thermal energy storage medium. Nevertheless, the authors also indicated the drawbacks such as inevitable high cost of the system and the complexity of the storage system due to large amount of PCM units. Therefore, they suggested conducting experimental work to investigate the system in technical and economical ways. Tamasauskas et al. (2012) numerically studied the efficiency of solar assisted heat pump with sensible and latent heat storage options where a tank with ice slurry was taken into account for thermal energy storage medium. They took electric heaters as reference to compare the efficiency of solar-assisted water-to-water heat pumps throughout annual operation. The authors concluded that the heat pump with sensible heat storage uses 81% less energy compared to electric heaters, while this ratio is 86% for the heat pump with latent heat storage. Besides, the solar fraction of the system and the *COP* of the heat pump were calculated as 0.88 and 8.22, respectively. Another relevant work was considered by Uçar and İnallı (2008) which dealt with thermal and economic comparisons of solar heating systems with a seasonal TES unit. In the numerical work, basically three different storage tanks were considered for comparison, which are the storage tank with and without insulation and the underground storage tank. It was concluded that the underground storage tank was more beneficial for enhanced thermal performance and lower payback time. Relatedly, Trinkl et al. (2009) also suggested using an uninsulated latent heat storage tank buried underground, which can thermally interact with the soil as a storage medium, for heat pump applications. Lv et al. (2016) investigated the impacts of thermal energy storage integration to ground-source heat pumps putting an emphasis on operational expenses with and without TES unit. The authors strongly recommended using thermal energy storage tank, which not only attained higher *COP* but also saved 35.2% and 18.3% cost saving in winter and summer, respectively, related to the off-peak electricity utilization thanks to thermal energy storage.

Bearing in mind that latent heat thermal energy storage units are not also for water-to-water heat pumps but also they can be used together with air-source heat pumps, Niu et al. (2013) studied the performance and thermal charging/discharging behavior of an air-source heat pump, which can also supported by solar energy system, depending on its operation mode. Also, a novel thermal energy storage unit act as a triple-sleeve heat exchanger was introduced in the experimental work. Apart from being a medium for solar energy storage and prevent instable operation in the system, this heat exchanger also acted as the evaporator of the heat pump. It was reported by the authors that the latent heat unit significantly improved the performance, which provided a *COP* up to 3.9 in the heat pump unit. Another work dealing with an air-source heat pump integrated with solar energy was conducted by Wu et al. (2019). In their experimental work, the authors proposed a system where the heat pump had air-source and solar evaporators (regenerator), which were able to be utilized interchangeably or in combination. After conducting daily tests at different ambient temperatures, they concluded that *COP* and exergy efficiency of the heat pump system were enhanced by 70% and 67% using solar regenerator system, respectively, compared to conventional air-source heat pump. As a result of the study, the authors recommended using the proposed system in the regions where the weather conditions are cold but mostly sunny.

Performance of a thermal energy storage integrated heat pump is of great importance from the first as well as second law of thermodynamics. In this regard, Utlu et al. (2014) experimentally studied a solar-assisted heat pump that had a latent heat storage unit connected to its evaporator. The authors considered a phase change material with a phase-change temperature in the interval of 42°C-44°C, which was filled in cylindrical containers vertically located inside the latent heat storage tank. A short-term, i.e., daily heat storage and release was taken into account, and measurements were taken continuously for about 20 days. Energy and exergy efficiencies of different components of the heat pump were monitored throughout this period. According to the data provided, the daily heat pump *COP* was varying in the range of 4 to 5. The daily average overall energy and exergy efficiencies of the latent heat storage unit during throughout the experiment days were found to be around 58% and 2.3%, respectively. A similar study on the experimental rig was conducted by the same research group (Aydin et al., 2015), and it was concluded that a PCM with the phase change interval of 35°C –

40°C would be more beneficial and efficient for increasing the share of solar energy due to easier phase change process even in cloudy weather conditions where the solar radiation is low. Qu et al. (2015) investigated a solar-assisted heat pump system, which had two different thermal energy storage tank. One of the tanks contained PCM, while the other one had water only. The water tank and the PCM tank had a volume of 850 L and 800 L, respectively, and sodium-sulfate-decahydrate ($Na_2SO_4 \cdot 10H_2O$) were used as PCM packed in aluminum cans. The researchers experimentally tested three different working conditions for daily operation, and they concluded that the peak *COP* reached up to 10.03 in the case of using dual-tank latent heat storage, which was reported to be approximately 3.5 times higher compared to the case of water only thermal energy storage. Besides, the authors indicated that the energy consumption of the compressor slightly changed during the operation of different cases, hence, using dual tank latent heat storage was found to be beneficial. Youssef et al. (2017) considered an indirect expansion solar-assisted heat pump to explore the effect of latent heat utilization on the performance and system stability. They considered the heat pump for domestic hot water purposes, and a PCM heat exchanger, which contains 30 kg of paraffin having a phase change temperature of 17°C, was integrated to the evaporator of the heat pump system. The stored thermal energy was designated by the researchers to be used in night-time or when the solar radiation is too low. The results of the study showed that using PCM brought an enhancement in the heating *COP* by 6.1% for sunny days and 14.0% in cloudy days.

It was proven by the literature studies given in the previous paragraph that integration of thermal energy storage systems can attain higher thermal efficiencies due to maintaining a relatively higher temperature at the evaporator and avoiding defrost requirements in cold weather, as well as increasing the share of renewable energy utilization. In addition to that, especially combined with PCM, using thermal energy storage can stabilize the fluctuations sourced by the intermittency of solar energy, meaning that storing solar thermal energy instead of using it directly at the heat pump evaporator can avoid the instabilities in the performance as well as intermittent heat pump operation (Gu et al., 2023). Similar benefits are also obtained for ground source heat pumps coupled with thermal energy storage units involving PCM (Alavy et al., 2021; Mousa et al., 2022; Qi et al., 2016). Even though integrating thermal energy storage systems to the heat pump evaporators has numerous benefits, especially in solar-assisted heat pumps, their capability to manage the demand side is questionable without using a thermal energy storage unit at the condenser of the heat pump. More clearly, the supplied thermal energy by the heat pump should be stored in a medium by sensible or latent means, and it should be used depending on the heating demand or electricity grid conditions. Hence, energy flexibility can be attained this way. Nonetheless, the operational conditions and limits as well as system performance can be different regarding the utilization of thermal energy storage unit at the condenser or at the evaporator. As mentioned previously, utilization of TES unit at the evaporator is more focused on the stabilization and efficiency, while using it at the condenser of heat pumps is rather dedicated to demand side management, i.e., load shifting or peak clipping.

Development in the electricity generation by the renewable energy sources, such as solar and wind, has brought questions about the proper management of instabilities and fluctuations in the electricity grid due to the intermittent nature of renewable energy sources (You et al., 2024). In addition to that, as the investments on heat pump technology, manufacturing, and utilization is sharply accelerating, there has been a concern due to the excess and disorganized utilization of electricity, which leads to a significant increase in the peak electricity demand, due to electrification of heating, even though heating by heat pump is an efficient way and is also a promising solution to reduce instabilities by proper demand side management (Knittel et al., 2024). Moreover, coupling heat pumps with thermal energy storage can enhance energy flexibility by contributing to the load shifting or peak clipping operations (Arteconi et al., 2013; Jin et al., 2023). Thus, researchers recently conducted various studies on the demand side management activities attained by heat pumps coupled with sensible or latent heat storage units. Arteconi et al. (2013) conducted a study that emphasizes the role of heat pump and thermal energy storage combination in demand side management techniques. They modelled and analyzed the utilization of heat pump coupled with a TES unit to shift the load to off-peak periods, where the on-peak period was considered between 16:00 and 19:00, during heating a room in Northern Ireland case. The authors stated that an acceptable indoor temperature control was achieved even if the heat pump was turned off during the aforementioned on-peak time interval. Furthermore, they pointed out that a cost saving can be achieved using appropriate tariff. In another work with a similar scope, Baeten et al. (2017) studied the effect of attaining energy flexibility by using heat pumps with thermal energy storage on the consumer, i.e., end user, costs, considering multi-objective control strategies. The authors highlighted that adding a storage tank to the system with heat pump remarkably helps reducing peak loads. Besides, they reported that larger storage tanks attain a larger amount of load shifting, nonetheless, it was underlined that applying demand management always brings additional costs to the end user, compared to the cases where no storage tank used, or load shifting is implemented. Hence, the authors recommended that heat pump users should be encouraged to participate to such strategies by renumeration of their expenses. Another modelling work was carried out by Renaldi et al. (2017), by emphasizing the importance of decarbonization and flexibility in domestic heating systems in the United Kingdom. Within this scope, they compared the thermal energy storage integrated heat pump systems to the conventional natural gas boiler heating systems. Using an 8.5 kW heat pump system with 300 L thermal energy storage unit attained 37% of cost and emission savings. Nevertheless, similar to the findings of the previously mentioned study (Baeten et al., 2017), the researchers underlined that equipment and operational costs of heat pumps are higher than the conventional heating systems. However, integration of TES and time-of-use tariffs can help reducing these costs in the heat pump heating systems. Furthermore, government incentives about renewable energy can also boost up these savings and attract the end users in the UK to use heat pump. Arteconi and Polonora (2018) investigated three different cases where a TES unit is connected to heat pump condenser for different purposes including energy efficiency and demand side management. Different focal points were considered in these cases where a ground-source or air-source heat pump is utilized together with a TES tank. The authors concluded that the case with ground-source heat pump can effectively postpone the energy utilization using TES tank, which can reach up to 8 hours when underfloor heating is considered. A similar emphasis was put on the issue by Campos et al. (2020) where the authors investigated four different residential heating scenarios in rural areas of Hungary, taking into account the annual number of building retrofits, utilization of heat pumps and hot water storage tanks, and yearly demographic trends in the selected regions. The scenarios took different percentage of the retrofitted buildings yearly, such as 1.25% as standard renovation and 2.5% as advanced energy efficiency retrofitting, as well as nearly-zero energy building concept. It was found that modest building retrofit actions provided relatively small energy savings which are insignificant, while more effective scenarios including a larger rate of retrofitting ensured 23% to 69% reduction in final energy consumption. Moreover, using heat pump with a hot water storage tank in well-insulated dwellings was found to provide theoretical energy flexibility reaching 3.4 kWh per 24h each year.

Since PCMs can significantly contribute to the thermal energy storage capacity of the storage tanks integrated to heat pumps, which expectedly results in an improved energy flexibility, some recent studies in the field focuses on latent heat utilization to augment the storage capacity and load shifting capability. Besides, this improvement in the thermal energy storage capacity of heat pump storage tanks can also provide a reduction in the required tank volume. To this end, Kelly et al. (2014) used a detailed building simulation model to investigate the thermal buffering needed to achieve a sufficient load shifting regarding the Economy 10 tariff for a typical detached dwelling in United Kingdom. The researchers considered a buffer tank with and without PCM for comparison. Striking findings were reported by the authors such as the volume of the buffer tank was halved by using PCM, quantitatively from 1000 L to 500 L. This amount was found to be sufficient to fully shift the load to off-peak period without violating the end user’s needs. On the other hand, the results of the work highlighted that the electrical demand of the heat pump increased by 60% due to load shifting, which leads to increased cost and CO_2 emissions. This notable penalty of energy consumption was reported to be sourced by decreasing efficiency of heat pump during thermal charging process as well as the heat losses from the buffer tanks. As a similar work focusing on storage volume and demand response, Hirmiz et al. (2019) investigated the performance of a thermal energy storage tank integrated with a heat pump for load shifting. The outcomes of the study showed that substantial volume saving can be attained using a hybrid tank involving 75% PCM, compared to a storage tank with water only. The authors indicated that the *COP* of the heat pump remarkably decrease as the storage temperature increases, and thus, the total daily electricity consumption increases. Quantitative analysis showed that the heat pump *COP* decreased from 3.4 to 2.5 during thermal charging from the storage temperature of 40°C to 50°C. As a result, the authors concluded that utilization of thermal energy storage coupled with heat pump condenser is not a solution for energy efficiency, and this action would even lead to higher energy consumption due to larger storage temperatures and heat losses. Nonetheless, this issue is still controversial and some studies in the literature reported the opposite conclusion or interpretation, especially in the presence of PCM (Arteconi and Polonara, 2018; Qureshi et al., 2011; Xu et al., 2021). At this point, in order to achieve energy efficiency and flexibility at the same time, advanced smart control units can be used, as reported by Lizana et al. (2018). End user electricity bill and the retailer electricity cost were respectively reduced by 20% and 25%, despite an increase of 8% in the final energy consumption. A similar finding was also stated by Fitzpatrick et al. (2020) where a residential building heating was simulated as a case study considering a hybrid heat pump together with thermal energy storage unit, and a gas boiler. The findings of this study revealed that the considered demand response strategies led to both higher thermal energy storage utilization and higher gas boiler utilization, which were stated to be 17.1% and 12.1% in maximum demand response intensity, respectively. Consequently, this resulted in higher overall primary energy consumption values that were reported to be between 1.6% and 9.1%. Jin et al. (2021b) investigated a solar assisted air-source heat pump performance for different volumetric flow rates of heat transfer fluid at the condenser side of the HP. Furthermore, they used a latent heat storage tank integrated to the heat pump. The authors concluded that a significant increase in the energy efficiency of the HP, which reaches up 57.5%, is achieved when solar energy is introduced compared to single HP system. In addition to that, the authors pointed out that the volumetric energy density is 25.97% higher in hybrid TES tank that uses sodium acetate trihydrate urea as PCM, compared to the TES tank using sensible heat only. Hence, a volume reduction of 21% can be ensured. The same research group (Jin et al., 2023) conducted a modelling work to evaluate the peak demand shifting potential of an air-source heat pump integrated with thermal energy storage, which was designed to meet domestic hot water demand. Four different setpoint temperatures and four different PCMs with different phase change temperature intervals were taken into account. Moreover, four different volume fractions of PCM inside the TES tank were considered to evaluate the appropriate amount of PCM in a latent heat storage unit used for the aforementioned purpose. As a result of the study, the authors recommended 75% of volume to be filled with PCM and assign higher setpoints for energy efficiency, nevertheless, adjusting the setpoint at 60°C resulted in a higher electricity consumption. In wintertime, the energy consumption was found to be decreased by 5.9% to 8.3% depending on operation strategy. Considering PCM selection, the researchers indicated that the phase change temperature interval should be around 50°C, rather than 30°C and 60°C, and selecting 50°C of phase change temperature interval respectively reduce operational cost by 0.7% and 11%, compared to other mentioned phase change temperature intervals, respectively. Considering time-varying energy tariff, the night water heating strategy brought a significant cost saving, quantitatively 13.6%, due to the concessionary rate gained by the night tariff. Another recent work was conducted by Lin et al. (2022) focused on a novel heat exchanger where the refrigerant of the heat pump conducts a direct interaction with the PCM where the heat loss is reduced. The authors investigated the effects of geometrical parameters of the heat exchanger as well as different PCM configurations, namely single-stage and three-stage, and it was found that three-stage PCM is superior to the single-stage in terms of energy and exergy efficiency. Targeting at combining energy flexibility with enhanced energy efficiency, Xu et al. (2021) conducted a numerical study and investigated four different system configurations where a desuperheater and a booster were used to enhance the energy efficiency. The authors concluded that using both desuperheater and booster was an efficient way for achieving energy efficient load shifting.

Increasing popularity of the heat pumps in space heating and domestic hot water applications results in a remarkable augmentation of the number of studies in the field as well as the investments to these efficient heating devices, especially in developed and developing countries such as USA, China, Türkiye, and EU countries. Nevertheless, intensely electrification of heating processes by heat pumps leads to the increasing risk of excessive grid loads. To eliminate this, thermal energy storage is considered, which can provide energy efficiency and flexibility. Furthermore, TES can increase the beneficially utilization of renewable solar energy. For these reasons, researchers accelerate their studies, and they recently focus on the TES integration to heat pumps. For this purpose, thermal energy storage units can be coupled with evaporator or condenser, and researchers investigate them one by one. Nevertheless, the studies usually focus on one of these systems, although each of these two systems has different advantages, which need to be evaluated from the efficiency and flexibility point of views. Therefore, this thesis work aims at contributing to the literature by evaluating the energy efficiency and flexibility of these systems and make recommendations accordingly.

3. MATERIALS AND METHODS

This thesis work consists of several stages including experimental and numerical works carried out on two different heat pump systems separately, namely a solar-assisted heat pump system where a thermal energy storage system integrated to its evaporator and an air-source heat pump that has the thermal energy storage system integrated to its condenser. Therefore, the present part of the text has been divided into several subsections providing details about the experimental and numerical studies conducted for both considered systems, separately. To be clearer, the thesis work includes three major chapters, which are about the CFD studies, experimental evaluation of the considered TES integrated heat pump systems, and the mathematical modeling of the two investigated heat pump systems. The CFD studies were carried out in order to comparatively assess the phase change behavior in the straight- and corrugated-wall tubes, which helps selecting the appropriate PCM container type to be used in the following experimental studies. Moreover, the average convective heat transfer coefficients for different cases are estimated by the aforementioned CFD studies, which constitute an input for the mathematical model which is established for the operation of the TES integrated heat pump systems. The second major chapter of the work covers the experimental studies for both systems. In the experiments, thermal behavior of the TES materials, namely water and the PCM, inside the TES unit is elaborated as well as the operational performance of the heat pump systems in different conditions. Besides, the operational heat pump data obtained from these experiments are partly used as inputs in the following mathematical model established in order to allow numerically simulate the operations and thermal behavior of the heat pump system and TES unit, respectively. In addition to that, phase change behavior of the PCM is also assessed by the experiments. Lastly, the operations of the examined TES integrated heat pump systems are mathematically modeled with the aid of experimentally obtained data. Thereby, within the experimental study ranges, the operation of the heat pump is simulated for different circumstances such as different TES materials or weather conditions.

For the outline of this chapter, first of all, the preliminary CFD studies for the selection of PCM tubes from two alternatives were presented. Then, the experimental rig and the process together with instrumentation details are presented. Thereafter, the numerical methods for the evaluation of dynamic working behavior of the heat pump systems as well as energy flexibility relations are explained.

3.1. Numerical Implementation for PCM Tube Selection

One of the major issues in latent heat storage applications by phase change materials is the incomplete melting or solidification that hinders the benefits of latent heat utilization. The main reasons for this phenomenon are the low thermal conductivity of the PCM, and the thermal resistance of the container in which the PCM is located. Hence, it is utmost important to enhance the thermal conductance from the heat transfer fluid to the PCM, and the selection of container material and design are crucial at this point.

For the selection of vertical tubes to be integrated into the TES tank, two different tube types were considered within the study, namely the standard straight surface tube and corrugated surface tube available in the market, and these were compared regarding their capability of heat transfer and contribution to the phase change process of the PCM. To evaluate their effect on the phase change phenomenon inside the TES tank, a set of computational fluid dynamics (CFD) analysis were carried out on the commercial CFD software licensed in Kocaeli University, ANSYS Fluent, simulating the fluid flow and heat transfer around the tubes. This simulation study was presented under three subsections involving the description of the problem along with the governing equations and boundary conditions as well as the assumptions, the validation of the numerical procedure, and the grid and time step independence tests.

3.1.1. Description of the Problem and the Numerical Implementation

Considering the large volume of the tank and detailed surface geometry of the tube surfaces, the problem was simplified in order to obtain an overview of the comparison between the standard and corrugated tubes. Thus, a small portion of each tube, which are the same diameter but 4.5% height, filled with a PCM of Rubitherm® RT26 was considered, and they were investigated inside a three-dimensional fluid domain where the heat transfer fluid flows in a turbulent regime. To evaluate the fluid flow effects, two different flow orientations, namely in the crossflow and axial flow were taken into account in two different fluid domains. The fluid domains with the simplified tube geometry are shown in Figure 3.1. The *a*, *b*, and *c* respectively stand for the height, width, and length of the fluid domains. The inlet and outlet sections are indicated in the figure, while the dimensions of the fluid domain created for the crossflow case (see Figure 3.1a) are a=0.045 m, b=0.2 m, c_1=0.27 m, c_2=0.57 m, and c_3=0.9 m. In the fluid domain of axial flow case, these dimensions are considered a=0.05 m, b=0.1 m, c_1=0.09 m, c_2=0.045 m, and c_3=0.225 m.

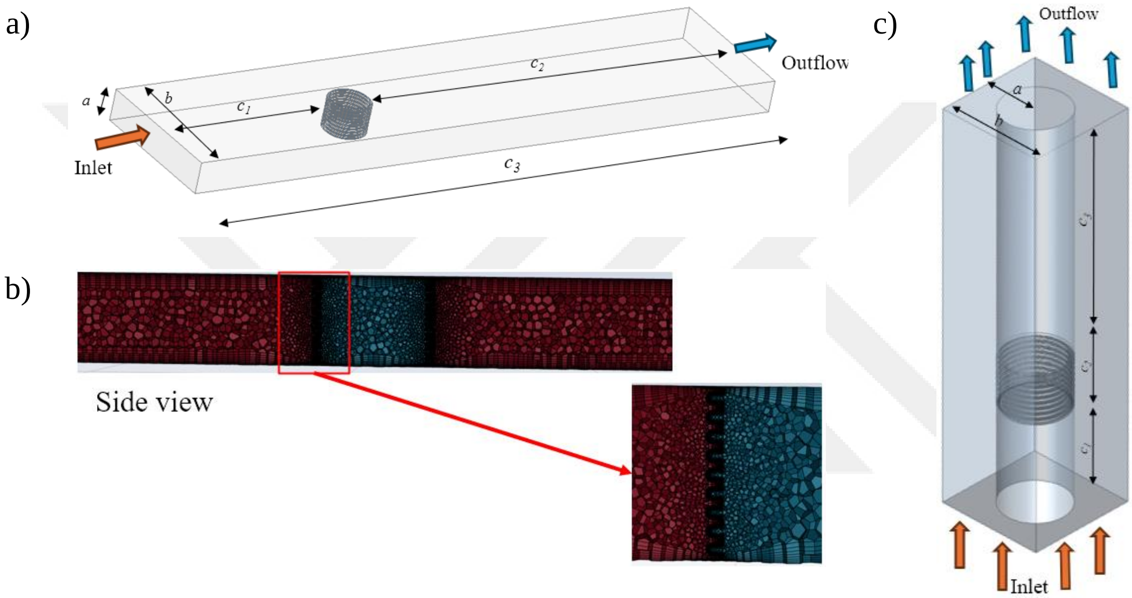

Figure 3.1. Simplified fluid domains with PCM tube portion and the utilized mesh structure for the crossflow case

Considering the possible fluid flow velocity inside the TES tank, three different mass flow rates ($\dot{m}$=0.45, 0.90, and 1.80 kg/s) were considered, which correspond to the presumed flow velocities in the tank. The inlet temperature of the heat transfer fluid was taken into account in accordance with the planned storage temperatures in the System-1. Three different storage temperatures, which are T_{st}=35°C, 45°C, and 55°C, were planned to be tested within the experimental studies. Therefore, the inlet temperature of the HTF in the CFD studies were taken as 45°C. With the considered momentum and thermal boundary conditions, it was aimed to estimate the fluid flow and heat transfer behavior between the water inside the tank and the PCM inside the tubes.

The governing equations of the problem, ensuring the conservation of mass, momentum and energy, are given as follows in the Equations (3.1), (3.2) and (3.3) (Bathcelor, 1967):

$$\frac{\partial \rho}{\partial t} + \nabla \cdot \left(\rho \vec{V}\right) = 0 \tag{3.1}$$

$$\frac{\partial}{\partial t}\left(\rho \vec{V}\right) + \left(\rho \vec{V} \cdot \nabla\right)\vec{V} = -\nabla p + \nabla \cdot \left(\mu\left(\rho \vec{V} + \rho \vec{V}^{T}\right) - \frac{2}{3}\mu \nabla \cdot \vec{V} I\right) + \rho \vec{g} + \vec{F} \tag{3.2}$$

$$\rho C_p \left[\frac{\partial T}{\partial t} + \left(\vec{V} \cdot \nabla\right)T\right] = \nabla \cdot (k \nabla T) \tag{3.3}$$

Regarding the turbulent flow of the heat transfer fluid considered in the fluid domain, the k-ε turbulence model was applied, which is mathematically expressed in the Equations (3.4), (3.5) and (3.6) as follows:

$$\frac{\partial(\rho k^{*})}{\partial t} + \frac{\partial}{\partial x_i}(\rho k^{*} u_i) = \frac{\partial}{\partial x_j}\left[\left(\mu + \frac{\mu_t}{\sigma_k}\right)\frac{\partial k^{*}}{\partial x_j}\right] + G_k - \rho \varepsilon \tag{3.4}$$

$$\frac{\partial(\rho \varepsilon)}{\partial t} + \frac{\partial}{\partial x_i}(\rho \varepsilon u_i) = \frac{\partial}{\partial x_j}\left[\left(\mu + \frac{\mu_t}{\sigma_\varepsilon}\right)\frac{\partial \varepsilon}{\partial x_j}\right] + C_{1\varepsilon}\frac{\varepsilon}{k}G_k - C_{2\varepsilon}\rho\frac{\varepsilon^2}{k^{*}} \tag{3.5}$$

$$\mu_t = C_\mu \frac{k^{*2}}{\varepsilon} \tag{3.6}$$

In the above equations, σ_k, σ_ε, $C_{1\varepsilon}$, and $C_{1\varepsilon}$ are constants, which have the values of σ_k=1, σ_ε=1.3, $C_{1\varepsilon}$=1.44, $C_{2\varepsilon}$=1.92.

The above given governing equations were solved by finite volume method integrated into the aforementioned commercial software ANSYS Fluent. Second order upwind scheme was considered for the discretization of momentum and energy equations, while the turbulent kinetic energy and turbulence dissipation equations were taken into account by the first order upwind scheme. Besides, the pressure-velocity coupling was treated by SIMPLE algorithm.

As briefly mentioned previously, the boundary condition at the inlet of the fluid domain was taken as mass flow rate with constant temperature, which was 318.15 K for melting simulations and 283.15 K for solidification processes. Symmetry boundary condition was considered along the remaining walls of the fluid domain to avoid Venturi effects, which may deteriorate the fair comparison.

Apart from the flow of the heat transfer fluid inside the domain, PCM is located in the tube, which is placed inside the fluid domain. For the treatment of phase change phenomenon, enthalpy-porosity technique was implemented. Besides, Boussinesq approximation was employed to deal with the buoyancy-driven convective motion of the melted PCM inside the domain. The governing equations for the phase change process of the PCM, which are respectively the continuity, momentum, and energy equations, are shown by Equation (3.7), (3.8), and (3.9), respectively, as follows (Mahdi et al., 2020), (Duan et al., 2020):

$$\frac{\partial \rho}{\partial t} + \nabla \cdot \left(\rho \vec{V}\right) = 0 \tag{3.7}$$

$$\frac{\partial}{\partial t}\left(\rho \vec{V}\right) + \nabla \cdot \left(\rho \vec{V} \cdot \nabla\right)\vec{V} = -\nabla p + \mu \nabla^2 \vec{V} + \rho \beta \vec{g}(T - T_0) + \vec{S} \tag{3.8}$$

$$\frac{\partial}{\partial t}(\rho H) + \nabla \cdot \left(\rho \vec{V} H\right) = \nabla \cdot (k \nabla T) \tag{3.9}$$

The initial temperature of the PCM domain was set to 25°C for melting simulations and 26°C for solidification simulations, according to the solidus and liquidus temperatures of the material. Furthermore, fixed mass flow rates at the inlet of the domain were taken into account for each case, while outflow condition was employed at the outlet of the domain. The surrounding walls were kept adiabatic, while the PCM tube wall was considered thermally conductive with negligible thermal resistance since the tubes to be utilized were planned to be made of steel with 0.25 mm wall thickness. Besides, the thermophysical properties of the heat transfer fluid (water) and PCM (RT26) considered in the CFD studies are given in Table 3.1.

Table 3.1. Thermophysical properties of the water and RT26 considered in the CFD studies

	ρ (kg/m^3)	Cp (J/(kgK))	k (W/(mK))	μ (Pa·s)	L_H (J/kg)	β (1/K)
Water	996	4183	0.622	0.00079	-	-
RT26	825	2000	0.2	0.0035	110000	0.00058

3.1.2. Validation of the Numerical Procedure

In order to validate the numerical procedure considered on ANSYS Fluent, an experimental work conducted by Mahdi et al. (2019) was considered. In the given experimental work, the melting process of a paraffin based PCM in a double tube latent heat storage unit was observed, and temperature measurements were taken from six different points inside the PCM. The inner tube of the latent heat storage unit has an outer diameter of 23 mm, and the outer tube that contains PCM has a diameter of 70 mm, while the length of the tube is 460 mm. The measurement points were named by the authors as A and B for the radial directions respectively from the center with the suffix of 1, 2, and 3 representing the axial direction. Paraffin wax was considered in the study, which has a melting temperature range of 48.3°C – 62°C, latent heat capacity of 114540 J/kg, specific heat of 2000 J/kgK, thermal conductivity of 0.14 W/mK, dynamic viscosity of 0.033 Pa·s, and a density of 820 kg/m^3. Water was considered heat transfer fluid flowing inside the inner pipe of the latent heat storage unit, and the flow regime of the water was turbulent.

In the numerical computations, thermophysical properties of the heat transfer fluid, water, were taken constant, and the fluid flow was considered turbulent as indicated in the examined literature work. For the paraffin wax, the thermophysical properties were also taken constant, except density, which was treated by Boussinesq approximation. The pressure-velocity coupling was carried out by SIMPLE algorithm, and the discretization of convective terms were treated by second order upwind scheme. The equations for turbulent kinetic energy and dissipation rate were discretized by second order upwind scheme. Since a numerical analysis were also conducted by the authors, the numerical model was established in consistency with the information provided in the relevant paper (Mahdi et al., 2019).

In order to compare the temperature results obtained in the experimental work and computed by the present numerical study in the thesis, three temperature measurement points along different directions, i.e., radial and axial, are selected. The temperature variations obtained by the numerical study and those indicated by data points were given in Figure 3.2. As seen from the figure, the experimental data and the present numerical outcomes have a significant consistency in terms of their trends and values.

The differences between the numerical and experimental outcomes at some specific points, which are lower than 10%, can be attributed to the assumptions in the present numerical model as well as the laboratory condition and experimental nature of the literature study considered.

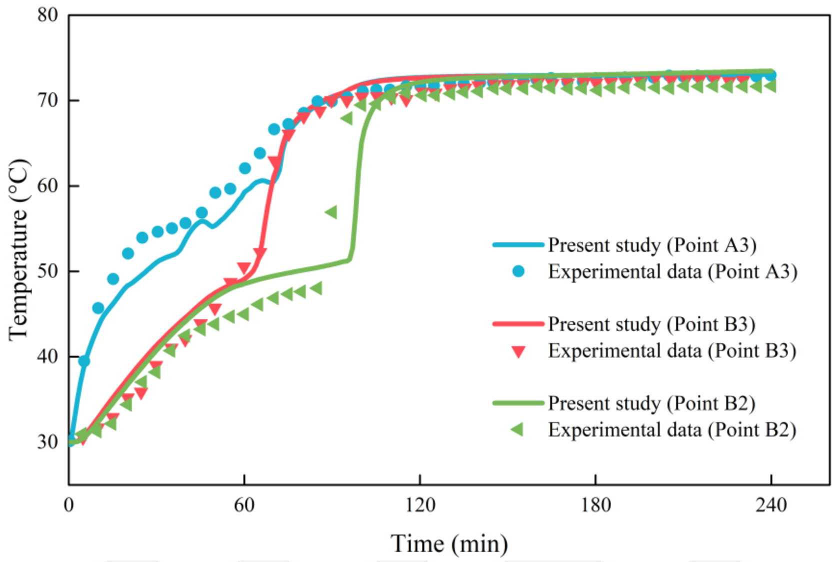

Figure 3.2. Validation results against temperature measurements from different points

3.1.3. Grid and Time Step Size Independence Tests

The solution of a numerical work must be independent from the grid size and time step size. Therefore, several numerical tests including different mesh and time step size should be systematically carried out for each considered fluid domain geometry. In this study, three different mesh structures with polyhedral elements of which the sizes are indicated by element numbers of 796212, 957256, and 1312726 were created for the fluid domain involving corrugated tube geometry in crossflow case. The results obtained for the melting process were elaborated in terms of average heat flux on the tube surface and average liquid fraction values of the PCM (RT26), as given in Figure 3.3. As seen from the results, using 957256 and 1312726 elements yielded the same heat flux results, while there were even marginal differences between the liquid fraction values obtained using these two mesh structures. Thus, the mesh with 957256 polyhedral elements were considered for further analyses in order to reduce computational cost.

a)

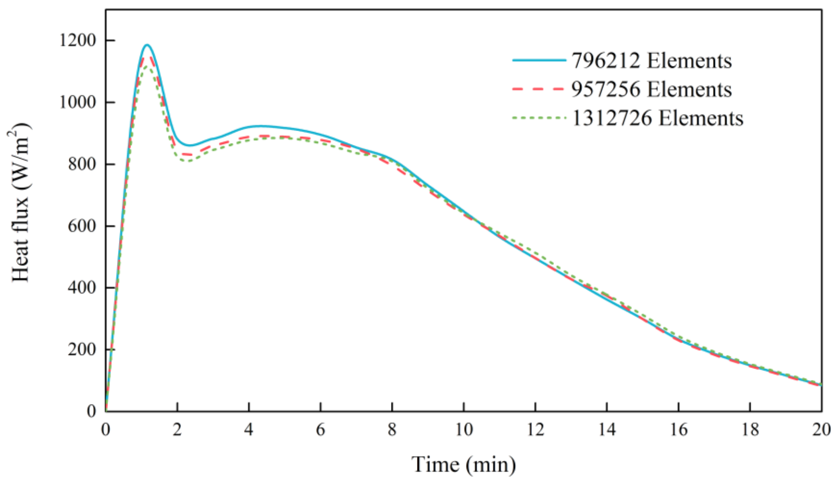

b)

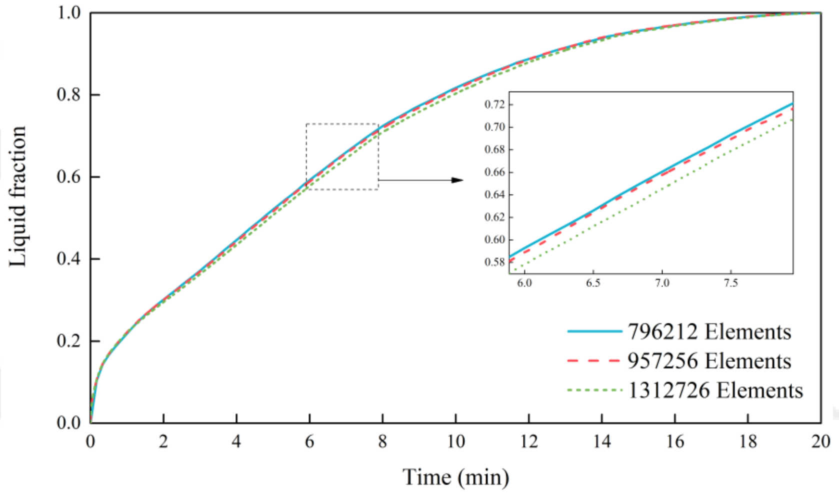

Figure 3.3 Grid independence test results for the crossflow case in terms of a) heat flux and b) liquid fraction

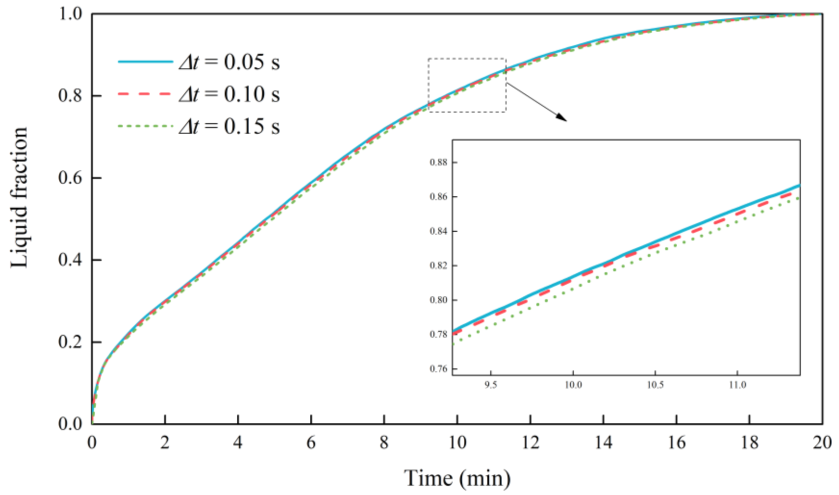

Figure 3.4. Time step independence test results for the crossflow case

After completion of grid independence test and determination of the most suitable mesh structure, the solution was ensured to be independent from the time step size by conducting melting analyses considering three different time steps, namely Δt=0.05, 0.10, and 0.15 s, separately. As a result of these analyses, the corresponding liquid fraction values were given in Figure 3.4, and it was noticed that insignificant differences occurred between Δt=0.05 s and Δt=0.10 s; hence, the time step size for the following analyses were chosen as Δt=0.10 s to save computational time. It is noteworthy that the time step size was considered Δt=0.1 s for the aforementioned analyses with different meshes.

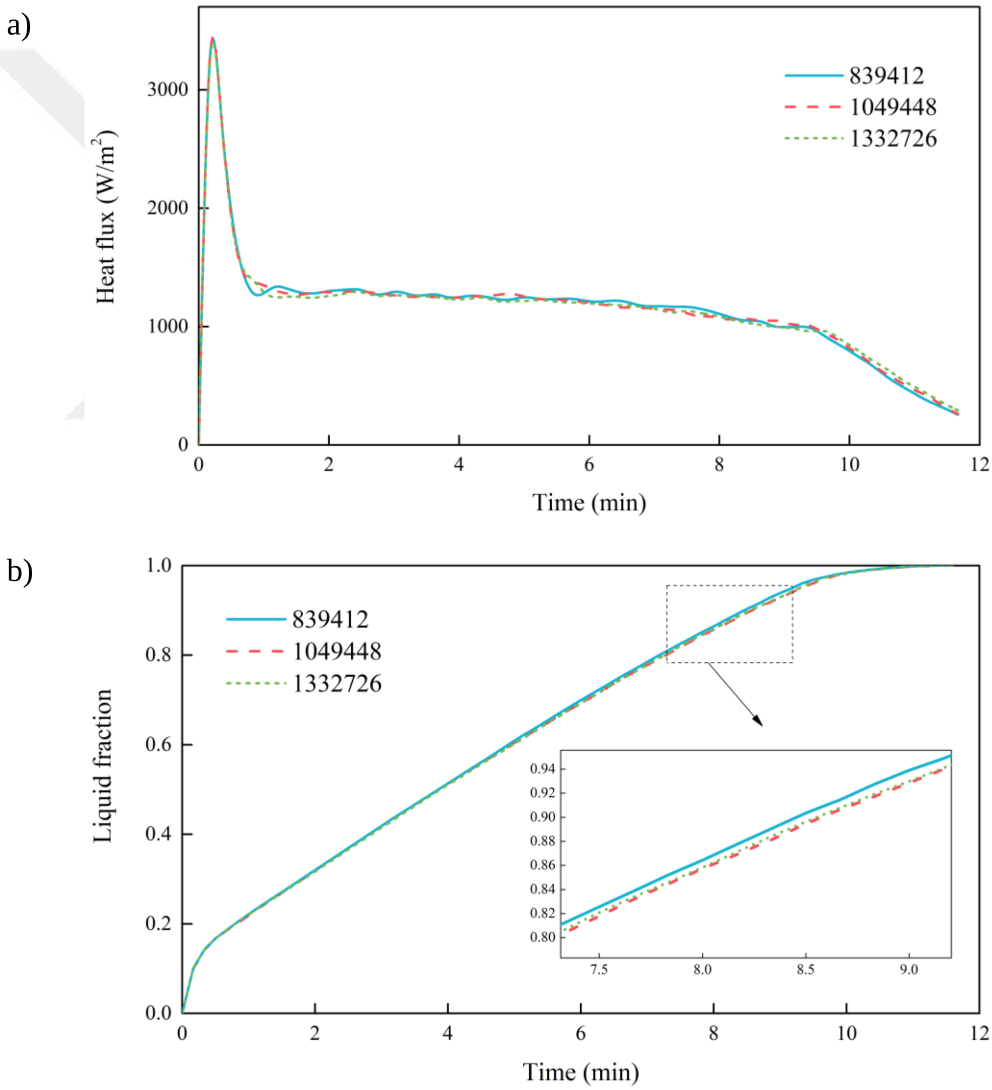

Figure 3.5. Grid independence test results for the fluid domain of the axial flow case

For the cases where the fluid flow was considered from bottom to top of the domain, i.e., axial flow cases, an additional grid and time step independence test was conducted since the geometry of the fluid domain includes some differences. Hence, three different grid structures were tested where the results are presented in Figure 3.5 in terms of both heat flux and liquid fraction variation, in order to observe the effect of grid structure on both parameters. Yet, there was no significant difference observed between the heat flux values obtained by the mesh structures having element number of 839412, 1049448, and 1332726. Similarly, liquid fraction values were also found to be close to each other. In order to ensure the grid independent solutions, a close-up examination was considered, and the mesh structure with the element number of 1049448 was selected for further computations of axial flow cases.

A set of time step independence tests was carried out to determine an appropriate time step for the solutions ensuring the most possible computational time saving. The results of the time step independence test are given in Figure 3.6. Regarding the obtained outcomes, the time step of 0.05 s was selected for further computations, which would give accurate solutions with reasonable computational cost.

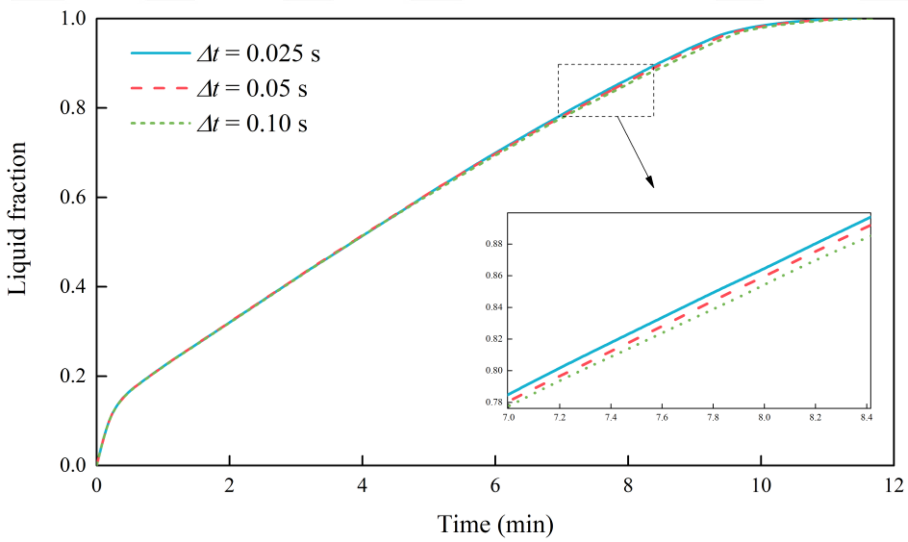

Figure 3.6. Grid independence test results for the fluid domain of axial flow case

3.2. Experimental Setup

A comprehensive heat pump experimental rig existing in Kocaeli University, as shown in Figure 3.7, was considered for the experimental works after integrating a thermal energy storage unit and a solar collector tank with electric heater to experimentally simulate the operation of a solar-assisted heat pump. The experimental heat pump system was designed and manufactured to be able to work as a water-to-water heat pump as well as an air-to-water heat pump thanks to having a cold-water accumulation tank (CAT) and an air-source evaporator at the same time in the back of the device, of which the operation is controlled by electro-valve depending on user demand.

Figure 3.7. A view of heat pump experimental rig

The heat pump utilized for the tests include two accumulation tanks, namely hot and cold accumulation tanks having a volume of about 150 L. In addition, a 2-hp Copeland ZB15KQE scroll compressor is used to ensure the circulation of refrigerant, which is R407c, in the vapor compression refrigeration cycle. While the evaporation of the refrigerant is carried out by the help of a plate heat exchanger where the heat transfer fluid is water, there are two different options in the device for condenser, which are a plate heat exchanger and a coil heat exchanger located inside the hot accumulation tank (HAT). The heat pump system is able to implement a relay-controlled on/off system for the compressor, which can be connected to a temperature value at any point or value interval, and the photographs of the compressor and the process-controller mounted on the system are shown in Figure 3.8.

Figure 3.8. The scroll compressor in the system (left) and the on/off relay-based process controller (right)

The thermal energy storage system integrated to the aforementioned heat pump setup consist of a high-density-polyethylene (HDPE) cylindrical tank with a 1.2-m-length and 630 mm internal diameter. The PCM module mounted into the tank includes 32 corrugated-wall steel tubes 2 inches in diameter and 1 meter in length, which are filled with PCM during tests. The reason behind the selection of this type of tubes relies on the computational fluid dynamics (CFD) simulations of which the details were given in the next subsection. Eighteen J-type thermocouples were mounted at different locations along the radial and axial directions on the tank, as well as at the two inlets and two outlets, in order to comprehensively measure the temperature distribution of water inside the thermal energy storage tank. In addition to that, ten different T-type thermocouples were immersed into the six of the PCM tubes to monitor their temperature variations. At this point, it is worth noting that four of the six PCM tubes contained one thermocouple immersed up to their midpoint along axial direction, namely $H/2$ considering the total PCM-filled height of the tube as H, and two of the PCM tubes included three thermocouples located at the heights $0.35H$, $0.60H$ and $0.85H$, so that any axial variation in the temperature along the PCM inside the tubes could be monitored. A photograph of the insulated thermal energy storage tank equipped with thermocouples is given in Figure 3.9. Additionally, the schematic front view of the TES tank and the schematic top-view of the PCM module inside the tank are shown in Figure 3.10. As seen from the figure, the temperature of the water inside the TES tank was measured at 9 points in axial direction, from T_5 to T_{13}, while it was measured at 5 points in radial directions, from T_{14} to T_{18}. In addition to that, the inlet and outlet temperatures at both sides of the tank are measured, and they are labeled as T_1, T_2, T_3, and T_4, for inlet-1, outlet-1, inlet-2, and outlet-2, respectively. Besides the water temperatures, different PCM tubes were selected for the placement of thermocouples in order to measure the PCM temperatures and evaluate if there is any significant difference in melting/solidification rates regarding the position of the tubes inside the tank. An organized distribution of tubes equipped with thermocouples was ensured within the tank geometry in order to monitor the temperature variations of the PCM tubes that are relatively closer to the inlets and outlets, as well as to the center of the tank.

Figure 3.9. Photograph of the thermal energy storage tank with insulation and thermocouples

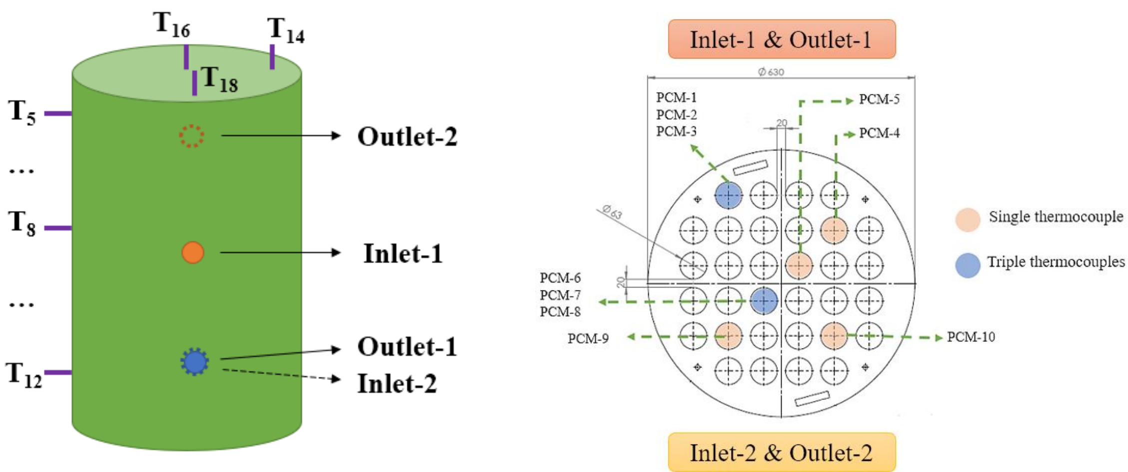

Figure 3.10. Schematic front view of the TES tank (left) and schematic top view of the PCM module inside the TES tank with thermocouple numbers and locations

In addition to the previously mentioned thermocouples located in the thermal energy storage tank and PCM tubes, two thermocouples were utilized at the condenser inlet and outlet of the heat pump to measure the temperature of heat transfer fluid which is circulated through the hot accumulation tank to reject the heat produced by the heat pump. Furthermore, an ENTES MPR63 network analyzer (±1%) (see Figure 3.11) was used in the heat pump system to monitor the energy consumption of the scroll compressor. The volume flow rates of the circulating heat transfer fluid via circulation pumps in the thermal energy storage tank as well as in the hot accumulation tank were measured using glass-tube float flowmeters. Universal data loggers of ORDEL UDL100 (±1%) were utilized to monitor and log the temperature data, while the electrical power data were transferred by ENTES RS485-USB converters (±0.015%) to the computer software, as shown in Figure 3.11. For the System-1, uncertainties arisen from various instruments were analyzed using a well-known method (Moffat, 1988), and the highest uncertainty was found in calculation of *COP* value which was ±8.25% in this system. Furthermore, the uncertainties in the measurement of volume flow rate, condenser inlet-outlet temperatures and electric power drawing from the network were within the maximum range of ±0.11 L/h, ±0.28°C, and ±0.011 W, respectively.

Figure 3.11. Photographs of the network analyzer (left), RS485-USB converter (middle), and the universal temperature data logger (right)

3.3. Investigated Heat Pump System Layouts and Experimental Procedures

In the beginning of the explanation of the experimental procedures, it should be highlighted that two different heat pump systems, both integrated with thermal energy storage unit by different considerations, were investigated within this thesis work in order to separately evaluate their operational performance as well as their benefits and drawbacks. Thus, first, the thermal energy storage unit described in the previous section was integrated to the evaporator of the water-source heat pump to provide a heat source, considering renewable energy utilization. This system was labeled as “System-1” in this work. At this point, the focus was on the effect of thermal energy storage utilization on the heat pump performance and augmentation of renewable energy utilization, which is considered solar energy. In the second system, which is named as “System-2”, the thermal energy storage unit was integrated to the condenser of the heat pump, which uses air as the heat source. Hence, in this system, the thermal energy is continuously stored by accumulating the heat provided by the air-source heat pump into the thermal energy storage tank up to a certain temperature value. Then, the charging process is ceased, and the stored thermal energy is directly used for the heating purpose, which significantly contributes to the load shifting operations depending on the electricity tariff.

3.3.1. Integration of Thermal Energy Storage Unit to the Evaporator (System-1)

Within the concept of this configuration of heat pump and TES combination along with renewable energy utilization, the solar energy can be stored in the diurnal period where the heating needs of a residential building is not very high, and this stored energy can be used as a heat source for the heat pump in nocturnal period, leading to a more efficient heating as well as organized utilization of solar thermal energy. Thus, this system was considered as a solar-assisted water-source heat pump system integrated with a TES unit. A schematic diagram to illustrate the system is given in Figure 3.12. An additional 50-liter insulated tank incorporated with a 3-kW electric heater was externally coupled with the TES tank in order to experimentally simulate a solar collector tank (SCT). There were two main reasons for the utilization of an additional tank with electric heater: First, the duration of the experiments in order to increase the water temperature inside the TES tank would be so high that it would not allow the similar circumstances for all considered cases. Secondly, the electrical energy supplied was measured by the network analyzers, which allowed the amount of energy provided to heat up the water, and this would not be possible if the experiments would have conducted using actual solar collectors. Moreover, thanks to the measurement of electrical energy, the total thermal energy stored as well as the thermal energy supplied to the heat pump evaporator could be estimated by this way. By using the aforementioned electric heater, the heat transfer fluid heated up was circulated between the SCT and TES tank in order to thermally charge the TES unit. The heat pump rig has a cold accumulation tank (CAT) connected to TES tank and a hot accumulation tank (HAT) acting as the condenser. In addition to that, an external chiller unit was used to reject the heat that is accumulated in the HAT as a result of heat pump operation and simulate a residential building to be heated. The heat load that is rejected by the chiller was adjusted by the flowrate of the heat transfer fluid which is controlled by a valve.

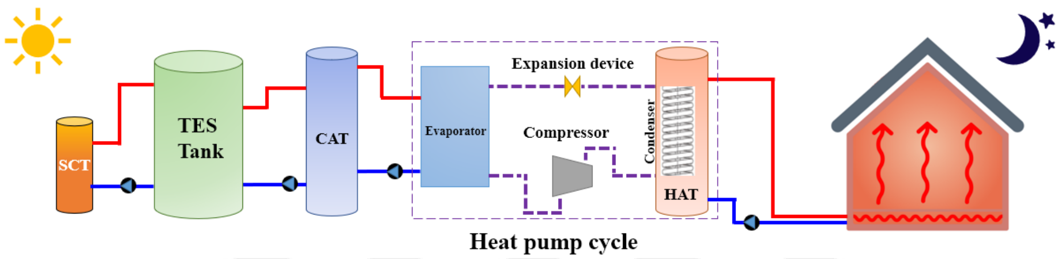

Figure 3.12. Schematic diagram of the investigated solar-assisted heat pump with TES unit (System-1)

As the thermal energy storage tank is integrated to heat pump evaporator in this system, the phase change temperature interval is of great importance since it must be suitable for the operation of the water-to-water heat pump system. Therefore, a commercially available PCM by Rubitherm GmbH was considered because of several reasons. First, the experimental procedure was considered to be finished when the water temperature in the TES tank reaches down 20°C, which is explained in detail in the upcoming paragraphs concerning the experimental procedure. Hence, a phase change temperature of around 25°C – 28°C would be appropriate for this application. Secondly, temperature stability was taken into account, and it was foreseen that a temperature just above 20°C would ensure an efficient operation of the heat pump, hence, it was crucial to make the evaporation temperature stable around the temperatures about 20°C and fairly above. Thirdly, the PCM was desired to have a sufficient amount of latent heat capacity to be able to store a significant amount of thermal energy. Last but not least, the availability and price of the PCM were taken into consideration. Regarding all these reasons, Rubitherm RT26 was selected as the PCM to be used in the tubes inside the thermal energy storage tank due to its appropriate and highly stable phase change interval between 25°C and 26°C, a combined heat capacity, namely the latent and sensible heat, around 180 kJ/kg between 19°C and 35°C, and relatively low-cost compared to the equivalent products. The considered PCM in its 10-kg-packing is shown in Figure 3.13, while its thermophysical properties taken from the manufacturer are shown in Table 3.2 (Rubitherm, 2023).

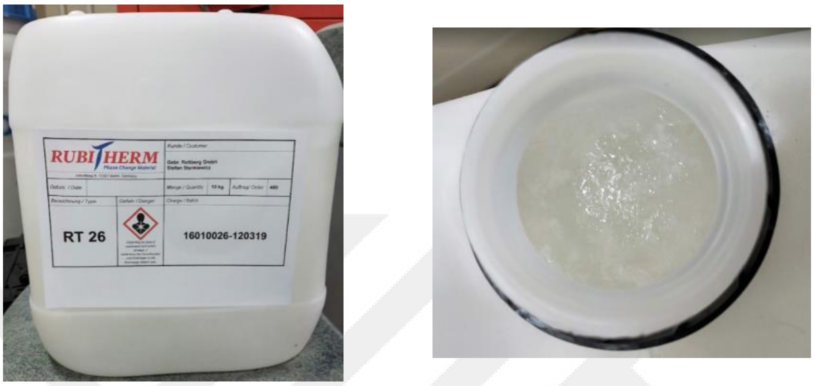

Figure 3.13. Photograph of the utilized PCM, RT26 in its package

Table 3.2. Thermophysical properties of the RT26 used in experimental works (Rubitherm, 2023)

Parameter	Value
Density (kg/m^3)	880 (solid) / 750 (liquid)
Specific heat capacity (J/(kg·K))	2000
Thermal conductivity (W/(m·K))	0.2
Solidus/Liquidus temperature (°C)	25 / 26
Heat storage capacity (J/kg)	180000
Maximum operation temperature (°C)	60

Here, it should be stressed that the heat storage capacity value given by the manufacturer covers not only the phase change enthalpy of the material but also the sensible heat storage. In other words, the heat storage capacity covers the combined thermal storage of the material in the temperature range of 19°C to 34°C (Rubitherm, 2023). At this point, the temperature-enthalpy diagram of the material provided by the manufacturer is given in Figure 3.14 (Rubitherm, 2023). As seen from the figure, the heat storage capacity of the material around 25-26°C is about 104 to 120 kJ/kg.

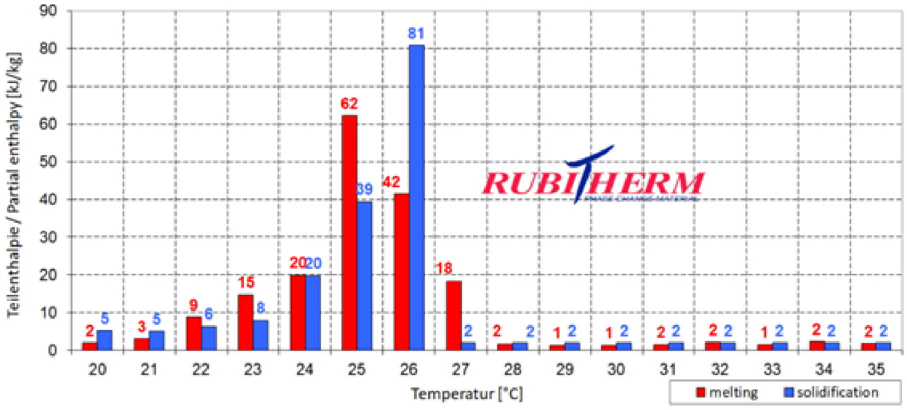

Figure 3.14. Temperature-enthalpy diagram of RT26 (Rubitherm, 2023)

Experimental procedure for System-1: The experimental procedure of the tests conducted for this heat pump system where the TES was integrated to its evaporator (System-1) can be divided into two major periods, namely, charging and discharging. In the first step of the experiment, the heat transfer fluid (water) inside the solar collector tank (SCT), TES tank, and cold accumulation tank (CAT) is maintained at 20°C by pre-heating or cooling operations. Thereafter, the electric heater inside the SCT is activated to thermally charge the thermal energy storage unit until the central temperature in the TES tank, which is the reading of thermocouple T_8, reaches a certain value. This temperature value is defined as storage temperature, T_{st}, and its effect is also investigated for T_{st} =35°C, 45°C, and 55°C. After the central tank temperature reaches the predefined storage temperature, the electric heater is turned off, and the thermal charging process is completed. At this point, it should be noted that the valves between the TES tank and the cold accumulation tank of the heat pump are kept closed, which means that the CAT temperature is maintained at 20°C. Besides, the condenser temperature, which is initially equal to the temperature of the hot accumulation tank (HAT), is also maintained at 35°C for the initial conditions of the tests. Once the charging process is completed, the valves between the TES tank and CAT are opened, and the heat pump compressor and the chiller are activated simultaneously. The temperature setpoint for the chiller is specified as 30°C, and this ensures that the return temperature of the heat transfer fluid to the HAT is maintained around 30°C, while the supply temperature of the water at the exit of HAT is around 35°C. The thermocouple measuring the water temperature at the exit of the HAT is connected to the on/off relay controller, and the compressor is automatically turned off when the temperature reaches

35.4°C, and it is turned on again when the temperature reaches down 35.0°C. By this on/off cycle, the temperature of the water circulated through the heating space remains around 35°C, which is an appropriate heating temperature considered for underfloor heating systems. Since the thermal energy is continuously rejected from the HAT by the chiller, this on/off operation becomes a continuous cycle, which depends on several parameters such as heat rejection rate and the temperature of the water inside the TES unit. In order to test the thermal behavior at different heating loads, five different volume flow rates of the heat transfer fluid circulating between the HP condenser and the chiller unit were considered, which are namely $\dot{V}$ = 400, 600, 800, 1000, and 1200 L/h, and consideration of these HTF flow rates correspond to the heat loads ranging approximately between $\dot{Q}_{load}$ = 1.4 to 3.8 kW. The operation of the heat pump system is ceased when the TES tank temperature, T_8, reaches down 20.0°C. In the experiments, the discharging process started from T_8=35°C, 45°C, or 55°C, and it ended when T_8=20°C. Therefore, a PCM with a phase change temperature of 26°C was presumed to be suitable for this process as it could exhibit appropriate melting and solidification behavior in both charging and discharging processes.

The experimental procedure of the System-1 is summarized by block diagrams as shown in Figure 3.15.

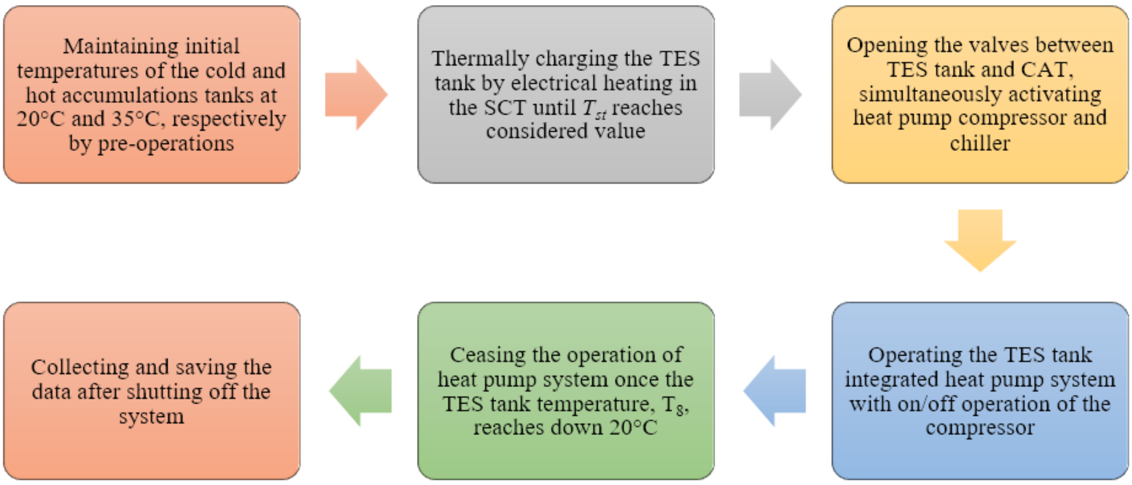

Figure 3.15. Block diagram for the experimental procedure summary of System-1

In the experimental process of the System-1, the collected temperature and energy data over time are analyzed to obtain the performance results, such as thermal charge and discharge times, time ratio of compressor operation (*COTR*), the total supplied heating energy to the load (the rejected heat by the chiller) and the total consumed electrical energy of the compressor over the total test time, of which the ratio yields the energy-based coefficient of performance (*COP*) value of the heat pump. The average rate of heat rejection from the hot accumulation tank integrated to the condenser, $\dot{Q}_{load}$, is calculated by taking the average of thermocouple readings at the inlet and outlet, that is $T_{HAT,i}$ and $T_{HAT,o}$, into account, together with the measured volumetric flow rate, $\dot{V}$, by flowmeter. Assuming that the density and specific heat of the heat transfer fluid, which are denoted by ρ and C_p, remains constant, this value is calculated as given in Equation (3.10) (Xu et al., 2021):

$$\dot{Q}_{load} = (\rho \dot{V} C_p)(T_{HAT,o} - T_{HAT,i}) \tag{3.10}$$

In order to obtain the amount of total thermal energy rejected from the heat pump condenser, i.e., from the hot accumulation tank (HAT), by the circulation of heat transfer fluid, water, the heat transfer rate values presented in the previous expression are integrated over the total heating period, i.e., total test time until the heat pump operation is ceased. Therefore, total energy obtained from the heat pump is expressed by Equation (3.11) as follows (Jin et al., 2021b):

$$Q_{load} = \int_{t_{start}}^{t_{end}} \dot{Q}_{load} dt \tag{3.11}$$

In the above equation, t_{start} and t_{end} respectively indicates the start and end times of the test where the heat rejection from the hot accumulation tank continuously takes place.

Utilizing the network analyzer, the electrical power drawn by the heat pump compressor, *P*, is measured, and the total electrical energy consumed by the compressor, *W*, is expressed in Equation (3.12) (Jin et al., 2021a):

$$W = \int_{t_{start}}^{t_{end}} P dt \tag{3.12}$$

Here, it should be underlined that the compressor operation is not continuous in this system layout (System-1); hence, the power drawn by the compressor can be zero in certain time intervals between t_{start} and t_{end}, whenever the outlet temperature of the HAT is at the predefined value, that is 35.4°C.

Considering the total heating time and the start/stop operation of the heat pump compressor during this period, a performance parameter named as compressor operation time ratio (*COTR*) is defined for this system in order to evaluate the share of compressor operation, i.e., electrical energy utilization, in the total heating period, and this parameter is expressed in Equation (3.13) as follows:

$$COTR = \frac{t_{compressor}}{t_{total}} \tag{3.13}$$

where $t_{compressor}$ and t_{total} indicate the total time when the compressor is active and the total time of the system operation, i.e., total discharging period.

The average coefficient of performance (*COP*) of the heat pump based on its energy consumption and heating energy supply is defined to evaluate the performance of the heat pump at different heat load levels regarding the PCM existence inside the TES tank, and it is shown in Equation (3.14):

$$COP = \frac{\dot{Q}_C}{P} \tag{3.14}$$

One of the aims of the design of the TES integrated solar-assisted water source heat pump (SAWSHP), which was labeled as System-1 within this thesis work, is to clip the electric loads during the peak periods, and thus, enhance the energy flexibility of the system. To quantify the peak clipping potential of the system under different circumstances such as operational conditions, PCM utilization, thermal charging status, etc., a peak clipping index (*PCI*) was defined, which takes into account the consumed electrical energy by the compressor during on-peak period. For this purpose, the ASHP within the same experimental rig was considered as the baseline case to meet the same heating demand, and the *COP* of the ASHP was calculated from the obtained data in an ambient temperature of 11°C. The peak period energy consumption values were compared regarding Equation (3.15):

$$PCI = \frac{W_{baseline,peak} - W_{actual,peak}}{W_{baseline,peak}} \tag{3.15}$$

3.3.2. Integration of Thermal Energy Storage Unit to the Condenser (System-2)

Another option for the integration of thermal energy storage units to heat pumps is to couple the TES unit to the condenser of the heat pump. Thereby, the thermal energy can be transferred to the TES tank, and this energy can be used in a period where it is needed, or when it is more convenient to use ensuring energy flexibility. Although different energy sources can be used for heat source of the heat pump, the most common type for this configuration considered in the literature is an air-source heat pump (ASHP), mainly used as air-to-water heat pumps when integrated with thermal energy storage, due to its simplicity and suitability for applications (Ermel et al., 2022).

In this system investigated, an air-to-water heat pump is utilized to store thermal energy into the storage medium inside the TES tank during off-peak periods, and this stored thermal energy is considered to be used in the on-peak period. This type of an operation attains a significant energy flexibility, particularly load shifting. The system design explained in the previous section was modified to construct the system schematically given in Figure 3.16. As shown in the figure, the system consists of an air-source evaporator, a compressor, an expansion valve, and the hot accumulation tank (HAT) coupled with the condenser of the heat pump. The TES tank is integrated to the HAT at the condenser side of the heat pump where the thermal energy is stored into the TES tank by the circulation of the heat transfer fluid, water, by the help of a circulation pump. The stored thermal energy inside the HAT and TES tank is rejected by the chiller unit, which simulates the heat load for the space heating purpose, after thermal charging process is completed. The heat loads in the discharging process are determined by the volume flow rate of the heat transfer fluid and the temperature controller of the chiller, which allows discharging the thermal energy inside the thermal energy storage tank at different heat loads.

Similar to the previously mentioned system, the tests were also conducted with and without PCM in this system. However, since the TES tank is integrated to the condenser, the temperature of the water inside the TES tank is increased from a reference temperature (35°C) to the storage temperature of 55°C in this application. Therefore, another PCM should be selected for utilization in the corrugated tubes inside the TES tank. A commercially available fatty-acid based PCM, lauric acid, was purchased to be used in System-2.

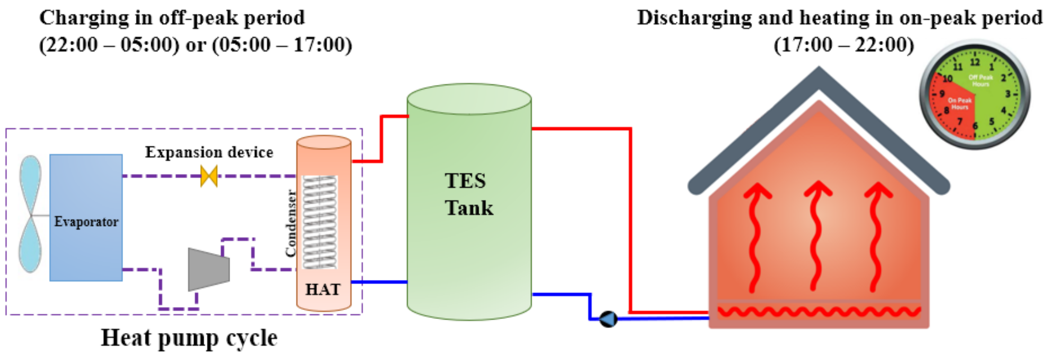

Figure 3.16. Schematic diagram of the investigated air-to-water heat pump with TES unit integrated to the condenser (System-2)

Even though it was not considered in a heat pump system experimentally investigated, to the best knowledge, this PCM is commonly considered in the investigation of various thermal energy storage systems in the literature (Kalapala and Devanuri, 2020; Mishra et al., 2022) due to its simplicity, availability in the market, inexpensive cost, and suitability for such applications with a phase change temperature interval between 41°C to 48°C and a latent heat capacity of around 160-180 kJ/kg. Considering that its phase change interval is between the lowest and highest storage temperatures taken into account in this system, namely 35°C and 55°, its utilization was foreseen to be suitable for both thermal charging and discharging during the operation of the System-2. Lauric acid is solid in the typical indoor ambient conditions, and it is produced in granular form as seen in Figure 3.17.

Figure 3.17. Lauric acid in granular form before DSC tests

It should be noted here that the density of this material is low in the granular form due to air gaps between the granules when poured into the tubes. Hence, the lauric acid in an amount of 50 kg is poured into the corrugated tubes, considering the safety limit preventing any leakage or outpouring effect, as well as the similar amount (~50 kg) considered in System-1. The thermophysical properties of the lauric acid available in the literature are given in Table 3.3 (Rocha et al., 2023; Shokouhmand and Kamkari, 2013).

Table 3.3. Thermophysical properties of lauric acid used in experimental works (Rocha et al., 2023)

Parameter	Value
Density (kg/m^3)	940 (solid) / 885 (liquid)
Specific heat capacity (J/(kg·K))	2180 (solid) / 2390 (liquid)
Thermal conductivity (W/(m·K))	0.16 (solid) / 0.14 (liquid)
Solidus/Liquidus temperature (°C)	43.5 / 48.2

Although thermophysical properties of the lauric acid are given as in the table by various literature studies, there may be some differences with the values depending on the chemical structure of the material. Therefore, differential scanning calorimetry (DSC) tests were conducted on the lauric acid purchased for this thesis work in order to reveal its latent heat capacity as well as melting and solidification temperature ranges. The results of these tests are given in Figure 3.18, and it is seen from the figure that the PCM exhibits melting behavior approximately between 44°C and 55°C with a peak point of 48°C, while its solidification process occur between 39°C and 41°C where the peak point is at 41°C. In addition to that, the latent heat capacity of the utilized material is about 160 kJ/kg, according to the test results. Besides, as the chemical stability of the material with respect to temperature variations is also important, hence, a thermogravimetric analysis (TGA) on the material was carried out in order to ensure that the material is chemically stable and suitable for the considered application. The result of the TGA for the considered lauric acid is given in Figure 3.19, and it is obviously noticed from the figure that this PCM is chemically stable up to around

200°C, and it does not exhibit any degradation below 115°C. Hence, this material is suitable for the utilization in thermal energy storage implementations for building heating or domestic hot water applications together with heat pumps without any concern of degradation.

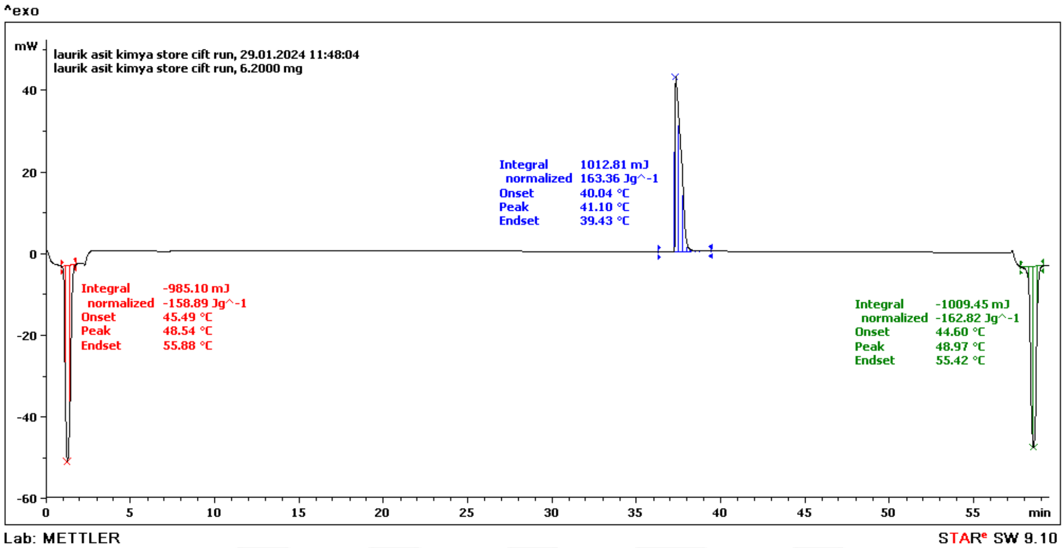

Figure 3.18. DSC test results of the utilized lauric acid

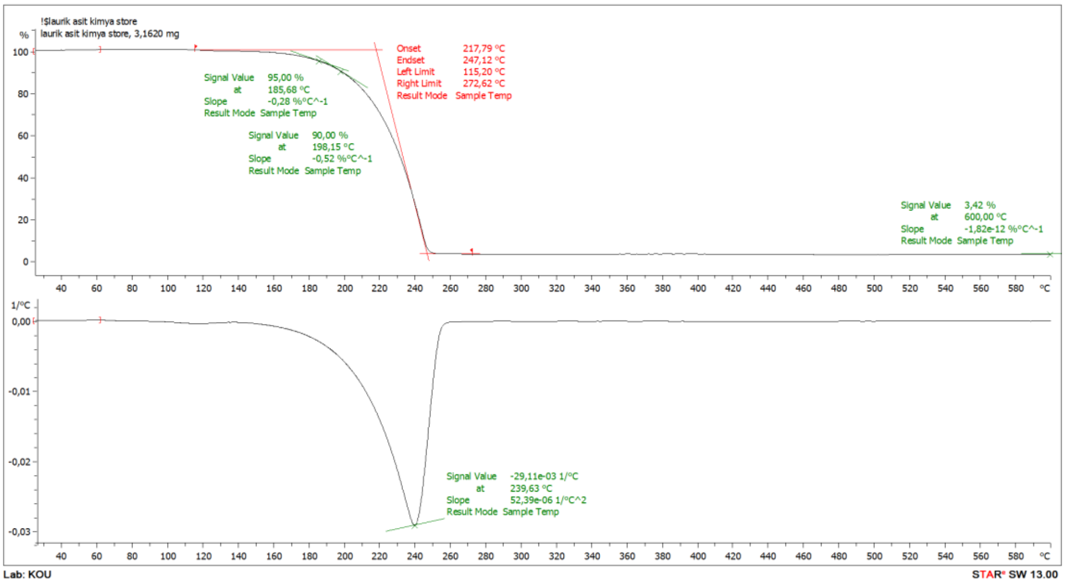

Figure 3.19. TGA results of the utilized lauric acid

To calculate the density of the purchased lauric acid, the weight of a certain amount of the material in liquid form is checked regarding a certain value of volume using a digital precision scale with a sensitivity of 0.001 g and a beaker glass, respectively. According to the measurement and observation, the density of the material is found to be around 850 kg/m^3, which is consistent with the values given in various literature works (Rocha et al., 2023).

Experimental procedure for System-2: Similar to the procedure considered in System-1, the total test can be divided into two main periods as thermal charging and discharging. Different from the System-1, the charging process is carried out by the continuous operation of the air-source heat pump of which the condenser temperature starts with 35°C. By the continuous operation of the air-to-water heat pump, the water temperature inside the thermal energy storage tank (T_{st}) is risen from T_{st} =35°C to T_{st} =55°C to store thermal energy. During the charging process, the temperature variations inside the tank, the power drawn by the compressor and the elapsed time are monitored. Once the T_8, which is the reference temperature in the middle point of the TES tank, reaches the required storage temperature (T_{st} =55°C), the charging process is ended. Thereafter, the vanes between the TES tank and the chiller are opened, and the discharging process is started by the aid of chiller unit rejecting heat from the TES tank. Different heating loads are adjusted by the volumetric flow rate of the heat transfer fluid and the temperature controller of the chiller unit, and the thermal behavior of the water and PCM (in cases of presence) are monitored along with the total discharging time. When the reference temperature, T_8, reaches back 35°C, the discharging operation is finished, considering that 35°C inlet water temperature is usually minimum acceptable temperature for space heating, e.g., for underfloor heating operations. The experimental procedure for System-2 is summarized by the diagram given in Figure 3.20.

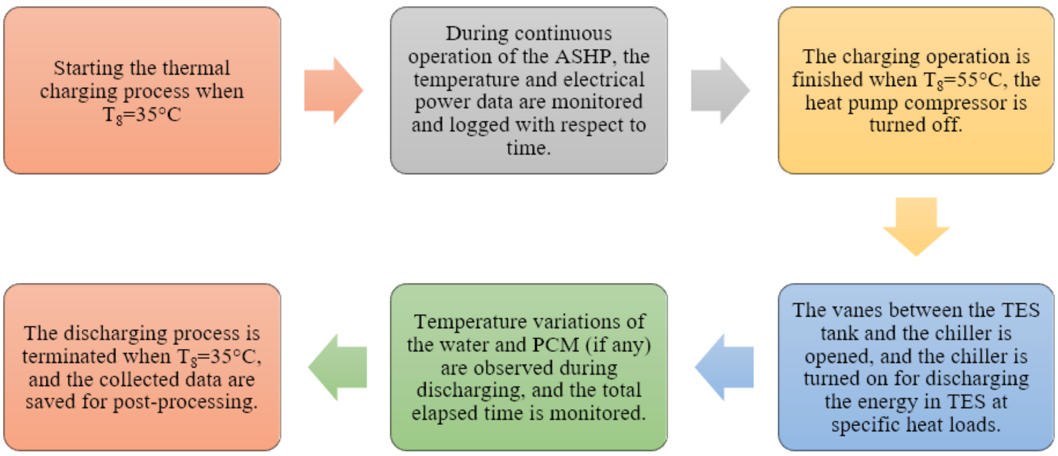

Figure 3.20. Block diagram for the experimental procedure summary of System-2

During the continuous operation of System-2 in thermal charging process, the heat rejected from the heat pump condenser, $\dot{Q}_{cond}$, is estimated by the thermocouple measurements located at the inlet and outlet of the HAT, and the volume flow rate measurement is considered by the glass-tube flowmeter, as the same way given for the System-1 in the previous section. Besides, the electrical power drawn by the compressor is noted using the network analyzer. The *COP* is defined by the ratio of heating load of the condenser ($\dot{Q}_C$) to the power drawn by the compressor (*P*) during charging, and it is expressed in Equation (3.16):

$$COP = \frac{\dot{Q}_C}{P} \tag{3.16}$$

Considering its operation principle, the heat pump system denoted by System-2 is beneficial for energy efficient load shifting operations ensuring energy flexibility. Storing the thermal energy during off-peak periods for the purpose of using it during on-peak periods without (or with smaller amount of) electrical energy consumption means a load shifting operation, which is one of the various activities for energy flexibility. In order to quantify the load shifting, the load shifting index (*LSI*) is defined regarding the ability to use previously stored thermal energy in peak periods to shift the electrical load to off-peak periods. This energy flexibility parameter can be defined as given in Equation (3.17) (Awan and Ma, 2023; Jin et al., 2023):

$$LSI = 1 - \frac{\int_{t_{peak,start}}^{t_{peak,end}} Pdt}{\int_{t_{start}}^{t_{end}} Pdt} \tag{3.17}$$

Related to the shifted load from the on-peak to off-peak periods, a significant cost saving can be attained as well, due to the noticeably varying electricity prices with respect to the tariffs. Considering the off-peak period where the thermal charging by the heat pump is carried out and the utilization share of the thermal energy during on-peak period, the cost saving rate can be calculated by the ratio of payment for electricity during charging period in an off-peak period to the payment of the same amount of electricity in the on-peak period. This performance parameter evaluates the potential of the cost saving in case of thermal charging in off-peak periods, compared to the thermal charging or heating in the on-peak period. Hence, this comparative parameter, cost saving ratio (*CSR*), was defined within Equation (3.18):

$$CSR = 1 - \frac{[LSR \times C_{off-peak}] + [(1 - LSR) \times C_{on-peak})]}{C_{on-peak}} \tag{3.18}$$

Here in the above equation, the symbol C represents the electricity cost during the relevant period, namely on-peak or off-peak, as mentioned in the subscripts.

3.4. Mathematical Modeling of TES Integrated Heat Pump Systems

Mathematical models for each investigated TES integrated heat pump systems were created under consideration of the experimental data, which are used to characterize the heat pump performance for the investigated cases, and the simulation algorithms were established by FORTRAN along with the mathematical model. The heat pump performances for each system (System-1 and System-2) were characterized by regressions regarding the time-dependent TES tank temperature and compressor power drawn, which is one of the methods within the context of grey-box modeling, for the estimation of heat pump performance by mathematical modeling (Baster, 2017; Song et al., 2023).

The in-house built codes are capable of predicting the total charging and discharging times for each system given the required heat load within the range of experimental data. Furthermore, the temperature variations in each tank including solar collector tank, TES tank, accumulation tanks, and an exemplary PCM tube, as well as average compressor energy consumption, *COP* values, and total compressor operation time are among the simulation outputs. The details of the mathematical modeling of each system are given in the following sections.

3.4.1. Mathematical Modeling of System-1 (TES integrated SAWSHP)

Starting with the mathematical model of System-1 where the TES is integrated to evaporator side of the heat pump, the assumptions taken into account can be listed as follows:

- The water inside all the tanks, i.e., the solar collector tank (SCT), thermal energy storage tank (TES), hot and cold accumulation tanks (HAT & CAT) were considered lumped system, due to the slight variations in the temperature values in axial and radial directions inside the TES tank according to the measurement values.

- As the compressor power drawn has a slight variation between setpoint temperatures for on/off cycle as well as the suction/discharge pressures, this was taken a constant value as the average power consumption value.
- The heat transfer inside the PCM medium was assumed one-dimensional, namely, in radial direction only. Hence, the phase change occurred also in one-dimension. The natural convective effects were implemented using a Nusselt number correlation derived for PCMs in vertical cylinders (Kim et al., 1989).
- The thermophysical properties of the PCM, namely the density, thermal conductivity, and specific heat capacity were taken constant.
- The density and specific heat of the heat transfer fluid, water, were considered to be constant.

Along with the above-mentioned assumptions, the mathematical model of the System-1 where the TES unit is used to create a heat source environment for the heat pump can be expressed by Equations (3.19) to (3.22) for thermal discharging process as follows, regarding the energy balance for each tank:

$$m_{SCT}C_p\frac{dT_{SCT}}{dt} = \dot{m}_{SCT}C_p(T_{TES} - T_{SCT}) \tag{3.19}$$

$$m_{TES}C_p\frac{dT_{TES}}{dt} = \dot{Q}_{SCT} - \dot{Q}_{CAT} + \dot{Q}_{Tube-total} \tag{3.20}$$

$$m_{CAT}C_p\frac{dT_{CAT}}{dt} = \dot{m}_{CAT}C_p(T_{TES} - T_{CAT}) - \dot{Q}_E \tag{3.21}$$

$$m_{HAT}C_p\frac{dT_{HAT}}{dt} = \dot{Q}_C - \dot{Q}_{load} \tag{3.22}$$

Here, m, C_p, T, and $\dot{Q}$ represent the mass of the water inside the relevant tank, specific heat of water, temperature, and heat transfer rate, respectively. The subscripts SCT, TES, CAT, HAT, Tube-total, load, C and E respectively stand for the solar collector tank, thermal energy storage tank, cold accumulation tank, hot accumulation tank, heating load, the condenser and the evaporator of the heat pump. As the tanks containing water are considered lumped system, the temperatures with relevant subscripts represent the water temperature exiting the aforementioned tank. While the heat transferred to the HAT by the heat pump condenser, $\dot{Q}_C$, depends on the heat pump performance, the heating load is varied by the volume flow rate of the heat transfer fluid

($\dot{V}$), and the inlet and exit temperatures of the heat transfer fluid circulating between the HAT and the chiller unit, which are measured by the thermocouples at these locations. Hence, the heat load is represented in Equation (3.23) as follows:

$$\dot{Q}_{load} = \rho \dot{V} C_p (T_{HAT,e} - T_{HAT,i}) \tag{3.23}$$

The heat transfer through the PCM including phase change process was carried out in radial direction only as it was assumed that there would be negligible difference in the axial direction of the vertical tubes inside the tank, due to the significantly uniform temperature distribution of water. Hence, the governing equations for the heat transfer through the PCM during no-phase-change condition and phase change situation was respectively expressed by the following equations, and thereafter was the equation given for the heat exchange between the tubes and the water in the TES tank. Here, it should be noted that the transferred sensible and latent heat from/to one PCM tube is calculated, and its amount is considered for all the tubes located in the TES unit.

$$\rho C_p \frac{\partial T}{\partial t} = \frac{1}{r} \frac{\partial}{\partial r}\left(kr \frac{\partial T}{\partial r}\right) \tag{3.24}$$

$$\rho C_p \frac{\partial T}{\partial t} = \frac{1}{r} \frac{\partial}{\partial r}\left(kr \frac{\partial T}{\partial r}\right) - \rho L_H \frac{\partial f}{\partial t} \tag{3.25}$$

$$\dot{Q}_{Tube} = hA_{surf}(T_{r=R} - T_{TES}) \tag{3.26}$$

$$\dot{Q}_{Tube-total} = \sum_{i=1}^{n} \dot{Q}_{Tube(i)} \tag{3.27}$$

In the above given equations ρ, C_p, T, k, L_H, and f stand for the density, specific heat, temperature, thermal conductivity, latent heat capacity and liquid fraction of the PCM inside the tubes, respectively. Besides, r, t, h, and A_{surf} respectively denote the distance in radial direction, time, convective heat transfer coefficient between the PCM medium and the water medium where the thermal resistance of the steel tubes was negligible, and the surface area of the tubes. The value of the average convective heat transfer coefficient along the tube surface was estimated by the aid of previously conducted CFD simulations. Besides, it was presumed that the convective thermal resistance at the outer side of the PCM tubes would be much lower compared to the conductive thermal resistance within the PCM medium, due to the low thermal conductivity of the PCMs. In other words, the dominant thermal resistance would be sourced by the PCM, while the thermal resistance at the outer side of the tubes would be relatively slight, and this phenomenon was also justified by the numerical computations in the section of the discussion of the results of the mathematical model for the System-1.

Integration of solar collector into the model of System-1: Thermal charging and discharging performances of the TES unit integrated to System-1 were investigated and discussed over the established numerical model considering five representative days from each month in the heating season. Therefore, the FPSC was included into the mathematical model even though it was not present in the experimental studies. The flat plate solar collector (FPSC) utilized in the study of Kim et al. (2018) was considered in the mathematical model, and the tilt angle of the solar collectors was taken as 35°, and their azimuth was taken into account as south facing. The useful heat gain from the solar collectors and the outlet temperature were respectively calculated using following equations (Kim et al., 2018):

$$\dot{Q}_{sc} = A_{sc}F_R[(\tau\alpha)G_\beta - (U_L)(T_{sc,in} - T_{amb}) \qquad (3.28)$$

$$T_{sc,out} = \frac{\dot{Q}_{sc}}{\dot{m}_{sc}C_p} + T_{sc,in} \qquad (3.29)$$

Here in the above equations, A_{sc}, $T_{sc,in}$, $T_{sc,out}$, T_{amb}, G_β, $\dot{Q}_{sc}$, $\dot{m}_{sc}$, and C_p respectively stand for the solar collector area, solar collector inlet temperature, solar collector outlet temperature, ambient temperature, incident solar radiation on the tilted surface, mass flow rate of the heat transfer fluid, and the specific heat of the heat transfer fluid, which is water. In addition to that, the multiplicated terms with the heat removal factor denoted by $F_R(\tau\alpha)$ and $F_R(U_L)$ signify the absorption coefficient and heat loss coefficient of the flat plate solar collectors. Considering the utilized solar collectors, the values of these terms were given as 0.883 and 4.865 W/m^{2}K, respectively (Kim et al., 2018). In the simulations, these values of the solar collectors were taken constant as it was assumed that there was no variation with the mass flow rate of the circulation pump between the TES tank and solar collectors as well as the convective heat transfer coefficient between the collector surface and the ambient air was taken a constant average value, as similarly taken in the considered literature work. Yet, the ambient temperature values were taken as variable considering the meteorological data. Two of the aforementioned solar collectors were considered in this thesis work where each one has a collector area of A_{sc}=1.68 m^2.

3.4.2. Mathematical Modeling of System-2 (TES integrated ASHP)

For the mathematical modeling of the operation of System-2 where the TES tank is integrated to the condenser side of the heat pump, the assumptions presented for the System-1 about the thermal behavior of the HAT and TES tank as well as the heat exchange between the water and the PCM were considered. Exceptionally in this case, the power drawn by the compressor is correlated with the temperature variation of the TES tank by a regression regarding the experimental data since the operation of the compressor is continuous, and hence, the power drawn by the compressor increases due to the augmentation in the water temperature in the TES tank along with the discharge pressure of the refrigerant at the compressor. Relatedly, the air-source evaporator load, $\dot{Q}_E$, could be also correlated with the TES tank temperature. Apart from the modeling of phase change process, the mathematical modeling for the thermal behavior of the water inside the thermal energy storage tank was taken into account regarding Equation (3.30):

$$m_{TES}C_p\frac{dT_{TES}}{dt} = \dot{Q}_C - \dot{Q}_{load} + hA_{surf}(T_{r=R} - T_{TES}) \tag{3.30}$$

Following conditions, which are expressed in Equation (3.31) and Equation (3.32) were applied for the above given equation, during thermal charging and discharging processes, respectively:

$$If\ P \neq 0 \begin{cases} \dot{Q}_C = \dot{m}_c C_p(T_{cond,o} - T_{cond,i}) \\ \dot{Q}_{load} = 0 \end{cases} \tag{3.31}$$

$$If\ P = 0 \begin{cases} \dot{Q}_C = 0 \\ \dot{Q}_{load} \neq 0 \end{cases} \tag{3.32}$$

The aforementioned two different models established for System-1 and System-2 have some limitations due to the considered assumptions and experimental data driven inputs for some performance parameters characterizing the heat pump performance. Hence, the assumptions & limitations of the models can be listed as follows:

- The water in all the tanks connected to the systems was considered lumped system regarding the negligible differences in the experimental data. Hence, additional mathematical expressions should be included to the model in case existence of stratified water tanks.

- Phase change process was taken into account as in radial direction only, and the heat transfer in radial direction was treated by conduction only. Yet, the natural convective effects were taken into consideration using a Nusselt number correlation derived for PCMs in vertical cylinders (Kim et al., 1989). To be more precise, the convective terms should be included.
- The compressor power drawn in the System-1 was taken constant at an average level of value although it was observed that there were slight variations during the operation. Nevertheless, as the heat pump in System-1 operates intermittently, the compressor operates at specific pressure ranges, hence, the variations become slight. In addition to that, some differences in the power drawn may be also sourced by the electric network.
- As the variation of evaporator load and compressor power were estimated using experimental data, the models are specific to the investigated systems and tested heat load values. Nevertheless, modifications such as tank dimensions, the PCM type, PCM amount, addition of renewable energy sources for thermal and electric energy etc., are possible and suitable for the model. Yet, in case of employing appropriate performance inputs for different heat pumps, the model could be applicable for them as well.
- The water tanks used in the system were observed to exhibit a lumped system behavior according to the temperature measurements. Hence, the water inside the tanks were treated as lumped system in the mathematical models as well, and this means that the model is applicable for systems having similar thermal behavior in the water tanks. Thus, different approaches should be implemented for the water storage tanks exhibiting a strong thermal stratification.

3.4.3. Numerical Implementation and Estimation of Heat Pump Performance

The differential equations in the above given mathematical modeling of the System-1 and System-2 were solved by finite difference method implementing an explicit discretization scheme. The temporal terms were discretized by forward difference, while the spatial terms were discretized in consideration of central difference scheme. As the water mediums in the tanks were taken as lumped system, the energy equation including phase change phenomena was solved as one-dimensional in radial direction where the convection boundary condition was applied between the water in the tank and PCM in the tubes, with the consideration of convective heat transfer coefficient by the aid of the outcomes obtained in CFD studies. The spatial and temporal step sizes were taken as Δr=1 mm and Δt=0.25 s after consideration of step size independence tests.

Different approaches exist to estimate the performance of a heat pump for implementation into numerical models. These can be categorized into three main groups, which are namely black-box models, grey-box models, and component based models (Baster, 2017; Green and Garimella, 2021; Murphy et al., 2013).

Black box models are fully empirical representation of a system using measured data. As these models are non-transparent and based only upon input-output relation, the knowledge about the system operation is usually not required, and the heat pump performance can be quickly modeled using this method. However, the results may not be highly interpretable, and some of the quantities or terms may not have a physical meaning. In grey-box model approaches, the models are usually based on the essential information about the system operation and physical phenomena, however, the key performance parameters or quantities are based on empirical relations. Yet, additional algorithms for the system operation are added into the model. Hence, a balance is considered between the empirical data and component knowledge in grey box models, which make them called partially transparent, and this approach is balanced between predictivity and interpretability. Lastly, the component-based models are established by modeling each component in the system individually. Thus, they require a large amount of precise information about the components as well as the system. Therefore, the modeling structure is remarkably complex, and there should be individual sub-models for each component in the system, reflecting the dynamic behavior of each component in the refrigeration cycle. These three major approaches along with their highlighting points were summarized in Figure 3.21. In the mathematical modeling established within the present thesis work, the approach used is regarded as a grey-box model with particular algorithms.

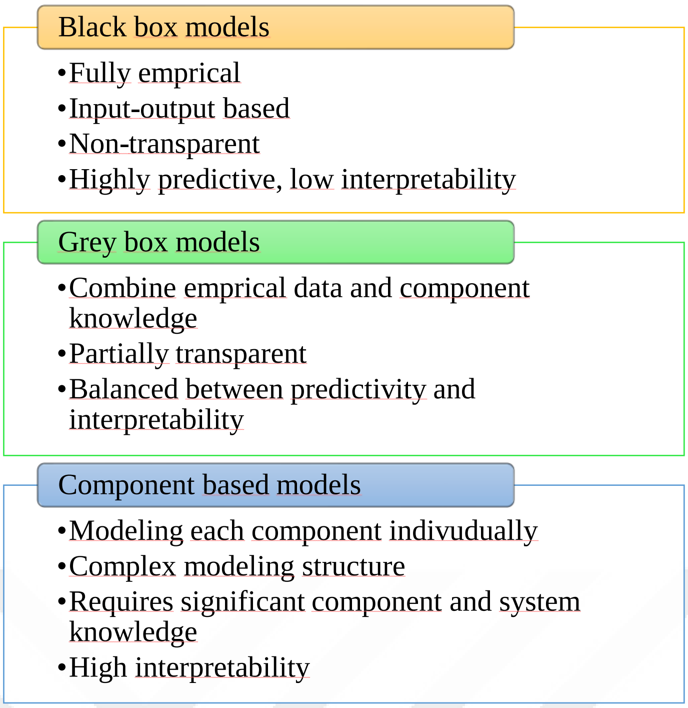

Figure 3.21. Summary of the modeling approaches for heat pump performance estimation

The evaporator load, $\dot{Q}_E$, is determined as an average value considering the total thermal energy given by the electric heater and consumed by the heat pump during the experimental tests for System-1. As the heat rejection by the evaporator varies with respect to the heat load specifying the operational frequency of the heat pump compressor, the evaporator load is correlated with the average heat load by linear regression.

On the other side, due to the continuous operation of the heat pump in System-2, the temperature of the TES tank represented by T_8 increases uninterruptedly, along with the compressor power drawn. Thus, the correlation between the water temperature in the TES tank and compressor power drawn as well as the relation between the TES tank temperature and evaporator load can be approached by a linear regression. Hence, regarding the measured thermal behavior of the TES unit and the HP, the compressor power, evaporator load, and relatedly condenser load was estimated and used in the numerical model.

The heat pump in the numerical model operates with respect to the regression data for the compressor and evaporator loads determining the heat pump performance characteristics. Hence, by only giving an input of heating load, the model can predict the charging time of the TES tank, the temporal variations of the water temperature inside the TES tank and temperature distribution inside the PCM tubes, as well as the *COP* value, within the specified conditions in accordance with the limits of the correlation. After completing the charging process, i.e., reaching the specified storage temperature, the model switches to the discharging mode, and it discharges the thermal energy at the given heat load estimating the total discharging time as well as the temperature variations inside the water and the PCM during this process. Thereby, it is possible to determine the energy consumed for charging process via considered heat pump, and the sufficiency of the thermal energy for different cases can be interpreted. Furthermore, this procedure can be used for different PCMs.

3.4.4. Validation of the Model Established for System-1

Validation of the established mathematical model was carried out by a set of comparisons with respect to experimental data obtained on System-1. First of all, the temperature variations of the TES tank and cold accumulation tank (CAT) during the discharging process in System-1, i.e., during the heat pump operation, were compared in case of using water storage tank with a storage temperature of T_{st}=45°C along with a HTF volume flow rate of 800 L/h, and the results were shown in Figure 3.22. The trends of the temperature variations showed a remarkable consistency despite the assumptions taken into account for the model. The maximum discrepancy at local points between the numerical and experimental results were found to be 3.5 K and 2.1 K for T_4 and T_8, respectively, while the average discrepancies were 2.2 and 1.7 K, respectively.

Secondly, variation of PCM temperatures with respect to time were compared at the same storage temperature and HTF volume flow rate, as given in Figure 3.23. In the comparison, four different temperature values were considered. The numerically obtained two different temperature variations represent the average PCM temperature in the tank and the temperature at the center point of the PCM. On the other hand, the experimentally obtained PCM temperature variations, PCM-1 and PCM-2 were taken from the tube near the SCT and near the CAT, respectively. The temperature variations were found to be consistent, especially during the phase change process. The maximum discrepancy of the numerically obtained average PCM temperature at a specific data point was calculated as 1.9 K and 2.9 K with respect to PCM-1 and PCM-10, respectively. Also, the average discrepancy was found as 0.5 K, proving the accuracy of the numerical model estimating the PCM temperature variations.

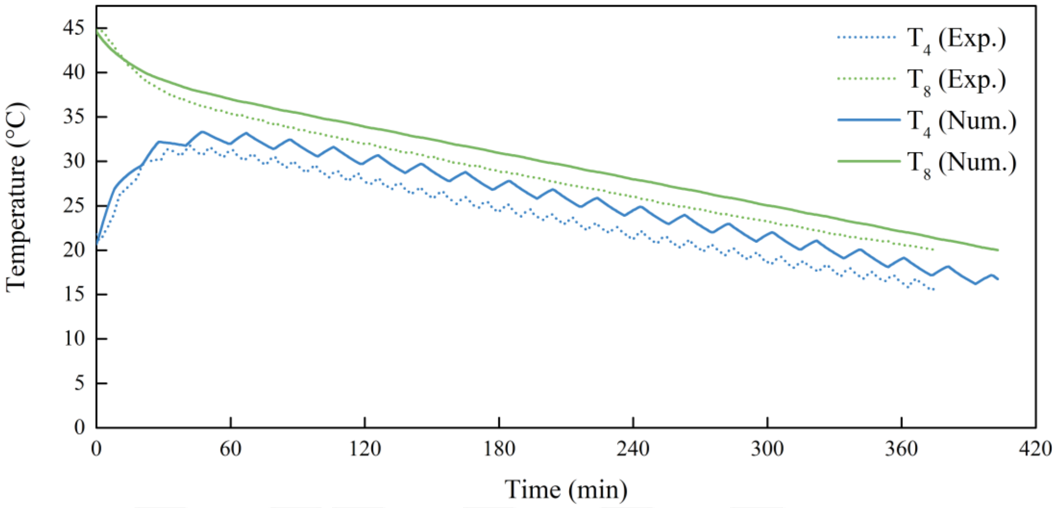

Figure 3.22. Comparison of the experimental and numerical temperature outcomes for System-1 during heat pump operation

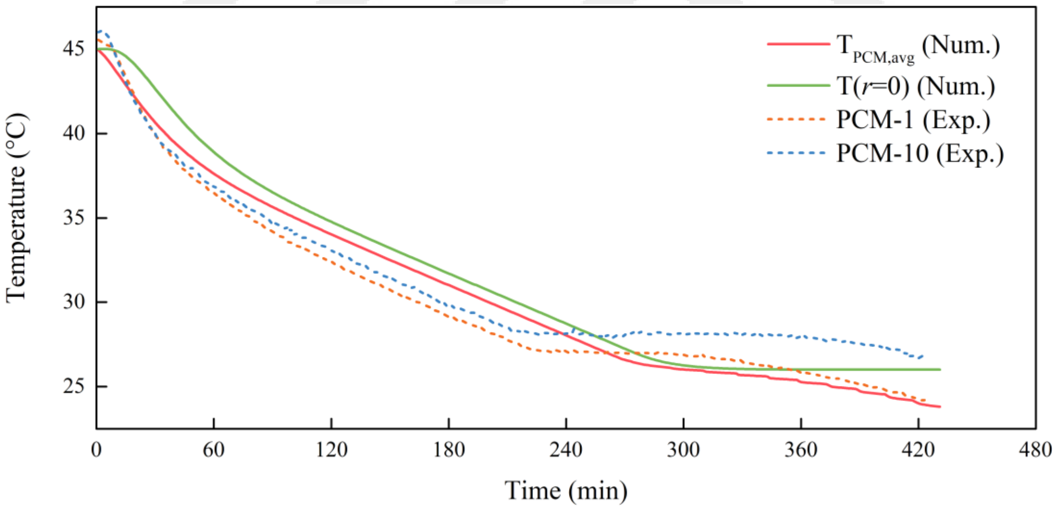

Figure 3.23. Comparison of PCM temperatures in System-1

Thirdly, the compressor operation trends obtained by the numerical model were compared to the experimental data, considering the case with no-PCM and T_{st}=45°C. As the compressor operation is intermittent in System-1, the start/stop operation is an important parameter to evaluate the heat pump performance along with thermal energy storage. Therefore, the compared data of the power drawn by the compressor were shown in Figure 3.24. The data illustrated in the figure evidently revealed that the compressor operation trends in numerical and experimental works were remarkably consistent. Furthermore, the numbers of start/stops in the experimental work and numerical model were the same, which was 38 in this case. Nevertheless, the compressor power drawn increased during the experimental tests due to the fact that the pressure continuously increased during compression which causes a larger energy use of the compressor. On the other hand, a constant power value was considered in the numerical model. Yet, the average values are significantly close to each other within 2.9% discrepancy.

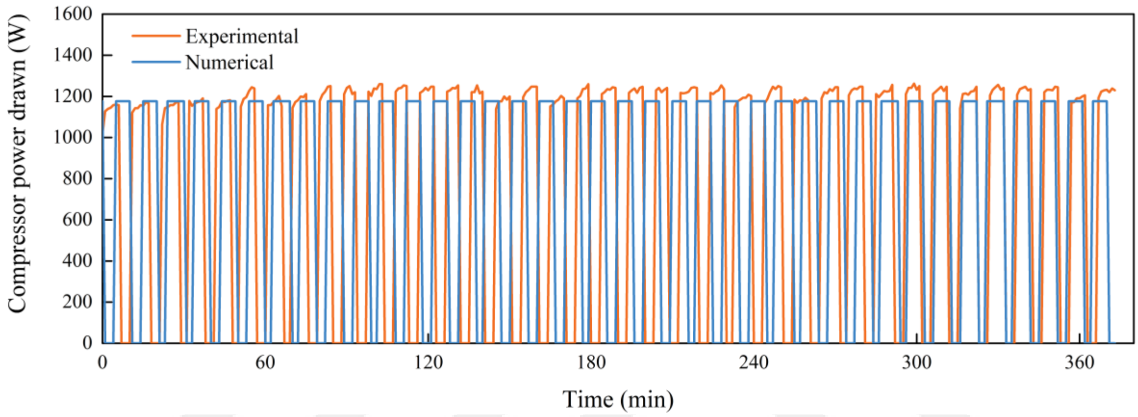

Figure 3.24. Comparison of compressor power values

In the experimental studies conducted for the System-1, the TES tank was charged using electric heater and the heat pump operation was started once the charging was completed. Thus, the heat pump was utilized to discharge the stored energy inside the TES tank. Comparing the total system operation time results, i.e., discharge time results, for the case including PCM at $\dot{V}$=800 L/h and T_{st}=45°C, the comparison outcomes were given in Figure 3.25. Furthermore, another comparison for the *COP* values was presented. As seen from the figures that the discharge times measured in the tests and computed by the numerical model were significantly consistent for all considered storage temperatures, T_{st}. Furthermore, *COP* values that were calculated regarding the heating energy by the heat pump condenser and the energy consumed by the compressor, and they were compared against experimentally obtained values, as presented in Figure 3.25b. The discrepancies in heating time were calculated as 3.3%, 6.4%, and 9.3% for the storage temperatures of T_{st}=35°C, 45°C, and 55°C, respectively.

Also, the discrepancy rates in *COP* values were 4.8%, 0.3%, and 2.3% for the same storage temperatures, respectively.

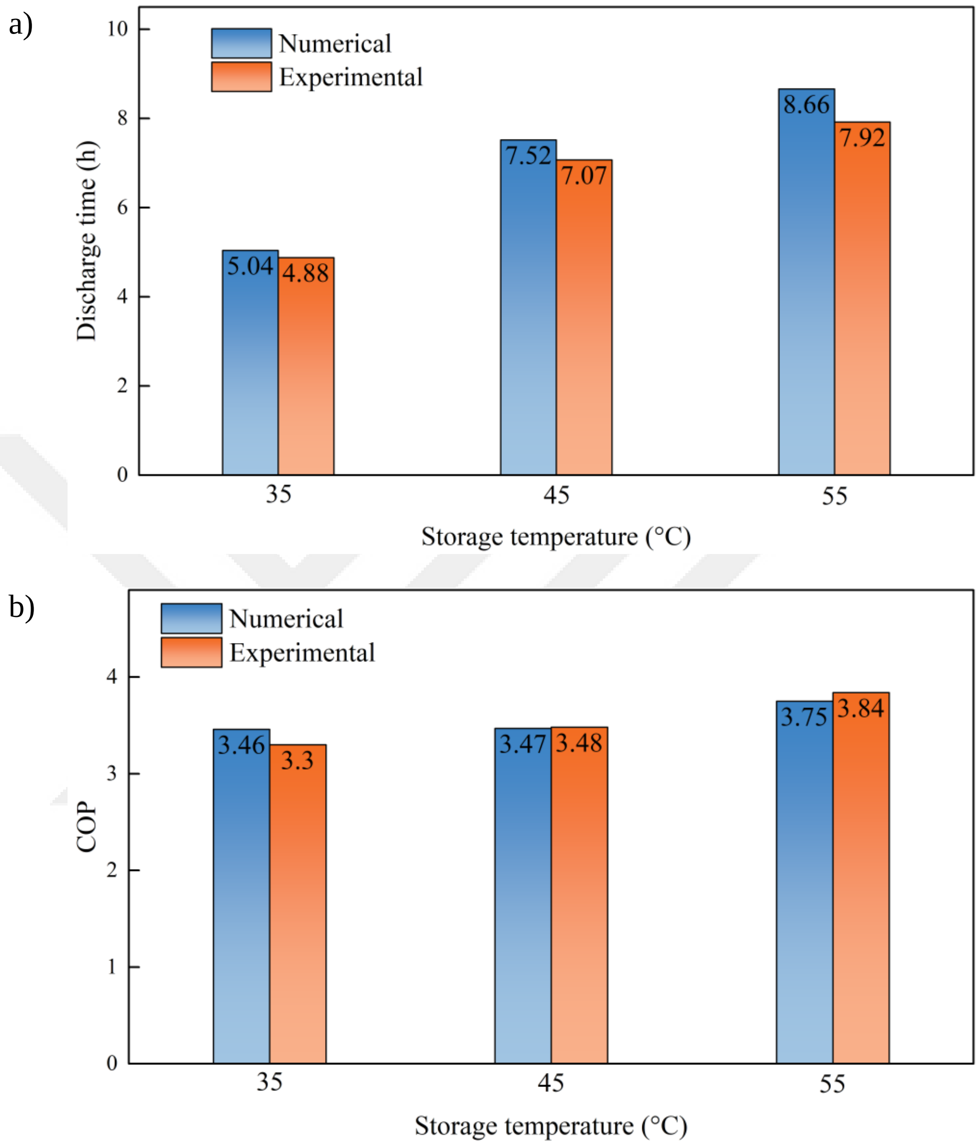

Figure 3.25. Comparison of system operation times and *COP* in discharge process using PCM at different storage temperatures

3.4.5. Validation of the Model Established for System-2

Similar to the numerical model established for System-1, another numerical model was created for System-2 considering the experimental data, as previously presented. The credibility of the established numerical model was tested comparing the numerical and experimental results in terms of temperature variations of the water and PCM in the tank, as well as thermal charge and discharge times. First, the variations of water temperature inside the TES tank (T_8) were presented in Figure 3.26 in terms of numerical and experimental outcomes when the discharge rate was 4.4 kW. As obviously seen from the figure that the temperature variations were overlapping in the majority of the thermal charge process, i.e., when the temperature was increasing from 35°C to 55°C. A slight deviation was seen which can be attributed to the intense exchange of latent heat which slows down the rapid temperature rise. In addition to that, a deviation was noticed just after the discharging process starts, namely after the temperature reached T_8=55°C. The reason for this deviation was the time taken for opening the vanes for the discharge process in laboratory conditions. Nonetheless, the temperature values became also remarkably consistent once the discharging process started, until it ended.

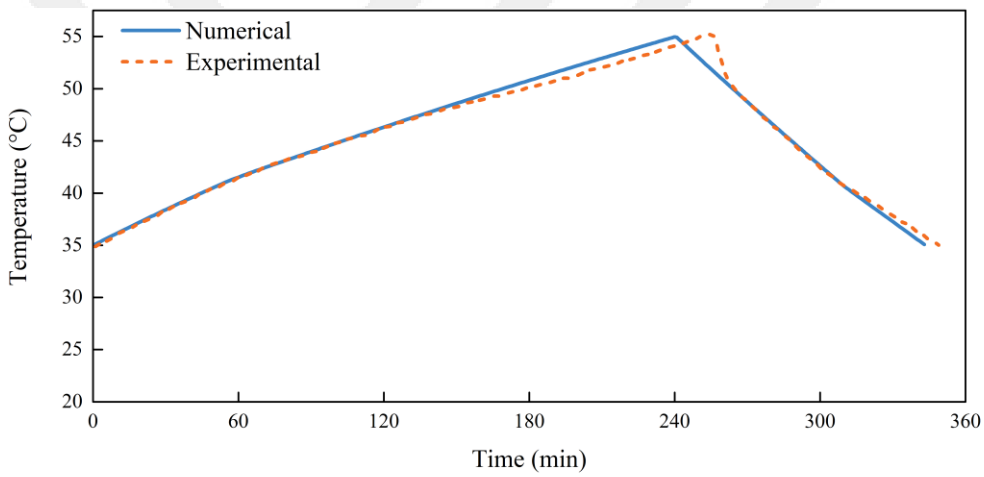

Figure 3.26. Comparison of numerically and experimentally obtained TES tank water temperatures

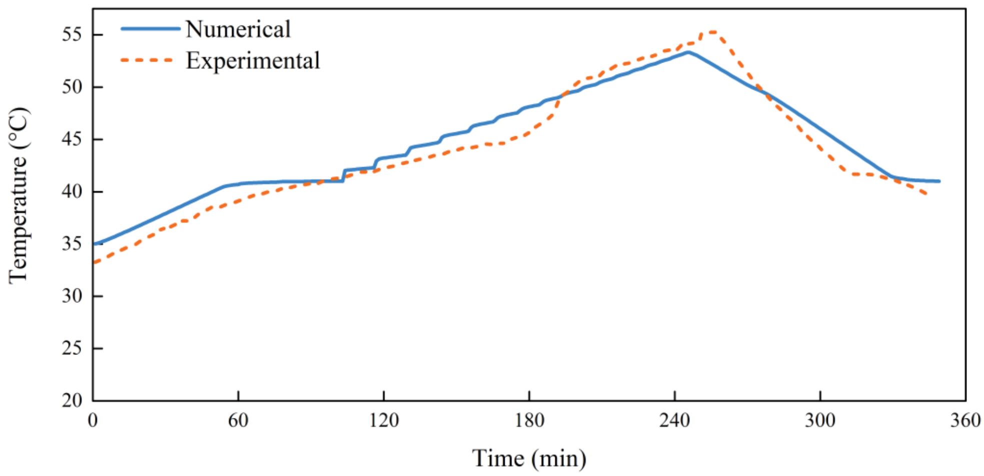

Figure 3.27. Comparison of PCM temperatures during thermal charge and discharge

Comparison of the variation of PCM temperatures in was given in Figure 3.27. As seen from the variations of the temperatures obtained by the experimental results and numerical model, it can be interpreted that the trends of the temperature curves are considerably consistent in both charging and discharging periods including phase change intervals, and it should be noted that the maximum discrepancy was around 3 K at specific time interval which was no longer than 5 minutes, while the average discrepancy throughout the whole process was 0.68 K.

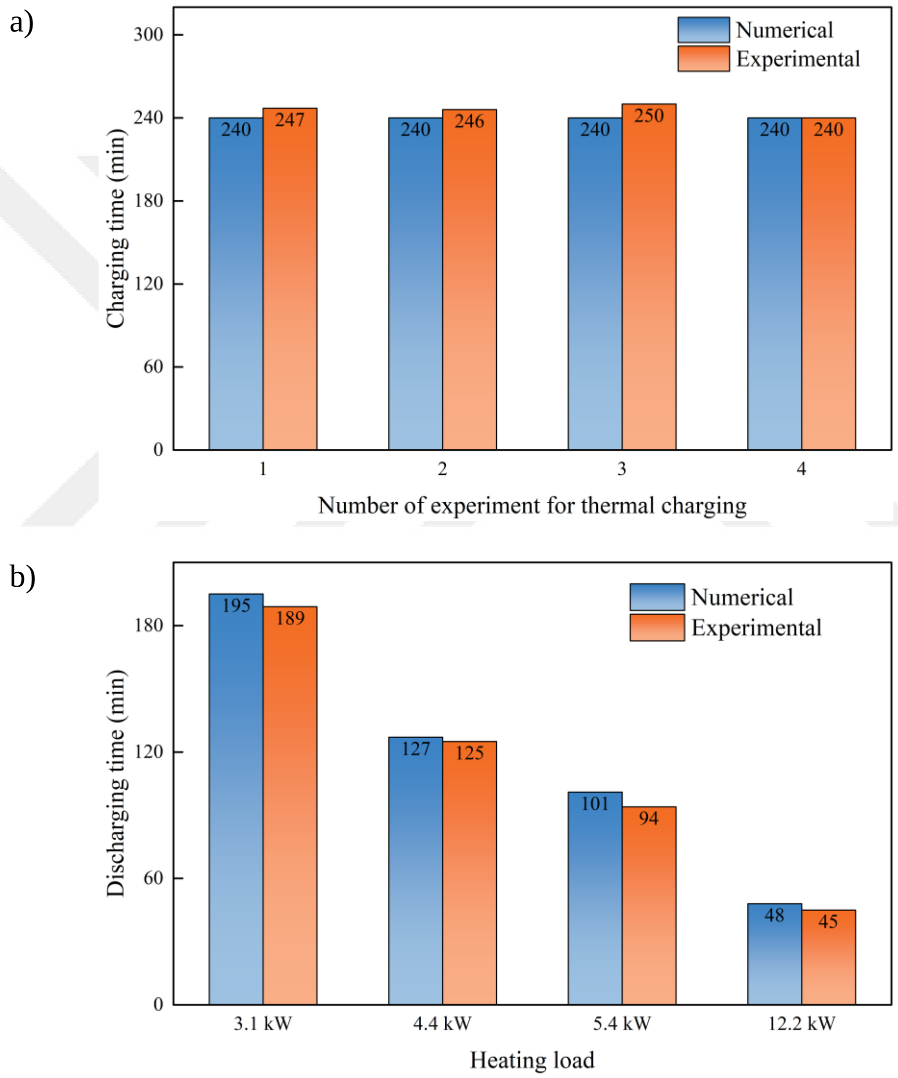

Figure 3.28. Comparison of thermal charging and discharging times of TES tank in case of using PCM

As another crucial point, the thermal charging and discharging times of the TES unit were compared where the results were presented in Figure 3.28. The charging times computed by the numerical code were not dependent on the case and they were all 240 minutes since the heat pump performance was evaluated and implemented into the numerical computations by the aid of experimentally obtained data, as also indicated by several works (Murphy et al., 2013; Patel et al., 2018; Simon et al., 2016). On the other hand, the charging times in practical test conditions varied from case to case due to the laboratory conditions. Nevertheless, these differences reached only up to 10 minutes maximally that corresponds a deviation of 4.2%. Considering the discharge temperatures shown in the figure, it can be observed that the values are remarkably consistent with each other with a deviation involving couple of minutes. Although the differences are within a few minutes, the percentage deviation was calculated to be between 1.6% to 7.4%, which are also in acceptable ranges.

4. RESULTS AND DISCUSSION

Integrated with thermal energy storage unit, two different heat pump systems were investigated within this thesis work where one of the systems uses thermal energy storage unit as a heat source at the evaporator side (System-1), while the other system uses it as a heat sink to store the thermal energy before final use (System-2).

Prior to the experimental studies, a CFD study was conducted to select a tube geometry from two alternatives available in the market, which are standard steel tube with straight wall and corrugated-wall steel tube. Hence, a set of CFD simulations were carried out in simplified domains, and the results including heat flux, heat transfer rate, and liquid fraction were obtained and discussed. Thereafter, the thermal energy storage unit was integrated to the existing heat pump experimental rig to create the layout of System-1. After completing the experiments regarding the PCM existence, i.e., PCM and no-PCM cases, the layout of the experimental rig was switched to the configuration of System-2 by the modifications in the assembly. By the time the experiments were conducted in a similar way, the experimental data obtained from both systems were used to establish the mathematical models of each system.

4.1. CFD Studies for Tube Selection

The selection of the appropriate geometry for PCM container was based on two alternatives available in the market, which are namely a standard straight-walled tube and a corrugated-wall tube. In order to provide an insight to their effects on the thermal behavior of the PCM in case of a heat transfer fluid flow around their body, a set of CFD analyses were carried out. Considering that the thermal energy storage tank used in the study was significantly large and require a remarkable amount of computational cost, the simplified models were established. These models include the crossflow situation and axial flow direction situations, which are named as crossflow and axial flow cases considering that the PCM containers were placed vertically in the fluid domain. In fact, a more complex flow structure was already expected inside the TES tank. Thus, to observe the fluid flow and thermal behaviors in a simplified way, these two different configurations were taken into account. Three different mass flow rates ($\dot{m}$=0.45, 0.90, and 1.80 kg/s) at the inlet of the domains were taken into consideration for the simulations regarding the expected fluid velocities inside the tank. Both melting (thermal charging) and solidification (thermal discharging) conditions were numerically analyzed, hence, the inlet temperatures were taken as 45°C (318.15 K) and 10°C (283.15 K), respectively, for melting and solidification cases. The reason for the selection of the temperatures is that the medium thermal storage temperature is specified as 45°C for the study, while the return temperature from the evaporator was assumed to be around 10°C.

4.1.1. Thermal Charging and Discharging Behavior in Crossflow Orientation

Evaluation of the thermal behavior of the PCM was evaluated over the average heat flux and heat transfer rate values along the tube walls with respect to elapsed time in the process, and their effects on the liquid fraction evolution of the PCM was discussed. The aforementioned heat flux, heat transfer rate, and volume fraction variations were presented in Figure 4.1. As clearly noticed from the set of figures, the heat flux values on the walls of both tubes exhibited a significant increase in the first quarter of the process, especially the standard tube, and then it started to decrease until the end of melting, which was due to the temperature difference between the tube walls and the heat transfer fluid that was first large and then decreased through the end of the process. Strikingly, heat flux values of the standard tube were found to be significantly large compared to those of corrugated tubes in the crossflow case. This may indicate that the fluid flow could not beneficially affect the heat transfer between the heat transfer fluid (HTF) and PCM tube wall. In a clearer explanation, the corrugated structure of the tubes may decrease the effectiveness of the convective heat transfer due to deteriorating flow patterns of the HTF around the tube wall. Therefore, the average heat flux value, which is directly related to the convective heat transfer coefficient, of the standard tube could become 1.5 times higher than that of the corrugated tube within the first half of the melting process. Considering the effect of inlet mass flow rate, it can be deduced that it had a slight effect on the heat flux. Nonetheless, it is also evident that increasing mass flow rate increased heat flux values throughout the melting process.

Apart from the heat flux values, the heat transfer rate is an important and determinative parameter for the thermal charging process of the PCM because it indicates the amount of energy transferred from the HTF into the PCM located inside the tubes. Here, the beneficial effect of increased surface area of the corrugated tubes on the thermal performance was profound, as seen from Figure 4.1b. Even though the heat flux values were higher for the standard tube, it was evidently noticed that the increased surface area of the corrugated tubes provided remarkably higher heat transfer rate through the tube walls in the beginning of the process, as can be seen from the scale-up portion of in the figure. Thereafter, the rate of heat transfer through the corrugated walls decreased and became lower than that of the standard tube, which can be attributed to the higher natural convection effects inside the standard tubes once relatively larger portion of the PCM was melted.

As one of the most important parameters in thermal charging and discharging processes, the liquid fraction evolution for the two types of the PCM tubes was given in Figure 4.1c. The high heat transfer rate through the corrugated walls at the beginning of the process remarkably affected the variation of liquid fraction with respect to time. Since the heat transfer was significantly higher in corrugated tubes, the solid PCM, especially near the corrugated inner walls, rapidly melted. The effect of remarkably large thermal energy input in the first quarter of the process resulted in a higher melting rate inside the corrugated tubes. Although the total melting times were significantly close to each other, which were around 20 minutes, the melting rates of the corrugated tubes were higher. In addition, this phenomenon became more profound when the mass flow rate was increased. This can be also noticed from the scale-up portion. The liquid fraction of the PCM in the corrugated wall tube is noticeably higher until the end of the process when the mass flow rate was 1.80 kg/s. Therefore, even though the heat flux values on the walls of the standard tubes were higher, the liquid fraction values of the PCM located inside the corrugated tube were noticeably higher. Since the liquid fraction evolution is a solid indicator for thermal energy storage performance, it can be inferred that using the corrugated wall tubes are more beneficial in terms of thermal energy storage. More importantly, in thermal energy storage systems, the phase change processes can occur partly, which means that thermal charging or discharging may have to be ceased or stopped due to the other circumstances such as heat source or heat sink conditions.

a)

b)

c)

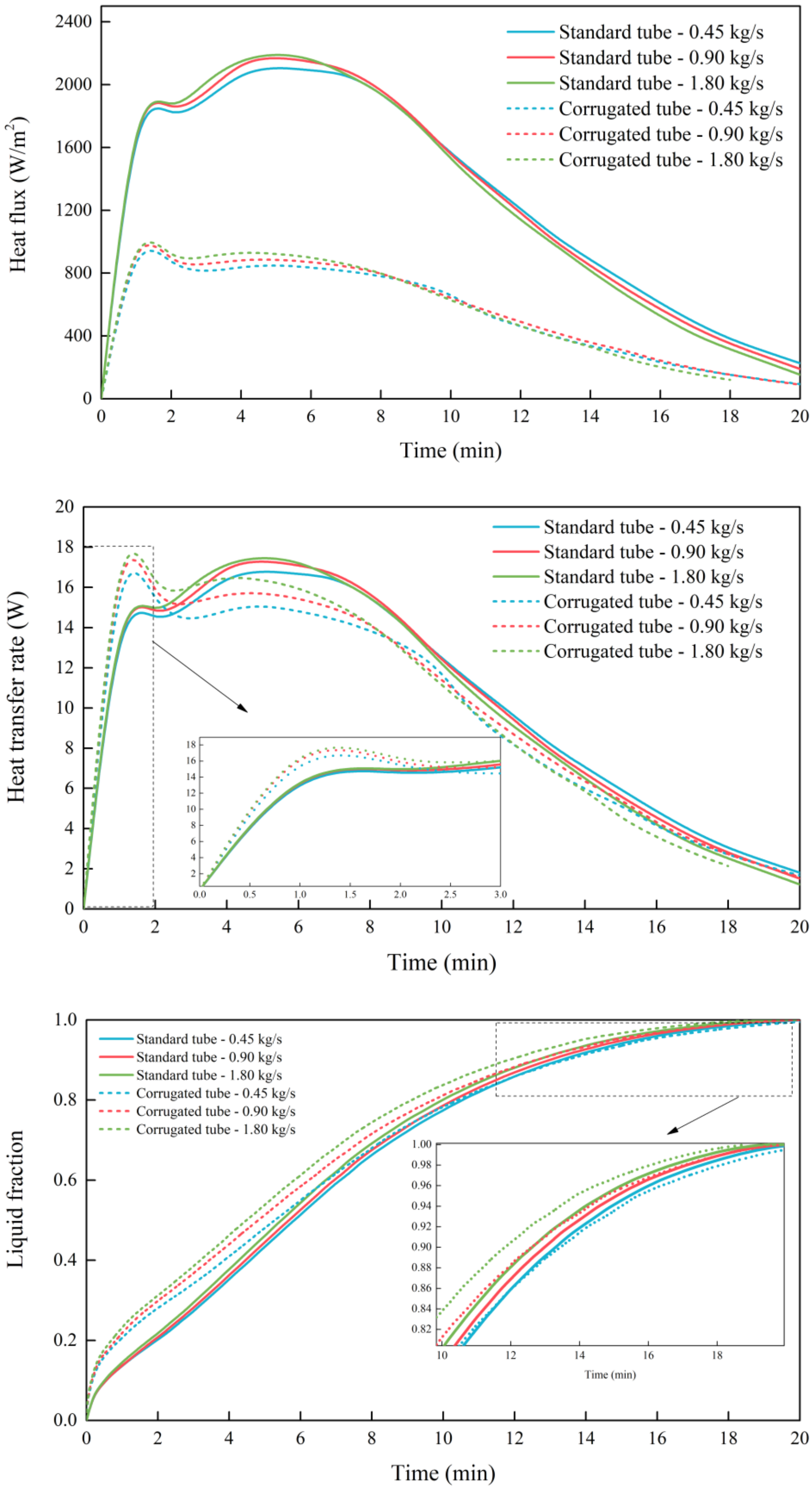

Figure 4.1. Variation of a) average heat flux, b) average heat transfer rate at the tube walls and c) average volume fraction of PCM in the tubes at different mass flow rates in crossflow orientation during thermal charging

To present a numerical result deduced from the aforementioned figure, the PCM inside the corrugated wall tube would store 3.3% more thermal energy compared to the PCM inside the standard straight-walled tube when the process was stopped after 10 minutes, meaning that 50% of the process. Considering a cease of process after 5 minutes from the start, which means the 25% of the process, this ratio would be 9.0%. At this point, the energy storage at a specific time could be higher using corrugated wall tubes. Nonetheless, the corrugated walls could be recommended to be designed at the inner side only with a straight outer wall of the tube, in order to prevent the deterioration of the fluid flow outside, which leads to a decrement in the heat flux.

Thermal discharging process which includes the solidification of the PCM inside the tubes is as crucial as melting process since it is also a significative point for effective utilization of latent heat. The numerical outcomes, namely the heat flux (a), heat transfer rate (b), and liquid fraction (c), were presented in Figure 4.2 for the thermal discharging process. Similar to the charging process, a significantly high heat flux was computed, which was caused by the difference between the inlet temperature of the HTF and the initial temperature of the PCM. When these temperature values became closer to each other, the heat flux values also decreased by time. In the same manner of the deduction made for melting process, the heat flux values were also larger when standard tubes were utilized as PCM container, compared to the corrugated ones, and this situation lasted till the end of the solidification process that took around 100 minutes.

As the heat transfer rates were examined, it was clearly seen that the corrugated tubes were superior in the beginning of the process until the first 25% of the period. Thereafter, the heat transfer rates at the walls of the standard and corrugated tubes were almost the same apart from insignificant differences. Therefore, considering the total thermal energy transfer, the corrugated tube walls became advantageous in the majority of the solidification period.

Reflection of the energy transfer to the thermal energy storage over the entire solidification process was shown in Figure 4.2c by liquid fraction lines. Similar to the liquid fraction curves in melting case, they exhibited noticeable differences between the standard and corrugated tubes. The high thermal energy input in the first era of the process was remarkably higher for corrugated tubes, thanks to its large surface area, and this resulted in an accelerated solidification process. Nonetheless, there was no significant difference observed in the total solidification times. Yet, the corrugated structure of the tubes can bring a considerable advantage when a partial energy storage would be the case. For example, when 50 minutes were elapsed in the solidification period where the mass flow rate was 0.90 kg/s, the liquid fraction of the standard and corrugated tubes were respectively 15.4% and 12.6%. This means that there would be a difference of 3.3% in the discharged thermal energy when the process was somehow stopped at this time. This ratio would be 5.7% when the process was ceased after 30 minutes of its start.

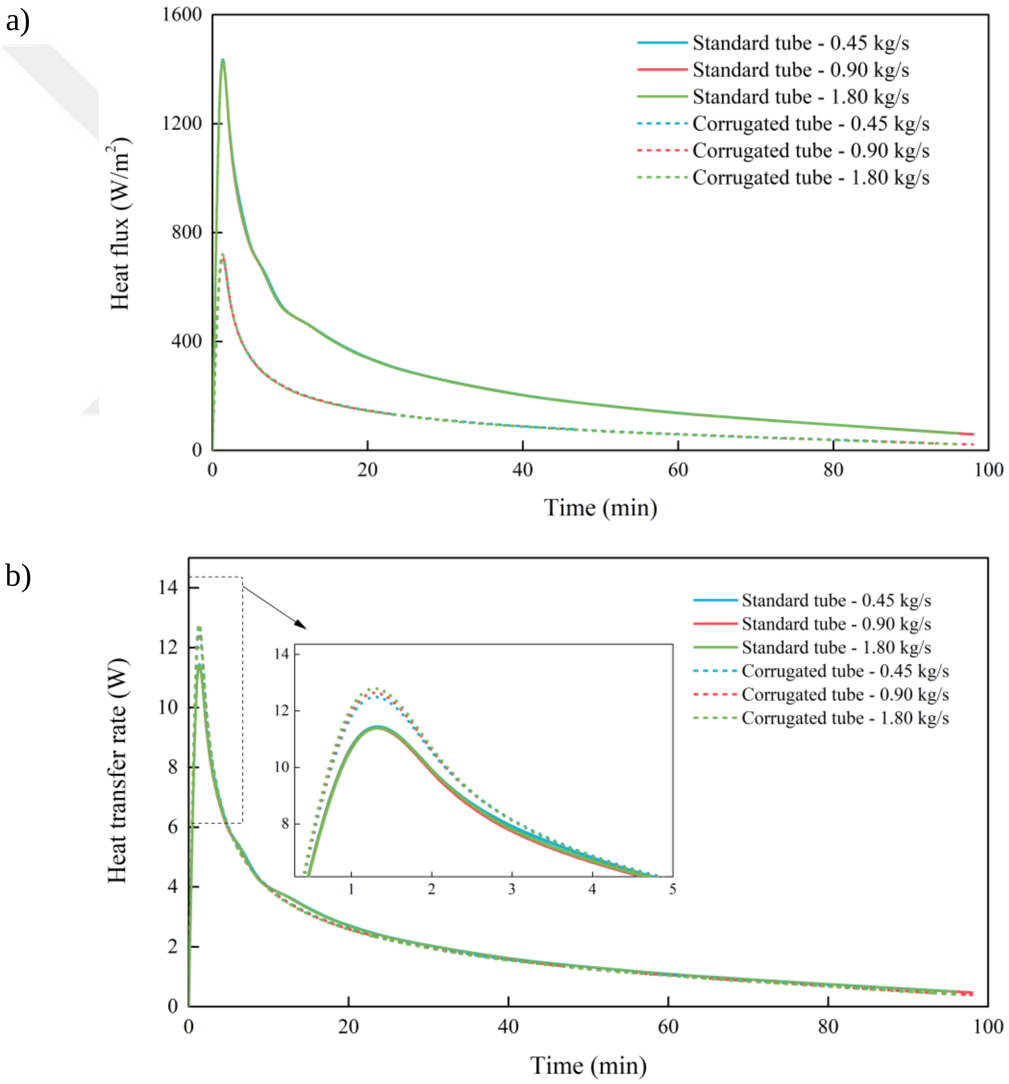

Figure 4.2. Variation of a) average heat flux, b) average heat transfer rate at the tube walls and c) average volume fraction of PCM in the tubes at different mass flow rates in crossflow orientation during thermal discharging

c)

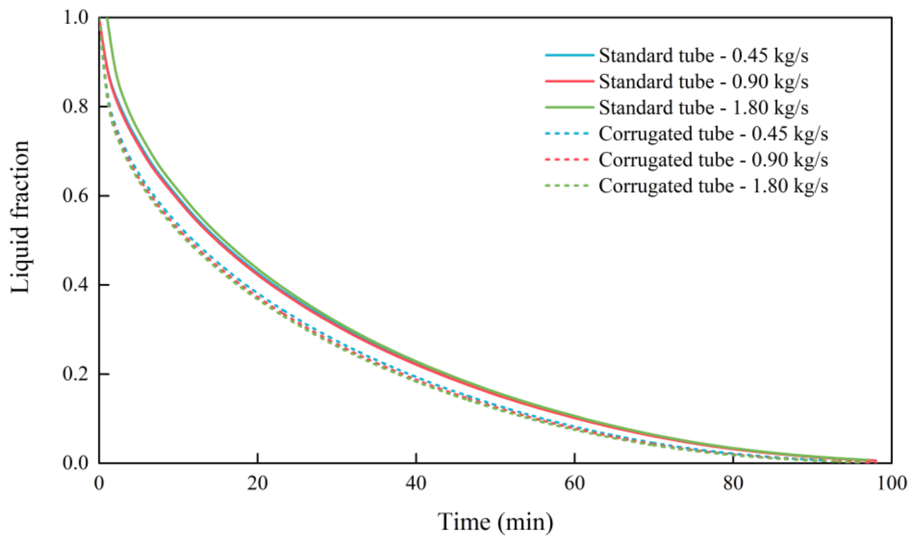

Figure 4.2. (Continued) Variation of a) average heat flux, b) average heat transfer rate at the tube walls and c) average volume fraction of PCM in the tubes at different mass flow rates in crossflow orientation during thermal discharging

4.1.2. Thermal Charging and Discharging Behavior in Axial Flow Orientation

The fluid flow around the PCM tubes inside the TES tank can be expected to be considerably complex where the fluid elements flow in rapidly changing various directions. Hence, the fluid flow around the tube walls and its effect on the phase change behavior of the PCM was investigated in two directions, namely in crossflow and axial flow, in a simplified way. Equivalent to the presentation structure of the crossflow case in the previous section, the heat flux, heat transfer rate, and liquid fraction variations with respect to time were illustrated and discussed in this part.

Starting with the thermal charging process, the variations of the aforementioned parameters, heat flux, heat transfer rate, and liquid fraction, were given in Figure 4.3. Evaluating the heat flux values, it was noted that the average heat flux variation on the wall of the standard straight-walled tubes was higher, compared to that of corrugated tubes, throughout the process. However, the difference between the values of standard and corrugated tube was lower in axial flow orientation, compared to crossflow one. Although the heat flux values of the standard tube were approximately 1.5 times higher than those of corrugated tube in crossflow orientation, this difference reached only up to 60%.

Related to the relatively lower difference in the heat flux values together with the high surface area of the corrugated tubes, the total heat transfer rates on the corrugated walls were found to be considerably higher, compared to those on standard tube walls. Besides, it should be highlighted that the heat transfer rates for the corrugated tubes were higher almost in the whole process, as seen from the figure, which clearly ensured a larger thermal energy transfer into the PCM. Quantitatively, the heat transfer to the PCM was about 70% higher for the corrugated tubes compared to standard straight ones in the initial steps of the process. Then, the difference was slowly decreased as the time elapsed. Yet the total heat transfer rate through the corrugated tube walls was about 30% higher in the halfway of the process, and it was 10 to 20% higher through the end of the process. The reason can be interpreted by the relatively complex flow adjacent to the corrugated tube walls, compared to the standard straight walls, especially in the grooves, which can contribute to the complexity of the fluid patterns. Hence, convective currents can be intensified in these locations due to the highly turbulent flow. This results clearly showed that a larger heat transfer can be attained by using corrugated wall tubes; hence, a higher melting rate was expected.

Liquid fraction curves shown in Figure 4.3c clearly justified the phenomenon occurred adjacent to the corrugated walls. Compared to the crossflow orientation, a larger difference between the liquid fraction curves of the two investigated tubes was pronounced. From the beginning to the end of the melting process, the PCM in the corrugated tubes had a higher melting rate due to the higher heat transfer because of the increased surface area and relatively more complex flow structure, as discussed in the previous paragraph. The total melting time of the PCM filled into the corrugated tube was remarkably low compared to the standard straight tube. The total melting time of the PCM in the corrugated tube and the standard straight tube were 12.3 and 17.8 minutes, respectively, which denotes that the melting time in the standard tube was 44.6% longer. Considering the partial melting at some specific points, the liquid fractions after the first five minutes of the process (t=5 min) were 0.41 and 0.56 for the standard and corrugated tubes, respectively. At t=10 min, these values were 0.72 and 0.94. This clearly proved that corrugated tubes would be remarkably superior to the standard tubes for both fully- and partially completed melting processes.

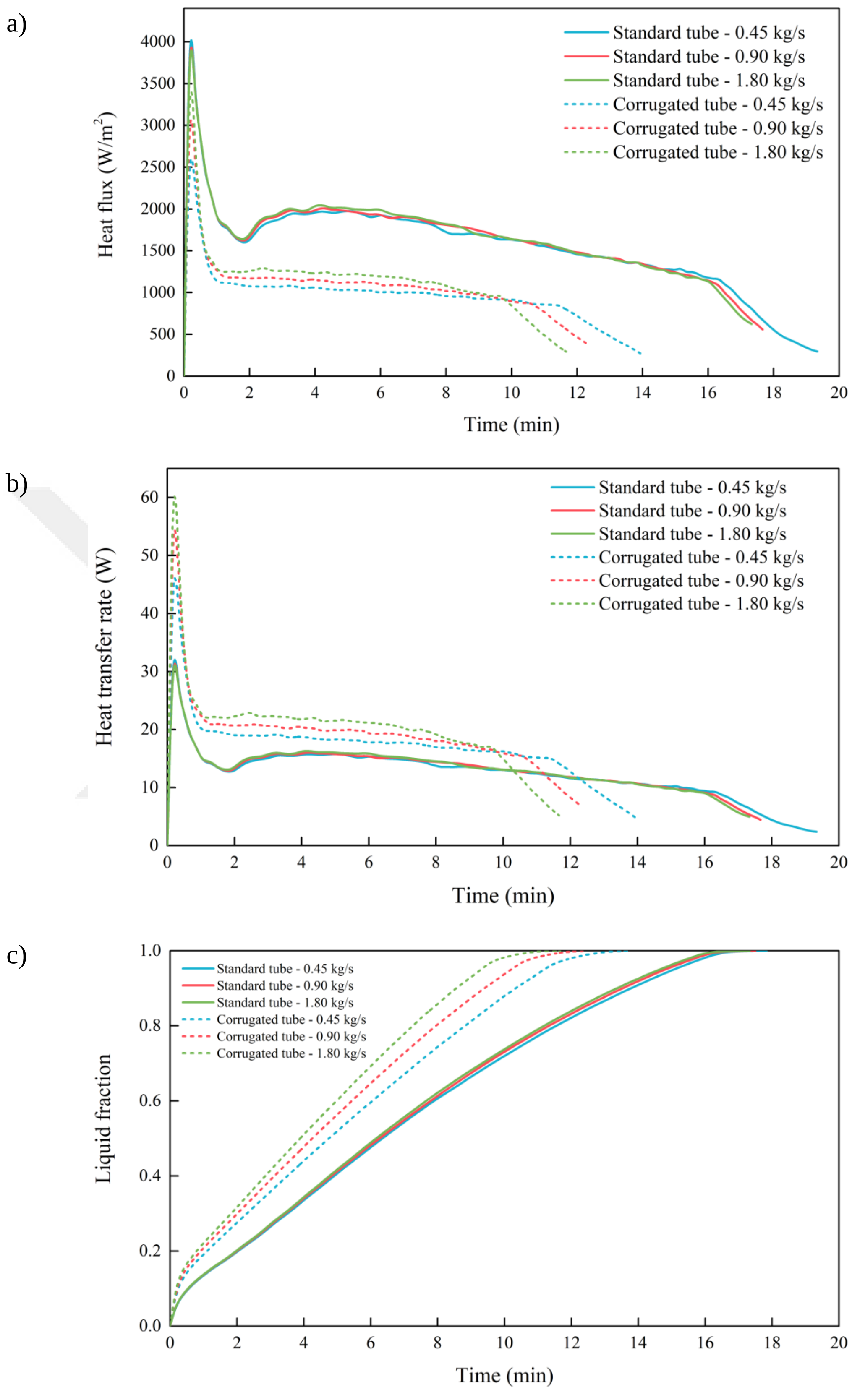

Figure 4.3. Variation of a) average heat flux, b) average heat transfer rate at the tube walls and c) average volume fraction of PCM in the tubes at different mass flow rates in axial flow orientation during thermal charging

Variation of the aforementioned three parameters were likewise given in Figure 4.4 for thermal discharging process. Starting with interpretation of heat flux values, it was evidently noticed that the heat flux values obtained for the standard straight tube were remarkably higher, compared to those of the corrugated tube walls. This situation was also similar in melting process, however, in solidification it was more pronounced due to the slight natural convection effects. Especially in the first minutes of the process, the difference reached up to two folds, yet this difference decreased as the progress continued. As the temperature gradient between the water and the tube surface decreased by time, the heat flux values also decreased, and the average heat flux on the standard and corrugated tube walls became closer to each other.

From the scale-up portions of the curves given for heat transfer rate in the figure, it was noticed that the rate of heat transfer was considerably high within the first minutes of the process when corrugated tubes were used instead of standard straight tubes even though the heat flux values were found to be higher. The significantly larger surface area of the corrugated tubes attained a higher heat transfer rate from water through the PCM, which consequently contributed to the energy release during the solidification process. Almost a two-fold difference was observed meaning that there was an energy transfer through the PCM twice as much compared to standard straight tubes. Hence, this situation led to a fast initiation of the phase change process. Thereafter, it was noticed from the figure that the heat transfer rate values on the corrugated tube walls were still above those of the standard tube at a rate around 5% to 20%.

Even if the difference between the heat transfer rate values decreased as the time elapsed, the effect of high heat transfer on the liquid fraction curves continued. A higher solidification rate was obtained for the PCM located in the corrugated tubes, initially, and this continued until the end of the process, providing a lower liquid fraction value at a given temporal point. The difference between the full solidification times was around 4% to 6%, depending on the mass flow rate. More importantly, in case of an incomplete solidification or a cease of process, the PCM in the corrugated tube would definitely release higher amount of energy.

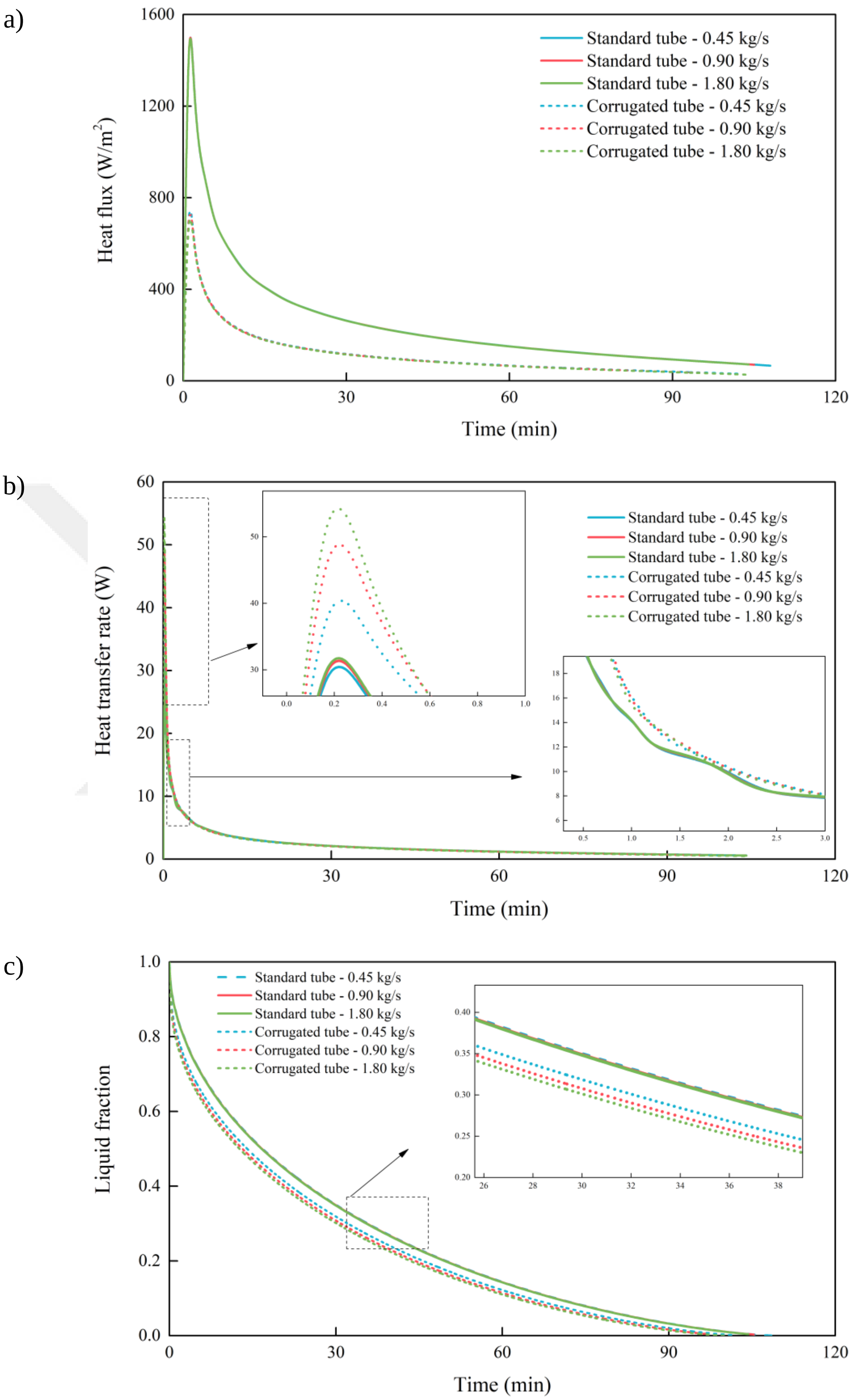

Figure 4.4. Variation of a) average heat flux, b) average heat transfer rate at the tube walls and c) average volume fraction of PCM in the tubes at different mass flow rates in axial flow orientation during thermal discharging

To sum up, using corrugated PCM tubes to contain the PCM inside the TES tank may cause a decrease in the heat flux, or similarly convective heat transfer coefficient, as the corrugated surface may restrict the fluid flow compared to the straight surface of standard tubes. Despite this adverse effect, the heat transfer rate through the surface of the corrugated tube is relatively larger and it affects the phase change rate in a beneficial way. Hence, using corrugated tubes is suggestible for similar engineering application, nevertheless, a straight outer surface and corrugated inner surface would be a more advantageous design. In addition to the obtained results, it is worth noting that the average convective heat transfer coefficient along the tube surface was found to be around 3000 W/m^{2}K which was later used in the established mathematical model of the TES integrated heat pump systems.

4.2. Experimental Studies for System-1

The tests for the layout of System-1 starts with a charging process of the solar collector tank (SCT) and thermal energy storage tank (TES) controlled by an electric heater. The process starts from T_8=20°C and lasts when T_8 reaches desired storage temperature, i.e., T_8=T_{st}=35°C, 45°C or 55°C. Thereafter, the heat pump is activated which uses the TES unit as a heat source, and the discharging process is started. For the discharging cases, five different volume flow rates of the heat transfer fluid at the condenser side ($\dot{V}$=400, 600, 800, 1000, and 1200 L/h) are considered, which represent different heat loads ranging from 1.4 kW to 3.8 kW. The process is finished when the TES tank temperature reaches down T_8=20°C.

4.2.1. Temperature Variations in the TES Tank without PCM

The temperature variation inside the thermal energy storage tank is shown in Figure 4.5 for different flow rates in the case of no PCM existence in the TES tank at T_{st}=45°C. The solid lines represent three of the temperature sensors gradually located in axial direction (T_5, T_8, and T_{11}), while dashed lines represent the sensors in radial directions (T_{14} to T_{18}). As seen from the figure, the temperature variations exhibited slight differences in both axial and radial directions in the cases of the lowest, the median, and the highest flow rates.

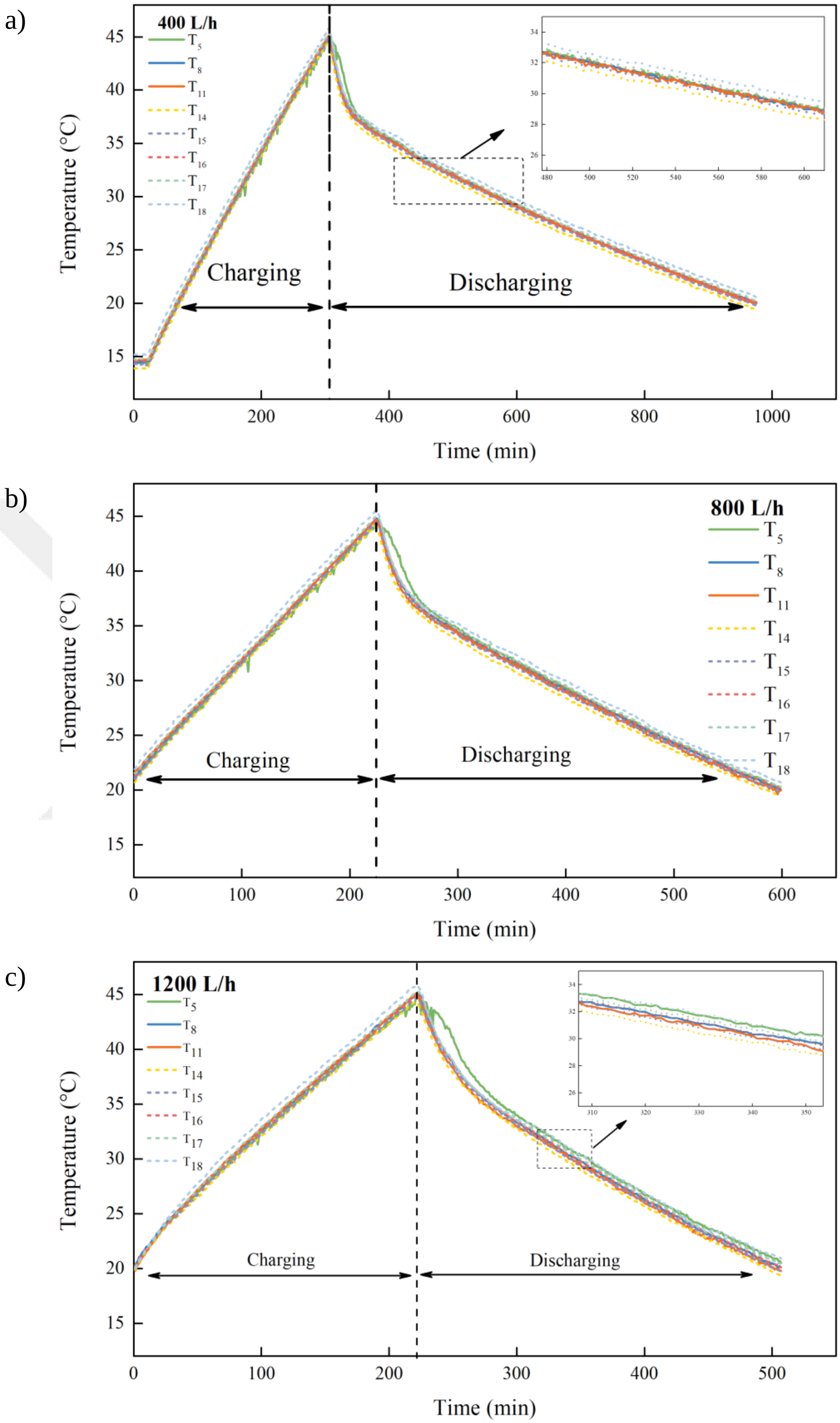

Figure 4.5. Temperature variations in the TES tank at different locations obtained by experimental measurements

Focusing on the close-up portions of the figures, the maximum difference between the highest and lowest temperatures inside the tank is about 1°C, which was caused by the fact that some of the sensors are close to the inlet and outlet ports where the hot or cold fluid stream is stronger. Yet, the temperature distribution inside the tank was relatively uniform. This outcome evidently showed and proved that the water inside the tank can be regarded as a lumped system, regardless of the heat load variation which affects the thermal discharge from the tank. In addition to this deduction, it was also seen that the charging time from the reference temperature, 20°C, to the storage temperature considered in this case (T_{st}=45°C) was about 220 minutes for all cases due to electric heating, and the discharging times depended on the heat rejection related to heat load, which ranged from 280 to 700 minutes. It is noteworthy to express that some experiments were started below the considered reference temperature (20°C) due to the ambient conditions, nevertheless, the charging and discharging times were considered with respect to the reference temperature.

4.2.2. Temperature Variations in the TES Tank with PCM

Comparing the PCM temperatures in axial direction in two different tubes at T_{st}=45°C, Figure 4.6 shows the temperature variation of PCM-1 & PCM-3 as well as PCM-6 & PCM-8. It is worth noting here that the PCM-1 & PCM-3 represent the temperature measurements from the tube located near the solar collector tank inlet/outlet sections, and PCM-1 represent the temperature at the upper part of the tube (H/3), while PCM-3 shows the temperature at the lower part of the same tube (2H/3). This is also the same for PCM-6 & PCM-8.

As the whole tank was electrically charged with a high flow rate and relatively high electric power, there was no noticeable difference in the PCM temperatures during charging process. It was noted that the PCM temperatures exhibit a variation in their trend indicating their melting process, and thereafter, their temperature rapidly become similar to that of water, pointing out that the melting process ends, and sensible heat is then stored. Here, it can be inferred that all the PCM in the tubes were melted during charging process. Then, discharging process started, and the latent heat utilization became evidently noticeable by the temperature variations during this process. As seen from the figures, the nearly isothermal regions are noticed, especially when the heating load, i.e., the HTF flow rate is low, due to the lower rate of heat rejection by the heat pump which operates in an on/off condition. As the flow rate was increased, the solidification process of the PCM, where the latent heat utilization is profound, became shorter since the test process was ceased when the water temperature T_8 reaches down 20°C. Hence, an incomplete solidification might be observed when the heat rejection is at a high rate. Nonetheless, apart from the individual analysis, the results should be compared to the no-PCM cases in order to reveal the contribution of latent heat of PCM, which was discussed in the upcoming sections.

a)

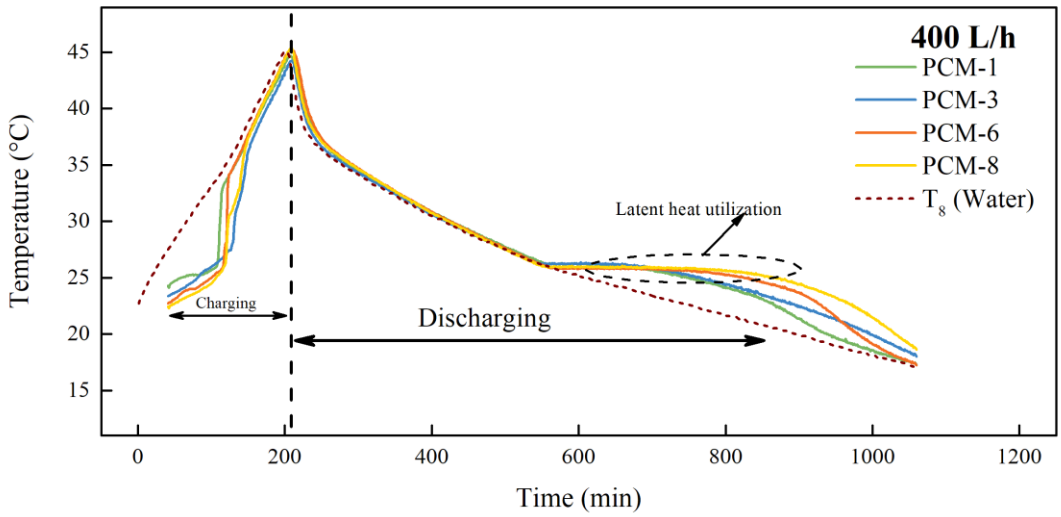

b)

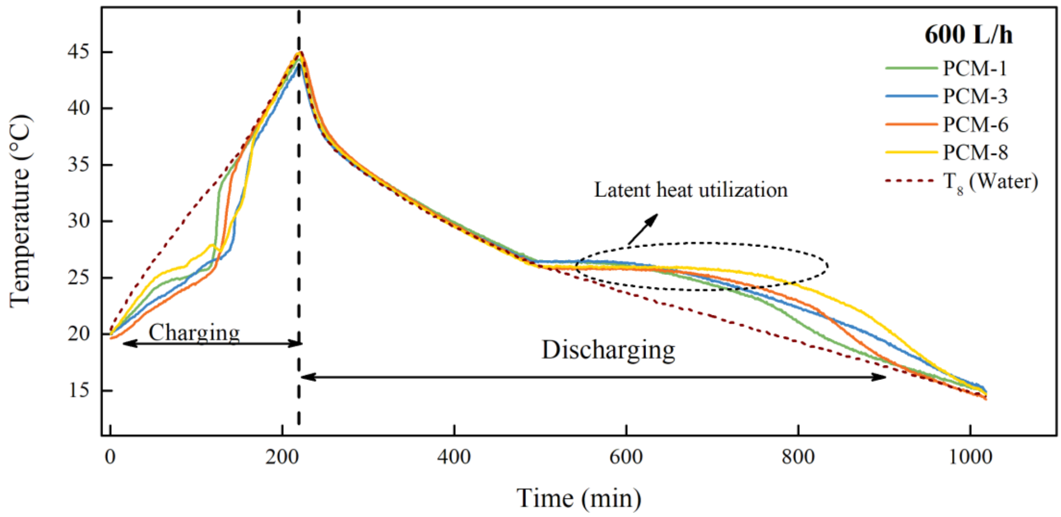

Figure 4.6. Temperature variations of PCM in axial direction regarding measurements

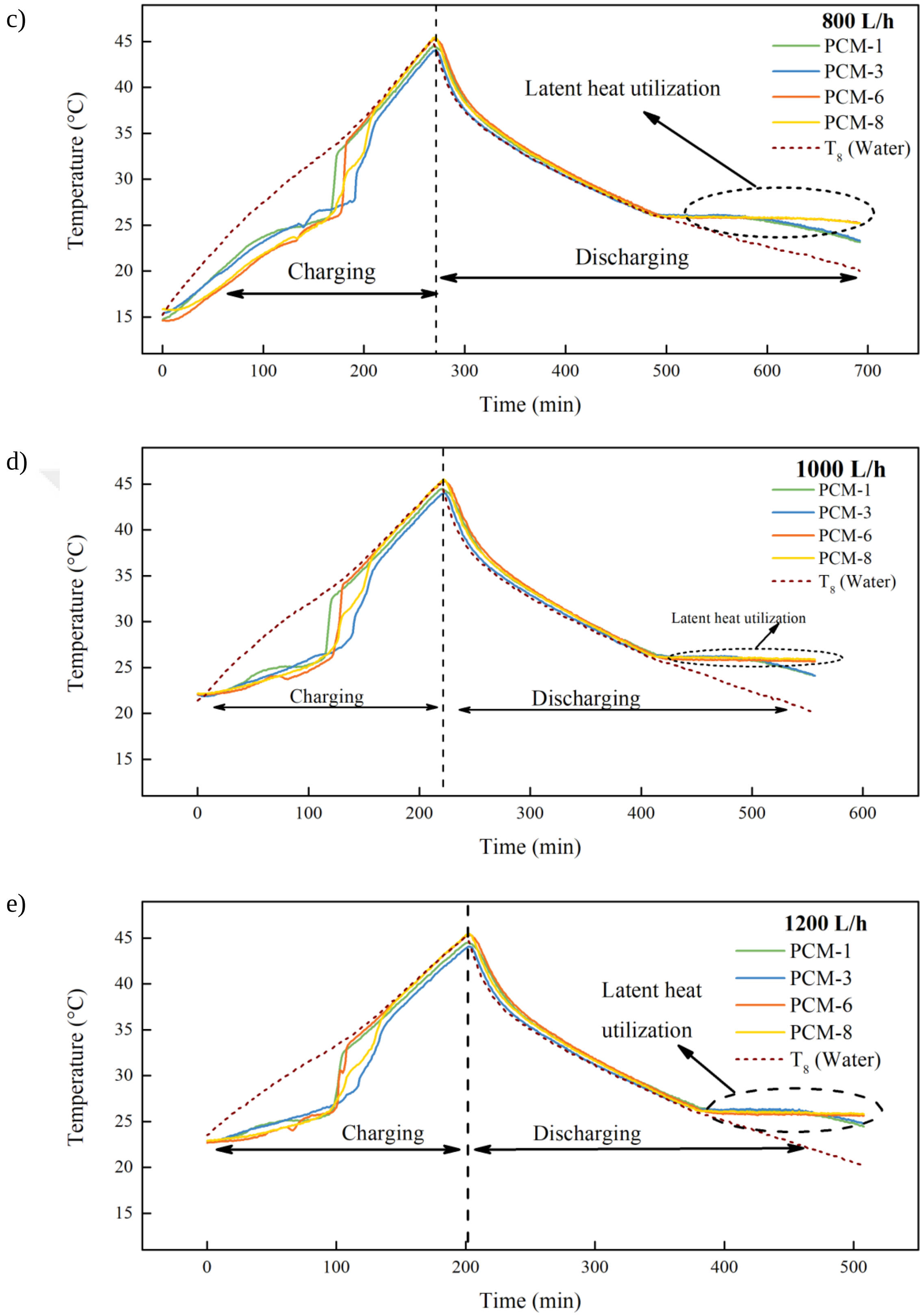

Figure 4.6. (Continued) Temperature variations of PCM in axial direction regarding measurements

Another deduction from the figures can be made upon the PCM tube and sensor locations. The figures show that the solidification of PCM-1 & PCM-3 was slightly more rapid compared to those of PCM-6 & PCM-8. Here, the reason of this small difference can be attributed to the fact that the tube including PCM-1 & PCM-3 was located near the inlet/outlet ports where the fluid velocity was expected to be relatively higher, causing a higher local convective heat transfer coefficient. On the other hand, the tube including PCM-6 & PCM-9 was located at the center region of the TES tank, hence, the fluid velocity is relatively lower since there was no strong fluid stream near the tube. Similarly, solidification process was slightly more rapid at the upper part of the tubes, which was attributed to the fluid stream inside the tank that was assumed to be stronger at the mid and upper parts of the tank due to the locations of the inlet and outlet ports.

Figure 4.7 depicts the temperature variation of PCM in three different tubes located in different parts of the tank for the investigated five flow rate values, together with the water temperature in the TES tank. To recall, PCM-2, PCM-5, and PCM-9 denote the PCM temperatures inside the tubes that are in the region near the SCT inlet/outlet ports, in the central part of the tank, and in the region near CAT inlet/outlet ports. According to the outcomes in the figure, a rapid melting process was seen for the PCM located in all three tubes, and once the melting was completed, the temperatures rapidly reached the TES tank temperature (T_8) with a slight difference. The reason for the slight difference between the temperatures of melted PCM and water is the high thermal conductivity of the steel tubes which leads to an insignificant thermal resistance between the two media. Considering the discharging process, the similar deduction can be made up to the point where solidification of PCM started. At all volume flow rates of the HTF, i.e., heating loads, a distinct isothermal region during the solidification process was observed in all considered three tubes. Yet, regardless of the heating load, the solidification process in the tube indicated by PCM-2 became more rapid, compared to those in the other two tubes. This can be attributed to the stronger fluid stream at the region due to high volume flow rate of water circulating between TES tank and SCT, leading to a higher local convective heat transfer coefficient.

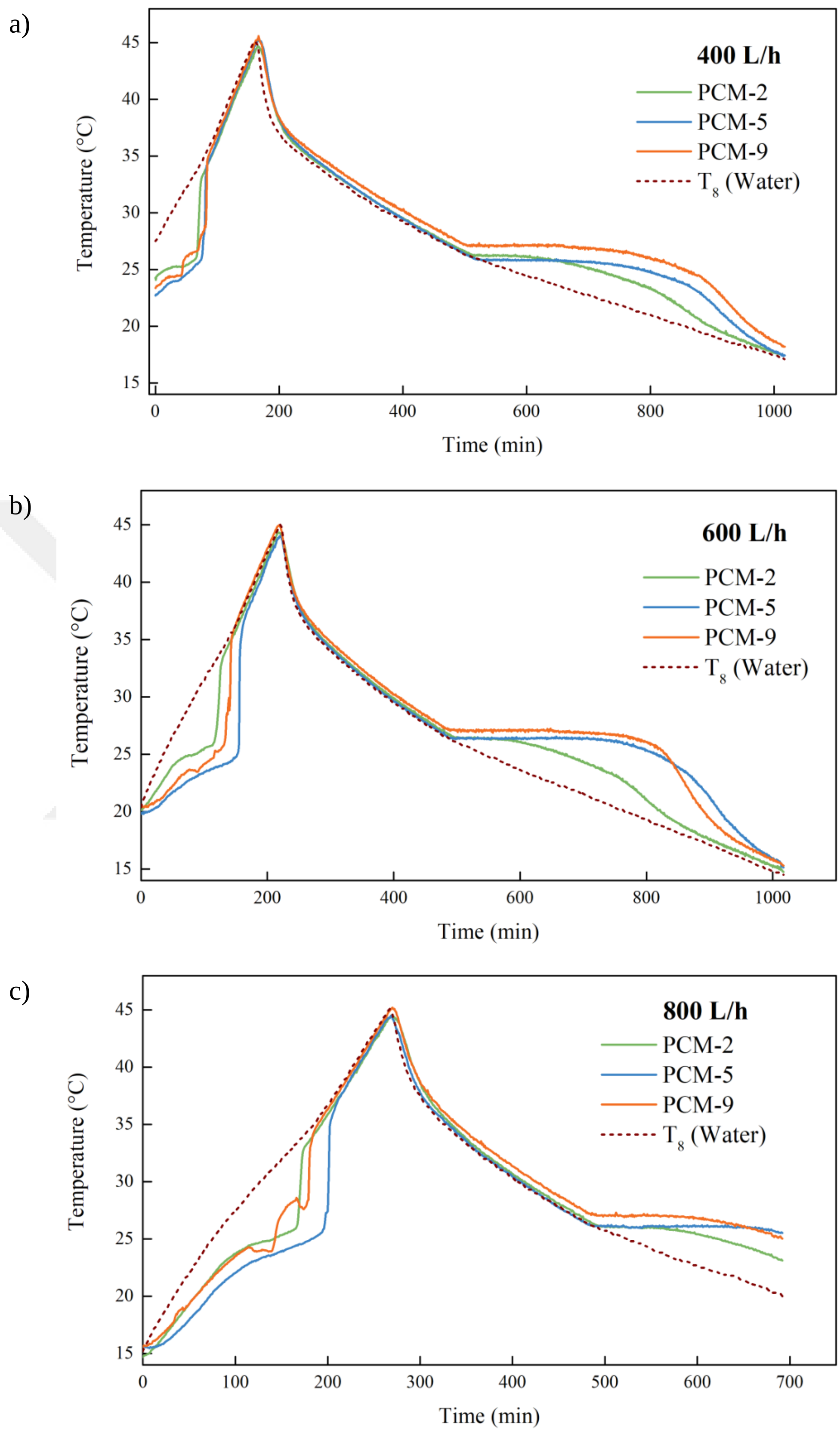

Figure 4.7. Temperature variations of PCM located in different locations of the TES tank

d)

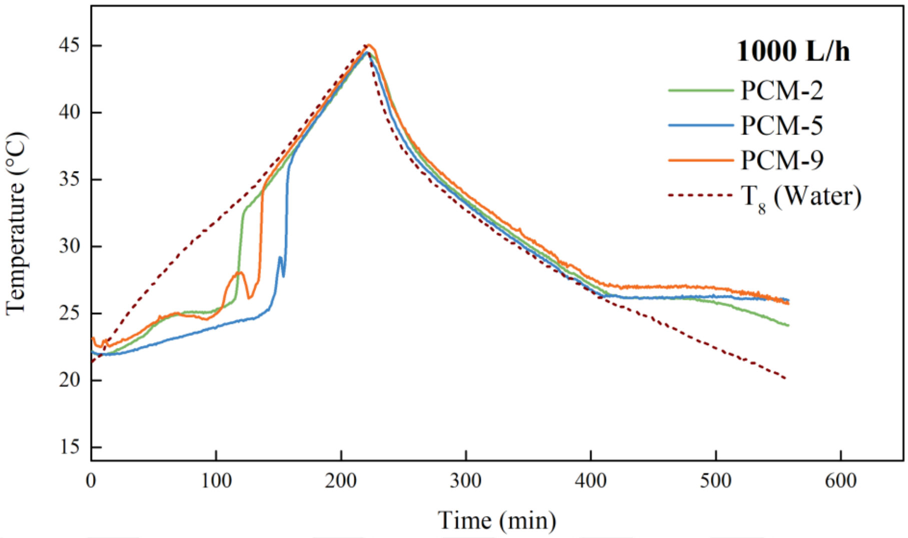

e)

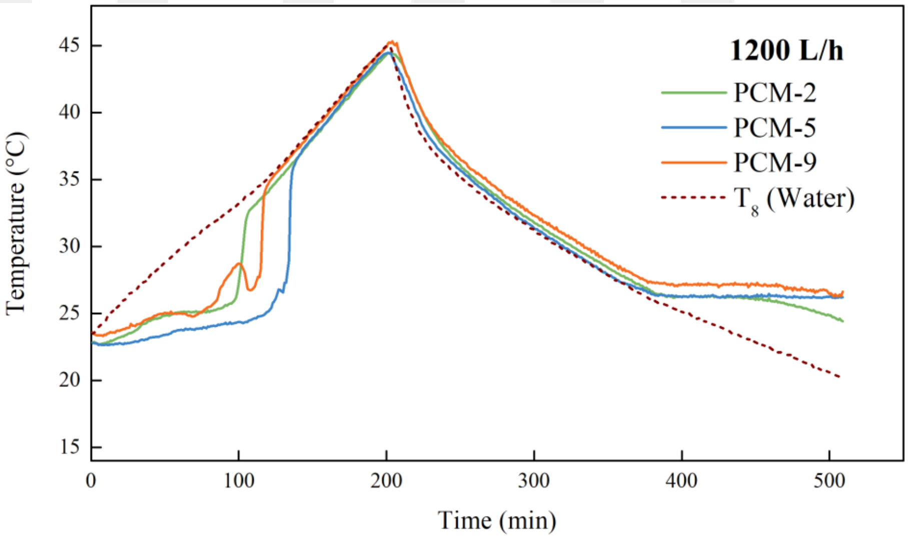

Figure 4.7. (Continued) Temperature variations of PCM located in different locations of the TES tank

Figure 4.8 exhibits the temperature variations of the water in the TES tank and the PCM in different tubes for the investigated storage temperatures, namely T_{st}=35°C, 45°C, and 55°C. The temperature variations do not exhibit a significant difference regarding different storage temperatures. However, it was noticed that, at T_{st}=35°C, the sensible heat storage may be slightly lower depending on the PCM tube location when the storage temperature is considered T_{st}=35°C. Yet, there was no incomplete melting situation at the investigated storage temperatures, especially at the lowest one, which might constitute this risk. However, in practical implementations, the relation between the phase change temperature interval of the PCM and the required storage temperature of the thermal energy storage tank should be attentively taken into account.

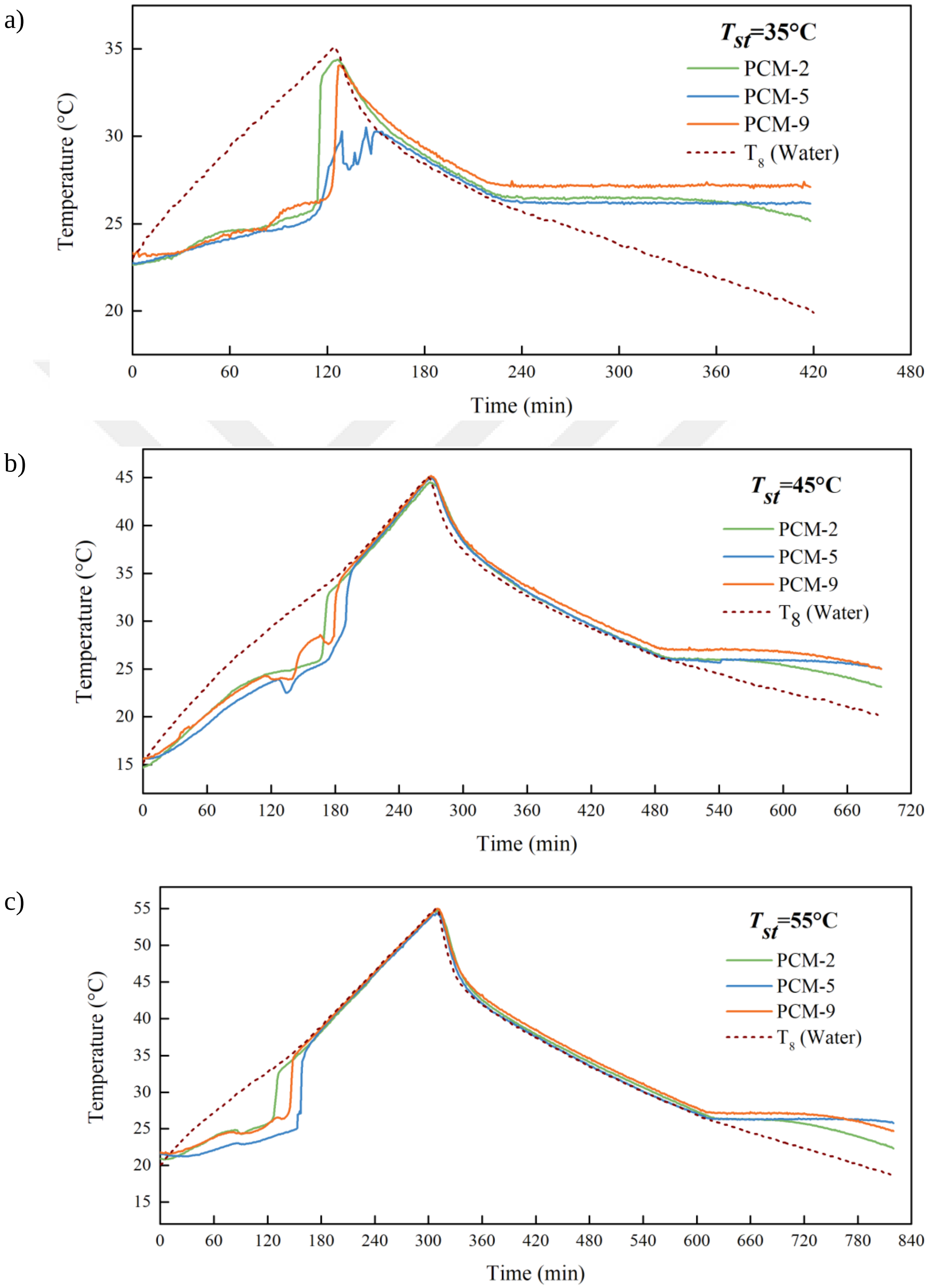

Figure 4.8. Temperature variations with respect to different storage temperatures

4.2.3. Variation of Heating Time by Heat Pump Integrated with TES System

Total heating time using heat pump is the utmost important parameter to quantitatively evaluate the system performance as well as the effects of enhanced thermal energy storage by using PCMs. Total heating time describes the overall period where the heat pump is activated. Hence, this process includes the thermal discharging of the energy in the TES unit during the heat pump operation. Figure 4.9 exhibits the total heating time using heat pump at different flow rates of the HTF, and at different storage temperatures together with the existence or inexistence of PCM. According to the data presented in the figure, as HTF flow rate, relatedly the heating load, increased, the total heating time decreased due to larger rate of heat rejection from the evaporator of the heat pump, which uses TES unit as the heat source. Similarly, increasing storage temperature leads to higher energy storage, especially as sensible heat, and thus, the heating time increased. Taking the case of $\dot{V}$=800 L/h into account for a quantitative interpretation, the heating time increased by 58.7% and 33.9% when the storage temperature was gradually increased from T_{st}=35°C to T_{st}=45°C and to T_{st}=55°C, respectively, in case of using no PCM in the TES tank. These increment rates respectively became 44.9% and 12.0% for the same gradual increment when the PCM (RT26) was considered in the tubes. Similar trends were observed in other flow rates as well. The reason is explained by the fact that water has a significantly higher specific heat capacity compared to the paraffin based PCM. Thus, increasing storage temperature at higher levels, both materials, namely water and PCM, stored sensible heat where the specific heat capacity is a determinative parameter. It should be noted that the phase change interval of the utilized PCM (RT26) is around 25-27°C, and beyond this interval, the material stores sensible heat along with a temperature increase when the heat input is continued. In addition to that, it can be inferred from the obtained time data that the elongation effect of increasing storage temperature decreases by increasing storage temperature, and a sharp decrement was observed especially beyond T_{st}=45°C.

Another significant interpretation about the heating times shown in the figure is the effect of PCM utilization, instead of water only. Utilization of PCM provided a significant extension in the total heating time at the investigated storage temperatures of T_{st}=35°C and T_{st}=45°C, while it showed an adverse effect when the storage temperature was considered T_{st}=55°C. Quantitative results revealed that using PCM at a low storage temperature such as T_{st}=35°C attained an elongation of 24.9%, 30.6% and 24.6% at the HTF flow rates of $\dot{V}$=400, 600, and 800 L/h, respectively. As the HTF flow rate increased, the improvement effect of the PCM also decreased; yet a significant enhancement in the total heating time was observed, which was around 16.9% at $\dot{V}$=1000 L/h and 15.3% at $\dot{V}$=1200 L/h. The PCM effect on the time elongation decreased when HTF flow rate was increased. Nevertheless, it is worth noting that the improvement observed at $\dot{V}$=600 L/h was larger compared to that at $\dot{V}$=400 L/h. This is due to the utilization of some amount of sensible heat after solidification process was finished, i.e., after latent heat of PCM was already exploited. Hence, as the sensible heat of water is considerably large compared to that of the PCM, the time extension becomes smaller compared to that at $\dot{V}$=600 L/h. Besides, the remarkable decrease in the aforementioned improvement ratio at $\dot{V}$=1000 and 1200 L/h occurred due to the rapid heat rejection from the tank, which hinders the full exploitation of latent heat from the PCM.

At T_{st}=45°C, the effect of PCM on the heating time extension diminished since the sensible heat of the materials (water and PCM) was more dominant in the process. Therefore, the rates of time extension were found to be in a range of 2.8% to 13.7% depending on the flow rate.

More strikingly, the presence of PCM exhibited an adverse effect on the heating time when the storage temperature was taken as T_{st}=55°C. In this case, the sensible heat of the water became dominant in the overall thermal storage process, hence, the water could store more thermal energy as sensible heat, compared to the PCM storing energy by latent and sensible means. The prominent reason for this phenomenon is the low sensible heat capacity of paraffin based PCM, which is around 2000 J/kgK, which is less than half of that of water. Therefore, the total heating time decreased by 8.9%, 6.5%, 5.0%, 4.5%, and 4.1% at the HTF flow rates of $\dot{V}$=400, 600, 800, 1000, and 1200 L/h, respectively.

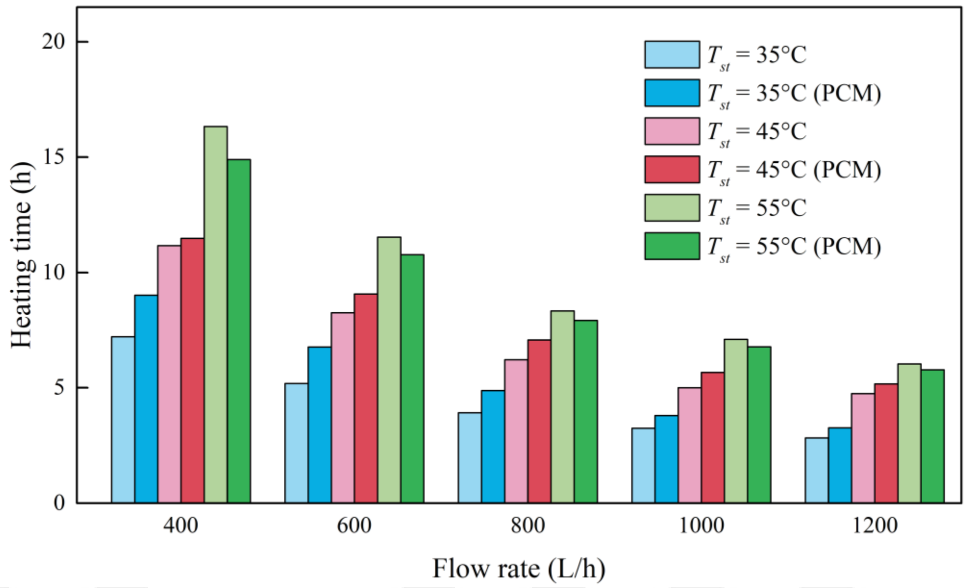

Figure 4.9. Variation of heating time in the considered cases in System-1

4.2.4. Effect of PCM Utilization on the Power Drawn by the Compressor

Electrical power drawn by the compressor was presented in Figure 4.10 for the investigated storage temperatures at $\dot{V}$=800 L/h which represents the medium heating load. First of all, the use of PCM brought a noticeable decrement in the compressor power drawn at all considered storage temperatures, which can be sourced by the relatively more stable temperature at the evaporator side of the heat pump, as similarly indicated in several studies (Gu et al., 2023; Youssef et al., 2017). Even though this reduction is around 20 to 100 W depending on the on/off cycle and storage temperature, this could bring a significant energy efficiency taking into account that heat pumps usually operate during a whole heating season. As seen from the zoomed-in portion of the figure given for T_{st}=45°C, it is obviously seen that the reduction in the compressor power drawn is around 100 W, which corresponds to an energy saving of 8%.

Another significant performance and efficiency metric at this point is the number of start/stops of the compressor during its operation in a specific time interval. Lower number of start/stops means a more efficient operation in heat pump systems because a considerable amount of energy is consumed during compressor starts overcoming the inertia. A stable operation with the existence of PCM may result in lower start/stop cycles for a given period and heat pump system. Taking the ending point of the shorter duration of the operation among the cases of PCM and no-PCM, the number of start/stop episodes reduced by the utilization of PCM. For instance, at T_{st}=35°C, the number of start/stop episodes was observed to be 26 when PCM did not exist in the TES tank, and the number reduced to 25 when PCM was included, achieving a reduction of 3.8%. Nonetheless, the reduction in the number of start/stop cycles of the compressor was more prominent at higher storage temperatures such as T_{st}=45°C and 55°C. For the no-PCM and PCM cases, the number of start/stop episodes were respectively 38 and 34 at T_{st}=45°C, which indicated that incorporation of PCM decreased the start/stop cycles by 10.5%. Similarly, at T_{st}=55°C, these numbers were found to be 50 and 45 in the no-PCM and PCM cases, respectively, corresponding to a reduction of 10%. A similar finding about the benefits of reduction of start-stop cycles was reported in a numerical study about a thermal energy storage tank integrated heat pump, which was carried out by Lyu et al. (2022).

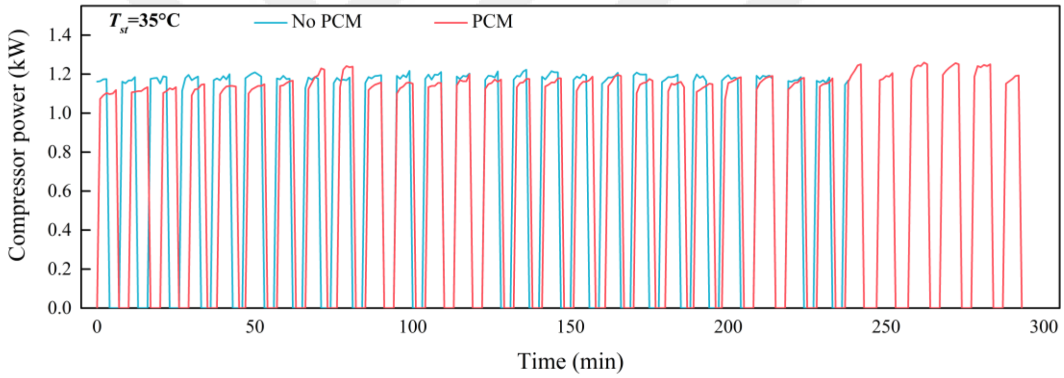

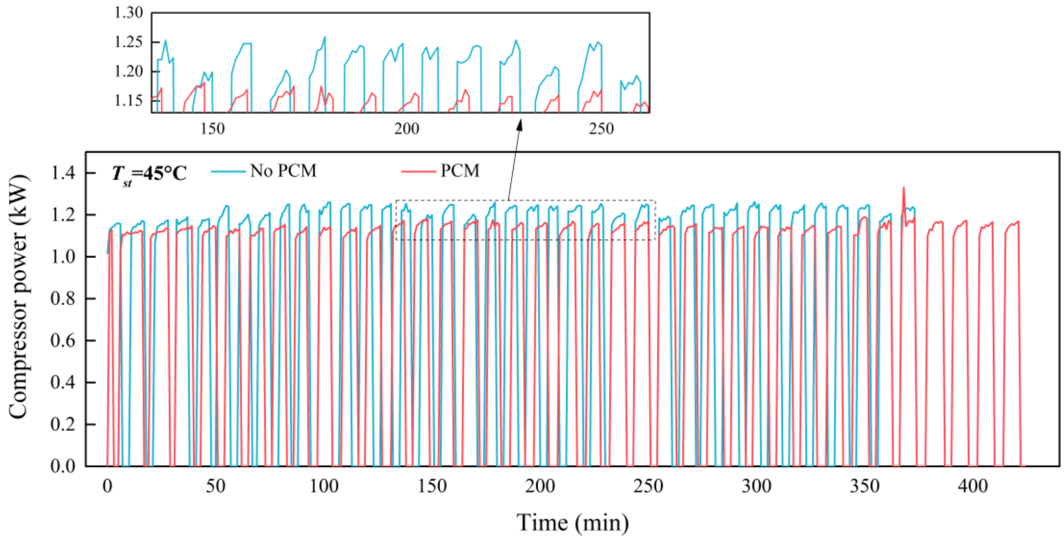

Figure 4.10. Compressor power values measured with respect to time regarding PCM existence

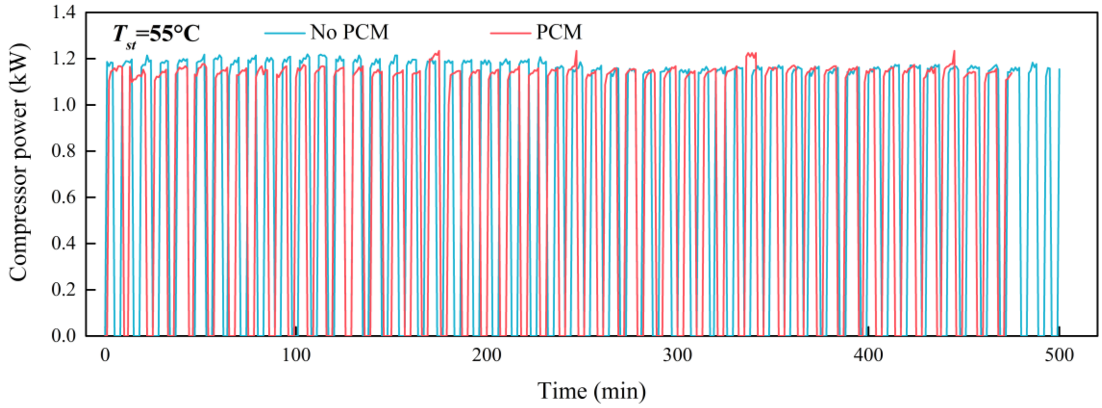

Figure 4.10. (Continued) Compressor power values measured with respect to time regarding PCM existence

4.2.5. Effect of PCM Utilization on the Compressor Operation Time Ratio and Peak Clipping Index

The share of compressor-active periods in a heating process presents significant information about the energy efficiency of the process. The compressor operation time ratio (*COTR*), which was previously defined as the ratio of the time when the compressor is active to the total time of heating, was illustrated in Figure 4.11. An overview to the figure reveals that increasing HTF flow rate results in higher *COTR* value, which means that the heat pump compressor operated for a longer time within the total heating period in order to meet the larger heating demand. Furthermore, it was noticed that the compressor operation time over the entire heating period was slightly lower when storage temperature was increased, which was grounded upon the shorter compressor operation at higher evaporation temperatures. As a general deduction, this relation between the evaporation temperature and heat pump efficiency was highlighted by several researchers, e.g., Zhu et al. (2015) and Wu et al. (2019), to cite a few. A more striking finding here was the variation of *COTR* with respect to the existence of PCM at each storage temperature. It was found that the existence of PCM remarkably help reducing *COTR* value at the low storage temperature, T_{st}=35°C, while it increases the *COTR* at the high storage temperature, T_{st}=55°C, for low heating loads. Especially at T_{st}=35°C, addition of PCM into the TES tank significantly mitigated the *COTR* and relatedly achieved a considerable energy saving.

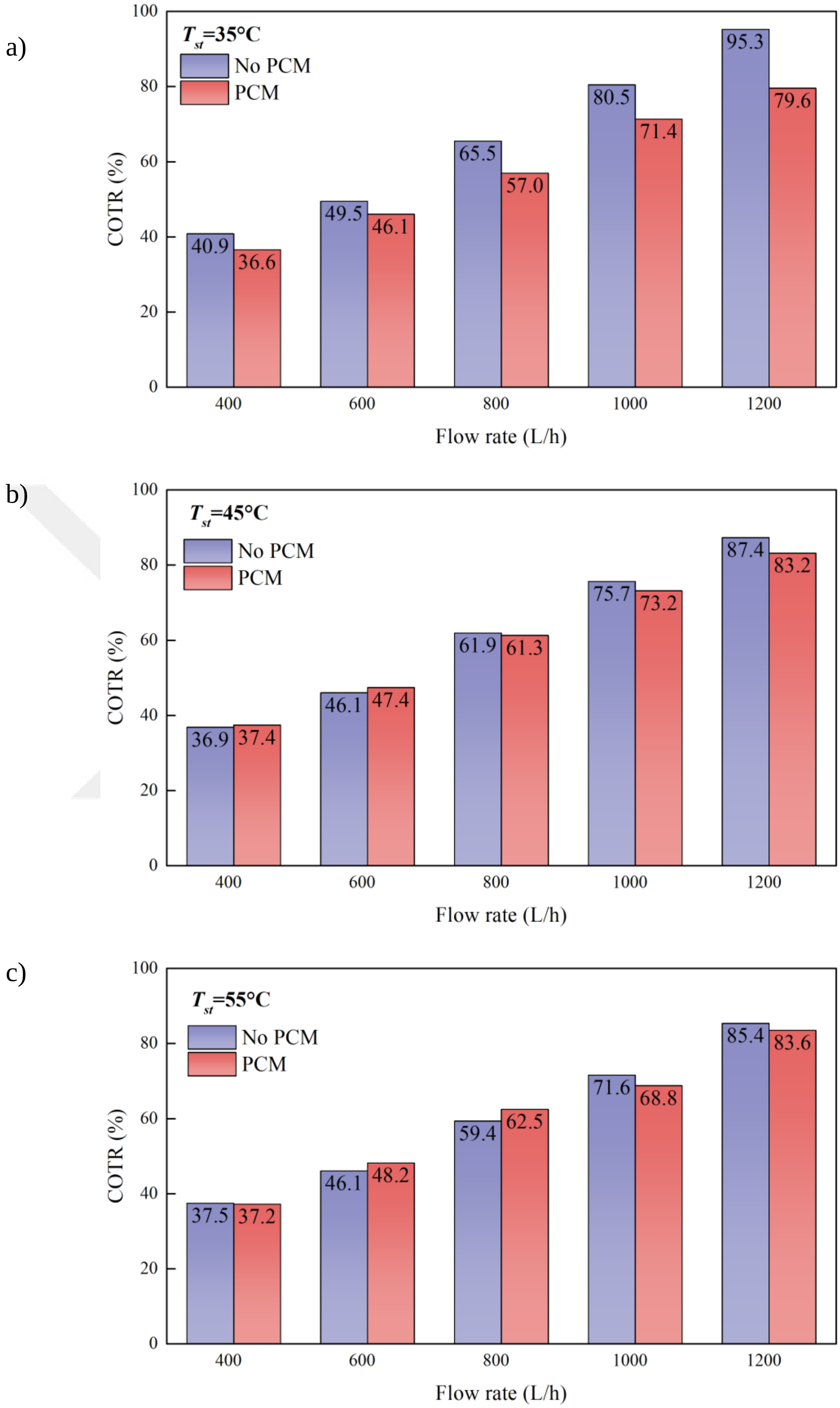

Figure 4.11. Compressor operation time ratio (*COTR*) in the investigated cases calculated by the experimental data

As the obtained data revealed, PCM integration to the TES unit connected to heat pump evaporator led to a reduction in the share of compressor-active time during the heating period (*COTR*) by 10.47%, 6.99%, 13.02%, 11.32%, and 16.48% at the heat transfer fluid flow rates of $\dot{V}$=400, 600, 800, 1000, and 1200 L/h, respectively. However, at higher storage temperatures, such as T_{st}=45°C and T_{st}=55°C, inclusion of PCM did not exhibit an improvement in terms of *COTR* reduction at low flow rates. The quantitative evaluation for T_{st}=55°C showed that the *COTR* value increased by 15.73%, 4.56%, and 5.22% at the flow rates of $\dot{V}$=400, 600, 800 L/h, while it decreased by 3.91% and 2.11% at $\dot{V}$=1000 and 1200 L/h, respectively. This finding was physically interpreted by that the heat rejection from the TES tank was at a larger rate when higher volume flow rates were considered at the condenser side, resulting in a more frequent operation of the heat pump. Hence, a higher rate of heat exchange occurred between the PCM tubes and the water inside the TES tank at higher flow rates. On the other hand, at lower flow rates, the heat rejection from the PCM was at a lower rate.

Considering the fact that the comparison of the *COTR* is based on the compressor operation time and total duration of heating process, the ratio might not always be beneficial although a full solidification occurred. Because the sensible heat of water at a large temperature difference can be more advantageous compared to PCM inclusion, in terms of total heating time. Here, it should be also highlighted that the incorporation of PCM can be more advantageous in all investigated cases when the reference heating time was taken a fixed value for both no-PCM and PCM cases.

Peak clipping index is highly related to the compressor operation ratio as it was defined as the reduction in the energy consumption during peak times with respect to the reference case, which was the air-source heat pump in the same operational conditions where the ambient temperature was around 11°C. Reduced *COTR* led to higher *PCI* values due to reduced electrical energy consumption of compressor, hence, it contributed to the energy flexibility of the system in peak hours. For example, Figure 4.12 shows the peak clipping index values calculated by the experimentally obtained data for three different storage temperatures at $\dot{V}$=1000 L/h. As seen from the figure, using PCM remarkably contributed to the improvement of *PCI* at a given storage temperature, especially for lower storage temperatures such as T_{st}=35°C, where the *PCI* was improved from 14.6% to 23.7%. The reason was attributed to the effect of PCM on the heating time extension, as well as lower compressor operation ratio during the test period. Therefore, at the same storage temperature reached, using PCM was found to be significantly effective for enhancement of peak clipping index.

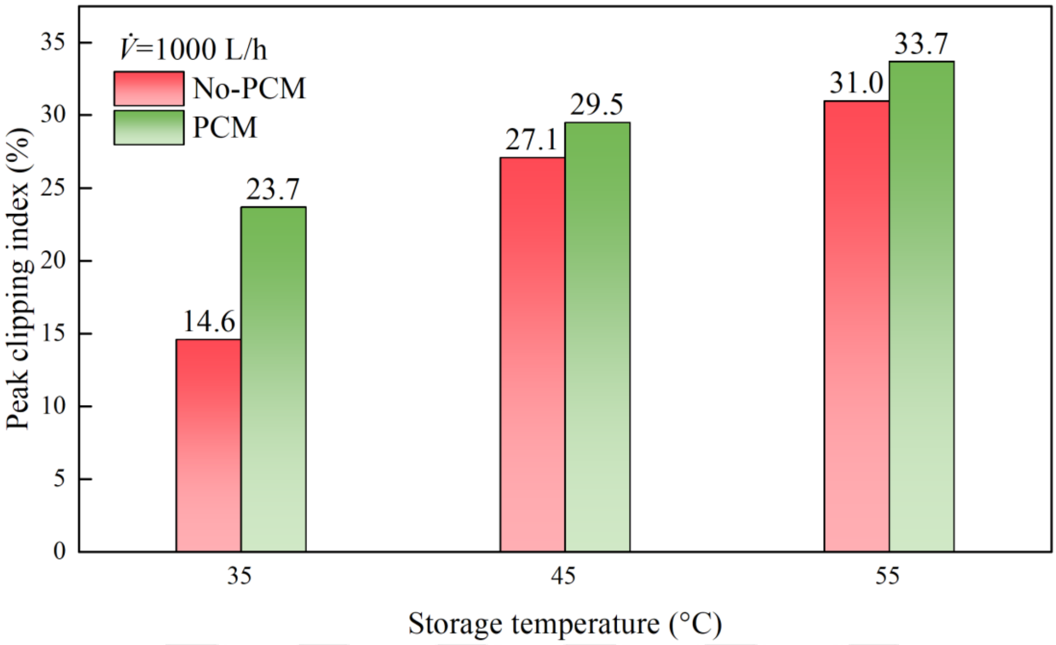

Figure 4.12. Peak clipping index values calculated by the experimentally obtained data for different storage temperatures at $\dot{V}$=1000 L/h

4.2.6. Variation of *COP* Values in the Investigated Cases

The coefficient of performance (*COP*) for the System-1 was defined to evaluate the relative performance of the system with respect to its thermal energy supply and electrical energy consumption over the total operation. Thereby, it has been possible to evaluate the effect of storage temperature and PCM existence. However, it should be underlined here that the compressor operation time ratio is also an important parameter affecting the overall heat pump *COP*, regarding the definition of *COP* in the previous section. According to the computed values given in Figure 4.13, increasing storage temperature had a positive impact on *COP* due to higher evaporation rate attained in the evaporator of the heat pump. Integration of PCM to the TES tank had a slight effect on the *COP*, nevertheless, it showed a significant impact at higher HTF flow rates, i.e., higher heating loads, as the *COP* value also depends on the total test (discharging) time and compressor time during the period.

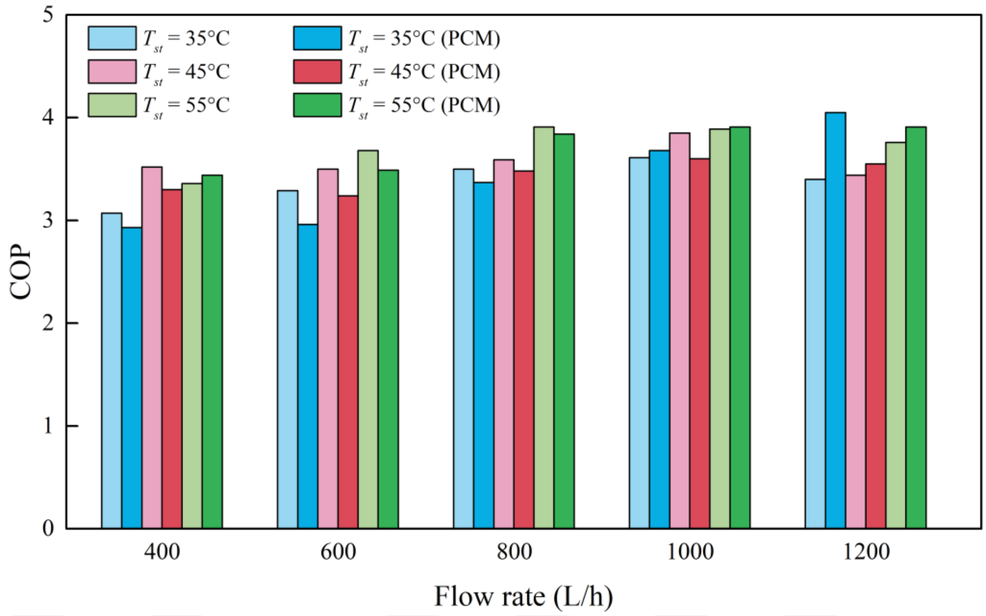

Figure 4.13. Variation of *COP* of System-1 in the investigated cases

Quantitative outcomes pointed out that gradually increasing storage temperature from T_{st}=35°C to 45°C and then to 55°C ensured an enhancement in the *COP* value by 2.6% and 8.9%, respectively, at a HTF volume flow rate of $\dot{V}$=800 L/h. Considering the addition of PCM, it was found that the *COP* values decreased at the low heating loads by up to 10% depending on the heating load and storage temperature. However, at higher heating loads, the *COP* was enhanced by up to 19.1%. Due to the fact that the *COP* is highly related to the balance between the latent and sensible heat utilization, the comparison of drawing energy from the TES unit in case of using water only and PCM integration was a critical point. Because although the PCM utilization increased the total discharging time, this also brought a larger compressor energy consumption. In addition, the sensible heat of the PCM is remarkably lower than that of water, roughly less than half of it. Thus, in case of PCM existence, utilization of a large portion of sensible heat from the PCM constituted a negative effect on the *COP* values, which could be seen in low heating load, i.e., low discharging rates. On the other hand, in high flow rates, the heating loads were larger, and the high latent heat of the PCM was more prominent compared to the sensible heat of water, which brought a larger energy drawn in comparison to water. Hence, the definition of the *COP* can be accordingly considered since there could be various aspects effecting the interpretation of comparative *COP* values, as similarly indicated by Hirmiz et al. (2019) and Belmonte et al. (2022).

4.3. Experimental Studies for System-2

The thermal energy storage tank was disassembled and connected to the condenser side of the heat pump in System-2, and thus, the heat pump was operated as an air-source heat pump (ASHP). Therefore, the system has a different operation strategy compared to that of System-1. First, the water and the PCM was thermally charged by the ASHP to provide energy flexibility by load shifting, and then the stored energy was drawn at different heating loads adjusted by the heat transfer fluid flow rate circulating between the TES tank and the chiller unit. Thereby, the TES unit was charged in the off-peak periods, and then the stored thermal energy was used during the on-peak periods.

4.3.1. Temperature Variations in the TES Tank

First of all, the temperature variations along the axial and radial directions during thermal charging and discharging processes were monitored to justify the hypothesis of lumped system approach to the water inside the TES tank. For this purpose, temperature variations at three locations, namely T_5 (axial, upper part), T_8 (axial, central part) and T_{14} (radial, near the tank wall), were given in Figure 4.14. Similar to the thermal behavior of the water discussed in the previous section for System-1, there was insignificant differences in the transient temperature profiles at various points inside the TES tank. The figure illustrates the temperature variations of the aforesaid points during both charging and discharging processes. It should be stressed that the charging process was carried out by the heat pump continuously within the performance limits of the heat pump. Yet, the discharging process was considered at different heating loads, and the highest discharging rate, which was attained at $\dot{V}$=1200 L/h and ΔT=10 K and corresponded to a heating load of approximately 12 kW, was selected for the evaluation of temperature variation in order to observe the differences more clearly since it was expected that a higher rate of heat transfer might cause larger local temperature gradients. Regarding the obtained data, the discrepancy between the temperatures at different locations that are far from each other was negligible, which proved that the water in the TES tank can be regarded as a lumped system.

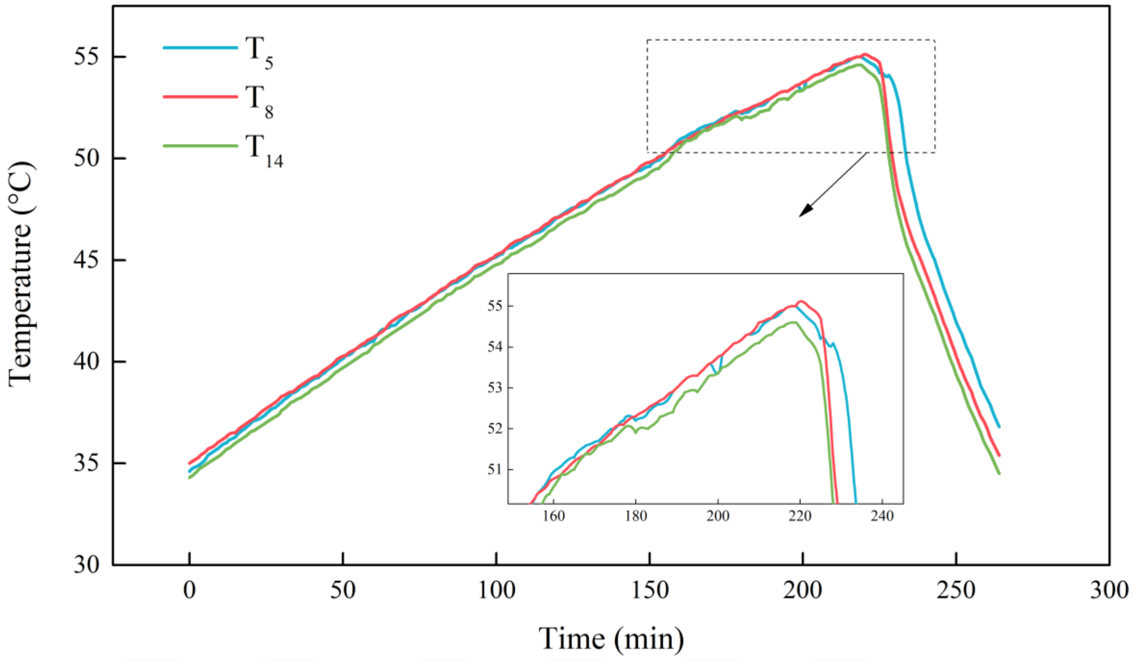

Figure 4.14. Water temperature variations measured in System-2

Variation of PCM temperatures along with the reference water temperature in the TES tank (T_8) is given in Figure 4.15 during charging by the ASHP and during discharging at different heating loads, as a whole. Although the charging processes were similar to each other due to the fact that the same heat pump was utilized in similar circumstances for thermal charging process, the temperature variations exhibit some differences with respect to the heating loads ($\dot{Q}_{load}$), i.e., the rate of heat rejection from the TES tank. As seen from the figures, a parallel trend between the T_8 and the PCM temperatures was observed starting from 35°C to about 43°C. As revealed by the DSC tests, the PCM utilized was expected to start changing its phase from solid to liquid at around 43°C, which was experimentally observed in the tests. It was observed by numerous tests that the PCMs in the tubes could be fully melted during the charging period until the water temperature inside the TES tank reaches T_{st}=55°C. As the charging process was common for all the cases, the temperature variations were similar to each other, and the thermal charging process took around 240–250 minutes in these cases, considering the thermal charging of the whole water inside the TES tank. As for the latent heat of PCM, the melting process of the PCM took about 120 to 170 minutes depending on the PCM tube being near an intense or weak flow stream. During the charging period, it can be evidently seen from the figure that the slope of the water temperature, T_8, decreased while the PCM was melting. This was because of the remarkably high latent heat storage of the PCM which stored a significant amount of thermal energy, hence, the increase rate of the water temperature decreased during the melting process occurred.

However, in the discharging processes, the elapsed time and temperature variations considerably changed depending on applied heating load, $\dot{Q}_{load}$. When lower heat loads were considered, it was slightly easier to reject the heat from the PCMs located in the tubes since larger time was allowed for the heat exchange even if it was at a lower rate. Thus, a larger amount of latent heat could be used. On the other hand, when the heating load was increased to 4.4 kW, 5.4 kW or even as large as 12 kW, the heat rejection from the TES tank became remarkably larger and faster. In addition to that, it was inferred from the obtained data that the temperature gradient between the PCM tube surfaces and the water medium was relatively lower. Therefore, larger times allowed for discharging the total thermal energy in the TES tank ensured larger latent heat utilization in this system.

Converse to the charging process, the slope of the water temperature, T_8, did not exhibit a significant slope change during solidification. One of the main reasons for this occurrence can be referred to the unexpected liquid-to-solid phase change temperature of the lauric acid. It is worth noting that the solidification was expected to initiate around 48°C according to the DSC tests conducted for the lowest possible heat rejection in the calorimetry settings. Nonetheless, the solidification was also started around 43°C in the numerous experimental tests conducted. This shows that thermal behavior of the lauric acid may be different in a practical application, compared to laboratory tests of the material. As a result of this situation, most of the PCMs in the tubes located in the TES tank could not fully finish the solidification process since the reference temperature for the tests were 35°C, meaning that the test was completed when T_8 reaches T_8=35°C. Hence, a significant amount of latent heat remained in the PCM and could not be transferred to the water medium to contribute to the building heating process.

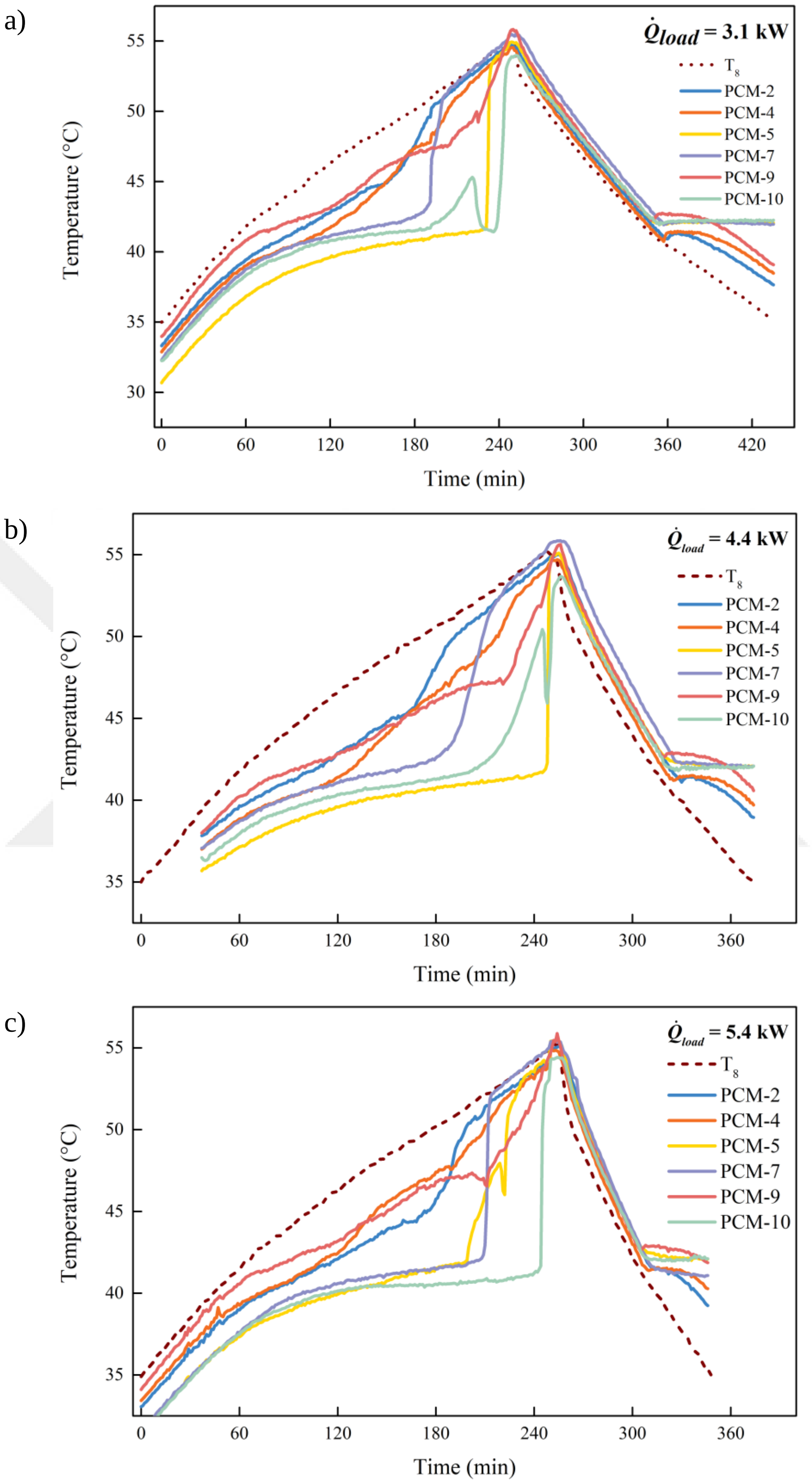

Figure 4.15. Variation of PCM temperatures during charging by ASHP and during discharging at a) 3.1 kW, b) 4.4 kW, c) 5.4 kW, and d) 12 kW

d)

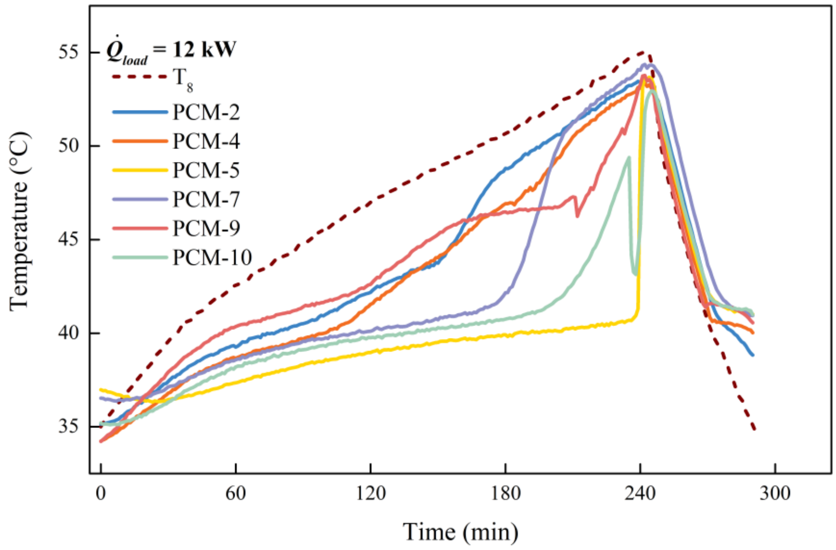

Figure 4.15. (Continued) Variation of PCM temperatures during charging by ASHP and during discharging at a) 3.1 kW, b) 4.4 kW, c) 5.4 kW, and d) 12 kW

4.3.2. Heat Pump Performance During Thermal Charging of the TES Unit

Considering the charging process carried out by the ASHP, the performance of the heat pump was evaluated regarding the experimental data. Within this scope, variations of the heat transfer rate from the condenser ($\dot{Q}_{condenser}$), the power drawn by the compressor (*P*), and the *COP* values with respect to time were presented in Figure 4.16 for the no-PCM and PCM cases. As seen from both figures, the heat transfer rate from the condenser decreased by the elapsed time, while the power drawn by the compressor increased. Relatedly, the *COP* value of the ASHP also decreased. The reason is that the temperature and pressure of the refrigerant at the compressor discharge as well as the temperature of the water inside the TES tank increased significantly as the time elapsed. Thereby, the difference between the refrigerant temperature and the water temperature inside the hot accumulation tank, which is the primary medium where the condensation occurred, decreased gradually. As a result, the heat rejection from the condenser reduced. In addition to that, as the discharge pressure of the compressor was gradually increased, the compression process became more difficult as the operation continued. Hence, the power drawn by the compressor was increased. The decline in the heat transfer at the condenser and the increase in the compressor power led to a significant reduction in the *COP* values of the ASHP.

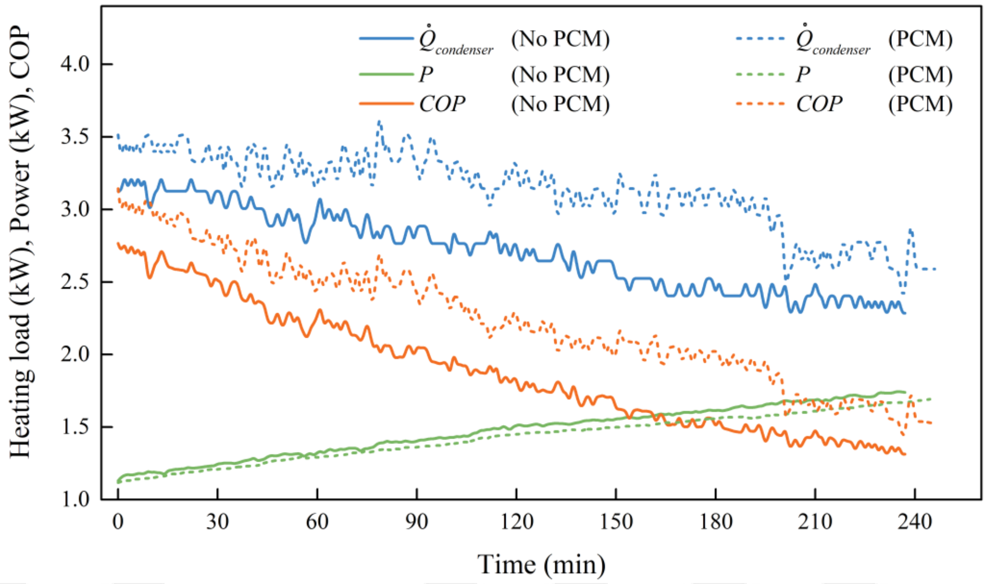

Figure 4.16. ASHP performance during thermal charging with and without PCM in the TES unit according to the experimental outcomes

Comparing the two cases regarding the presence of the PCM, it was noted that integration of PCM resulted in a more stable heat removal from the condenser, especially in the first half of the charging period. Then, the heat transfer rate from the condenser started to decrease slightly, and after 180 minutes of charging process, a more noticeable decrement was noticed. Because the existence of PCM ensured a more stable temperature variation in the TES tank since a large amount of thermal energy was transferred from water to the PCM during phase change process, which took place almost in an isothermal way. Hence, as the PCM stored the thermal energy in latent heat form, it slowed down the temperature rise of the water for a specific time interval, which was evidently noticed from the previously presented temperature variation figures. Nevertheless, the electric power drawn by the compressor was not considerably changed as the compressor discharge pressure and temperature continued increasing during the continuous operation. Yet, the stability in the heat transfer and a larger rate of heat removal from the condenser attained a larger overall *COP* value of the ASHP. Quantitative outcomes showed that the average *COP* values were 1.89 and 2.24 for the no-PCM and PCM cases, respectively, indicating an enhancement of 18.5% by using PCM inside the TES tank. Nonetheless, the charging time was slightly higher in case of PCM existence. The total charging time was 237 minutes when there was no PCM in the TES tank, while it was 247 minutes for the PCM case, and this means that 4.2%

longer time needed to thermally charge the TES tank including PCM in the same conditions where the ambient temperature was approximately 11°C throughout the process.

4.3.3. Discharging Time of the Stored Thermal Energy

Discharging time of the stored thermal energy into the TES tank is of great importance in such systems since they are determinative for satisfactorily meeting the heating demand during specific periods, such as peak times for the grid. In this way, discharging times were given in Figure 4.17 at the investigated heating loads for the cases including and not including PCM. Expectedly, the discharging time proportionally decreased with increasing heating load due to consuming the thermal energy at a larger rate when larger heating loads were considered. Interestingly, utilization of lauric acid as the PCM in the system did not help improving the discharging times, i.e., heating times for a specific space. Conversely, addition of lauric acid brought an adverse effect to the system at the considered heating loads. Quantitative outcomes obtained from the experiments indicated that the total heating time using the stored thermal energy in the TES tank decreased by 3 minutes (1.6%), 11 minutes (8.1%), 18 minutes (16.1%) and 2 minutes (4.3%) at the heating loads of 3.1 kW, 4.4 kW, 5.4 kW, and 12 kW, respectively. As inferred from the previously discussed temperature variations, the reason for this unexpected occurrence was the insufficient heat transfer from the lauric acid to the water inside the tank during solidification process. In other words, an insufficient solidification rate by the utilized lauric acid was observed. Consequently, the latent heat stored in the PCM could not be fully withdrawn within the required time period, i.e., until the water temperature inside the TES tank reached 35°C. Besides, it was noticed that the total discharge time of the no-PCM and PCM cases became closer to each other when heating load was decreased, e.g., when the heating load was gradually decremented from 5.4 kW to 4.4 kW and to 3.1 kW. The maximum considered heat load, around 12 kW, is an exception at this point. Since the thermal energy in the TES tank was rejected at a significantly high rate, the difference between the discharging times of no-PCM and PCM cases became insignificant. Besides, it should be stressed here that the solidification point of the lauric acid (41°C) was close to the reference temperature (35°C) where the system stopped operating. Therefore, a significant amount of thermal energy stayed in the lauric acid, resulting in a wasted latent heat potential, as similarly seen in the temperature variations. Moreover, it was observed during the trials and tests on the experimental setup that the lauric acid exhibited a supercooling behavior meaning that it resisted to solidify completely even if its temperature reduced below solidification point.

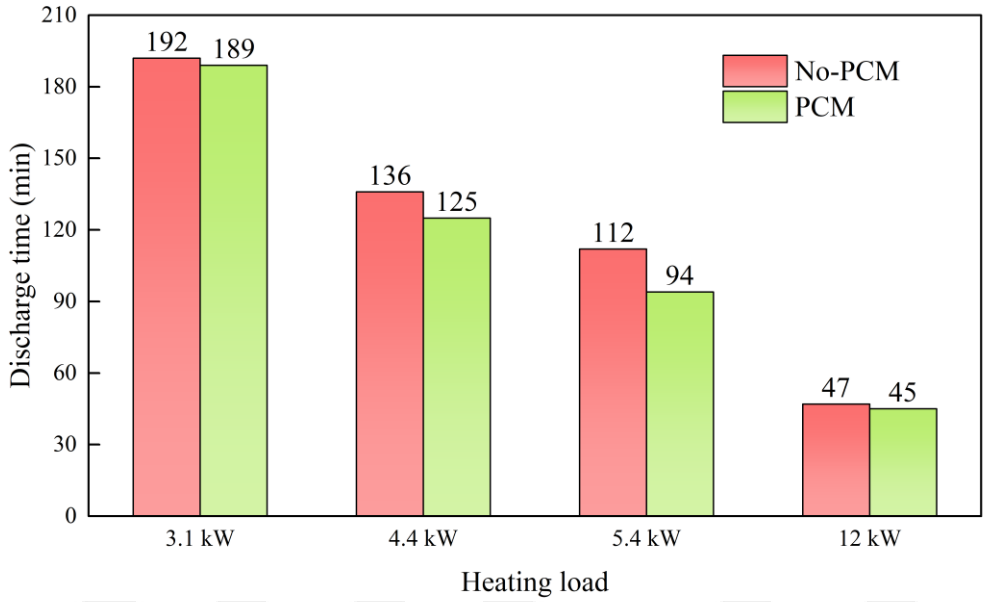

Figure 4.17. Discharging times measured in the tests of System-2

4.3.4. Electricity Tariff and the Load Shifting Index

Load shifting index (*LSI*) was defined to determine how capable the system was to meet the required thermal energy in the on-peak period without using electrical energy. In other words, this flexibility parameter shows what portion of electric energy requirement during on-peak period was met by the stored thermal energy during off-peak periods. To this end, the electricity tariff applied in Türkiye and the calculated *LSI* values were illustrated in Figure 4.18. As can be seen from the figure, a five-hour period is regarded as on-peak period in Türkiye. Before that, the periods between 05:00 – 17:00 and between 22:00 and 05:00 are considered as the day and night tariffs for the pricing of electricity, which depends on the intensity of the electricity use from the grid. Considering the figure on the *LSI*, 67.0% and 69.1% of the thermal energy demand in the on-peak period can be met by the stored thermal energy inside the TES tank at a heating load of 3.1 kW, without and with using PCM, respectively. Besides, this energy was charged by the ASHP as an efficient and cleaner way compared to conventional heating systems such as direct electric heating or natural gas boilers. Using PCM increased the load shift capability to some extend (3.2%) due to higher *COP* values during charging. As heating load was increased, the load shifting index decreased significantly since the thermal energy became insufficient to cover all the on-peak period when the demand is high. At the heating loads of 4.4 kW, 5.4 kW and 12 kW, the *LSI* values were found to be 48.3%, 38.4%, and 17.4% for the no-PCM case, respectively. In case of PCM inclusion to the TES unit, these *LSI* values became 50.1%, 41.5%, and 19.1%, respectively, which correspond to an increase of 3.9%, 8.2%, and 10.1%, respectively.

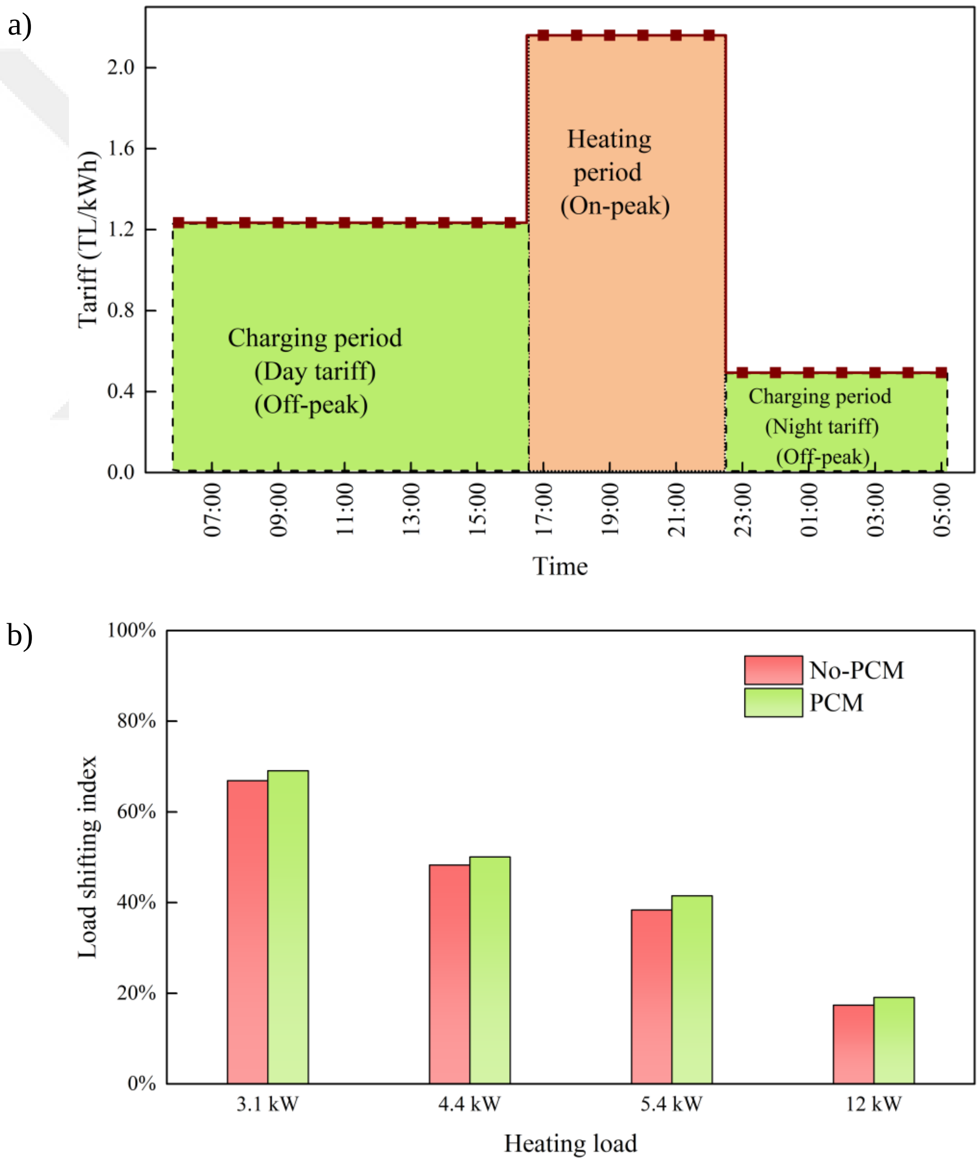

Figure 4.18. Electricity tariff in Türkiye (a) and the calculated *LSI* values (b)

Related to the load shifting strategies, a significant amount of reduction can be achieved in the electricity bills. Considering the electricity tariff and prices in Türkiye as given previously, the cost saving ratios (*CSR*) were given in Figure 4.19 with respect to investigated heating loads. The cost saving ratio was evaluated for two different options, which were the thermal charging within day-tariff and within night-tariff, separately. This means that the thermal energy was considered to be stored during the day-tariff or night tariff only, i.e., between 05:00 – 17:00 or 22:00 – 5:00, using the considered ASHP. Then, this thermal energy was considered to be maintained in the TES tank, and it was utilized during the on-peak period (17:00 – 22:00) until it was fully consumed. Hence, during its consumption, although the thermal energy could not shift the total on-peak load, it met the energy demand partly, as obviously seen from the *LSI* results. According to the cost saving ratio values calculated, a significant reduction in electricity bills can be attained, which reach up to 28.7%, 20.7%, 16.5%, and 7.5% for the heating loads of $\dot{Q}_{load}$=3.1 kW, 4.4 kW, 5.4 kW, and 12 kW, respectively, in case of no PCM existence in the storage tank. Inclusion of PCM brought an additional saving in the cost, and the saving rates became 29.6%, 21.5%, 17.8%, and 8.2%, respectively. When the thermal charging operation by the ASHP is considered in a night-tariff period, a more remarkable saving potential can be ensured due to time of use pricing, and these cost saving rates became 51.7%, 37.2%, 29.6%, and 13.4% for the heating loads of $\dot{Q}_{load}$=3.1 kW, 4.4 kW, 5.4 kW, and 12 kW, respectively, in the no-PCM case. Utilization of PCM brought a further cost saving potential, and these rates were found as 53.3%, 38.7%, 32.0%, and 14.8%, respectively. For the electricity prices in Türkiye in 2023, these rates correspond to monthly cost savings of around 132 to 156 TRY for charging in day-tariff, and 239 to 280 TRY for charging in night-tariff.

These results showed that using thermal energy storage integrated to heat pumps is significantly beneficial in terms of energy cost reduction and grid load shifting even though a partly load shifting was attained. Increasing the size of TES tank can be an alternative solution for increasing load shifting ratio, however, the thermal charging time and energy consumption should be also attentively considered to optimize the storage size. In addition to that, it should be emphasized that a notable amount of thermal energy could not be released from the PCM (lauric acid) due to its significantly low thermal conductivity (k ≈ 0.14 W/mK). Consideration of thermal conductivity enhancers can ensure a more effective utilization of PCM for energy efficiency, load shifting, and cost reduction.

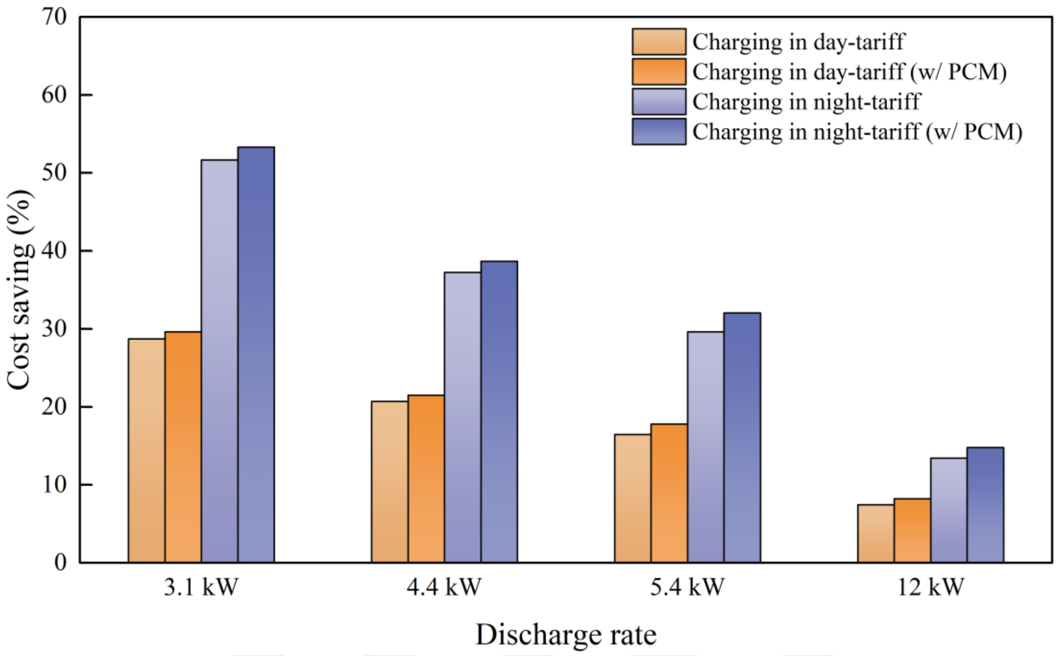

Figure 4.19. Cost saving rates sourced by the load shifting calculated by the experimental data

4.4. Numerical Evaluation of System-1 Considering Thermal Energy Storage/Release Capability and Energy Flexibility in Different Conditions

In this section of the thesis work, the performance of the thermal energy storage integrated heat pump system was evaluated utilizing the mathematical model that was established regarding the experimentally obtained data, as similarly approached in relevant literature works (Green and Garimella, 2021; Murphy et al., 2013) via black-box or grey-box models. Regarding the established mathematical model for System-1, it is possible to integrate solar panels and thermally charge the TES tank. Hence, impacts of variation of solar radiation in different months of heating season were investigated. For the numerical simulations evaluating the thermal charging and discharging behavior of the TES unit as well as the performance of the system, the city of Kocaeli, Türkiye, was considered, and one representative day was selected from each month in the heating period. The heating period was considered five months, from November to March. The heating load was taken constant at 3 kW. Besides, different PCMs were considered in the TES unit to elaborate the impacts of phase change temperature and latent heat capacity on the performance of the system.

The incident solar radiation data in the aforementioned five months for Kocaeli, Türkiye, were obtained using the database of Photovoltaic Geographical Information System (PVGIS), which is presented by EU Science Hub of European Commission and used by many researchers working in the field (Arıcı et al., 2020; Campos et al., 2020; Nižetić et al., 2018). Variations of the hourly incident solar radiations on a south-facing 35° tilted surface were given in Figure 4.20a for the selected representative days in the heating season months in 2020, and the variations of the ambient temperatures during these selected days in each month were also given in Figure 4.20b. The solar radiation data were obtained for clear days, and it was noticed that the incident solar radiation values were considerably higher in the transitional months, such as November and March, while they were significantly low in December and January where the days were usually severely cold. Besides, the number of sunny hours, i.e., the daylight period, was also lower in these two months, while it was higher in March. In order to collect the useful solar energy, two flat plate solar collectors (FPSC), which were used by Kim et al. (2018), were integrated to the system in the model. The FPSC had a surface area of 1.68 m^2, regarding its dimensions, and the detailed properties of the FPSC were given by the authors in the aforementioned study.

In the established mathematical model, the algorithm is based on thermal charging by the solar energy absorbed by the solar collectors. Hence, the useful heat gain is transferred to the thermal energy storage tank in order to thermally charge the water and PCM (if any) inside the TES unit. A circulation pump was considered within the system to circulate the heat transfer fluid in the pipelines. Thus, the heat transfer fluid is started to be circulated when there is adequate solar radiation incident onto the surface of the flat plate solar collector (FPSC). Thereafter, the circulation of the heat transfer fluid between the solar collector and the TES unit is stopped in two conditions in the model: i) reaching the specified maximum thermal storage temperature, and ii) when the heat loss from the solar collector exceeds the heat gain, i.e., when there is only heat loss from the collector, which occurs when the incident solar radiation is inadequate.

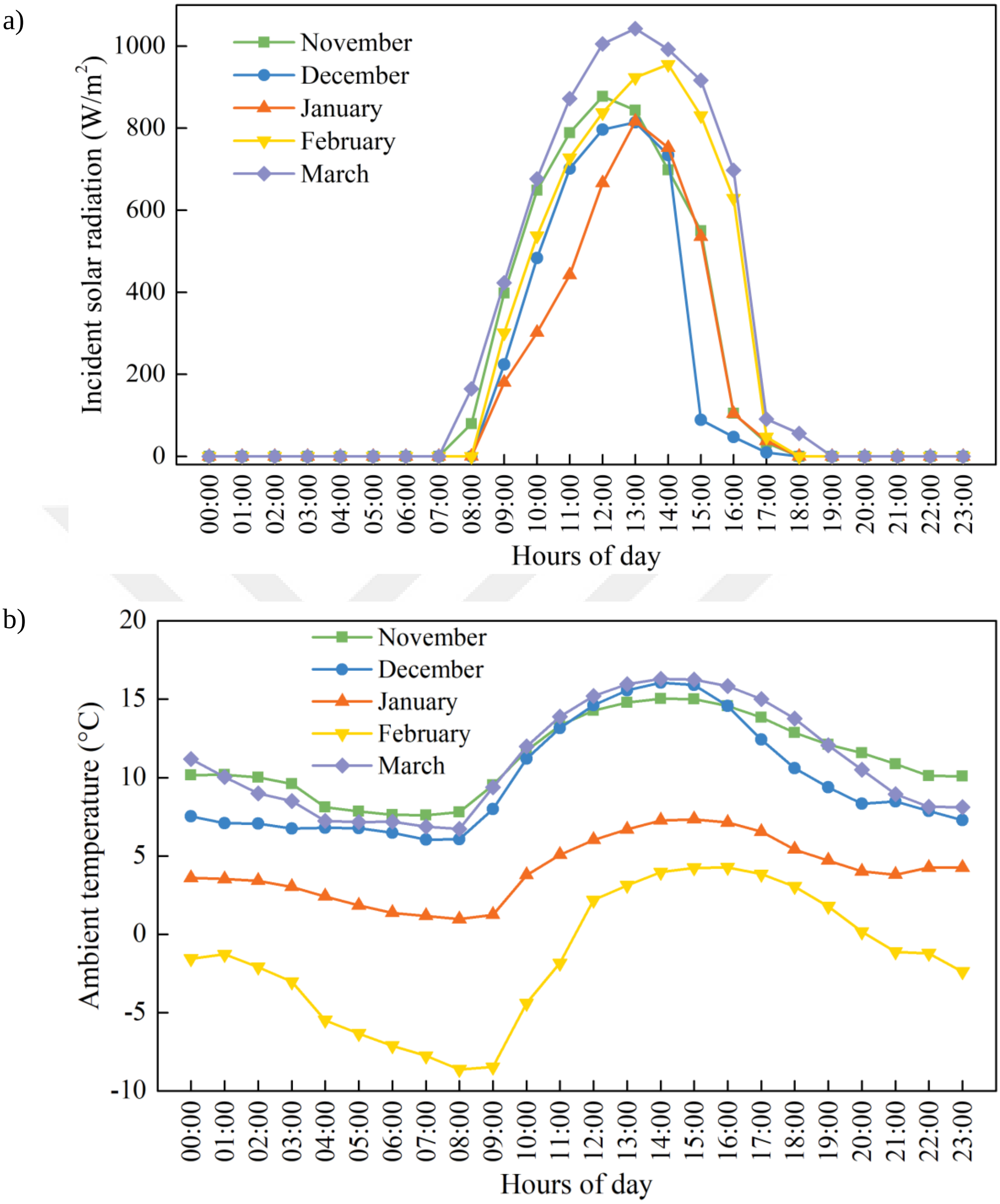

Figure 4.20. Hourly a) incident solar radiation and b) ambient temperature variations on the selected representative days in each month

In the discharging step, the modeled heat pump starts operating using the stored thermal energy in the TES unit as a heat source, and it continues its operation within start-stop cycles to provide the heating demand. The SAWSHP stops its operation once the water temperature inside the TES unit reaches the reference temperature (20°C), as exactly considered in the experimental works. Thanks to the established model, the effect of weather conditions on the thermal charging of the water and PCM inside the TES tank was investigated. More specifically, thermal behavior of commercially available different PCMs, such as Rubitherm RT24 HC, RT26, RT28 HC, and RT31 of which the thermophysical properties were given in Table 4.1, in terms of temperature variations and latent heat storage was examined under different weather conditions. Similarly in the discharging step, several parameters such as temperature variations, amount of energy release, total heating time, latent heat utilization and peak clipping index were interpreted considering the obtained numerical results.

Before the discussion of the results obtained by the mathematical models for the heat pump systems, it should be noted that the effect of convective heat transfer coefficient on the total heating time during discharging and the average *COP* was examined. As mentioned previously in the Section 3.4.1, the thermal resistance at the outer side of the PCM tubes was relatively negligible, compared to the thermal resistance in the PCM medium, which is much larger due to the low thermal conductivity of the PCMs, in both System-1 and System-2. Yet, a set of computations were carried out on the established mathematical model in order to see the impact of convective heat transfer coefficient at the outer side of the PCM tubes. According to the obtained results given in Table 4.2, the convective heat transfer coefficient value had almost no impact when it was increased beyond a certain point. In other words, if the value of the convective heat transfer coefficient is any larger than h=200 W/m^{2}K, its effect on the computed values becomes negligible. Here, it is noteworthy that the estimated convective heat transfer coefficients from the CFD studies were around h=3000 W/m^{2}K.

Table 4.1. Thermophysical properties of the PCMs used in the numerical study for System-1

Thermophysical property	RT24HC	RT26	RT28HC	RT31
Density (kg/m^3)	750	825	825	795
Specific heat (J/(kgK))	2000	2000	2000	2000
Thermal conductivity (W/(mK))	0.2	0.2	0.2	0.2
Phase change temperature (°C)	24	26	28	31
Latent heat of fusion (J/kg)	133000	110000	206000	106000

Table 4.2. Variation of heating times and *COP* values by convective heat transfer coefficient

h (W/(m^{2}K))	Heating time in discharging (h)	*COP*
50	4.94	3.67
100	5.31	3.67
200	5.40	3.65
500	5.40	3.65
1000	5.41	3.65
2000	5.41	3.65
3000	5.41	3.65
4000	5.41	3.65

4.4.1. Temperature Variations and Latent Heat Utilization of Different PCMs in System-1

Utilization of different PCMs inside the TES unit was elaborated via temperature and liquid fraction variations on each representative day selected from each five months in the heating period, from November to March, in order to reveal the potential of using PCMs in the TES units. For this purpose, temperature and liquid fraction variations of water and different PCMs as TES material were numerically investigated and the results were discussed in this section. Besides, the latent heat utilization for each PCM was computed to reveal their TES capabilities for each month. Figure 4.21 shows the temperature and liquid fraction variation of each considered TES material including water on the representative day in November. The thermal charging process started with the sunrise at 08:00 on this day, and the temperatures of the water and the PCM rapidly increased until 15:50 where the solar radiation was lastly sufficient to increase the temperature of the HTF. After this time, circulation of the water through the solar collectors would have resulted in heat loss to the outdoor ambient; hence, the thermal charging process was ceased. At this time, it was seen that the TES tank with water only had a slightly higher temperature compared to the TES tanks which contained PCM inside the tubes. The reason was the large amount of latent heat absorption of the PCMs in the tubes, which suppressed the rapid rise of the water temperature inside the TES tank. The thermal behavior of RT28 HC drew attention here due to having a noticeably smaller temperature when the thermal charging process ended. This occurrence was sourced by the high latent heat capacity of the RT28 HC, which absorbed relatively higher amount of latent heat from water, which resulted in a smaller temperature rise.

When it was 17:00, the heating process by the SAWSHP was started, and the temperatures began to decrease significantly as the water in the CAT and TES tank mixed at first. Meanwhile, the PCM temperatures was slightly higher than the water temperatures in the tank, having the same declining trend. It was evidently observed from the figure that the average PCM temperatures showed a nearly isothermal trend once they reached their phase change temperature. However, it was detected that the PCM temperatures could not reach the reference temperature, 20°C, at the end of the process when the water temperature reached the reference point, 20°C. This situation indicated that the possibility of presence of unused thermal energy inside the PCM media.

As inferred in the previous paragraph, the variation of liquid fraction was given in Figure 4.21b in order to evaluate the variation of latent heat storage and release during thermal charging and discharging processes on the representative day in November, respectively. It was noticeable that the PCMs stored some amount of sensible heat before melting started, and then liquid fraction started to increase rapidly, which indicated the latent heat storage, and this continued until the liquid fraction value reached unity (f=1). Yet, the thermal charging was not completed at that moment, and this means that the PCM continued to store sensible heat in liquid from. Here, it should be underlined that although the phase change temperature of RT28 HC is smaller than that of RT31 which caused RT28 HC to start melting earlier, the duration for latent heat storage was longer for RT28 HC, compared to RT31. This can be explained by the fact that the RT28 HC has a considerably higher latent heat capacity, which took it longer to be charged by latent heat. Nevertheless, during discharging, the latent heat of RT31 was almost completely released, while that of RT28 HC was not released completely and

17.9% of the latent heat was trapped in this material as an unused energy. This situation was even more dramatic for RT24 HC, due to its smaller phase change temperature, which was close to the reference point (20°C), and thus, it delayed the latent heat release process.

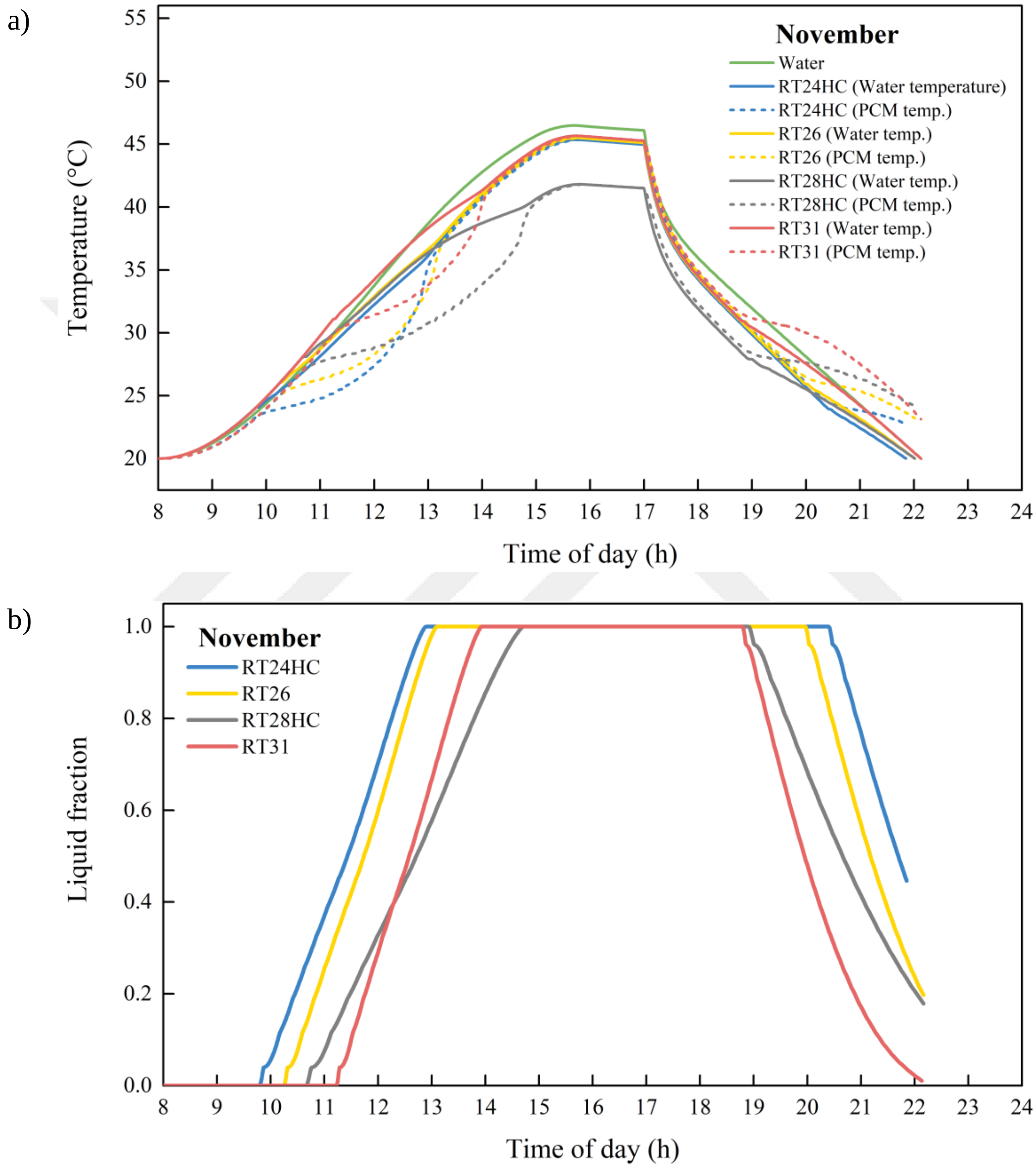

Figure 4.21. Temperature (a) and liquid fraction (b) variations of the considered TES materials on the representative day in November

The temperature and liquid fraction variations of the considered TES materials were given in Figure 4.22 for December. By an overview on the figure, it was evidently noticed that the temperature of the TES materials was not as high as in November due to the fact that the solar radiation intensity was considerably lower in December. Therefore, in case of using water as a TES material, the storage temperature reached about T_{st}=40°C, and it was lower when PCM was used. A similar temperature trend was observed as interpreted for November during thermal charging and discharging, however, it was also noticed that the thermal charging process was shorter in December, compared to the process in November. This can be attributed to the weather conditions in December where the ambient temperature was significantly low, and the solar radiation intensity was relatively weaker. Hence, after 14:00, it was not reasonable to circulate water through the solar collector as it could bring a considerable heat loss, rather than charging the TES unit. The discharging process was initiated at 17:00, as planned in the model, and the temperatures dropped rapidly. Here, it should be noted that the temperature of RT28 HC was lower due to the same reason explained previously. It was also observed from the numerical computations that the RT28 HC struggled to store thermal energy, and thus, it had to start discharging process at a lower temperature compared to other TES materials. As the water did not store any latent heat, its temperature was at the highest level among the investigated materials.

a)

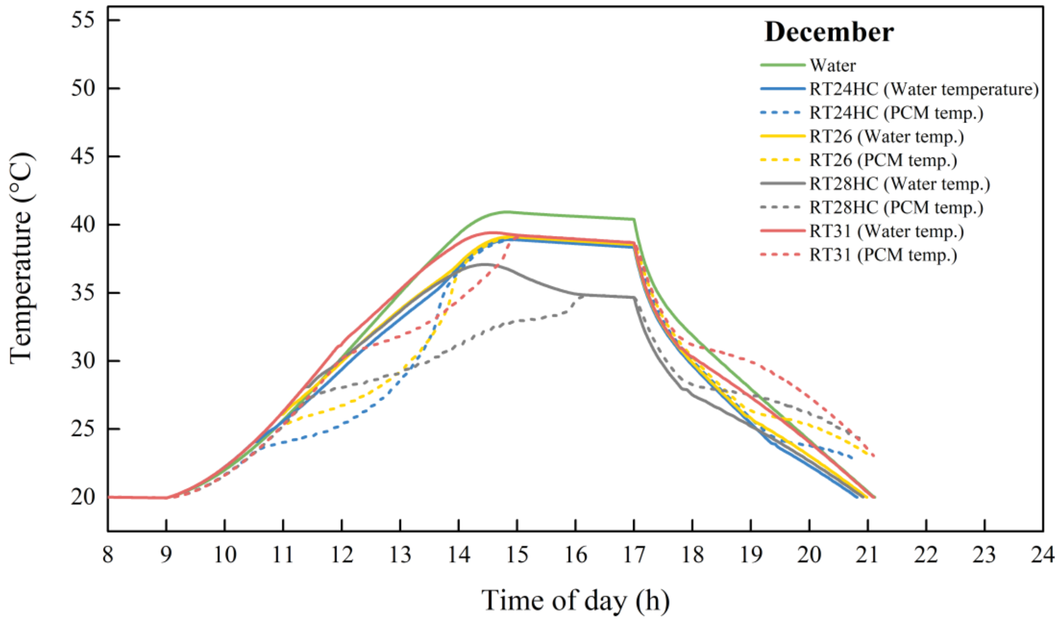

Figure 4.22. Temperature (a) and liquid fraction (b) variations of the considered TES materials on the representative day in December

b)

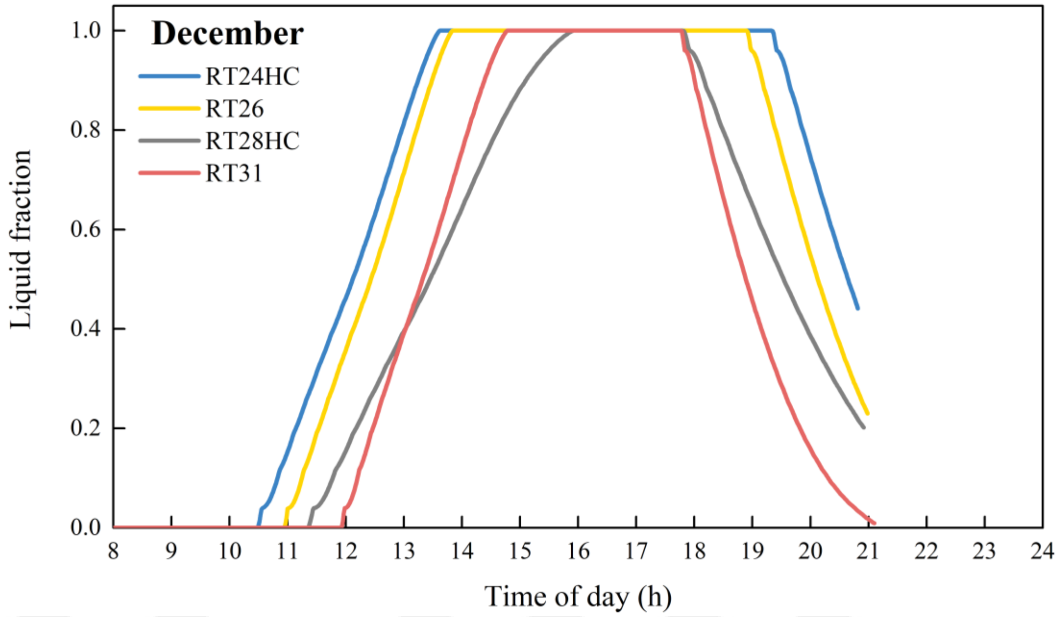

Figure 4.22. (Continued) Temperature (a) and liquid fraction (b) variations of the considered TES materials on the representative day in December

A similar trend of liquid fraction curves to those obtained in November was observed also for December. Although there was no incomplete melting situation detected, the amount of sensible heat storage was different depending on utilized PCM. Here, the phase change point was of great importance. A phase change point close to the reference temperature of 20°C, i.e., smaller phase change temperatures, provided a more guaranteed latent heat storage; however, this became a significant drawback during discharging process ending up with incomplete solidification, i.e., ineffective latent heat utilization.

The charging process in January was even more struggling due to the low solar irradiation on the representative day, as given in Figure 4.23. The temperatures of the water and the PCMs could not reach 40°C, and some of them barely reached 35°C. Although a similar trend was observed as given in December, it was obvious that the representative day selected in January was significantly colder. Relatedly, a conspicuous occurrence was spotted, which was the probably incomplete melting of RT28 HC, due to inadequate solar radiation for the thermal charging of the large latent heat capacity of this material.

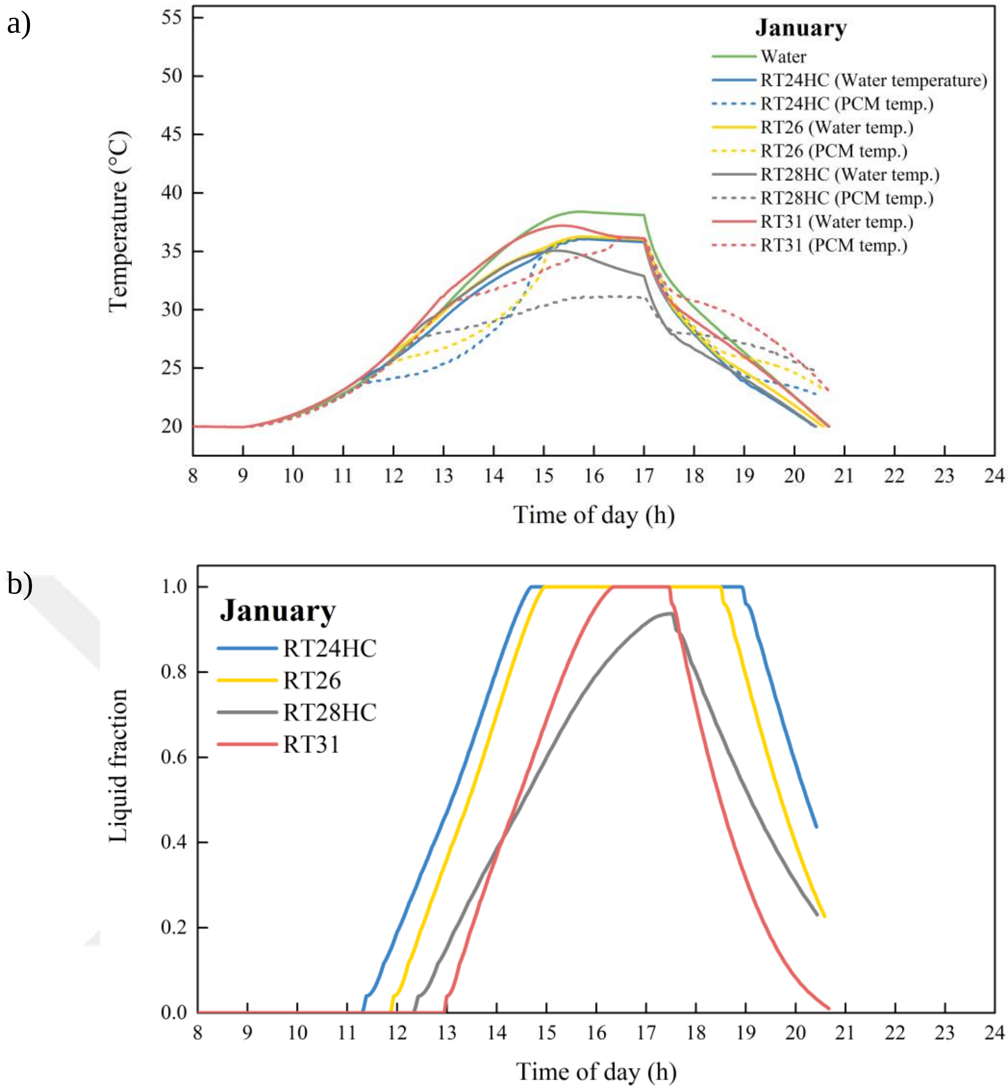

Figure 4.23. Temperature (a) and liquid fraction (b) variations of the considered TES materials on the representative day in January

The liquid fraction curves illustrated in Figure 4.23b provided a clear view about the latent heat storage and release of the PCMs. As inferred from the temperature variations, it was evidently seen that the PCM RT28 HC was unable to fulfill all the latent heat capacity it has. Due to inadequate solar radiation causing lower heat transfer to the TES tank as well as due to the high latent heat capacity of the PCM, 93.8% of the latent heat of RT28 HC was fulfilled. Yet, it started releasing its stored thermal energy as soon as charging was completed and discharge was started, and it covered the evaporator energy of the heat pump until around 21:00, which was similar to the discharging time of RT26 case.

On the day selected in February, the solar radiation values were obviously higher compared to other winter months, December and January. Therefore, the temperature and liquid fraction variations for February given in Figure 4.24 were similar to those obtained for November. The water temperatures inside the TES tank reached above 45°C, except for RT28 HC, which indicated that the TES materials stored a considerable amount of latent and sensible heat. The liquid fraction curves also confirmed this situation as seen from the figure, and they reached unity for all considered PCMs. Nevertheless, there was still an incomplete solidification observed for the PCMs, except RT31 which has relatively higher solidification point.

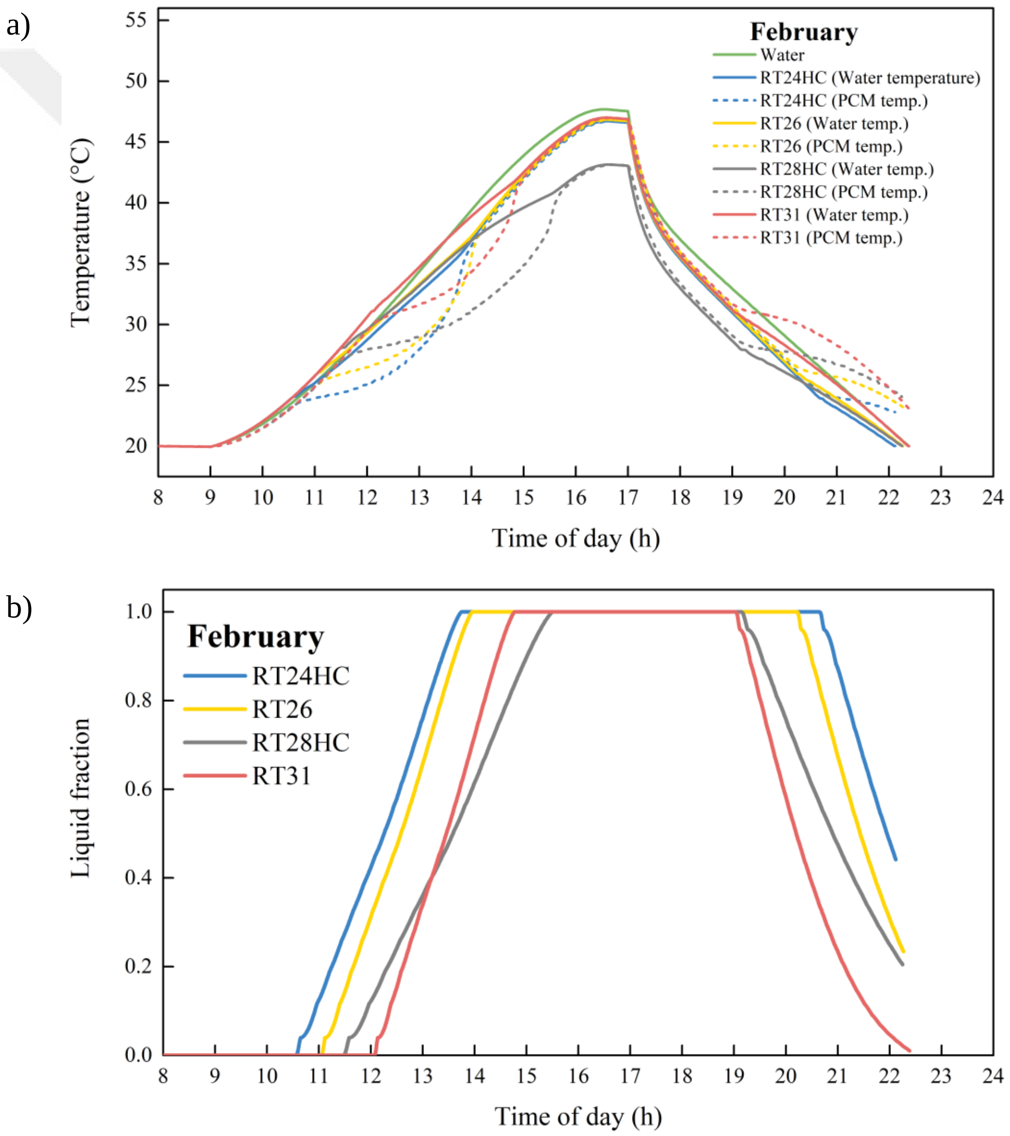

Figure 4.24. Temperature (a) and liquid fraction (b) variations of the considered TES materials on the representative day in February

March is usually the warmest month in a heating season in northern hemisphere. Due to high solar radiation, it was seen in Figure 4.25 that the water temperature inside the TES tank reached the upper limit of storage temperature, T_{st}=55°C. It should be underlined that all the considered PCMs stored latent and sensible heat, meaning that their temperatures reached the limit value, with the exception of RT28 HC, which had a temperature reduction due to intense latent heat storage. After a slight heat loss calculated to be around 162 W in a basement-like environment presumed at 15°C, the discharging process started at 18:00. Here, it is noteworthy that the discharging process started at 18:00 in March, due to longer sunshine time. Thereby, it was seen that the heating process by the SAWSHP continued until late night, such as 01:00.

Considering liquid fraction curves in Figure 4.25b, a large plateau region drew attention, which was due to the release of the large amount of sensible heat stored in the PCMs. Similar to the deductions for the other months, the PCMs except RT31 could not fully benefit the latent heat that they stored by solar energy during thermal charging. Therefore, this potential must be evaluated, which was discussed in the upcoming paragraph.

a)

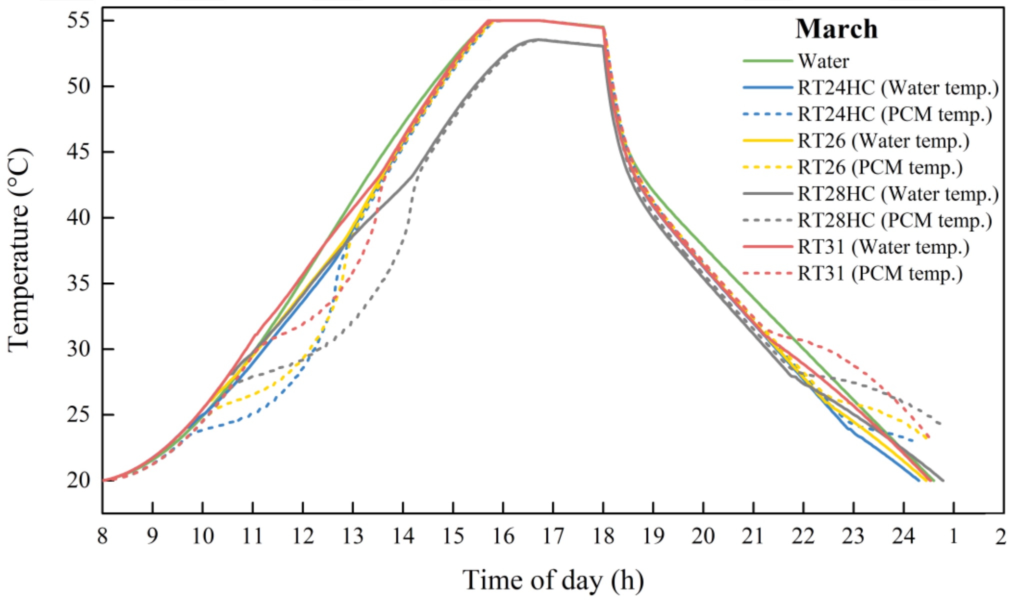

Figure 4.25. Temperature (a) and liquid fraction (b) variations of the considered TES materials on the representative day in March

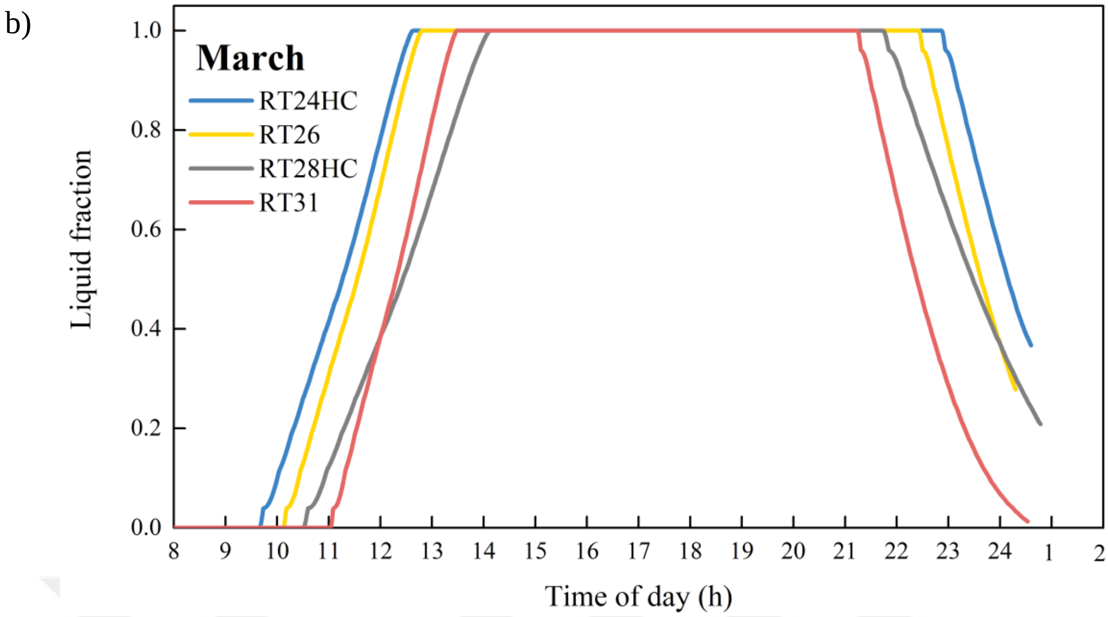

Figure 4.25. (Continued) Temperature (a) and liquid fraction (b) variations of the considered TES materials on the representative day in March

The latent heat utilization of the considered PCMs was presented in Figure 4.26 in terms of percentage utilization of the total capacity and total released thermal energy in kWh to elaborate the latent heat utilization behavior of the examined PCMs. Considering the ratio of the benefitted latent heat of the PCMs during discharging, it was noticed that almost all the stored latent heat (around 99%) by RT31 was released, due to its relatively high phase change point. On the other hand, only 55% to 60% of the latent heat stored in the RT24 HC was released to contribute to the energy of the water inside the TES tank. Besides, RT26 and RT28 HC provided a significant amount of the stored latent heat in every month, which were respectively around 75% to 80%. However, an exception was noted here about RT28 HC, which could not even release 40% of its stored latent heat in January. Related to the temperature and liquid fraction curves discussed previously, the reason for this phenomenon was the incomplete melting and consequently ineffective benefiting from this PCM.

On the other hand, considering the absolute amounts of latent heat release from the PCMs in interest, the computed outcomes were presented in Figure 4.26b, which revealed that RT28 HC contributed to the TES unit with a great amount of latent heat. Depending on the month, the total amount of latent heat RT28 HC discharged was from 100% to 200% larger compared to other examined PCMs. Combining the deductions from both figures evidently highlights the significant potential of thermal energy storage/release of RT28 HC. At this point, the common challenge of PCMs, the low thermal conductivity, comes up as a barricade in front of the effective utilization of latent heat in TES integrated solar-assisted heat pumps. Comparing the results obtained for RT28 HC to the RT26 that was used in the experiments, it was stated that RT28 HC was able to release 67% higher latent heat.

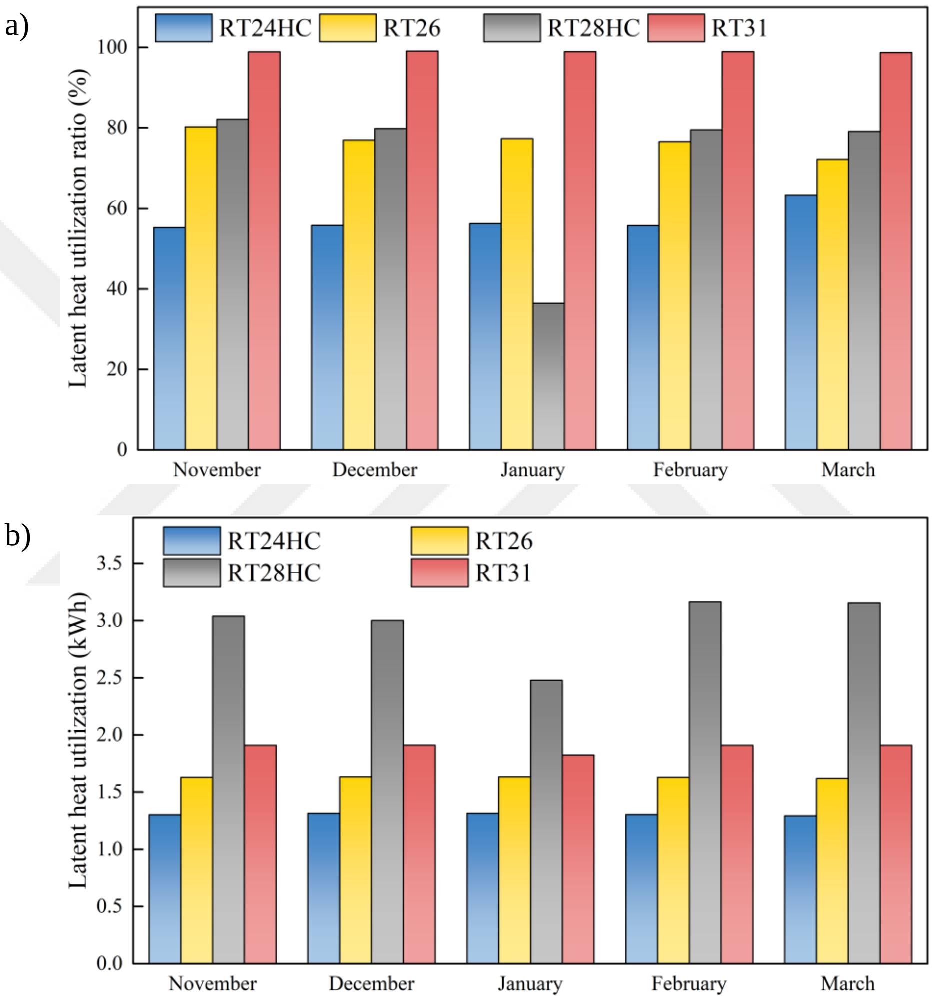

Figure 4.26. Latent heat utilization in numerical simulations in terms of a) percentage of the total capacity and b) total released energy during the discharging period

4.4.2. Evaluation of Using Different PCMs in terms of Charge/Discharge Times and Peak Clipping Potential in System-1

Thermal behavior of the TES materials, including water, and latent heat utilization performance of the PCMs are crucial parameters determining the charging and discharging times, which consequently characterizes the heating performance and energy flexibility of the system. The charging time in System-1 was highly dependent on the considered weather conditions, i.e., solar radiation and ambient temperature, while the considered PCMs have also an impact on this parameter. On the other hand, the discharge time was characterized by the effective use of stored thermal energy inside the TES tank since the operation of the system was terminated when the water temperature inside the TES tank reach 20°C.

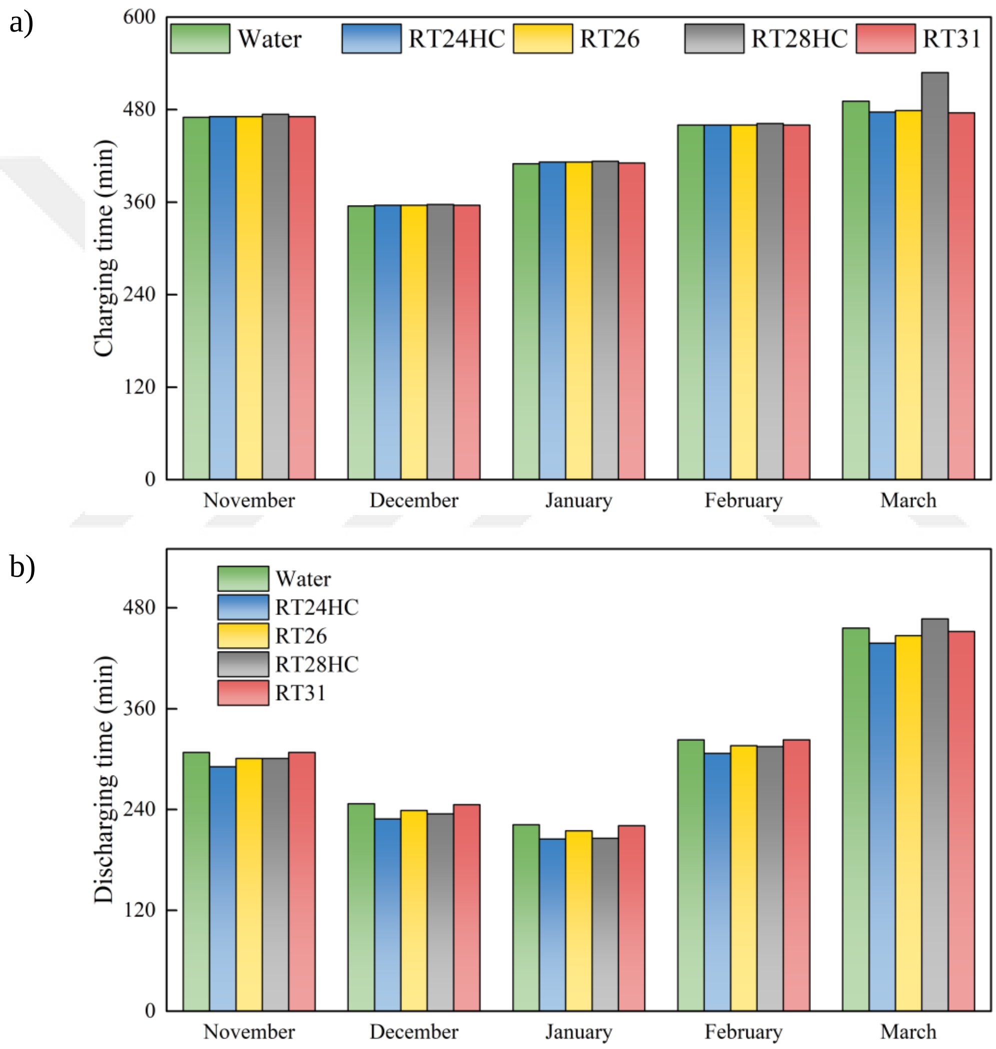

Figure 4.27. Charging and discharging times of the TES unit filled with different TES materials in System-1 obtained numerically for different PCMs

The charging and discharging times were respectively given in Figure 4.27. The thermal charging time exhibited only slight differences with respect to the TES material. However, in cold weather conditions such as the month December and January, the charging period was significantly low, due to insufficient solar radiation. This also led to lower sensible heat storage depending on water temperature inside the TES tank. Discharging times also showed slight differences with respect to considered TES material. The discharging times obtained by using water or RT31 were almost the same, while RT26 and RT28 HC yielded a slightly lower discharge time. However, RT28 HC exhibited an exceptional case in March, and the discharging time was markedly higher in this month, compared to all other TES materials. This was grounded upon the adequate thermal charging of the RT28HC. Hence, although the PCM utilization did not exhibit a remarkable benefit in terms of discharging time in almost all investigated cases, this occurrence evidently proved that appropriate PCM utilization with adequate thermal charging could be outperforming the water only TES units. For instance, in November, the discharging times obtained by using water and RT28HC were 308 min and 301 min, respectively. However, in March, these values were respectively 456 min and 467 min. The discharging time for the RT28 HC case was 2.3% shorter than that of water in November, while it was 2.4% longer in March, although it was not able to release all the stored thermal energy.

In order to elaborate the energy flexibility potential of the current system (System-1), the peak clipping index was determined previously, which indicates the reduction of the energy consumption for heating during peak period, which takes 5 hours between 17:00 and 22:00 in Türkiye. As the heating was considered with heat pump, the air-source heat pump considered in this thesis work was taken as the baseline case to determine the contribution of the utilization of TES integrated SAWSHP to the energy flexibility, i.e., the peak clipping. The *COP* of the considered ASHP was determined to be 2.74 at a condenser-side circulating HTF temperature of T_c=35°C, which is the same as the HTF temperature of the considered SAWSHP. Hence, the electric energy consumption of the reference ASHP in a continuous regime was 5.47 kWh during the 5-hour peak period. On some occasions, such as the days having high solar radiation or long sunshine time, the TES unit was charged at a high level that it could cover all the peak period, attaining a significant peak clipping. However, in relatively colder months or in case of ineffective PCM utilization, the TES unit could not be charged to cover all the 5-hour period to meet all the heating demand in the peak period. In such cases, the aforementioned ASHP was considered to start operating to complete the heating demand in the remaining peak period. In this case, the peak clipping was also calculated accordingly.

Peak clipping indexes of the each considered case were presented in Figure 4.28. As illustrated in the figure, utilization of TES integrated SAWSHP significantly help clipping the peak loads during the peak period thanks to its high efficiency and high heat storage capability using solar energy. At this point, the results showed that the degree of thermal energy storage was crucial for clipping the peak loads as it directly affects the efficient heating period. In November, February, and March, the TES tank was thermally charged up to a higher temperature compared to the days in December and January where the solar radiation was low. Hence, the efficient SAWSHP with TES unit was able to operate for a longer period during the peak times in the warmer months, consequently, the peak clipping index was found to be higher, meaning that a larger electric load was clipped. For example, the *PCI* was around 25% - 27% in November and February, and it even reached about 30% in March, meaning that the peak loads clipped by about 25% to 30% in these months. However, the *PCI* was between 15% and 20% in December or January depending on the utilized TES material.

A critical point was inferred from the numerical outcomes. The thermal energy storage material used inside the TES tank with PCM had a significant effect on the peak clipping index (*PCI*), in comparison to utilization of an ASHP. Although utilization of water as the TES material created a noteworthy peak clipping, utilization of PCMs inside the tubes rather than water had also a conspicuous potential. For instance, using RT31 provided 27.2% peak clipping, while using water attained 26.5%. Besides, the *PCI* of these two materials were almost the same in February and March. However, it should not be overlooked that the RT28 HC was not able to release all the stored latent heat, as inferred from the liquid fraction curves given previously. This means that using all the stored heat in the RT28 HC would be expected to yield a larger *PCI* value. Hence, the heat transfer enhancement techniques could be useful for exploiting the stored energy from the PCMs, and this issue was addressed in the following sections where a re-evaluation process for the PCM utilization was carried out within this context using the PCM with enhanced effective thermal conductivity.

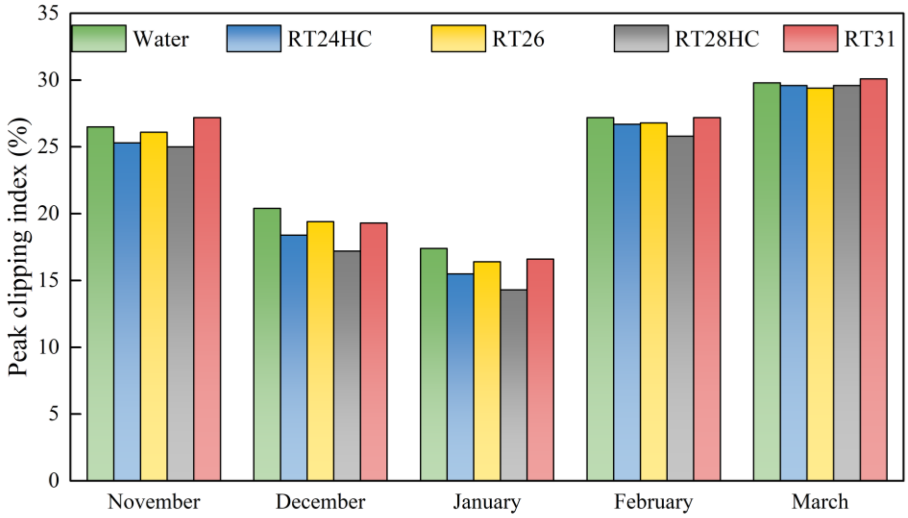

Figure 4.28. Peak clipping index for different PCMs investigated in System-1

4.4.3. Evaluation of Thermal Energy Storage and Volume Saving for TES Unit Using Different PCMs

To analyze the effectiveness of different PCMs in terms of thermal charging and relatedly their contribution to the volume saving, the total stored thermal energy into the water medium in the tank and into the tubes were given in Figure 4.29, separately. Examining the stored energy into the water inside the TES tank (~300 kg) for each case (see Figure 4.29a), it was noticed that the stored thermal energy was the highest in case of using water as a TES material inside the tubes, i.e., water case, rather than using PCM. In case of using PCM, the heat stored to the water slightly decreased due to large heat absorption of water. However, in warmer periods such as in March, the water inside the TES tank can store quite similar amount of thermal energy, due to the fact that the charging period was long enough to reach water temperatures at a certain value. Quantitatively, in case of using water as TES materials in tubes, the water inside the TES tank was able to store 6.4 kWh thermal energy in January and 12.2 kWh in March. In case of using RT28 HC as the TES material, the water inside the TES tank stored 5.3 kWh in January and 11.7 kWh in March. From these results, it was found that 20.8% and 4.3% more energy can be stored into the TES tank only, in case of using water as a TES material inside the tubes, rather than RT28 HC. However, it should be stressed that the energy store in the tubes were excluded in this computation. Considering the thermal energy stored in the tubes in case of using water or various PCMs given in Figure 4.29b, remarkably high values were noted by using RT28 HC, compared to all other TES materials including water. In the coldest month, January, the thermal energy values that were stored inside the tubes were 1.47 kWh and 3.57 kWh in case of using water and RT28 HC as a TES material, respectively. In the warmest month, these values were 2.81 kWh and 4.28 kWh for the same TES materials, respectively. Correspondingly, this result showed that using RT28 HC instead of water inside the TES tubes led to 142% and 52.5% higher thermal energy storage in January and March, respectively, because of large latent heat capacity of this material. It should be stressed that this latent heat stored inside the tubes by the PCM had a great potential for the improvement of effective thermal energy use, extension of heating time, and energy flexibility, as well as volume saving for the TES units.

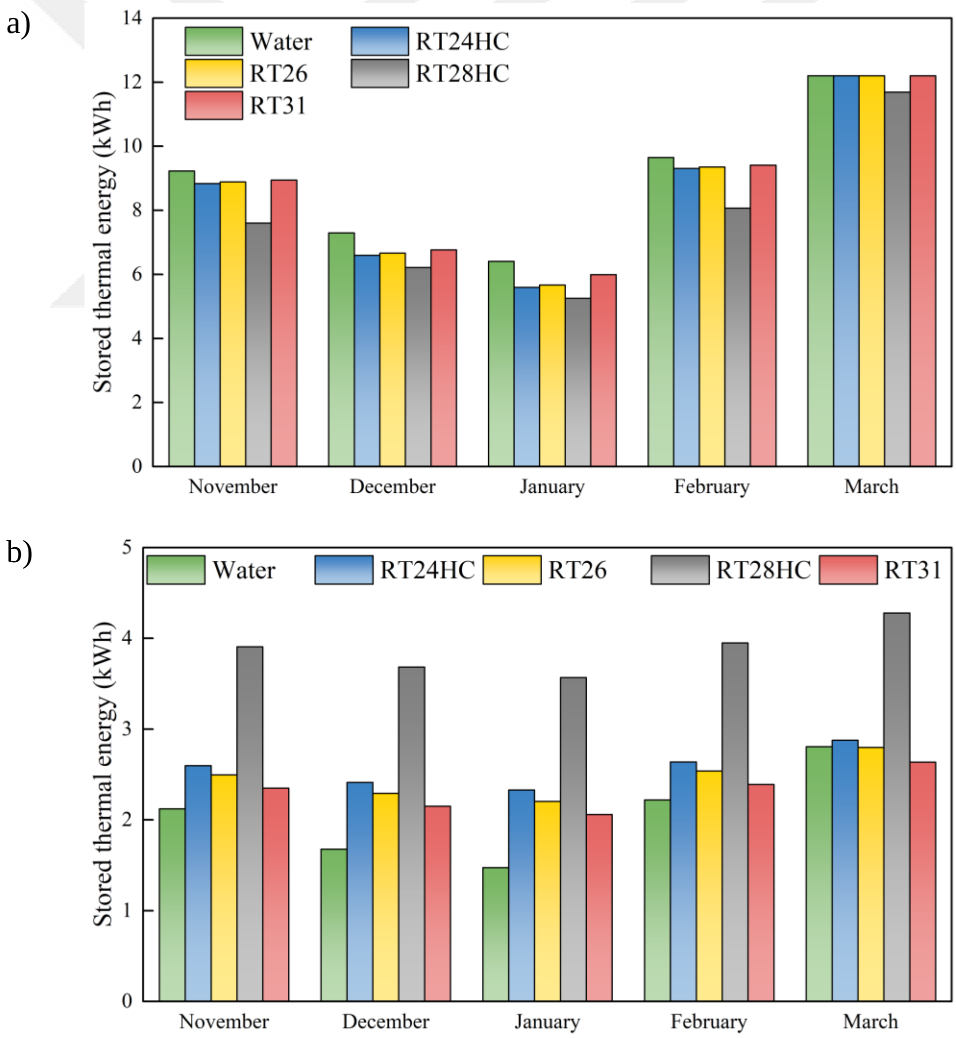

Figure 4.29. Stored thermal energy in the a) TES tank and b) PCM tubes at the end of the numerically simulated thermal charging process in System-1

Higher thermal energy storage can consequently lead to a noticeable amount of volume saving for the TES tank. Thanks to the high latent heat capacity of PCMs, they can add extra energy capacity per unit volume, which can ensure a volume saving. However, in case of using PCM, the latent and sensible heat storages should outperform the sensible heat storage of water in order to effectively obtain downsizing potential. In the present case with the given thermal energy storage data in Figure 4.29, utilization of PCM (RT28 HC) provided a remarkable volume saving especially in colder months, such as December and January, which reached up to 10.3% and 11.9%, respectively. Furthermore, in March, a significant volume saving of 6.4% was attained. However, the other considered PCMs did not significantly contribute to the volume saving, apart from improvements around 1% to 2%. Here, it was deduced that the considered PCM should store a significant amount of latent heat, i.e., the latent heat capacity should be high, besides, the PCM should also store a considerable amount of sensible heat in order to outperform water in TES applications. Hence, sensible heat storage capacity or capability according to the application should not be overlooked.

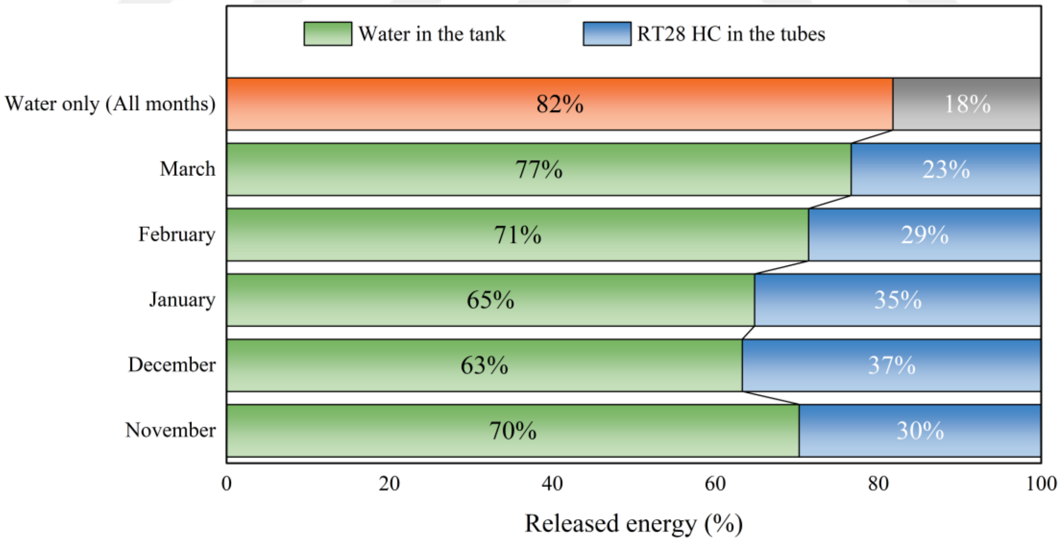

Figure 4.30. Ratio between the released thermal energy from the TES tank and from the tubes inside the tank regarding numerical computations

Figure 4.30 indicates the ratio between the released energy from the tank and from the tubes, during the discharging process. Regardless of the considered months, 82% of the thermal energy was stored in the TES tank and 18% was in the tubes in case of using water as a TES material. In this case, the thermal energy was all in sensible form. On the other hand, considering RT28 HC, a large portion of the thermal energy was supplied from the PCM inside the tubes, which corresponded up to 37% in December. Although the total energy storage was higher in case of using water by 4.3% to 11%, except March where it was 2% lower, it was shown that utilization of PCM had a significant potential when all the stored energy could be used.

4.4.4. Impact of Heat Transfer Enhancement by Effective Thermal Conductivity on Thermal Energy Storage Performance and Energy Flexibility of the System-1

In the previous three subsections, it was found by the computations and comparisons that using a PCM with high latent heat and appropriate phase change temperature, such as RT28 HC, had a remarkable potential to improve thermal energy storage capability. However, a challenging barrier, the inherent low thermal conductivity of PCMs, hinders the effective utilization of these materials in thermal energy storage since low thermal conductance led to incomplete melting or solidification, which consequently results in ineffective thermal energy storage. To overcome this drawback, various heat transfer enhancement techniques are utilized, such as addition of nanoparticles or attachment of fins. Thereby, the effective thermal conductivity can be significantly enhanced.

In the present work, it was found that using RT28 HC could remarkably enhance the energy storage capacity of the TES unit integrated to SAWSHP if the heat transfer through the PCM was appropriately increased. In order to simulate this enhancement in the present model, different effective thermal conductivity values were considered parametrically. To focus on the effect of k_{eff} on the thermal behavior of the system, the results were presented for the representative days in November, January, and March, which were illustrated in Figure 4.31 to Figure 4.33. Furthermore, the temperature variations were compared to the water only case taken as reference.

On the representative day selected in November, it was seen that the temperature in the water-only case was significantly higher compared to the water temperatures in PCM cases (see Figure 4.31a.). The reason was, as previously indicated, the high latent heat absorption of the material. As the thermal conductivity was increased, it was evidently seen from the figure that the slope of the temperature curves decreased during charging, due to the heat transfer from water to the PCM at a higher rate. Once the melting process was completed, the temperature curves in the PCM cases coincided, which showed that the variation of k_{eff} was more profound during phase change. This situation also went on during the discharging process, until the temperatures reached the solidification point. During solidification, a noticeable difference occurred between the water temperatures in each case of different k_{eff}. More clearly, it was seen that increasing k_{eff} of the PCM (RT28 HC) was remarkably beneficial in terms of releasing heat to the water inside the TES tank. Hence, it contributed to the discharging time as well.

a)

b)

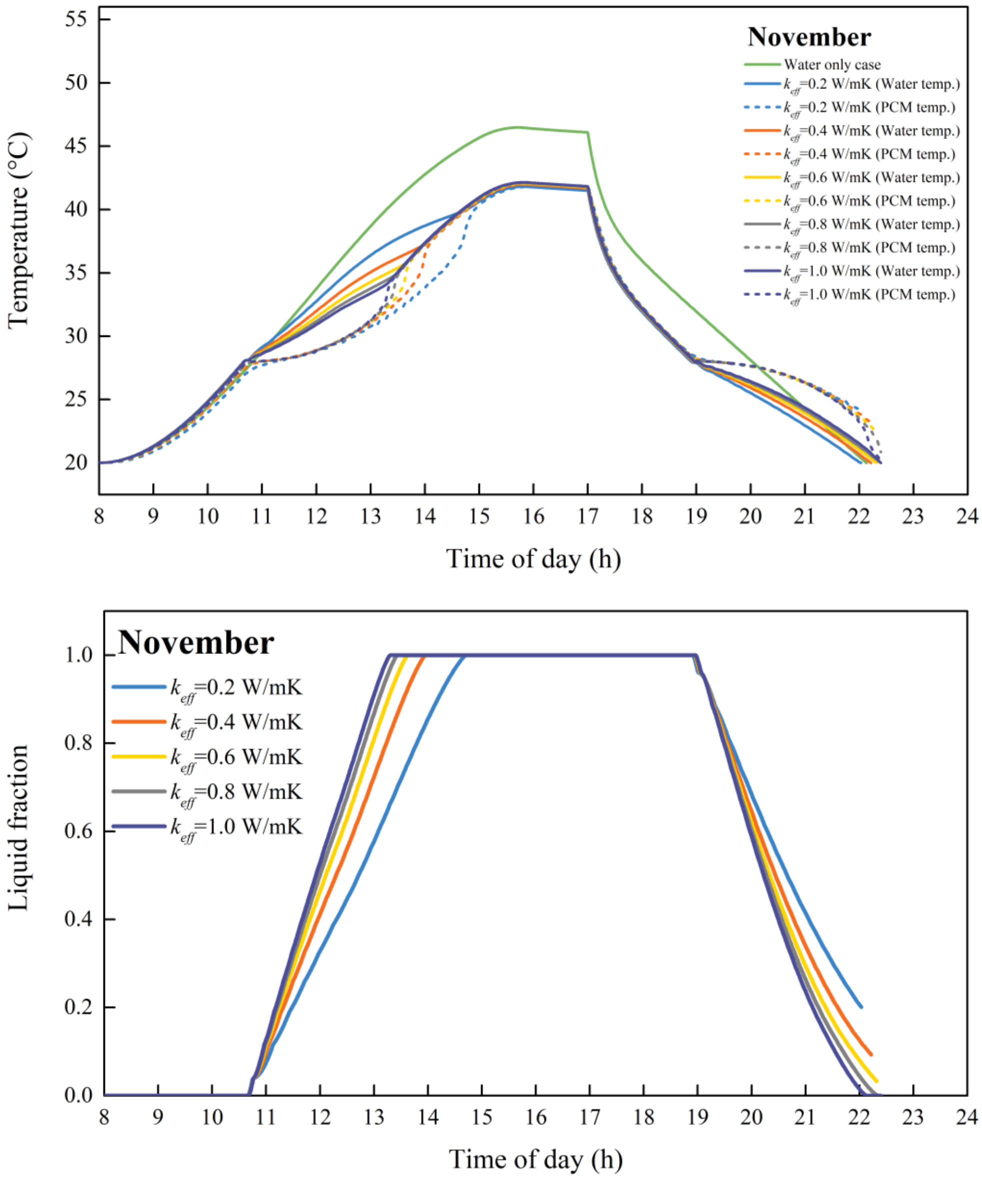

Figure 4.31. Temperature (a) and liquid fraction (b) variations of the considered TES materials with different k_{eff} on the representative day in November

The liquid fraction curves given in Figure 4.31b provided an important overview to the latent heat utilization. As inferred from the figure, the PCM was fully melted in each case in November, and they also stored a considerable amount of sensible heat. Besides, in discharging, it was noted that increasing k_{eff} of the PCM yielded a lower liquid fraction at the end of the process, meaning that a higher amount of latent heat was released. A point worth highlighting was that the liquid fraction curves became steeper when k_{eff} was gradually increased. However, the steepness of the curve with respect to increasing k_{eff} was limited to some extent.

As the coldest representative day considered within this study, it was seen from Figure 4.32 that the water temperatures could not reach 40°C in case of no PCM used and 35°C in case of PCM used. Besides, even though the k_{eff} was increased, the PCM was unable to store significant amount of sensible heat after melting was completed. This can be also inferred from the liquid fraction curves. The plateau region at f=1 was relatively shorter, indicating that the sensible heat storage was lower compared to other months. The original PCM with k_{eff} =0.2 W/mK was even not able to fulfill its latent heat capacity during charging, and it also could not release all the stored energy during discharging. However, increasing k_{eff} to k_{eff} =0.8 W/mK ensured a full discharge of the stored latent heat.

a)

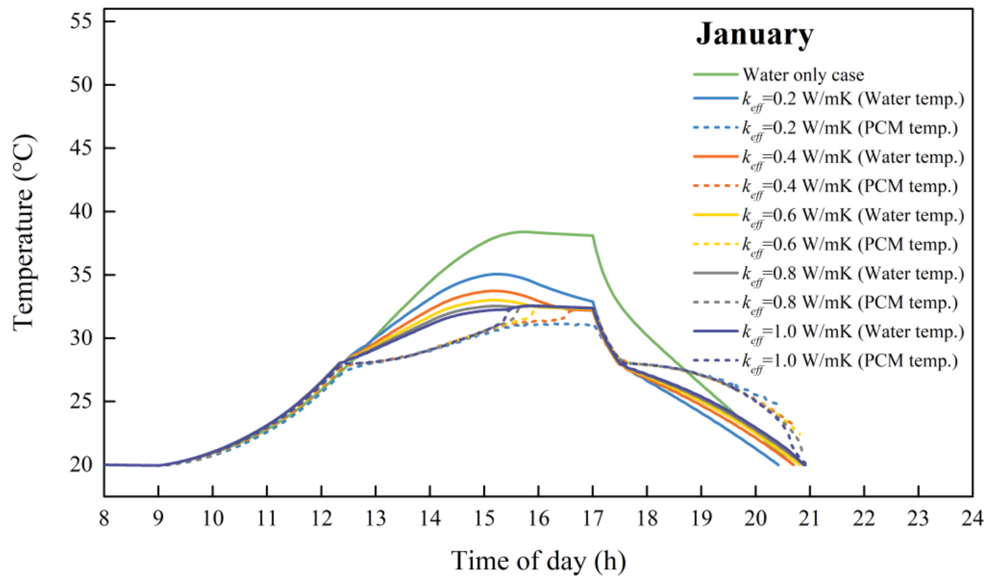

Figure 4.32. Temperature (a) and liquid fraction (b) variations of the considered TES materials with different k_{eff} on the representative day in January

b)

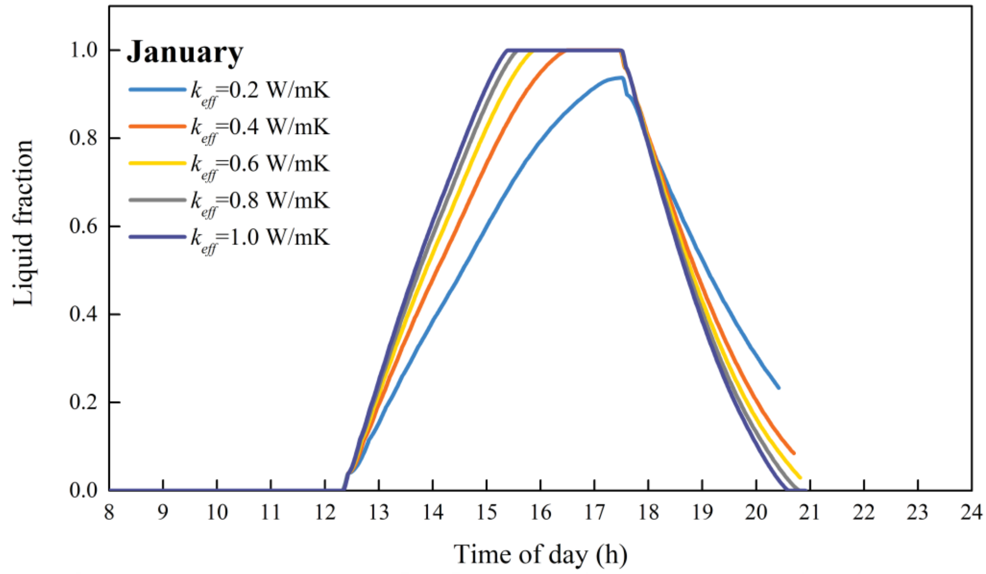

Figure 4.32. (Continued) Temperature (a) and liquid fraction (b) variations of the considered TES materials with different k_{eff} on the representative day in January

The representative day in March was the warmest one in the heating season, and it was noticed from Figure 4.33 that the water temperatures in no-PCM and PCM cases were relatively closer to each other compared to other months. In addition, it was evident that a significant amount of sensible heat was stored once the latent heat storage was completed because of the higher solar radiation and longer sunshine period that allowed to bring more heat input into the TES unit. Both from the temperature and liquid fraction curves, it was clear that a high amount of sensible heat was released, nevertheless, the k_{eff} should be higher, e.g., k_{eff} =0.8 W/mK in order to fully benefit the stored latent heat.

For quantitative analysis of the latent heat release, Figure 4.34 shows the utilization of latent heat in kWh as well as in percentage on the representative day in January. Since the latent heat utilization exhibited negligible differences regarding different months, the discussion was carried out on the coldest day. The computations revealed that the original PCM with k_{eff} =0.2 W/mK was unable to store all the latent heat with respect to its capacity, hence, the heat release in the discharge was also limited, which was quantitatively 70.4%. However, when k_{eff} was increased one step to k_{eff} =0.4 W/mK, a remarkable improvement was recorded. In this case, the RT28 HC was able to release 91.5% of its stored latent heat, which corresponded to 3.0 kWh. With this level of improvement of k_{eff}, the latent heat utilization was enhanced by 30%. Increasing k_{eff} gradually to k_{eff} =0.6 W/mK, k_{eff} =0.8 W/mK, and eventually k_{eff} =1.0 W/mK ensured an enhancement of 6% and 3%, respectively, while the latent heat use in case of k_{eff} =0.8 W/mK and k_{eff} =1.0 W/mK were identical. To sum up, increment of effective thermal conductivity provided a remarkable enhancement in latent heat utilization of PCM, however, its improvement effect decreased after k_{eff} =0.4 W/mK. Consideration of k_{eff}=0.8 W/mK allowed to fully utilize the stored latent heat.

a)

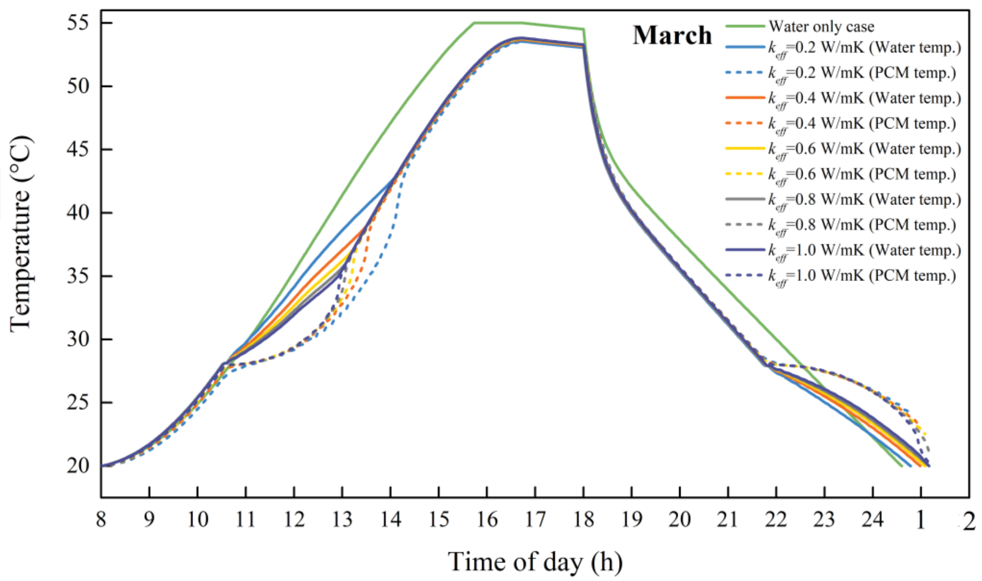

b)

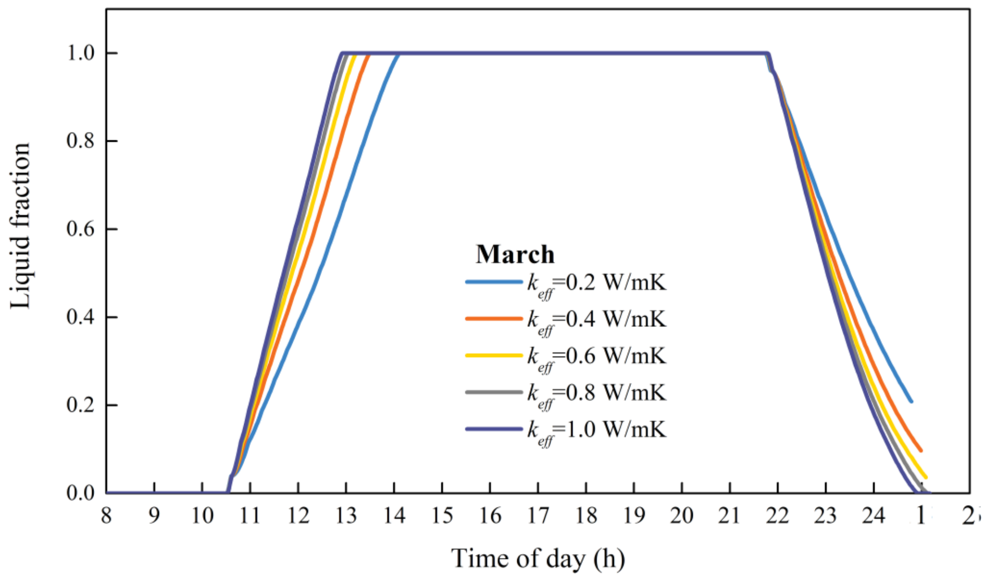

Figure 4.33. Temperature (a) and liquid fraction (b) variations of the considered TES materials with different k_{eff} on the representative day in March

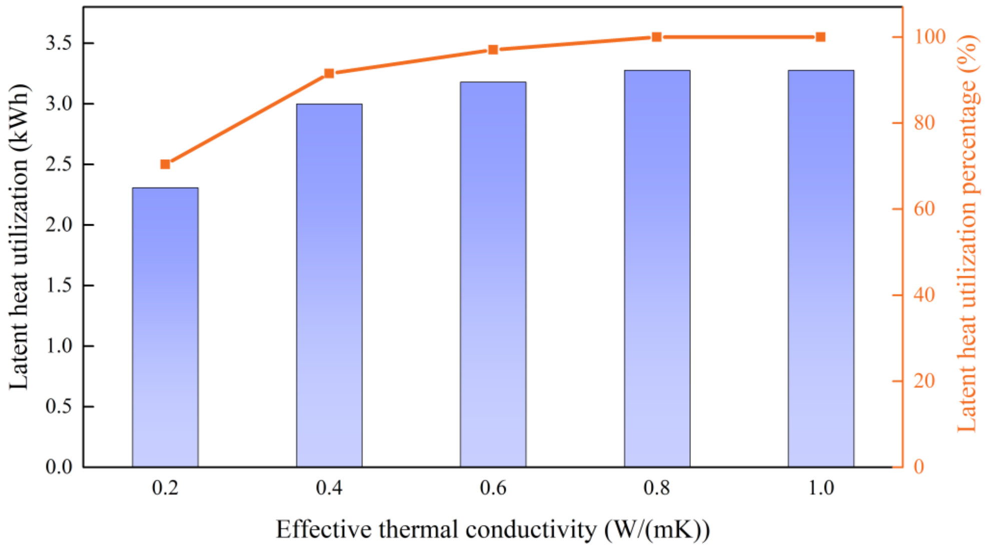

Figure 4.34. Latent heat utilization regarding different k_{eff} values on the representative day in January

Effective utilization of latent heat had a considerable impact on the discharging times in the TES integrated SAWSHP system. Hence, the computed discharge times on the selected days in November, January and March regarding different k_{eff} values of RT28 HC were given in Table 4.3 to elaborate the influence of k_{eff} on the heating time that was provided by the heat pump. It is worth recalling here that the discharging time was 307 min, 221 min, and 395 min on the representative days in November, January, and March, respectively. As seen from the values presented in the table, augmentation of k_{eff} had a remarkable impact on the elongation of the discharging time, i.e., the heating time by the HP before the thermal energy in the TES unit was consumed. Increasing keff one step, i.e., to k_{eff} = 0.4 W/mK ensured a noticeable elongation in the discharging time, which corresponded to an increase of 3.7%, 7.8% and 2.9% in November, January and March, respectively. This showed the prominent benefit of PCM utilization in cold weathers. On the other hand, increasing keff from k_{eff} = 0.2 W/mK to k_{eff} = 0.8 W/mK exhibited an enhancement in the discharging times by 7.3%, 13.7%, and 5.4% in November, January, and March, respectively. It was evidently deduced that improvement of latent heat utilization had a remarkable impact on the elongation of discharging times, which led to longer heating times by the SAWSHP.

Comparing the PCM utilization with enhanced effective thermal conductivity to the case of utilization only water in the TES unit, the computed discharging times were compared. First, the discharging times in case of using no-PCM was slightly higher in November and January, in comparison to the original PCM (RT28HC with k=0.2 W/mK). However, it was 3% higher in March. Increasing the effective thermal conductivity one step further, which is k_{eff} = 0.4 W/mK, the discharging times were respectively 1.6% and 6.1% higher for PCM case in November and March, compared to no-PCM case, while there was no improvement noted in January. Yet, augmentation of the k_{eff} to k_{eff} = 0.8 W/mK attained a remarkable enhancement compared to using only water in the TES unit. This enhancement in the discharging time was quantitatively 5.2%, 5.4%, and 8.6% in November, January, and March, respectively. A noteworthy point was found that a further increment of k_{eff} beyond k_{eff} = 0.8 W/mK brought no additional improvement. Therefore, a four-times enhancement of k_{eff} was adequate for effective latent heat utilization in this case.

Table 4.3. Impact of k_{eff} on the heating times (min) during discharge in different months

k_{eff} (W/(mK))	November	January	March
0.2	301	205	407
0.4	312	221	419
0.6	319	229	425
0.8	323	233	429
1.0	323	233	429

Increasing latent heat utilization of the PCM by enhancing the effective thermal conductivity led to some influences on the energy flexibility of the system, which was quantified by the peak clipping index (*PCI*). The computed *PCI* were given in Figure 4.35 for different k_{eff} values. It was deduced that increasing k_{eff} of the PCM ensured a larger *PCI* in the cold days, while there was negligible difference between them in the warmer days. On the other hand, it was noticed that the *PCI* of the PCM cases were slightly lower compared to no-PCM case. For example, increasing k_{eff} from k_{eff}=0.2 W/mK to 0.4 W/mK brought an enhancement of 5.2%, by improving it from 17.2% to 18.1%, in December. Augmenting k_{eff} one step further made the value 19.1%. A more remarkable enhancement was noticed in January, and the *PCI* increased from 14.3% to 18.1%. This means that effective utilization of latent heat could enhance the flexibility of the system by clipping the peak loads compared to ASHP systems. Hence, they can attain a significant reduction in the grid load. The *PCI* is a complex energy flexibility index that is dependent on the energy consumption which is related to the performance of the heat pumps as well as the thermal behavior of the discharged TES unit. TES units allowing a longer operation of the heat pump could also lead to slightly higher energy consumption, which could not always enhance the peak clipping index. All in all, the most important factor for the *PCI* was found as the charging capacity of the TES unit, which was directly related to the solar radiation intensity in this system, since the TES unit obtained the required energy directly from the renewable solar energy.

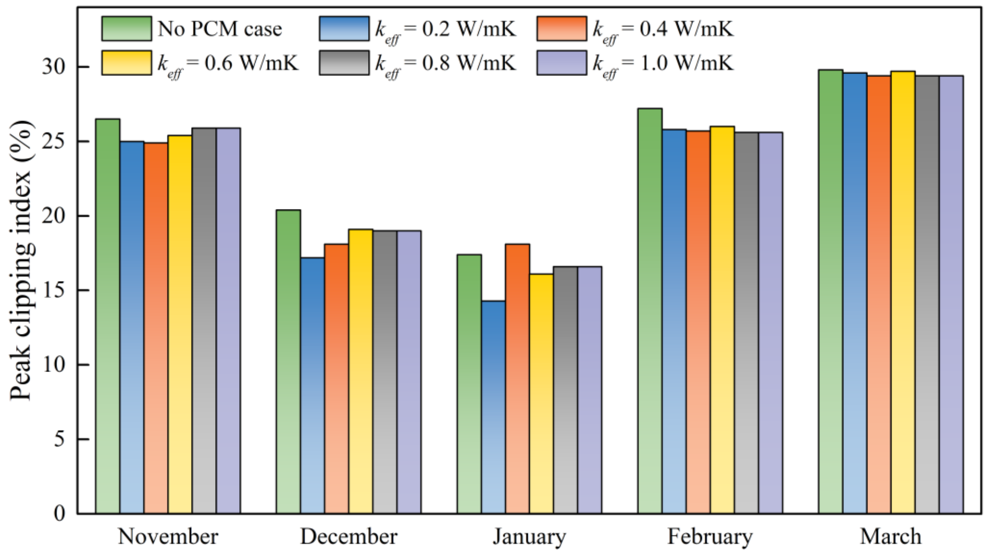

Figure 4.35. Impact of effective thermal conductivity on the peak clipping index

4.5. Numerical Evaluation of System-2 Considering Thermal Energy Storage/Release Capability and Energy Flexibility in Different Conditions

In the established model for System-2, the operation of the TES integrated ASHP system during thermal charging and discharging periods is simulated considering the ASHP performance obtained by the experimental data using grey-box modeling. Similar to the experimental works, the initial temperature of the water as well as PCM inside the TES tank were set to 35°C, and the thermal charging, i.e., melting, period of the TES unit was continued until the water temperature reached 55°C. During charging process, thermal behavior of the PCM was focused, hence, different PCMs, such as lauric acid, Rubitherm RT38, RT44 HC, and RT47 of which the thermophysical properties were given in Table 4.4, were numerically tested inside the TES unit. Thereafter, the discharging process was initiated, and the thermal behavior of the selected PCMs as well as their load shifting potential were evaluated during thermal discharge, i.e., solidification process. It should be noted that the thermal charging process would take about 4 hours. Then, as soon as the thermal charging process was completed, the discharging process was initiated.

Table 4.4. Thermophysical properties of the PCMs used in the numerical study for System-2

Thermophysical property	RT38	Lauric acid	RT44HC	RT47
Density (kg/m^3)	815	850	900	825
Specific heat (J/(kgK))	2000	2300	2000	2000
Thermal conductivity (W/(mK))	0.2	0.14	0.2	0.2
Phase change temperature (°C)	38	41	44	47
Latent heat of fusion (J/kg)	138000	155000	208000	136000

4.5.1. Temperature Variations and Latent Heat Utilization of Different PCMs in System-2

Temperature variations of the water and PCM inside the TES tank were shown in Figure 4.36. The solid lines represent the water temperature, while the dashed lines point out the average PCM temperatures in the tubes for each case. According to the numerical outcomes depicted in the figure, the charging process taking from 35°C to 55°C was the shortest in case of using water in the tubes, which can be expectable due to the rapid temperature rises along with relatively lower thermal resistance since there was water inside the tubes in the TES unit. On the other hand, it was noticed that the presence of PCM inside the tubes slowed down the temperature rise of the water inside the TES tank, and this decrement in the rate of change of temperature with respect to time was smaller when the phase change temperature was low, such as RT38, because its phase change process was initiated earlier, compared to other PCMs. Focusing on the PCM temperature variations, they exhibited a rise accompanying to the water temperature increase, meaning that they store sensible heat, and it was clearly noticed from the figure that the increment rate was decreased once the PCM temperatures reached their corresponding phase change temperatures. For the PCMs except RT38, which has a relatively lower phase change temperature, it was seen that their temperature could not reach that of water in the TES unit until thermal discharge started. This shows that there had still been a potential for the energy storage even if the material completed its phase change and fulfilled all its latent heat capacity, i.e., there could be still a potential for sensible heat storage into the PCM. Nonetheless, this could not happen due to the low thermal conductivity and relatively higher phase change temperatures of the PCMs.

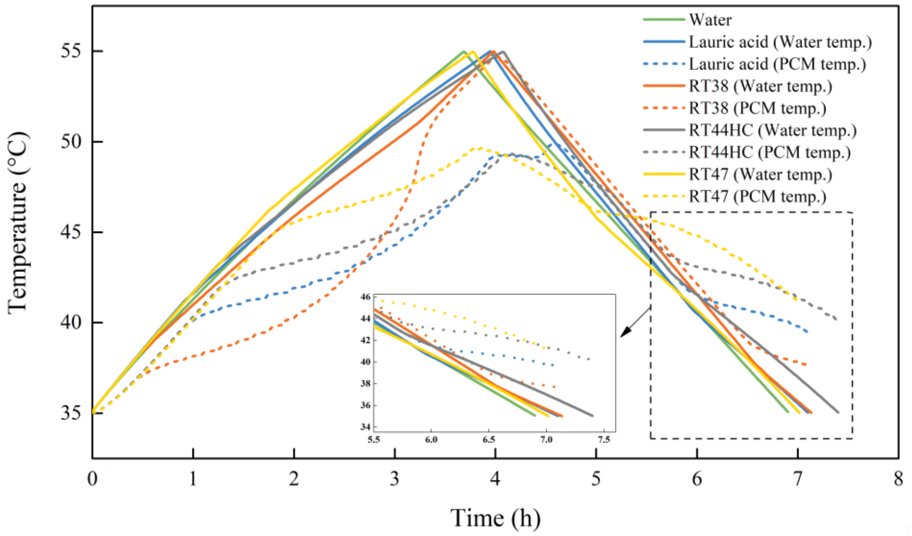

Figure 4.36. Water and PCM temperature variations computed numerically in case of using different PCMs in the TES unit in System-2

As soon as the charging process was completed, the heat pump operation was ceased, and the discharging was started to meet the heating load specified as 3 kW. Hence, the temperature of the water inside the tank started to decrease, and the PCM temperatures accompanied this decrement in the water temperature up to a point around the phase change temperature of the PCMs. This means that, the PCM used the sensible heat stored, and thereafter, it started to release the thermal energy stored in latent heat form. As seen from the figure as well as from the scale-up portion, a nearly isothermal temperature profile was noticed on the dashed PCM temperature curves, indicating the latent heat release. Nevertheless, the PCM temperatures were around the phase change point when the water temperature inside the tank reached the reference temperature, 35°C, which indicates the end of the process. So, it was highly expectable that a significant portion of latent heat stored inside the material could not be used during thermal discharging process. This phenomenon was examined over the liquid fraction curves (Figure 4.37) given in the next paragraph.

Variations of computed average liquid fraction values for the investigated PCMs were given in Figure 4.37 during the whole process, i.e., thermal charging and then discharging, continuously. Tracing the curves presented in the figure, it can be clearly seen that the liquid fraction values stayed at zero, which means that the material did not start changing its phase for a while, and it stored sensible heat in solid state during this period until its temperature reaches the phase change point. Once its temperature reaches that point, the liquid fraction started to increase rapidly indicating that the PCM was changing its phase from solid to liquid by storing thermal energy in latent heat form. It is worth noting here that the liquid fraction still continued to increase when the thermal charging period, which took nearly 4 hours, was over. The reason is that the process was turned from charging to discharging as soon as the storage temperature reaches T_{st}=55°C, and it started to decrease from 55°C to 35°C. At this point, the PCMs were at a lower temperature, and they sustained the energy absorption in both latent and sensible heat form, except RT47 which stored 91% of its total latent heat capacity, until the temperature of the PCM and the water equalized, which was due to the relatively higher phase change temperature of the RT47. Thereafter, the PCM started to release its sensible and latent heat to the water inside the TES tank. It is visible from the figure that the discharging process ended before the PCMs released all the latent heat they had previously stored. This clearly highlights that all the investigated PCMs were unable to fully discharge their latent heat during this discharging process.

Related to the liquid fraction curves, the latent heat utilization was computed and presented in Figure 4.38 since the key point of using PCM in a TES unit is the exploitation of latent heat. The columns in the figure denote the amount of discharged latent heat from the PCMs, while the line graph indicates the percentage use of the latent heat capacity of the PCM. The computations showed that the PCMs RT38, lauric acid, RT44 HC, and RT47 respectively released 0.52 kWh, 0.97 kWh, 1.79 kWh, and 1.34 kWh of latent heat. This corresponded to a latent heat utilization rate of 29%, 48%, 66%, and 76% for the RT38, lauric acid, RT44 HC, and RT47. Although the percentage use value was higher for RT47, the amount of latent heat utilization was the highest for

RT44 HC, indicating that it was the most beneficial PCM that could be used for the purpose of latent heat utilization in this TES integrated ASHP system. Here, it should be underlined that the phase change temperature and latent heat capacity are utmost important parameters for exploitation of latent heat. Relatedly, it can be deduced that using RT44 HC among the investigated PCMs could achieve the most beneficial latent heat utilization for both charging and discharging. Furthermore, it was revealed that the appropriate choice of TES material could further contribute to the energy flexibility of the system as well as reduction of storage volume, which were discussed in the following parts.

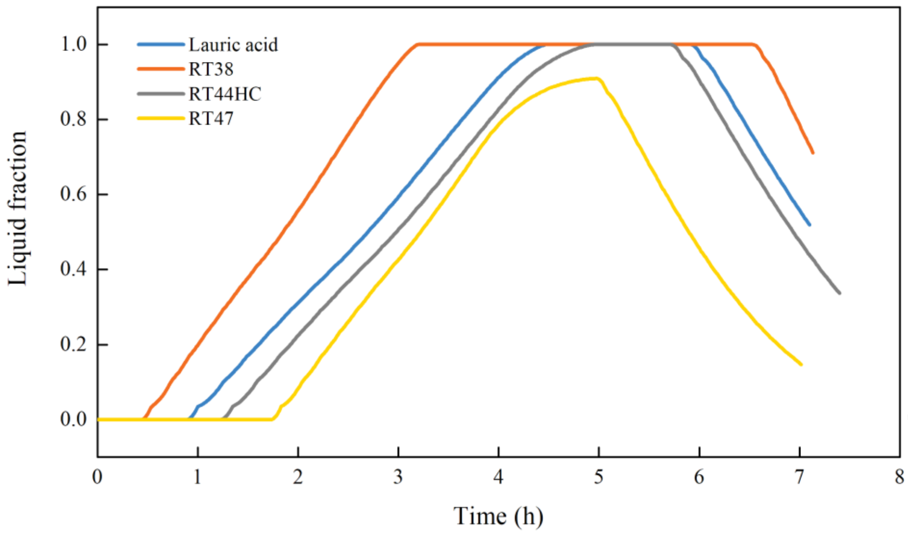

Figure 4.37. Variations of liquid fraction of each considered PCMs in the TES unit during thermal charging and discharging in System-2

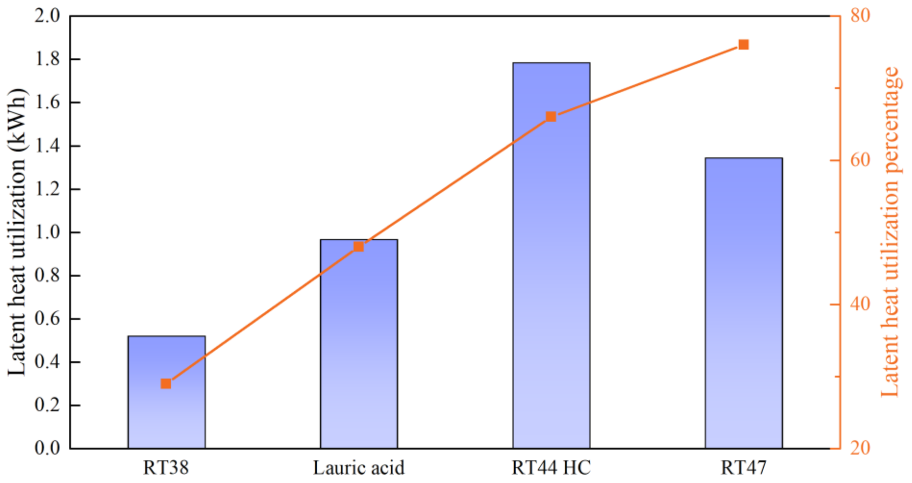

Figure 4.38. Latent heat utilization of different PCMs in System-2 regarding numerical simulations

4.5.2. Evaluation of Using Different PCMs in terms of Charge/Discharge Times and Load Shifting Potential

The time needed to charge the TES unit as well as the duration of using the stored thermal energy are significant metrics to determine the energy storage capability and energy flexibility potential of the TES unit integrated to the ASHP. Therefore, Figure 4.39 indicates the thermal charging and discharging times computed for different TES materials including water. Here, it was observed that using PCM instead of water inside the tubes located in the TES tank extended the time required to bring the water temperature from 35°C to 55°C. This duration was 222 minutes in case of having water inside the tubes, while it was 240, 238, 245, and 228 minutes when RT38, lauric acid, RT44 HC, and RT47 were used, respectively. Thus, the thermal charging time was found to be 8.0%, 7.2%, 10.4%, and 2.7% longer in case of using RT38, lauric acid, RT44 HC, and RT47, respectively, compared to water case. The reason for longer thermal charge duration in RT44 HC case can be attributed to its melting temperature which ensured an initiation of melting process in around half-time of the process and to its high latent heat that provided a larger heat absorption which led to a decrement effect in the rate of change of water temperature in the TES tank. On the other hand, the charging time was close to that of water when using RT47, and it was due to its relatively higher melting point as well as its incomplete latent heat storage situation.

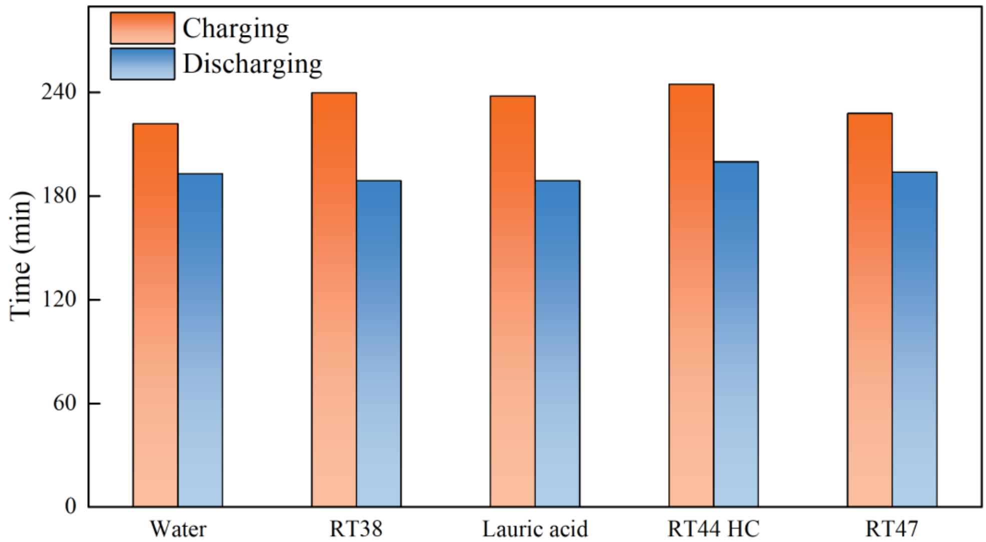

Figure 4.39. Thermal charging and discharging times in case of using different thermal energy storage materials in System-2

Thermal discharge times given in the figure showed that using RT44 HC attained a 3.6% longer discharge time compared to the case using water as a TES material. On the other hand, using RT47 yielded almost the same discharge time with the water case, while using RT38 or lauric acid exhibited a 2.1% decrement in the discharge time. It should be emphasized here that the discharge time has a particular importance since it is related to the meeting of the heating load during a space heating process as well as it has a strong relation with the energy flexibility of the system. Because longer discharge times without consuming electric energy improves load shifting capability of the system.

Load shifting was the focus point for the purpose of the layout of System-2, i.e., the air-source heat pump system charges the TES unit during off-peak periods, and this stored thermal energy is utilized during on-peak periods without consuming additional electric energy to operate the compressor. In other words, the electric energy that drives the compressor to operate the heat pump system is obtained from the grid during off-peak periods rather than operating it during on-peak times, hence, it attains a significant reduction of the excessive loads on the grid. Furthermore, it also benefits from the time-of-use tariffs which consequently led to lower electricity bills for the user. In addition to that, it also helps reducing CO_2 emissions since these emissions sourced by the electricity generation are also significantly high if the load is high in the on-peak periods. Therefore, the more electric energy shifted from on-peak to off-peak periods, the higher the benefits in terms of energy efficiency and energy flexibility.

The load shifting index as an energy flexibility indicator computed for the TES integrated ASHP system (System-2) were given in Figure 4.40 in case of using water and different PCMs as TES materials. According to the computed and presented numerical outcomes, the load shifting index was found as the lowest for water (64.9%) and the highest for RT44 HC (68.9%), which indicated that more than 2/3 of the grid load can be shifted to off-peak periods even though the PCM were not able to use all its stored latent heat. Besides, this outcome showed that 6.2% larger amount of electric load on the grid can be shifted when RT44 HC is used inside the TES unit, compared to using water. Basically, it was inferred that utilization of any PCM considered within the present work have a larger potential of load shifting, compared to that of water. The two main reasons here were that the relatively lower energy consumption of the heat pump compressor during thermal charging due to its repressing effect on the rapid rise of the water temperature which causes a larger energy consumption of the compressor during thermal charging. Secondly, the longer discharge duration in case of using PCM remarkably contributed to the load shifting, i.e., energy flexibility. Here, it should be significantly emphasized that the RT44HC showed a superior thermal discharging behavior even if its latent heat had not been fully exploited. This means that, there was still a significant amount of thermal energy trapped in the PCM, and the benefits of using this PCM inside the investigated TES unit could have been further enhanced by heat transfer enhancement techniques from various points of views such as energy efficiency, effective energy use, and energy flexibility.

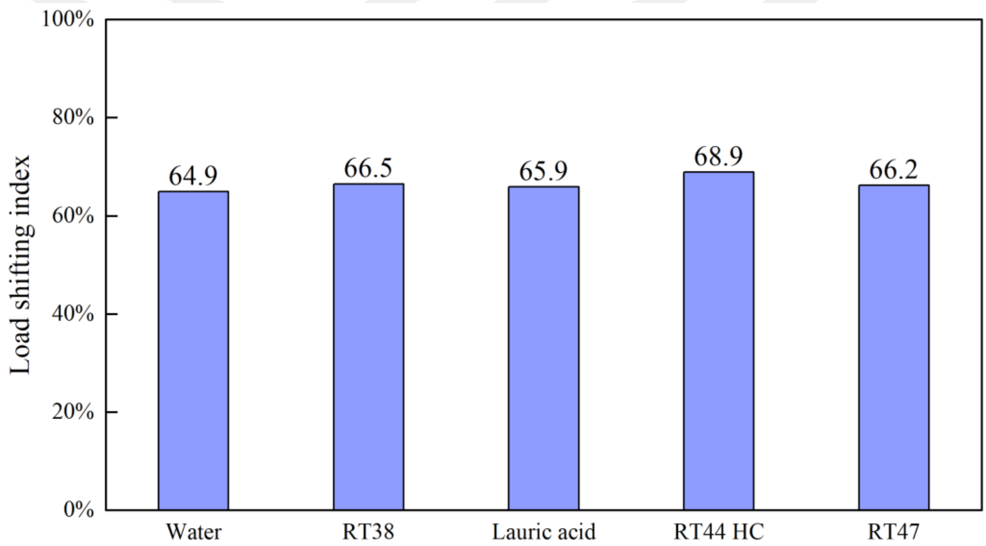

Figure 4.40. Load shifting index in case of using different TES materials

Shifting the grid loads from on-peak to off-peak periods using thermal energy storage systems can also contribute to the reduction of energy costs due to time-of-use pricing. Related to the amount of shifted loads, consuming energy in the off-peak periods rather than on-peak periods brought a significant cost saving, which was evaluated over the cost saving ratio (*CSR*) defined previously, and the results were given in Figure 4.41. Besides, the rate of cost saving can be different with respect to the time period of thermal charging, namely in day-tariff (05:00-17:00) or night-tariff (22:00-05:00). Using water as a TES material achieved a cost saving of 27.8% and 50.1% depending on charging in day-tariff or night-tariff, respectively. Using PCM instead of water brought a slight enhancement in CSR. Nevertheless, this enhancement was more profound when RT44 HC used as a TES material because of its high latent heat capacity and medium phase change temperature that is roughly between the initial and final storage temperatures as a median. The cost saving was around 1.8% when using lauric acid instead of water as a TES material. However, this enhancement was more pronounced when RT44 HC was used instead of water, which was quantitatively 6.2%. Hence, it was found from the computations that using a PCM having similar thermophysical properties to those of RT44 HC would be beneficial for load shifting and cost saving actions in the TES integrated ASHP system.

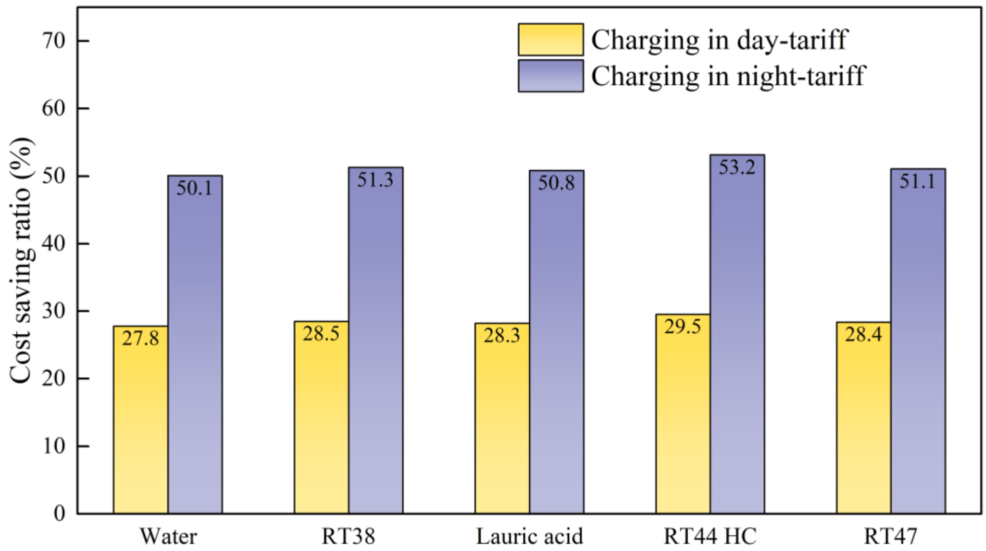

Figure 4.41. Cost saving obtained by load shifting operations for different PCMs

4.5.3. Evaluation of the Effects of Different PCMs on the Storage Volume Saving

Ensuring the previously mentioned energy efficiency and flexibility at the highest possible level is undoubtedly crucial for TES integrated heat pump systems. Yet another important parameter is the size of the storage tank since it is usually limited due to the space restrictions in many practical engineering applications. Therefore, the storage volume should be reduced as much as possible without sacrificing the thermal energy storage density. One of the best ways to achieve this is the phase change materials due to their high storage density per unit volume. In this subsection of the numerical study carried out for the System-2, the rate of volume saving was computed with respect to using water only inside the TES tank, and the results were presented in Figure 4.42. The volume saving ratio for the thermal energy storage was computed regarding the total thermal energy storage capacity of the TES unit including sensible and latent heat regarding the TES materials it contains. Thereby, the calculation results showed that a significant volume saving can be attained using PCM inside the TES units in the examined system, compared to using water only. Quantitatively, using RT38, lauric acid, RT44 HC, and RT47 could achieve considerable reductions in the TES unit volume, which reached up to 10.1%, 8.5%, 11.7%, and 3.7%, respectively. The reason why the volume saving rate was noticeably lower in case of using RT47 was that it was not able to benefit all the latent heat capacity it had, nor the full sensible heat capacity. Because RT47 could not be fully charged due to its relatively high melting temperature, which did not allow it to fully use its chargeable latent heat capacity before the ASHP system shut down at the limit storage temperature, T_{st}=55°C. Hence, it could not bring an improvement in volume reduction as large as the other PCMs were able to. On the other hand, using RT44 HC exhibited a considerable enhancement in the volume saving of the storage tank reaching up to 11.7%, thanks to its high latent heat capacity as well as suitable phase change temperature, which is approximately the mean of the initial and final water temperatures in the TES tank.

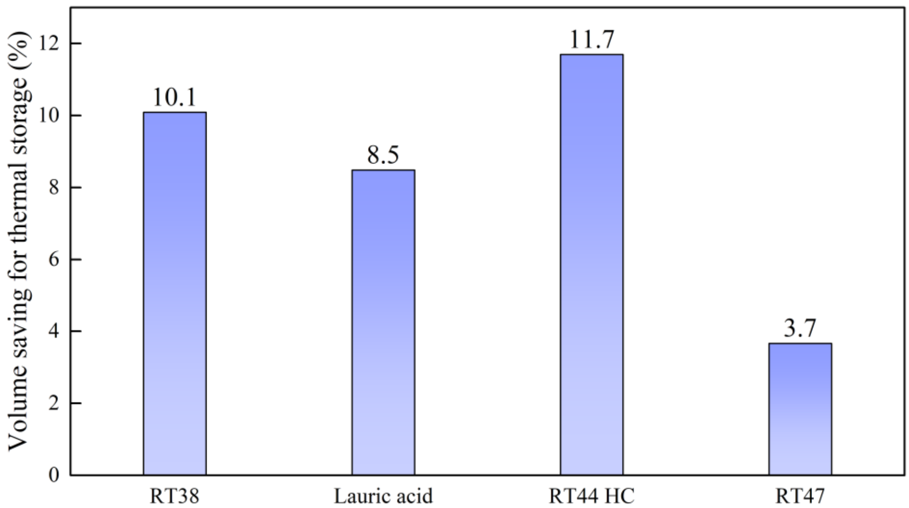

Figure 4.42. Rate of volume saving for thermal energy storage using different PCMs

Considering its benefits in thermal energy storage capacity, extension of heating time, enhancing energy flexibility by larger amount of load shifting, and a significant rate of TES tank volume reduction, the PCM labeled as RT44 HC were found as the appropriate alternative among the investigated PCMs, for the utilization in the TES unit in System-2, although it could not exploit all of the stored latent heat during discharging because of the limitation brought by the low thermal conductivity of these materials. Hence, it was inferred that a more pronounced improvement can be achieved using this PCM when the effective thermal conductivity would be higher, which was investigated and discussed in the upcoming section.

4.5.4. Impact of Heat Transfer Enhancement by Effective Thermal Conductivity on Thermal Energy Storage Performance and Energy Flexibility of the System-2

Previous computations clearly showed that RT44 HC is the most suitable thermal energy storage material to be used in the TES unit of the System-2, among the other investigated ones, thanks to its high latent heat capacity and appropriate phase change temperature that allows to store thermal energy by using all the latent heat capacity. However, the material could not use all the stored latent heat due to its low thermal conductivity, which is a common problem for PCMs. Enhancing its effective thermal conductivity can further highlight its benefits. Hence, a set of numerical simulations were carried out and discussed in this subsection by gradually increasing the effective thermal conductivity of the PCM from k_{eff}=0.2 W/mK to 1.2 W/mK by 0.2 W/mK steps. Following performance metrics were investigated according to the numerically tested effective thermal conductivity values:

- Temperature and liquid fraction variations
- Latent heat utilization
- Thermal charging and discharging times
- Load shifting index and corresponding operational cost reductions

Starting with the temperature and liquid fraction variations given in Figure 4.43, it was seen that, by the gradual increment of the effective thermal conductivity, the temperature curves of the PCM reached the temperature of the water inside the TES tank during thermal charging process, and their temperatures eventually reached T_{st}=55°C when the effective thermal conductivity was k_{eff}=0.4 W/mK or above, while the temperature of the PCM having an effective thermal conductivity of k_{eff}=0.2 W/mK could not reach the specified storage temperature by accompanying water temperature since the thermal discharging process started and the temperatures of the water and the

PCM started to decrease again. Apart from that, it was noticed that increasing the effective thermal conductivity led to a larger delay in the completion of the thermal charging process, and the slope of the temperature curves decreased during the time interval where the PCM stored a significant amount of thermal energy in latent form. After a time-shift of about 25 minutes compared to the original material with k_{eff}=0.2 W/mK, the discharging process was started for the PCMs with k_{eff} ≥0.4 W/mK. The temperature curves of the water and the PCM followed a similar trend up to the phase change temperature, and thereafter, the average PCM temperatures started to exhibit a nearly isothermal or a slowly decreasing profile, while the steepness of the water temperature curves reduced due to large thermal energy release from the PCM, which slowed down the reduction in water temperature inside the TES unit, which was a similar situation observed in the experimental works. The system stopped working when the water temperature reached 35°C, and it was seen from the figure that the PCM temperatures did not reach that temperature, indicating that they may still have useful thermal energy for the application, in sensible or latent form, which were evaluated by the liquid fraction curves.

The liquid fraction curves given in Figure 4.43b clearly pointed out that all the PCMs with various effective thermal conductivities managed to store all the latent heat regarding the capacity of material, which can be interpreted by the liquid fraction curves reaching f=1. Furthermore, it was also clear from the figure that the PCMs stored an amount of sensible heat before they started melting as well as after they completed the melting process. Considering that the thermal charging process took around 4.0 to 4.5 hours depending on the effective thermal conductivity, the PCMs with a k_{eff} ≥0.4 W/mK fully stored the latent heat, and they additionally stored sensible heat before thermal charging was completed. On the other hand, PCM with k_{eff} =0.2 W/mK stored an amount of latent heat approximately 85% of its latent heat capacity. Yet, the PCM continued to receive thermal energy from the water inside the TES tank that has a large thermal mass and larger temperature even if the discharging started. Thereby, the PCM with k_{eff} =0.2 W/mK was also able to store all its latent heat capacity. Nonetheless, there were two major drawbacks such as i) it could not store any sensible heat as the charging process completed, and ii) there had been a delay by the utilization of latent heat during discharging, which led this PCM to have a large amount of latent heat (33.7%) in its medium when the discharging process ended.

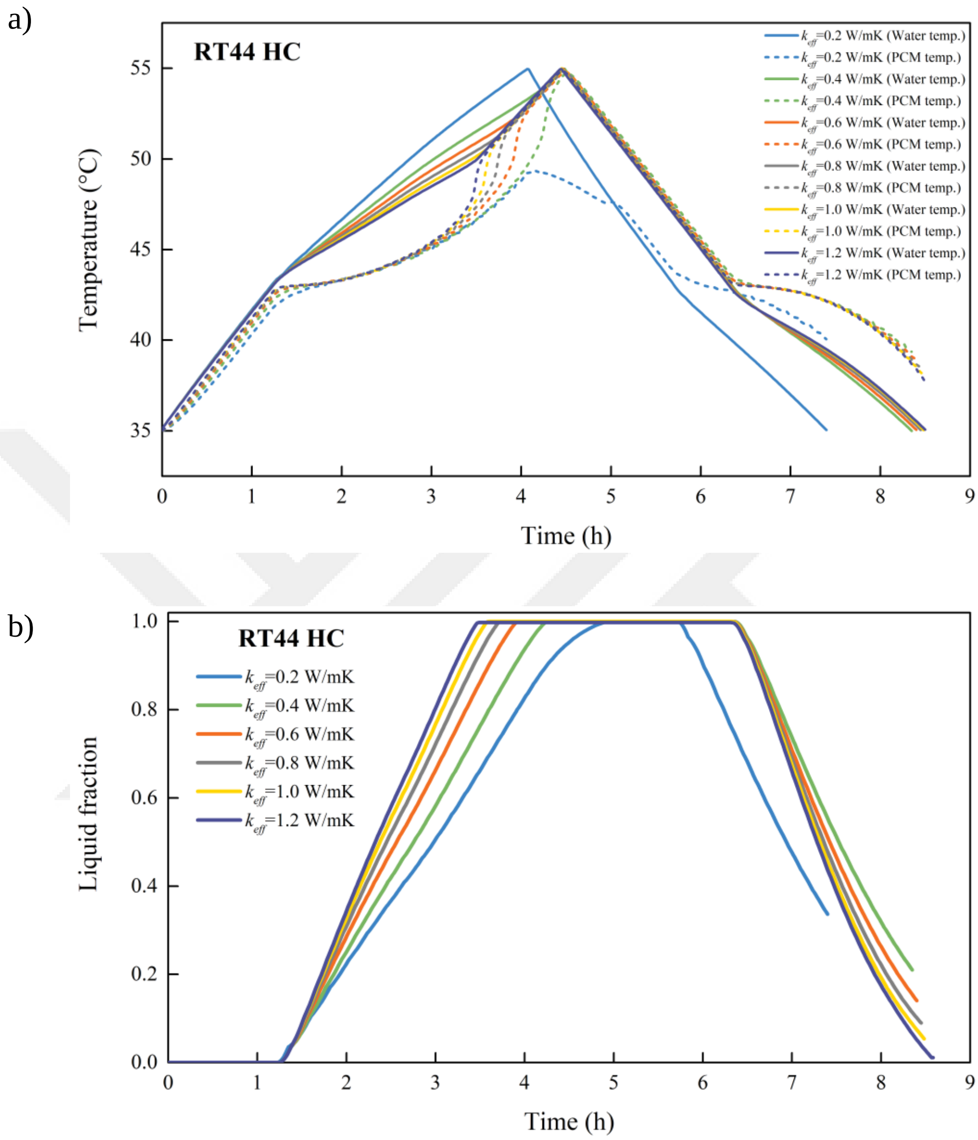

Figure 4.43. Effect of effective thermal conductivity on temperature and liquid fraction variations in System-2

For a more specific focus on the latent heat utilization during thermal discharging, Figure 4.44 illustrates the amount and percentage of latent heat use of PCMs with different k_{eff} during thermal discharging. Obviously, the gradual increase in the k_{eff} attained a larger amount of latent heat use. Especially the PCM with k_{eff} =0.4 W/mK exhibited a superior behavior in terms of latent heat utilization, compared to that with k_{eff} =0.2 W/mK. However, this impact became less pronounced by the further increment of the effective thermal conductivity. The numerical outcomes showed that 1.79 kWh of latent heat was discharged by the PCM with k_{eff} =0.2 W/mK, while it became 2.14 kWh by one step improvement of effective thermal conductivity, i.e., to k_{eff} =0.4 W/mK. This means that an improvement of 19.7% was achieved with this step. On the other hand, increasing k_{eff} from k_{eff} =1.0 W/mK to 1.2 W/mK brought only 5.3% of improvement in the latent heat use. Hence, it can be inferred that the major enhancement was ensured by increasing the effective thermal conductivity of RT44 HC from k_{eff} =0.2 W/mK to 0.4 W/mK. Besides, all the latent heat capacity was benefitted when the effective thermal conductivity was taken as k_{eff} =1.2 W/mK. As the augmentation beyond this value would result in sensible heat utilization of PCM, rather than relatively larger latent heat capacity, higher values of the effective thermal conductivity were not considered.

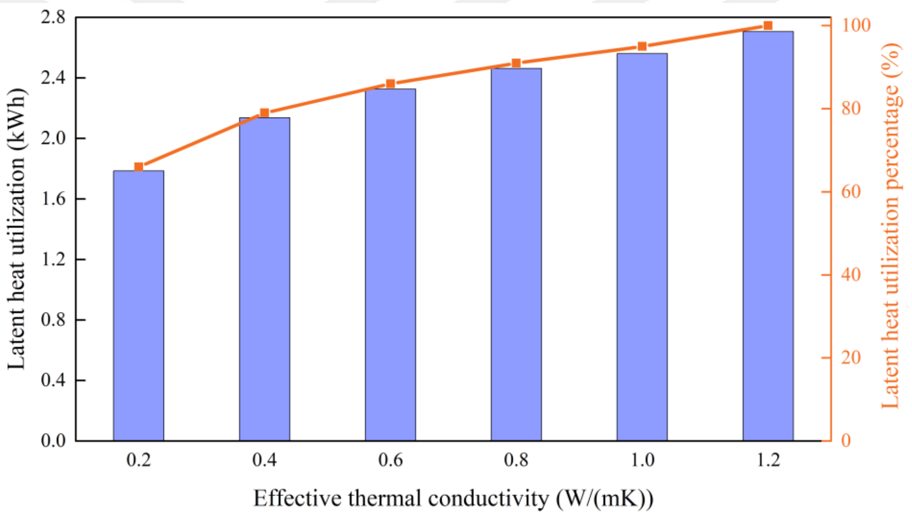

Figure 4.44. Latent heat utilization at different effective thermal conductivities during thermal discharging

The charging and discharging times were given in Figure 4.45 to evaluate the influence of heat transfer enhancements on temporal performance of the processes. As interpreted over the temperature curves, augmentation of k_{eff} led to an extension in both charging and discharging times. At the first sight, prolonged thermal charging times can be taken as a drawback; however, considering the TES applications for energy flexibility, especially in such a system, there could be a relatively larger off-peak time to store thermal energy. At this point, the discharging times would be more critical because they directly affect the heating time as well as shifted load. Hence, the charging time increased from 245 to 270 minutes when k_{eff} was augmented from k_{eff} =0.2 W/mK to 0.4

or larger, meaning that the charging time was not further extended by the increment of k_{eff}. The main reason for this occurrence was found as the lack of sensible heat storage after melting process as seen from the temperature curves. With higher k_{eff} values, the material was able to store larger sensible heat, which repressed the rise of water temperature and prolonged the charging time. As a more critical point, the discharging times were significantly improved by the increment of k_{eff}. While it was 200 minutes for k_{eff} =0.2 W/mK, the discharging times were significantly extended in a range of 232 to 247 minutes, for k_{eff} =0.4 W/mK and 1.2 W/mK. This clearly revealed the importance of heat transfer enhancement applications for PCMs. It is noteworthy here that the improvement is 32 minutes when k_{eff} was incremented from k_{eff} =0.2 W/mK to 0.4 W/mK, while the further improvement was 15 minutes when it was incremented from k_{eff} =0.4 W/mK to 1.2 W/mK. Hence, an effective thermal conductivity of k_{eff} =0.4 W/mK attained the major improvement in the discharging times.

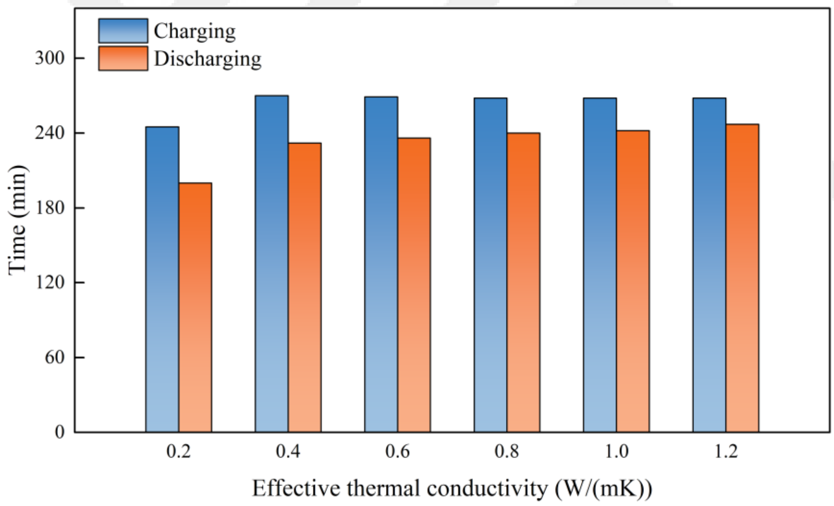

Figure 4.45. Impact of effective thermal conductivity on the charging and discharging times of the TES unit

As the energy flexibility indicator for the System-2, load shifting index (*LSI*) was defined and discussed previously. In this part, the effect of heat transfer enhancement on the *LSI* was presented in Figure 4.46a to evaluate the relation between the effective thermal conductivity of the PCM and energy flexibility of the system. In previous discussions, it was found that RT44 HC was successful for shifting 68.9% of the grid load from on-peak to off-peak periods, even though it had not used all its latent heat capacity. Hence, increasing effective thermal conductivity that can be ensured by various heat transfer enhancement techniques, the load shifting rate of the system was remarkably improved. Related to the augmentation in latent heat utilization, the load shifting index considerably increased from 68.9% to 78.4% when the k_{eff} was increased from k_{eff} =0.2 W/mK to 0.4 W/mK. Obviously, further increment in k_{eff} helped improving *LSI*, nonetheless, the rate of this enhancement was not as large. Increasing k_{eff} from k_{eff}=0.2 W/mK to 0.4 W/mK provided an improvement of 13.8% in the load shifting index, while further augmentation from k_{eff} =0.4 W/mK to 1.2 W/mK brought only 5% of an improvement in *LSI*, although the k_{eff} was increased 200%. To sum up, utilization of PCM with a proper and adequate heat transfer enhancement technique, or utilization of a suitable PCM with relatively high thermal conductivity can markedly contribute to the load shifting applications to improve energy flexibility of the TES integrated ASHP system and provide an efficient heating with lower grid load and lower carbon emissions.

Shifting the grid loads from on-peak to off-peak periods not only contribute to the energy flexibility of the system, but also it can relatedly reduce the electricity bills due to the time-of-use tariffs. Figure 4.46b indicates the cost saving rates (*CSR*) in two cases, namely when the TES unit was charged during daytime and during night-time, disregarding the heat loss from the TES tank. Using PCM (RT44 HC) with k_{eff} =0.2 W/mK brought a cost saving of 29.5% and 53.2% in case of thermal charging in the day-tariff and night-tariff, respectively, compared to the case where no load shifting was considered. Similar to the load shifting improvements, the increase of effective thermal conductivity from k_{eff} =0.2 W/mK to 0.4 W/mK achieved a cost saving of 33.6% and 60.5% with respect to charging in day-tariff and night-tariff, respectively, compared to the case with no load shifting implementations. This means that roughly an additional 14% cost saving can be attained with a slight heat transfer enhancement that can improve k_{eff} to k_{eff} =0.4 W/mK. Further increments also acquired additional savings, however, these were considerably slight in comparison. All in all, it was deduced here that achieving the thermal conductivity of PCMs to two-folds of the original value using a heat transfer enhancement technique, such as using fins in the application, can attain a significant cost saving. Hence, the additional implementation for the heat transfer enhancement should be carefully taken into account in order to avoid extra costs for any unnecessary improvements that would bring slighter contributions.

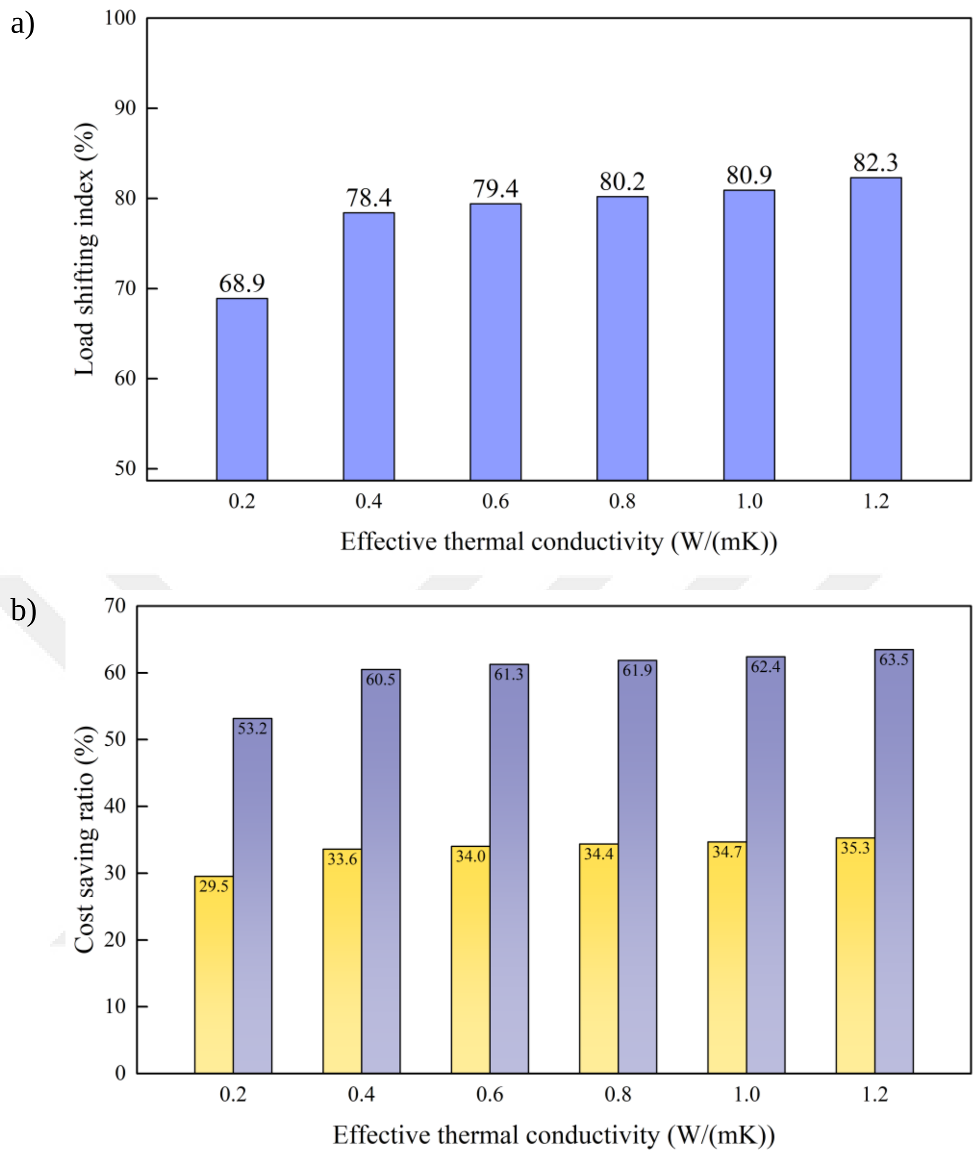

Figure 4.46. Impact of effective thermal conductivity on the load shifting and cost saving rates

5. CONCLUSIONS, RECOMMENDATIONS AND FUTURE WORK

Emphasizing the importance of thermal energy storage for effective space heating applications by heat pumps as well as enhancing their energy flexibility, this thesis work focused on elaboration of two different heat pump systems that are coupled with a thermal energy storage unit. As thermal energy storage units can be coupled with heat pumps via assembling the TES unit to the evaporator or condenser depending on utilization strategy and energy flexibility considerations, the present thesis work aimed at investigating both types of the system in terms of thermal behavior of the TES unit during charging and discharging, its interaction with the heat pump system, and the impacts on the system performance and energy flexibility indicators.

Prior to the study for the TES integrated HP systems, the tubes to be used as the modular PCM containers were selected from two alternatives available in the market, which were namely standard straight-wall tubes and corrugated-wall tubes. The effect of tube surface geometry on the melting and solidification of PCM was investigated by a set of CFD analyses. Thereafter, the experimental works were carried out for both systems.

The first system that was labeled as System-1 within this work consisted of a water source heat pump where the TES unit was integrated to its evaporator in order to constitute a high-temperature heat source for the heat pump. Solar-assisted heat pump systems were taken into scope within this part of the study; however, an electric heater was used during the experiments to thermally charge the TES unit in this system, by measuring the supplied electrical energy, which ensured a more standardized test procedure, while the solar radiation effects were later investigated by a numerical model established for the system. Rubitherm RT26 was used as phase change material inside the PCM modules considering the three thermal storage temperatures (T_{st}=35°C, 45°C, and 55°C) and the reference temperature (T_{ref}=20°C) considered in the system. In order to evaluate the thermal behavior of the System-1 at different heating loads, four different volume flow rates were considered allowing different heating loads. Regarding the experimental data obtained from the tests, a numerical model was established to elaborate the thermal performance of the system in a more comprehensive way including the effects of utilization of different PCMs and their effective thermal conductivities on the thermal charging and discharging behavior of the TES unit and system performance.

In the second step, the same TES unit was integrated to the condenser of the heat pump system, and it was thermally charged by the air-source heat pump. Thereby, utilization of stored thermal energy was considered to be used for heating purposes during on-peak periods to attain an enhanced load shifting. The reference temperature for the water located inside the tank was taken as 35°C considering an appropriate temperature for underfloor heating systems, and the TES unit was charged until the water temperature reached T_{st}=55°C. Similar to the procedure regarded in System-1, the tests were conducted for the cases where water was filled inside the tubes as well as for the cases having PCM inside the tubes, separately. Lauric acid was utilized as a PCM in the aforementioned TES integrated ASHP system. Thermal behavior of the system during charging and discharging processes was investigated. Thereafter, a mathematical model was established using the experimental data specifying the heat pump performance.

5.1. Conclusions

The major conclusions drawn from the CFD studies within the present thesis work can be listed as follows:

- In both considered orientations of the HTF fluid flow, namely the crossflow and axial flow, the heat flux values were found to be notably higher for standard straight wall tubes, compared to corrugated wall tubes, reaching up to 1.5 times at some specific time intervals. However, thanks to the large surface area of the corrugated tubes, the total heat transfer rate was noticeably higher, reaching up to 2 times at specific short time intervals and approximately 5% to 20% during the entire process, which consequently led to a higher phase change rate at the initial steps that continued until the end of the process.
- In crossflow orientation, both melting and solidification rates obtained for the corrugated tube were higher compared to straight wall tubes. Although the total time taken for the processes were almost the same, the liquid fraction curves of the corrugated tube walls had a larger curvature. Hence, at a given time between the start and the end of the phase change process, the melted or solidified portion of the PCM

was larger in corrugated tubes, which quantitatively reach up to 9.0% and 5.7% in melting and solidification, respectively.

- In bottom-heating orientation, on the other hand, a more remarkable difference was obtained in the liquid fraction values due to the previously mentioned reason about the high heat transfer rate by the large surface area of the corrugated tubes. The melting process took 18 to 20 minutes for the PCM in the standard straight wall tubes, depending on the inlet mass flow rate, while it took 12 to 14 minutes for the PCM in the corrugated wall tube. This indicated that the melting time in the standard tubes was about 50% longer, compared to corrugated walls. Relatedly, a significant difference was noticed during the whole melting process, which means that using corrugated tubes could be advantageous even if incomplete melting situations. Besides, the variation of melting rate with respect to inlet mass flow rate was profound in corrugated tubes, while there was negligible difference for the PCM in the standard tube. The solidification rates in this flow configuration were also higher for the corrugated wall tubes although the process ended at the same time for the two examined tube types.

Considering the experimental and numerical works carried out for the System-1, which denotes a solar-assisted heat pump system with a TES unit integrated to the heat pump evaporator, the major findings related to this system can be presented as follows:

- According to the temperature measurements, it was observed that the temperature variations of the water with respect to the location inside the tank were negligible. Hence, the water inside the TES tank could be suitable for lumped system approach. Although thermal stratification is usually desired in solar tanks to improve efficiency, uniform temperature distribution resulted in a more uniform melting and solidification of the PCM, in axial direction, which increased the phase change effectiveness. Relatedly, the measured PCM temperatures from the tubes also did not exhibit a significant difference in axial direction.
- At the storage temperatures of T_{st}=35°C and 45°C, addition of PCM attained a significant elongation in the total heating, i.e., discharging, times, compared to no-PCM cases. Especially at the low storage temperature (T_{st}=35°C), the heat pump could provide a longer heating period reaching up to 30.6%, compared to using only

water as TES material. When the storage temperature was increased to T_{st}=45°C, PCM utilization was still advantageous although the rate of heating time improvement was diminished, such as 2.8% to 13.7%, compared to using water only. Strikingly, at T_{st}=55°C, utilization of PCM showed an adverse effect on the discharging times. The reason was that the water utilized as TES material inside the tubes stored a larger sensible heat compared to the sensible and latent heat storage of the RT26 as the specific heat capacity of the water is 109% higher compared to that of RT26.

- Utilization of PCM noticeably decreased the *COTR* value, which denotes the share of compressor operation time during a whole operational process of the HP. By using PCM, the *COTR* remarkably decreased from 95.3% to 79.6% at T_{st}=35°C and $\dot{V}$=1200 L/h, i.e., the highest heating load about 3.8 kW, while this reduction was less profound at higher storage temperatures due to the diminishing share of latent heat in the total energy use. Similarly, when PCM was considered as a TES material, the *COP* values of the System-1 were found to be lower at low heating loads, while they were noticeably higher at high heating loads, which is due to the portion of latent heat utilization regarding the total energy use.
- Outcomes of the numerical study on the mathematical model established for System-1, it was found that using RT28 HC instead of RT26 can be remarkably more advantageous due to its larger latent heat value as well as higher phase change temperature. Since incomplete solidification occurred in this system, increasing the difference between the solidification point of the PCM and the reference temperature where the system stops operation would positively affect the latent heat utilization. Furthermore, compared to RT26 which is a PCM used in the experiments, utilization of RT28 HC attained 67% more thermal energy release. However, when a flat plate solar collector utilized in the system regarding the dynamic behavior of the weather conditions, it became challenging to thermally charge the TES unit up to high temperatures as in water-only case, because PCM absorbed significant amount of latent heat which restricted the increase of the water temperature inside the TES tank. Therefore, the discharging time was found to be slightly lower when RT28 HC utilized. Yet, it released about 3.0 kWh of latent heat, while RT26 used nearly 1.6

kWh on most of the considered days, which proved that RT28 HC had a remarkable potential when the heat transfer through the material could be enhanced.

- It should be underlined that PCMs, especially RT28 HC having a high latent heat and suitable phase change point, had a larger potential in colder weathers to contribute to the TES unit since the corresponding thermal energy storage of the water was relatively low in cold weathers. Hence, latent heat utilization could be profound. To achieve this, heat transfer enhancement techniques are strongly recommended. Quantitative outcomes showed that RT28 HC stored almost twice as much thermal energy compared to other TES materials; however, it was able to use only 38% to 81% of its latent heat, depending on considered month.
- Evaluation of the energy flexibility potential of the System-1 by the metric of peak clipping index (*PCI*), it was concluded that using water was more prominent using water, compared to using PCM in almost all cases, due to the fact that incomplete latent heat release from the PCMs significantly restrict the peak clipping potential of the system. On the other hand, consideration of a PCM with relatively high solidification temperature, such as RT31 in this case, the *PCI* yielded slightly higher compared to water.
- Regarding a holistic analysis of the obtained results, it was concluded that RT28 HC was the most suitable PCM for System-1, among the examined ones. However, the requirement of heat transfer enhancement applications for PCMs was evidently deduced from the obtained results, in order to prevent incomplete phase change that restricting heat absorption or release. According to the numerical results, the effective thermal conductivity of the RT28 HC should be at least k_{eff}=0.8 W/mK in order to allow the PCM to use 100% of its latent heat effectively. However, it was found that further increment of effective thermal conductivity did not bring any further enhancement within this scope.

In case of integrating the TES unit to the condenser of the ASHP (System-2), the system was focused on storing the thermal energy during off-peak periods and use it during on-peak periods in order to achieve load shifting. According to the obtained experimental and numerical results for the system, following conclusions and recommendations can be drawn from the thesis work:

- Experimental results showed that the utilized PCM, lauric acid, could completely melt and store latent heat during thermal charging period by the heat pump. However, incomplete solidification was observed during discharging period even though the heating load, i.e., the heat rejection rate from the TES unit, was considered at a low level, such as 3.1 kW. Hence, it was observed in all cases of different heating loads, the discharging time of the TES unit was longer when water was used, instead of lauric acid, at a ratio of ranging from 1.6% to 16.1%.
- The load shifting index (*LSI*) obtained from the test results indicated that utilization of this system can respectively shift the 67.0%, 48.3%, 38.4% and 17.4% of the peak loads to the off-peak periods when the heating loads were $\dot{Q}_{load}$=3.1 kW, 4.4 kW, 5.4 kW, and 12 kW, using only water as a TES material. Inclusion of PCM (lauric acid) was found to further improve *LSI* by 3.2%, 3.9%, 8.2%, and 10.1%, respectively, for the aforementioned heating loads.
- In order to shift the loads to the off-peak periods, the TES unit can be charged either in day-tariff or in night-tariff, which affects the cost saving ratio (*CSR*). The *CSR* in the electricity bills reached up to 8.2% to 29.6% in day-tariff charging and up to 14.8% to 53.3% in night-tariff charging in case of using PCM, depending on the considered heating load. Hence, it was concluded that a significant cost-saving can be attained by the TES integrated ASHP system, in consideration of time-of-use electricity pricing.
- Apart from lauric acid, different commercial PCMs were considered for the TES unit of the system using the established numerical model. RT44 HC was found to be the most suitable among the numerically investigated PCMs, and it achieved 3.6% longer discharge time compared to water at a discharge rate of 3.1 kW, while increasing the *LSI* from 64.9% to 68.9%, even though it could not release all the latent heat it stored due to its low thermal conductivity. Besides, it was computed that using RT44 HC can acquire a volume saving of TES tank reaching up to 11.7%.
- Numerical results showed that increasing thermal conductivity of RT44 HC from k_{eff}=0.2 W/mK to 0.4 W/mK provided a remarkable enhancement (19.7%) in the latent heat utilization. Thereby, 79% of the stored latent heat could have been discharged, while it was 66% when k_{eff}=0.2 W/mK. Also, the *LSI* increased from 68.9% to 78.4%, which significantly contributed to the energy flexibility of the

system. Increasing k_{eff} further enhanced the latent heat utilization, however, the rate of augmentation diminished. At k_{eff}=1.2 W/mK, 100% of the stored latent heat could have been used. In this case, the *LSI* increased up to 82.3%.

5.2. Recommendations

Regarding the deductions made from the CFD studies, it was revealed that using corrugated tubes can be significantly beneficial for accelerating the melting and solidification rates for a given period, compared to standard tubes with straight wall. Nevertheless, their corrugated structure may restrict the fluid flow around the outer surface of the tubes. Hence, utilization of corrugated structure only at the inner side of the tubes can be recommended. Alternatively, a straight wall tube can be used together with fins attached to the inner surface of the tube would be considerable beneficial for the heat transfer enhancement both at the outer and inner side of the PCM containers.

Experimental results obtained for System-1 led to the recommendation of using PCM for the cases where relatively lower storage temperatures reached by the water inside the TES tank. In other words, using PCM is not recommended when a significant amount of sensible heat of PCM is used during thermal charging and discharging, because the sensible heat capacity of PCMs is considerably low, compared to that of water. Hence, in such cases, using only water can be suggested. According to the numerical computations carried out for different weather conditions, using PCM in the TES unit in the months with relatively lower solar radiation is rather recommended. Nevertheless, in order to fully benefit the latent heat storage and release of PCMs, using heat transfer enhancement techniques to boost up the effective thermal conductivity of the PCM is strongly recommended. When such techniques are unavailable or when the solar radiation is high enough to thermally charge up the water inside the TES unit up to certain temperatures, using water-only TES units would be a better option from various point of views.

The deductions made from the results obtained for System-2 indicated that utilization of PCM in the TES tank integrated to ASHP has a remarkable potential for increasing heating time and enhancing load shifting ratio attaining a more flexible system. Nonetheless, implementation of heat transfer enhancement techniques such as fin attachment or nanoparticle addition is inevitable in order to acquire a significant benefit from the PCM. Otherwise, using water-only systems can be a more effective and reasonable option if there is a risk of incomplete phase change or low latent heat capacity of PCMs.

To conclude, both systems have advantages brought by integration of TES unit. Comparing two systems to each other, it can be concluded that the System-1 can be an efficient option for locations having high solar radiation and relatively longer sunshine times. On the other hand, System-2 can be a good option for locations where the solar radiation is weak, installation place is limited, and the load shifting activities are crucial due to time-of-use electricity tariffs as well as high grid loads. In both systems, utilization of PCM has a remarkable potential to further improve the thermal energy storage capacity per unit volume. Nevertheless, in case of incomplete melting or solidification, utilization of water can outperform the use of PCM. Moreover, when the temperature difference for thermal charging or discharging, i.e., the temperature difference between the lowest and the highest (initial & final) temperatures in the TES unit, is high, the PCM utilization can also bring a challenging situation due to its significantly low specific heat compared to water. Hence, PCM should be considered in applications where the temperature difference between the lowest and highest one. Besides, the heat transfer enhancement techniques should be inevitably applied to the PCM in order to outperform water. When the latent heat storage and release of the PCM can be appropriately assured, it can have a remarkable advantage for thermal energy storage applications coupled with heat pumps.

5.3. Future Work

The obtained results from the three major parts of this thesis work, namely the CFD studies, experimental tests, and numerical computations carried out for both TES integrated heat pump systems, led to several future work ideas, which can result in further improvements in the field. The future work ideas related to the present thesis work can be listed as follows:

- Investigation of the most effective PCM tube geometries to be used in similar TES units can be considered for a higher melting and solidification rates, which may consequently prevent incomplete thermal charging and discharging. At this point, a tube geometry with straight outer walls and corrugated inner walls is worth investigating to augment the heat transfer area at the PCM side without causing any blockage effect for the flow of the heat transfer fluid at the outer side.

- As the mathematical models established within the present thesis work are verified with respect to the experimentally obtained data, different climatic conditions and different PCM usage can be considered for the operation of System-1. Furthermore, the operational algorithms can be also enhanced for both System-1 and System-2 to improve the energy flexibility. Besides, different heat pump performance data can be also implemented to the numerical model to examine the systems for different heat pump cycles or operational characteristics.
- Consideration of the two systems in combination, namely with dual TES units at the evaporator and condenser side, can remarkably enhance energy flexibility potential in terms of both peak clipping and efficient load shifting. In this case, the combined system can be operated with a more advanced algorithm that allows a higher efficiency and higher flexibility for the thermal energy storage integrated heat pump system.
- Utilization of PCM in the thermal energy storage unit integrated heat pump systems similar to those in the present thesis work can lead to various cost depending on the design of the system as well as the PCM types. Furthermore, the duration of stable operation of the PCMs throughout the whole thermal charging and discharging cycles can differ. Therefore, consideration of a cost analysis, or more comprehensively, a life cycle cost analysis can be regarded as an important future work.

REFERENCES

Abdur Rehman, O., Palomba, V., Frazzica, A., & Cabeza, L. F. (2021). Enabling Technologies for Sector Coupling: A Review on the Role of Heat Pumps and Thermal Energy Storage. *Energies*, *14*(24), 8195. https://doi.org/10.3390/en14248195

Agyenim, F., & Hewitt, N. (2010). The development of a finned phase change material (PCM) storage system to take advantage of off-peak electricity tariff for improvement in cost of heat pump operation. *Energy and Buildings*, *42*(9), 1552–1560. https://doi.org/10.1016/j.enbuild.2010.03.027

Akeiber, H., Nejat, P., Majid, M. Z. A., Wahid, M. A., Jomehzadeh, F., Zeynali Famileh, I., Calautit, J. K., Hughes, B. R., & Zaki, S. A. (2016). A review on phase change material (PCM) for sustainable passive cooling in building envelopes. *Renewable and Sustainable Energy Reviews*, *60*, 1470–1497. https://doi.org/10.1016/j.rser.2016.03.036

Alavy, M., Peiris, M., Wang, J., & Rosen, M. A. (2021). Assessment of a novel phase change material-based thermal caisson for geothermal heating and cooling. *Energy Conversion and Management*, *234*, 113928. https://doi.org/10.1016/j.enconman.2021.113928

Ali, H. M. (2019). Applications of combined/hybrid use of heat pipe and phase change materials in energy storage and cooling systems: A recent review. *Journal of Energy Storage*, *26*(October), 100986. https://doi.org/10.1016/j.est.2019.100986

Arıcı, M., Bilgin, F., Nižetić, S., & Karabay, H. (2020). PCM integrated to external building walls: An optimization study on maximum activation of latent heat. *Applied Thermal Engineering*, *165*, 114560. https://doi.org/10.1016/j.applthermaleng.2019.114560

Arteconi, A., Hewitt, N. J., & Polonara, F. (2012). State of the art of thermal storage for demand-side management. *Applied Energy*, *93*, 371–389. https://doi.org/10.1016/j.apenergy.2011.12.045

Arteconi, A., Hewitt, N. J., & Polonara, F. (2013). Domestic demand-side management (DSM): Role of heat pumps and thermal energy storage (TES) systems. *Applied Thermal Engineering*, *51*(1–2), 155–165. https://doi.org/10.1016/j.applthermaleng.2012.09.023

Arteconi, Alessia, & Polonara, F. (2018). Assessing the demand side management potential and the energy flexibility of heat pumps in buildings. *Energies*, *11*(7), 1–19. https://doi.org/10.3390/en11071846

Awan, M. B., & Ma, Z. (2023). Building energy flexibility: definitions, sources, indicators, and quantification methods. In *Building Energy Flexibility and Demand Management*. INC. https://doi.org/10.1016/B978-0-323-99588-7.00003-1

Aydin, D., Utlu, Z., & Kincay, O. (2015). Thermal performance analysis of a solar energy sourced latent heat storage. *Renewable and Sustainable Energy Reviews*, *50*, 1213–1225. https://doi.org/10.1016/j.rser.2015.04.195

Badescu, V. (2003). Model of a thermal energy storage device integrated into a solar assisted heat pump system for space heating. *Energy Conversion and Management*, *44*, 1589–1604. www.elsevier.com/locate/enconman

Baeten, B., Rogiers, F., & Helsen, L. (2017). Reduction of heat pump induced peak electricity use and required generation capacity through thermal energy storage and demand response. *Applied Energy*, *195*, 184–195. https://doi.org/10.1016/j.apenergy.2017.03.055

Bampoulas, A., Saffari, M., Pallonetto, F., Mangina, E., & Finn, D. P. (2021). A fundamental unified framework to quantify and characterise energy flexibility of residential buildings with multiple electrical and thermal energy systems. *Applied Energy*, *282*(October 2020). https://doi.org/10.1016/j.apenergy.2020.116096

Baster, E. (2017). *Air source heat pump modelling for dynamic building simulation tools based on standard test data*. University of Strathclyde.

Bathcelor, G. K. (1967). *An introduction to fluid dynamics*. Cambridge University Press.

Belmonte, J. F., Díaz-Heras, M., Almendros-Ibáñez, J. A., & Cabeza, L. F. (2022). Simulated performance of a solar-assisted heat pump system including a phase-change storage tank for residential heating applications: A case study in Madrid, Spain. *Journal of Energy Storage*, *47*(April 2021). https://doi.org/10.1016/j.est.2021.103615

Benli, H., & Durmuş, A. (2009). Evaluation of ground-source heat pump combined latent heat storage system performance in greenhouse heating. *Energy and Buildings*, *41*(2), 220–228. https://doi.org/10.1016/j.enbuild.2008.09.004

Bisengimana, E., Zhou, J., Binama, M., & Yuan, Y. (2022). Numerical investigation on the factors influencing the temperature distribution of photovoltaic/thermal (PVT) evaporator/condenser for heat pump systems. *Renewable Energy*, *194*, 885–901. https://doi.org/10.1016/j.renene.2022.05.154

Bouckaert, S., Pales, A. F., McGlade, C., Remme, U., & Wanner, B. (2021). Net Zero by 2050: A Roadmap for the Global Energy Sector. In *International Energy Agency*. https://www.iea.org/reports/net-zero-by-2050

Boumaza, B., Laouer, A., Teggar, M., Agagna, B., Ismail, K. A. R., & Arıcı, M. (2023). Effect of heating tube arrangement on nano-enhanced thermal energy storage. *Energy, Ecology and Environment*. https://doi.org/10.1007/s40974-023-00291-8

Brahim, T., & Jemni, A. (2017). Economical assessment and applications of photovoltaic/thermal hybrid solar technology: A review. *Solar Energy*, *153*, 540–561. https://doi.org/10.1016/j.solener.2017.05.081

Campos, J., Csontos, C., Harmat, Á., Csüllög, G., & Munkácsy, B. (2020). Heat consumption scenarios in the rural residential sector: the potential of heat pump-based demand-side management for sustainable heating. *Energy, Sustainability and Society*, *10*(1), 1–16. https://doi.org/10.1186/s13705-020-00271-4

Chu, J., & Cruickshank, C. A. (2014). Solar-Assisted Heat Pump Systems: A Review of Existing Studies and Their Applicability to the Canadian Residential Sector. *Journal of Solar Energy Engineering*, *136*(4), 1–9. https://doi.org/10.1115/1.4027735

Dahash, A., Ochs, F., Janetti, M. B., & Streicher, W. (2019). Advances in seasonal thermal energy storage for solar district heating applications: A critical review on large-scale hot-water tank and pit thermal energy storage systems. *Applied Energy*, *239*, 296–315. https://doi.org/10.1016/j.apenergy.2019.01.189

Date, J., Candanedo, J. A., & Athienitis, A. K. (2021). A Methodology for the Enhancement of the Energy Flexibility and Contingency Response of a Building through Predictive Control of Passive and Active Storage. *Energies*, *14*(5), 1387. https://doi.org/10.3390/en14051387

Dawe, D. (2022). *Cloverleaf - Air Source Heat Pump Efficiency*. https://www.cloverleafmaintenance.co.uk/how-does-an-air-source-heat-pump-work/

Desai, F., Sunku Prasad, J., Muthukumar, P., & Rahman, M. M. (2021). Thermochemical energy storage system for cooling and process heating applications: A review. *Energy Conversion and Management*, *229*, 113617. https://doi.org/10.1016/j.enconman.2020.113617

Dincer, I., Dost, S., & Li, X. (1997). Performance analyses of sensible heat storage systems for thermal applications. *International Journal of Energy Research*, *21*(12), 1157–1171. https://doi.org/10.1002/(SICI)1099-114X(19971010)21:12<1157::AID-ER317>3.0.CO;2-N

Duan, J., Xiong, Y., & Yang, D. (2020). Study on the effect of multiple spiral fins for improved phase change process. *Applied Thermal Engineering*, *169*(August 2019). https://doi.org/10.1016/j.applthermaleng.2020.114966

Ermel, C., Bianchi, M. V. A., Cardoso, A. P., & Schneider, P. S. (2022). Thermal storage integrated into air-source heat pumps to leverage building electrification: A systematic literature review. *Applied Thermal Engineering*, *215*(July). https://doi.org/10.1016/j.applthermaleng.2022.118975

Fallahi, A., Guldentops, G., Tao, M., Granados-Focil, S., & Van Dessel, S. (2017). Review on solid-solid phase change materials for thermal energy storage: Molecular structure and thermal properties. *Applied Thermal Engineering*, *127*, 1427–1441. https://doi.org/10.1016/j.applthermaleng.2017.08.161

Fang, W.-Z., Tang, Y.-Q., Yang, C., & Tao, W.-Q. (2020). Numerical simulations of the liquid-vapor phase change dynamic processes in a flat micro heat pipe. *International Journal of Heat and Mass Transfer*, *147*, 119022. https://doi.org/10.1016/j.ijheatmasstransfer.2019.119022

Feng, B., Tu, J., Sun, J.-W., Fan, L.-W., & Zeng, Y. (2019). A molecular dynamics study of the effects of crystalline structure transition on the thermal conductivity of pentaerythritol as a solid-solid phase change material. *International Journal of Heat and Mass Transfer*, *141*, 789–798. https://doi.org/10.1016/j.ijheatmasstransfer.2019.07.017

Fitzpatrick, P., D'Ettorre, F., De Rosa, M., Yadack, M., Eicker, U., & Finn, D. P. (2020). Influence of electricity prices on energy flexibility of integrated hybrid heat pump and thermal storage systems in a residential building. *Energy and Buildings*, *223*. https://doi.org/10.1016/j.enbuild.2020.110142

Gaur, A. S., Fitiwi, D. Z., & Curtis, J. (2021). Heat pumps and our low-carbon future: A comprehensive review. *Energy Research and Social Science*, *71*(August 2020). https://doi.org/10.1016/j.erss.2020.101764

Gelazanskas, L., & Gamage, K. A. A. (2014). Demand side management in smart grid : A review and proposals for future direction. *Sustainable Cities and Society*, *11*, 22–30. https://doi.org/https://dx.doi.org/10.1016/j.scs.2013.11.001

Givoni, B. (1977). Underground longterm storage of solar energy-An overview. *Solar Energy*, *19*(6), 617–623. https://doi.org/10.1016/0038-092X(77)90021-4

Gómez, M. A., Collazo, J., Porteiro, J., & Míguez, J. L. (2018). Numerical study of an external device for the improvement of the thermal stratification in hot water storage tanks. *Applied Thermal Engineering*, *144*, 996–1009. https://doi.org/10.1016/j.applthermaleng.2018.09.023

Green, C., & Garimella, S. (2021). Residential microgrid optimization using grey-box and black-box modeling methods. *Energy and Buildings*, *235*. https://doi.org/10.1016/j.enbuild.2020.110705

Gu, H., Chen, Y., Yao, X., Huang, L., & Zou, D. (2023). Review on heat pump (HP) coupled with phase change material (PCM) for thermal energy storage. *Chemical Engineering Journal*, *455*(September 2022), 140701. https://doi.org/10.1016/j.cej.2022.140701

Gustafsson, A. M., Westerlund, L., & Hellström, G. (2010). CFD-modelling of natural convection in a groundwater-filled borehole heat exchanger. *Applied Thermal Engineering*, *30*(6–7), 683–691. https://doi.org/10.1016/j.applthermaleng.2009.11.016

Han, Z., Zheng, M., Kong, F., Wang, F., Li, Z., & Bai, T. (2008). Numerical simulation of solar assisted ground-source heat pump heating system with latent heat energy storage in severely cold area. *Applied Thermal Engineering*, *28*(11–12), 1427–1436. https://doi.org/10.1016/j.applthermaleng.2007.09.013

Hesaraki, A., Holmberg, S., & Haghighat, F. (2015). Seasonal thermal energy storage with heat pumps and low temperatures in building projects - A comparative review. *Renewable and Sustainable Energy Reviews*, *43*, 1199–1213. https://doi.org/10.1016/j.rser.2014.12.002

Hirmiz, R., Teamah, H. M., Lightstone, M. F., & Cotton, J. S. (2019). Performance of heat pump integrated phase change material thermal storage for electric load shifting in building demand side management. *Energy and Buildings*, *190*, 103–118. https://doi.org/10.1016/j.enbuild.2019.02.026

IEA – International Energy Agency. (2020). *IEA*. https://www.iea.org/reports/heat-pumps (Visiting date: 17 January 2023)

IEA – International Energy Agency. (2021). *IEA Heat Pump Report of 2021*.

Imran Khan, M., Asfand, F., & Al-Ghamdi, S. G. (2023). Progress in research and development of phase change materials for thermal energy storage in concentrated solar power. *Applied Thermal Engineering*, *219*(March 2022). https://doi.org/10.1016/j.applthermaleng.2022.119546

Jensen, S. Ø., Marszal-Pomianowska, A., Lollini, R., Pasut, W., Knotzer, A., Engelmann, P., Stafford, A., & Reynders, G. (2017). IEA EBC Annex 67 Energy Flexible Buildings. *Energy and Buildings*, *155*(2017), 25–34. https://doi.org/10.1016/j.enbuild.2017.08.044

Jin, X., Wu, F., Xu, T., Huang, G., Wu, H., Zhou, X., Wang, D., Liu, Y., & Lai, A. C. (2021). Experimental investigation of the novel melting point modified Phase–Change material for heat pump latent heat thermal energy storage application. *Energy*, *216*, 119191. https://doi.org/10.1016/j.energy.2020.119191

Jin, X., Zhang, H., Huang, G., & Lai, A. C. (2021). Experimental investigation on the dynamic thermal performance of the parallel solar-assisted air-source heat pump latent heat thermal energy storage system. *Renewable Energy*, *180*, 637–657. https://doi.org/10.1016/j.renene.2021.08.067

Jin, X., Zheng, S., Huang, G., & CK Lai, A. (2023). Energy and economic performance of the heat pump integrated with latent heat thermal energy storage for peak demand shifting. *Applied Thermal Engineering*, *218*(August 2022). https://doi.org/10.1016/j.applthermaleng.2022.119337

Kalapala, L., & Devanuri, J. K. (2020). Energy and exergy analyses of latent heat storage unit positioned at different orientations – An experimental study. *Energy*, *194*, 1–14. https://doi.org/10.1016/j.energy.2020.116924

Kalidasan, B., Pandey, A. K., Saidur, R., Kothari, R., Sharma, K., & Tyagi, V. V. (2023). Eco-friendly coconut shell biochar based nano-inclusion for sustainable energy storage of binary eutectic salt hydrate phase change materials. *Solar Energy Materials and Solar Cells*, *262*, 112534. https://doi.org/10.1016/j.solmat.2023.112534

Karaipekli, A., Sarı, A., & Biçer, A. (2016). Thermal regulating performance of gypsum/(C18–C24) composite phase change material (CPCM) for building energy storage applications. *Applied Thermal Engineering*, *107*, 55–62. https://doi.org/10.1016/j.applthermaleng.2016.06.160

Kelly, N. J., Tuohy, P. G., & Hawkes, A. D. (2014). Performance assessment of tariff-based air source heat pump load shifting in a UK detached dwelling featuring phase change-enhanced buffering. *Applied Thermal Engineering*, *71*(2), 809–820. https://doi.org/10.1016/j.applthermaleng.2013.12.019

Kendrick, C., Ogden, R., Wang, X., & Baiche, B. (2012). Thermal mass in new build UK housing: A comparison of structural systems in a future weather scenario. *Energy and Buildings*, *48*, 40–49. https://doi.org/10.1016/j.enbuild.2012.01.009

Khan, Z., Khan, Z., & Ghafoor, A. (2016). A review of performance enhancement of PCM based latent heat storage system within the context of materials, thermal stability and compatibility. *Energy Conversion and Management*, *115*, 132–158. https://doi.org/10.1016/j.enconman.2016.02.045

Kim, T., Choi, B. Il, Han, Y. S., & Do, K. H. (2018). A comparative investigation of solar-assisted heat pumps with solar thermal collectors for a hot water supply system. *Energy Conversion and Management*, *172*(April), 472–484. https://doi.org/10.1016/j.enconman.2018.07.035

Kim, Y., Honda, T., & Kanzawa, A. (1989). The Role of Natural Convection During Melting and Solidification of Pcm in a Vertical Cylinder. *Chemical Engineering Communications*, *84*(1), 43–60. https://doi.org/10.1080/00986448908940334

Knittel, T., Palmer-Wilson, K., McPherson, M., Wild, P., & Rowe, A. (2024). Heating electrification in cold climates: Invest in grid flexibility. *Applied Energy*, *356*(November 2023), 122333. https://doi.org/10.1016/j.apenergy.2023.122333

Lakhdari, Y. A., Chikh, S., & Campo, A. (2020). Analysis of the thermal response of a dual phase change material embedded in a multi-layered building envelope. *Applied Thermal Engineering*, *179*, 115502. https://doi.org/10.1016/j.applthermaleng.2020.115502

Lazzarin, R. (2020). Heat pumps and solar energy: A review with some insights in the future. *International Journal of Refrigeration*, *116*, 146–160. https://doi.org/10.1016/j.ijrefrig.2020.03.031

Lee, K. S. (2010). A Review on Concepts, Applications, and Models of Aquifer Thermal Energy Storage Systems. *Energies*, *3*(6), 1320–1334. https://doi.org/10.3390/en3061320

Li, D., Wu, Y., Wang, B., Liu, C., & Arıcı, M. (2020). Optical and thermal performance of glazing units containing PCM in buildings: A review. *Construction and Building Materials*, *233*, 117327. https://doi.org/10.1016/j.conbuildmat.2019.117327

Li, G. (2016). Sensible heat thermal storage energy and exergy performance evaluations. *Renewable and Sustainable Energy Reviews*, *53*, 897–923. https://doi.org/10.1016/j.rser.2015.09.006

Li, Han, Wang, Z., Hong, T., & Piette, M. A. (2021). Energy flexibility of residential buildings: A systematic review of characterization and quantification methods and applications. *Advances in Applied Energy*, *3*(July), 100054. https://doi.org/10.1016/j.adapen.2021.100054

Li, Hexin, Zhuang, Y., Feng, J.-C., & Huang, S.-M. (2023). Experimental study on the solidification and melting performances of magnetic NEPCMs composited with optimized filling metal foam in a uniform magnetic field. *Solar Energy*, *263*, 111927. https://doi.org/10.1016/j.solener.2023.111927

Li, Yantong, Ding, Z., & Du, Y. (2020). Techno-economic optimization of open-air swimming pool heating system with PCM storage tank for winter applications. *Renewable Energy*, *150*, 878–890. https://doi.org/10.1016/j.renene.2020.01.029

Li, Yuanyuan, Mojiri, A., Rosengarten, G., & Stanley, C. (2021). Residential demand-side management using integrated solar-powered heat pump and thermal storage. *Energy and Buildings*, *250*. https://doi.org/10.1016/j.enbuild.2021.111234

Lin, Y., Fan, Y., Yu, M., Jiang, L., & Zhang, X. (2022). Performance investigation on an air source heat pump system with latent heat thermal energy storage. *Energy*, *239*, 121898. https://doi.org/10.1016/j.energy.2021.121898

Lizana, J., Friedrich, D., Renaldi, R., & Chacartegui, R. (2018). Energy flexible building through smart demand-side management and latent heat storage. *Applied Energy*, *230*(May), 471–485. https://doi.org/10.1016/j.apenergy.2018.08.065

Lottner, V., Schulz, M. E., & Hahne, E. (2000). Solar-assisted district heating plants: Status of the German programme Solarthermie-2000. *Solar Energy*, *69*(6), 449–459. https://doi.org/10.1016/S0038-092X(00)00125-0

Luc, K. M., Heller, A., & Rode, C. (2019). Energy demand flexibility in buildings and district heating systems–a literature review. *Advances in Building Energy Research*, *13*(2), 241–263. https://doi.org/10.1080/17512549.2018.1488615

Lugolole, R., Mawire, A., Okello, D., Lentswe, K. A., Nyeinga, K., & Shobo, A. B. (2019). Experimental analyses of sensible heat thermal energy storage systems during discharging. *Sustainable Energy Technologies and Assessments*, *35*(February), 117–130. https://doi.org/10.1016/j.seta.2019.06.007

Lv, J., Wei, Z., & Zhang, J. (2016). Running and economy performance analysis of ground source heat pump with thermal energy storage devices. *Energy and Buildings*, *127*, 1108–1116. https://doi.org/10.1016/j.enbuild.2016.06.072

Lyu, W., Wang, Z., Li, X., Deng, G., Xu, Z., Li, H., Yang, Y., Zhan, B., & Zhao, M. (2022). Influence of the water tank size and air source heat pump size on the energy saving potential of the energy storage heating system. *Journal of Energy*

Storage, *55*(August). https://doi.org/10.1016/j.est.2022.105542

Mahdi, J. M., Mohammed, H. I., Hashim, E. T., Talebizadehsardari, P., & Nsofor, E. C. (2020). Solidification enhancement with multiple PCMs, cascaded metal foam and nanoparticles in the shell-and-tube energy storage system. *Applied Energy*, *257*(June 2019). https://doi.org/10.1016/j.apenergy.2019.113993

Mahdi, M. S., Hasan, A. F., Mahood, H. B., Campbell, A. N., Khadom, A. A., Karim, A. M. em A., & Sharif, A. O. (2019). Numerical study and experimental validation of the effects of orientation and configuration on melting in a latent heat thermal storage unit. *Journal of Energy Storage*, *23*(November 2018), 456–468. https://doi.org/10.1016/j.est.2019.04.013

Miglioli, A., Aste, N., Del Pero, C., & Leonforte, F. (2023). Photovoltaic-thermal solar-assisted heat pump systems for building applications: Integration and design methods. *Energy and Built Environment*, *4*(1), 39–56. https://doi.org/10.1016/j.enbenv.2021.07.002

Mishra, G., Memon, A., Gupta, A. K., & Nirmalkar, N. (2022). Computational study on effect of enclosure shapes on melting characteristics of phase change material around a heated cylinder. *Case Studies in Thermal Engineering*, *34*(March). https://doi.org/10.1016/j.csite.2022.102032

Moffat, R. J. (1988). Describing the uncertainties in experimental results. *Experimental Thermal and Fluid Science*, *1*(1), 3–17. https://doi.org/10.1016/0894-1777(88)90043-X

Mohanraj, M., Belyayev, Y., Jayaraj, S., & Kaltayev, A. (2018). Research and developments on solar assisted compression heat pump systems – A comprehensive review (Part A: Modeling and modifications). *Renewable and Sustainable Energy Reviews*, *83*(February 2017), 90–123. https://doi.org/10.1016/j.rser.2017.08.022

Moreno, P., Castell, A., Solé, C., Zsembinszki, G., & Cabeza, L. F. (2014). PCM thermal energy storage tanks in heat pump system for space cooling. *Energy and Buildings*, *82*, 399–405. https://doi.org/10.1016/j.enbuild.2014.07.044

Moreno, P., Solé, C., Castell, A., & Cabeza, L. F. (2014). The use of phase change materials in domestic heat pump and air-conditioning systems for short term storage: A review. *Renewable and Sustainable Energy Reviews*, *39*, 1–13. https://doi.org/10.1016/j.rser.2014.07.062

Mousa, M. M., Bayomy, A. M., & Saghir, M. Z. (2022). Long-term performance investigation of a GSHP with actual size energy pile with PCM. *Applied Thermal Engineering*, *210*, 118381. https://doi.org/10.1016/j.applthermaleng.2022.118381

Murphy, G., Counsell, J., Baster, E., Allison, J., & Counsell, S. (2013). Symbolic modelling and predictive assessment of air source heat pumps. *Building Services Engineering Research and Technology*, *34*(1), 23–39.

https://doi.org/10.1177/0143624412462592

Nair, A. M., Wilson, C., Huang, M. J., Griffiths, P., & Hewitt, N. (2022). Phase change materials in building integrated space heating and domestic hot water applications: A review. *Journal of Energy Storage*, *54*(March), 105227. https://doi.org/10.1016/j.est.2022.105227

Nazir, H., Batool, M., Bolivar Osorio, F. J., Isaza-Ruiz, M., Xu, X., Vignarooban, K., Phelan, P., Inamuddin, & Kannan, A. M. (2019). Recent developments in phase change materials for energy storage applications: A review. *International Journal of Heat and Mass Transfer*, *129*, 491–523. https://doi.org/10.1016/j.ijheatmasstransfer.2018.09.126

Niessink, R. J. M. (2019). *Ground-source heat pump (GSHP) – households*. https://energy.nl/data/ground-source-heat-pump-gshp-households/

Ninikas, K., Hytiris, N., Emmanuel, R., Aaen, B., & McMillan, S. (2014). A renewable heat solution for water ingress in the Glasgow subway tunnel system. *WIT Transactions on Ecology and the Environment*, *186*(December), 161–171. https://doi.org/10.2495/ESUS140141

Niu, F., Ni, L., Yao, Y., Yu, Y., & Li, H. (2013). Performance and thermal charging/discharging features of a phase change material assisted heat pump system in heating mode. *Applied Thermal Engineering*, *58*(1–2), 536–541. https://doi.org/10.1016/j.applthermaleng.2013.04.042

Nižetić, S., Arıcı, M., Bilgin, F., & Grubišić-Čabo, F. (2018). Investigation of pork fat as potential novel phase change material for passive cooling applications in photovoltaics. *Journal of Cleaner Production*, *170*, 1006–1016. https://doi.org/10.1016/j.jclepro.2017.09.164

Nouri, G., Noorollahi, Y., & Yousefi, H. (2019). Solar assisted ground source heat pump systems – A review. *Applied Thermal Engineering*, *163*, 114351. https://doi.org/10.1016/j.applthermaleng.2019.114351

Nowak, T. (2023). *European Heat Pump Market and Statistics Report*.

Olsthoorn, D., Haghighat, F., & Mirzaei, P. A. (2016). Integration of storage and renewable energy into district heating systems: A review of modelling and optimization. *Solar Energy*, *136*, 49–64. https://doi.org/10.1016/j.solener.2016.06.054

Osterman, E., & Stritih, U. (2021). Review on compression heat pump systems with thermal energy storage for heating and cooling of buildings. *Journal of Energy Storage*, *39*(April). https://doi.org/10.1016/j.est.2021.102569

Pardiñas, Á., Alonso, M. J., Diz, R., Kvalsvik, K. H., & Fernández-Seara, J. (2017). State-of-the-art for the use of phase-change materials in tanks coupled with heat pumps. *Energy and Buildings*, *140*, 28–41. https://doi.org/10.1016/j.enbuild.2017.01.061

Pardo, P., Deydier, A., Anxionnaz-Minvielle, Z., Rougé, S., Cabassud, M., & Cognet, P. (2014). A review on high temperature thermochemical heat energy storage. *Renewable and Sustainable Energy Reviews*, *32*, 591–610. https://doi.org/10.1016/j.rser.2013.12.014

Patel, V. K., Gluesenkamp, K. R., Goodman, D., & Gehl, A. (2018). Experimental evaluation and thermodynamic system modeling of thermoelectric heat pump clothes dryer. *Applied Energy*, *217*(February), 221–232. https://doi.org/10.1016/j.apenergy.2018.02.055

Péan, T. Q., Salom, J., & Costa-Castelló, R. (2019). Review of control strategies for improving the energy flexibility provided by heat pump systems in buildings. *Journal of Process Control*, *74*, 35–49. https://doi.org/10.1016/j.jprocont.2018.03.006

Pereira da Cunha, J., & Eames, P. (2016). Thermal energy storage for low and medium temperature applications using phase change materials - A review. *Applied Energy*, *177*, 227–238. https://doi.org/10.1016/j.apenergy.2016.05.097

Pinamonti, M., Beausoleil-Morrison, I., Prada, A., & Baggio, P. (2021). Water-to-water heat pump integration in a solar seasonal storage system for space heating and domestic hot water production of a single-family house in a cold climate. *Solar Energy*, *213*(October 2020), 300–311. https://doi.org/10.1016/j.solener.2020.11.052

Pinel, P., Cruickshank, C. A., Beausoleil-Morrison, I., & Wills, A. (2011). A review of available methods for seasonal storage of solar thermal energy in residential applications. *Renewable and Sustainable Energy Reviews*, *15*(7), 3341–3359. https://doi.org/10.1016/j.rser.2011.04.013

Plytaria, M. T., Tzivanidis, C., Bellos, E., & Antonopoulos, K. A. (2018). Energetic investigation of solar assisted heat pump underfloor heating systems with and without phase change materials. *Energy Conversion and Management*, *173*, 626–639. https://doi.org/10.1016/j.enconman.2018.08.010

Qaiser, R., Khan, M. M., Khan, L. A., & Irfan, M. (2021). Melting performance enhancement of PCM based thermal energy storage system using multiple tubes and modified shell designs. *Journal of Energy Storage*, *33*, 102161. https://doi.org/10.1016/j.est.2020.102161

Qi, D., Pu, L., Sun, F., & Li, Y. (2016). Numerical investigation on thermal performance of ground heat exchangers using phase change materials as grout for ground source heat pump system. *Applied Thermal Engineering*, *106*, 1023–1032. https://doi.org/10.1016/j.applthermaleng.2016.06.048

Qi, Q., Deng, S., & Jiang, Y. (2008). A simulation study on a solar heat pump heating system with seasonal latent heat storage. *Solar Energy*, *82*(8), 669–675. https://doi.org/10.1016/j.solener.2008.02.017

Qu, M., Xia, L., Deng, S., & Jiang, Y. (2012). An experimental investigation on reverse-cycle defrosting performance for an air source heat pump using an electronic expansion valve. *Applied Energy*, *97*, 327–333. https://doi.org/10.1016/j.apenergy.2011.11.057

Qu, S., Ma, F., Ji, R., Wang, D., & Yang, L. (2015). System design and energy performance of a solar heat pump heating system with dual-tank latent heat storage. *Energy and Buildings*, *105*, 294–301. https://doi.org/10.1016/j.enbuild.2015.07.040

Qureshi, W. A., Nair, N. K. C., & Farid, M. M. (2011). Impact of energy storage in buildings on electricity demand side management. *Energy Conversion and Management*, *52*(5), 2110–2120. https://doi.org/10.1016/j.enconman.2010.12.008

Ren, H., Sun, Y., Albdoor, A. K., Tyagi, V. V., Pandey, A. K., & Ma, Z. (2021). Improving energy flexibility of a net-zero energy house using a solar-assisted air conditioning system with thermal energy storage and demand-side management. *Applied Energy*, *285*(December 2020). https://doi.org/10.1016/j.apenergy.2021.116433

Renaldi, R., Kiprakis, A., & Friedrich, D. (2017). An optimisation framework for thermal energy storage integration in a residential heat pump heating system. *Applied Energy*, *186*, 520–529. https://doi.org/10.1016/j.apenergy.2016.02.067

Rendall, J. D., Gluesenkamp, K. R., Worek, W., Abu-Heiba, A., Nawaz, K., & Gehl, T. (2020). Empirical characterization of vertical-tube inlets in hot-water storage tanks. *International Communications in Heat and Mass Transfer*, *119*(November). https://doi.org/10.1016/j.icheatmasstransfer.2020.104838

Reuss, M., Beck, M., & Müller, J. P. (1997). Design of a seasonal thermal energy storage in the ground. *Solar Energy*, *59*, 247–257.

Reynders, G., Nuytten, T., & Saelens, D. (2013). Potential of structural thermal mass for demand-side management in dwellings. *Building and Environment*, *64*, 187–199. https://doi.org/10.1016/j.buildenv.2013.03.010

Reynders, Glenn, Amaral Lopes, R., Marszal-Pomianowska, A., Aelenei, D., Martins, J., & Saelens, D. (2018). Energy flexible buildings: An evaluation of definitions and quantification methodologies applied to thermal storage. *Energy and Buildings*, *166*, 372–390. https://doi.org/10.1016/j.enbuild.2018.02.040

Reynders, Glenn, Diriken, J., & Saelens, D. (2017). Generic characterization method for energy flexibility: Applied to structural thermal storage in residential buildings. *Applied Energy*, *198*, 192–202. https://doi.org/10.1016/j.apenergy.2017.04.061

Risueño, E., Faik, A., Gil, A., Rodríguez-Aseguinolaza, J., Tello, M., & D'Aguanno, B. (2017). Zinc-rich eutectic alloys for high energy density latent heat storage applications. *Journal of Alloys and Compounds*, *705*, 714–721. https://doi.org/10.1016/j.jallcom.2017.02.173

Rocha, T. T. M., Trevizoli, P. V., & de Oliveira, R. N. (2023). The role of the phase-change material properties, porosity constant, and their combination for melting problems using the enthalpy-porosity scheme. *Thermal Science and Engineering Progress*, *46*(September). https://doi.org/10.1016/j.tsep.2023.102198

Rodrigo-ilarri, J., Jin, S., Blum, P., & Bayer, P. (2010). Geostatistical characterisation of heterogeneous aquifers for the application of open shallow geothermal systems Geostatistical characterisation of heterogeneous aquifers for the application of open shallow geothermal systems Geothermal energy is the ener. *GEOENER 2010 Segundo Congreso Sobre La Energía Geotérmica En La Edificación y En La Industria*.

Romero Rodríguez, L., Sánchez Ramos, J., Guerrero Delgado, Mc., Molina Félix, J. L., & Álvarez Domínguez, S. (2018). Mitigating energy poverty: Potential contributions of combining PV and building thermal mass storage in low-income households. *Energy Conversion and Management*, *173*(April), 65–80. https://doi.org/10.1016/j.enconman.2018.07.058

Rubitherm. (2023). *Rubitherm GmbH Product List*. https://www.rubitherm.eu/en/index.php/productcategory/organische-pcm-rt

Sartor, K., & Dewallef, P. (2017). Optimized Integration of Heat Storage Into District Heating Networks Fed By a Biomass CHP Plant. *Energy Procedia*, *135*, 317–326. https://doi.org/10.1016/j.egypro.2017.09.523

Schibuola, L., & Scarpa, M. (2016). Experimental analysis of the performances of a surface water source heat pump. *Energy and Buildings*, *113*, 182–188. https://doi.org/10.1016/j.enbuild.2015.12.048

Sezen, K., Tuncer, A. D., Akyuz, A. O., & Gungor, A. (2021). Effects of ambient conditions on solar assisted heat pump systems: a review. *Science of The Total Environment*, *778*, 146362. https://doi.org/10.1016/j.scitotenv.2021.146362

Shahjalal, M., Shams, T., Islam, M. E., Alam, W., Modak, M., Hossain, S. Bin, Ramadesigan, V., Ahmed, M. R., Ahmed, H., & Iqbal, A. (2021). A review of thermal management for Li-ion batteries: Prospects, challenges, and issues. *Journal of Energy Storage*, *39*(May). https://doi.org/10.1016/j.est.2021.102518

Sharda, S., Singh, M., & Sharma, K. (2021). Demand side management through load shifting in IoT based HEMS: Overview, challenges and opportunities. *Sustainable Cities and Society*, *65*(October 2020). https://doi.org/10.1016/j.scs.2020.102517

Sharma, A., & Chauhan, R. (2022). Integrated and separate collector storage type low-temperature solar water heating systems with latent heat storage: A review. *Sustainable Energy Technologies and Assessments*, *51*, 101935. https://doi.org/10.1016/j.seta.2021.101935

Sharma, A., Pitchumani, R., & Chauhan, R. (2023). Melting and solidification performance investigation of latent heat storage unit designs for low-temperature solar thermal applications. *Journal of Energy Storage*, *66*, 107323. https://doi.org/10.1016/j.est.2023.107323

Sharma, R. K., Ganesan, P., Tyagi, V. V., Metselaar, H. S. C., & Sandaran, S. C. (2015). Developments in organic solid–liquid phase change materials and their applications in thermal energy storage. *Energy Conversion and Management*, *95*, 193–228. https://doi.org/10.1016/j.enconman.2015.01.084

Shen, C., Li, X., Yang, G., Wang, Y., Zhao, L., Mao, Z., Wang, B., Feng, X., & Sui, X. (2020). Shape-stabilized hydrated salt/paraffin composite phase change materials for advanced thermal energy storage and management. *Chemical Engineering Journal*, *385*(2999). https://doi.org/10.1016/j.cej.2019.123958

Shi, G.-H., Aye, L., Li, D., & Du, X.-J. (2019). Recent advances in direct expansion solar assisted heat pump systems: A review. *Renewable and Sustainable Energy Reviews*, *109*, 349–366. https://doi.org/10.1016/j.rser.2019.04.044

Shokouhmand, H., & Kamkari, B. (2013). Experimental investigation on melting heat transfer characteristics of lauric acid in a rectangular thermal storage unit. *Experimental Thermal and Fluid Science*, *50*, 201–212. https://doi.org/10.1016/j.expthermflusci.2013.06.010

Simon, F., Ordoñez, J., Reddy, T. A., Girard, A., & Muneer, T. (2016). Developing multiple regression models from the manufacturer's ground-source heat pump catalogue data. *Renewable Energy*, *95*, 413–421. https://doi.org/10.1016/j.renene.2016.04.045

Solé, A., Martorell, I., & Cabeza, L. F. (2015). State of the art on gas–solid thermochemical energy storage systems and reactors for building applications. *Renewable and Sustainable Energy Reviews*, *47*, 386–398. https://doi.org/10.1016/J.RSER.2015.03.077

Solé, A., Miró, L., Barreneche, C., Martorell, I., & Cabeza, L. F. (2015). Corrosion of metals and salt hydrates used for thermochemical energy storage. *Renewable Energy*, *75*, 519–523. https://doi.org/10.1016/j.renene.2014.09.059

Song, Y., Peskova, M., Rolando, D., Zucker, G., & Madani, H. (2023). Estimating electric power consumption of in-situ residential heat pump systems: A data-driven approach. *Applied Energy*, *352*(June). https://doi.org/10.1016/j.apenergy.2023.121971

Sterner, M., & Stadler, I. (2019). *Handbook of Energy Storage* (M. Sterner & I. Stadler (eds.); 2nd ed.). https://doi.org/10.1007/978-3-662-55504-0

Sunku Prasad, J., Muthukumar, P., Desai, F., Basu, D. N., & Rahman, M. M. (2019). A critical review of high-temperature reversible thermochemical energy storage systems. *Applied Energy*, *254*, 113733. https://doi.org/10.1016/J.APENERGY.2019.113733

Tamasauskas, J., Poirier, M., Zmeureanu, R., & Sunyé, R. (2012). Modeling and optimization of a solar assisted heat pump using ice slurry as a latent storage material. *Solar Energy*, *86*(11), 3316–3325. https://doi.org/10.1016/j.solener.2012.08.021

Teggar, M., Ajarostaghi, S. S. M., Yıldız, Ç., Arıcı, M., Ismail, K. A. R., Niyas, H., Lino, F. A. M., Mert, M. S., & Khalid, M. (2021). Performance enhancement of latent heat storage systems by using extended surfaces and porous materials: A state-of-the-art review. *Journal of Energy Storage*, *44*(September), 103340. https://doi.org/10.1016/j.est.2021.103340

Topcu, F. E. (2022). *Business News*, *AA*. National News Agency, Türkiye. https://www.aa.com.tr/tr/sirkethaberleri/teknoloji/mitsubishi-electric-uretim-kapasitesine-113-milyon-dolar-yatirim-yapacak/673161

Trinkl, C., Zörner, W., & Hanby, V. (2009). Simulation study on a domestic Solar/Heat pump heating system incorporating latent and stratified thermal storage. *Journal of Solar Energy Engineering, Transactions of the ASME*, *131*(4), 0410081–0410088. https://doi.org/10.1115/1.3197845

Tunçbilek, E., Yıldız, Ç., Arıcı, M., Ma, Z., & Awan, M. B. (2023). Thermal energy storage for enhanced building energy flexibility. In Z. Ma, M. Arıcı, & A. Shahsavar (Eds.), *Building Energy Flexibility and Demand Management* (1st ed., pp. 89–119). Elsevier. https://doi.org/10.1016/B978-0-323-99588-7.00004-3

Ucar, A., & Inalli, M. (2008). Thermal and economic comparisons of solar heating systems with seasonal storage used in building heating. *Renewable Energy*, *33*(12), 2532–2539. https://doi.org/10.1016/j.renene.2008.02.019

UN Environment Programme. (2019). 2019 Global Status Report for Building and Construction - Towards a zero-emissions, efficient and resilient buildings and construction sector. In *Global Status Report*.

Utlu, Z., Aydin, D., & Kincay, O. (2014). Comprehensive thermodynamic analysis of a renewable energy sourced hybrid heating system combined with latent heat storage. *Energy Conversion and Management*, *84*, 311–325. https://doi.org/10.1016/j.enconman.2014.04.024

V R, S., & Chanda, S. (2023). Thermal performance evaluation of PCM-MF composite heat sinks under varying ambient conditions. *International Journal of Heat and Mass Transfer*, *206*, 123927. https://doi.org/10.1016/j.ijheatmasstransfer.2023.123927

Venkitaraj, K. P., & Suresh, S. (2019). Effects of Al2O3, CuO and TiO2 nanoparticles son thermal, phase transition and crystallization properties of solid-solid phase change material,. *Mechanics of Materials*, *128*, 64–88. https://doi.org/10.1016/j.mechmat.2018.10.004

Walker, I. S., Less, B. D., & Casquero-Modrego, N. (2022). Carbon and energy cost impacts of electrification of space heating with heat pumps in the US. *Energy and*

Buildings, *259*, 111910. https://doi.org/10.1016/j.enbuild.2022.111910

Wang, X., Zheng, M., Zhang, W., Zhang, S., & Yang, T. (2010). Experimental study of a solar-assisted ground-coupled heat pump system with solar seasonal thermal storage in severe cold areas. *Energy and Buildings*, *42*(11), 2104–2110. https://doi.org/10.1016/j.enbuild.2010.06.022

Wolisz, H., Kull, T. M., Müller, D., & Kurnitski, J. (2020). Self-learning model predictive control for dynamic activation of structural thermal mass in residential buildings. *Energy and Buildings*, *207*. https://doi.org/10.1016/j.enbuild.2019.109542

Wu, J., Xian, T., & Liu, X. (2019). All-weather characteristic studies of a direct expansion solar integrated air source heat pump system based on PCMs. *Solar Energy*, *191*, 34–45. https://doi.org/10.1016/j.solener.2019.08.057

Wu, Y., Li, D., Jiang, W., Zhu, S., Zhao, X., Arıcı, M., & Tunçbilek, E. (2022). Energy storage and exergy efficiency analysis of a shell and tube latent thermal energy storage unit with non-uniform length and distributed fins. *Sustainable Energy Technologies and Assessments*, *53*(May). https://doi.org/10.1016/j.seta.2022.102362

Xi, Z., Yao, R., Li, J., Du, C., Yu, Z., & Li, B. (2021). Experimental studies on hot gas bypass defrosting control strategies for air source heat pumps. *Journal of Building Engineering*, *43*, 103165. https://doi.org/10.1016/j.jobe.2021.103165

Xu, J., Wang, R. Z., & Li, Y. (2014). A review of available technologies for seasonal thermal energy storage. *Solar Energy*, *103*, 610–638. https://doi.org/10.1016/j.solener.2013.06.006

Xu, T., Humire, E. N., Chiu, J. N., & Sawalha, S. (2021). Latent heat storage integration into heat pump based heating systems for energy-efficient load shifting. *Energy Conversion and Management*, *236*, 114042. https://doi.org/10.1016/j.enconman.2021.114042

Yang, X., Sun, L., Yuan, Y., Zhao, X., & Cao, X. (2018). Experimental investigation on performance comparison of PV/T-PCM system and PV/T system. *Renewable Energy*, *119*, 152–159. https://doi.org/10.1016/j.renene.2017.11.094

Yıldız, Ç., Arıcı, M., & Nižetić, S. (2023). Heat transfer enhancement of phase change materials. In *Phase Change Materials for Heat Transfer*. https://doi.org/10.1016/B978-0-323-91905-0.00006-X

You, Z., Lumpp, S. D., Doepfert, M., Tzscheutschler, P., & Goebel, C. (2024). Leveraging flexibility of residential heat pumps through local energy markets. *Applied Energy*, *355*, 122269. https://doi.org/10.1016/j.apenergy.2023.122269

Youssef, W., Ge, Y. T., & Tassou, S. A. (2017). Effects of latent heat storage and controls on stability and performance of a solar assisted heat pump system for domestic hot water production. *Solar Energy*, *150*, 394–407.

https://doi.org/10.1016/j.solener.2017.04.065

Yu, M., Li, S., Zhang, X., & Zhao, Y. (2021). Techno-economic analysis of air source heat pump combined with latent thermal energy storage applied for space heating in China. *Applied Thermal Engineering*, *185*, 116434. https://doi.org/10.1016/j.applthermaleng.2020.116434

Yu, M., Zhang, C., Fan, Y., Zhang, X., & Zhao, Y. (2021). Performance study of phase change charging/discharging processes of condensing heat storage in cold regions based on a mathematical model. *Applied Thermal Engineering*, *182*(July 2020). https://doi.org/10.1016/j.applthermaleng.2020.115805

Yumrutas, R., & Kaşka, Ö. (2004). Experimental investigation of thermal performance of a solar assisted heat pump system with an energy storage. *International Journal of Energy Research*, *28*(2), 163–175. https://doi.org/10.1002/er.959

Zhang, L., Jiang, Y., Dong, J., & Yao, Y. (2018). Advances in vapor compression air source heat pump system in cold regions: A review. *Renewable and Sustainable Energy Reviews*, *81*, 353–365. https://doi.org/10.1016/j.rser.2017.08.009

Zhou, C., Li, Y., Wang, F., Wang, Z., Xia, Q., Zhang, Y., Liu, J., Liu, B., & Cai, W. (2023). A Review of the Performance Improvement Methods of Phase Change Materials: Application for the Heat Pump Heating System. *Energies*, *16*(6), 2676. https://doi.org/10.3390/en16062676

Zhu, C., Li, B., Yan, S., Luo, Q., & Li, C. (2021). Experimental research on solar phase change heat storage evaporative heat pump system. *Energy Conversion and Management*, *229*(December 2020). https://doi.org/10.1016/j.enconman.2020.113683

Zhu, N., Hu, P., Lei, Y., Jiang, Z., & Lei, F. (2015). Numerical study on ground source heat pump integrated with phase change material cooling storage system in office building. *Applied Thermal Engineering*, *87*, 615–623. https://doi.org/10.1016/j.applthermaleng.2015.05.056

Zilberberg, E., Trapper, P., Meir, I. A., & Isaac, S. (2021). The impact of thermal mass and insulation of building structure on energy efficiency. *Energy and Buildings*, *241*. https://doi.org/10.1016/j.enbuild.2021.110954

Zou, D., Ma, X., Liu, X., Zheng, P., Cai, B., Huang, J., Guo, J., & Liu, M. (2017). Experimental research of an air-source heat pump water heater using water-PCM for heat storage. *Applied Energy*, *206*(August), 784–792. https://doi.org/10.1016/j.apenergy.2017.08.209

PUBLICATIONS AND WORKS

Abdulkadhim, A., Hamzah, H. K., Ali, F. H., **Yıldız, Ç.**, Abed, A. M., Abed, E. M., & Arıcı, M. (2021). Effect of heat generation and heat absorption on natural convection of Cu-water nanofluid in a wavy enclosure under magnetic field. *International Communications in Heat and Mass Transfer*, *120*(November 2020). https://doi.org/10.1016/j.icheatmasstransfer.2020.105024

Arıcı, M., Tükel, M., **Yıldız, Ç.**, Li, D., & Karabay, H. (2020). Is the thermal transmittance of air-filled inclined multi-glazing windows similar to that of vertical ones? *Energy and Buildings*, *229*, 110515. https://doi.org/10.1016/j.enbuild.2020.110515

Arıcı, M., Tütüncü, E., **Yıldız, Ç.**, & Li, D. (2020). Enhancement of PCM melting rate via internal fin and nanoparticles. *International Journal of Heat and Mass Transfer*, *156*, 119845. https://doi.org/10.1016/j.ijheatmasstransfer.2020.119845

Arıcı, M., **Yıldız, Ç.**, Nižetić, S., Shahsavar, A., & Campo, A. (2021). Implications of boundary conditions on natural convective heat transfer of molten phase change material inside enclosures. *International Journal of Energy Research*, *45*(5), 7631–7650. https://doi.org/10.1002/er.6344

Boulaktout, N., Mezaache, E. H., Teggar, M., Arıcı, M., Ismail, K. A. R., & **Yıldız, Ç.** (2021). Effect of Fin Orientation on Melting Process in Horizontal Double Pipe Thermal Energy Storage Systems. *Journal of Energy Resources Technology*, *143*(7). https://doi.org/10.1115/1.4050904

Faraji, H., **Yıldız, Ç.**, Arshad, A., Arıcı, M., Choukairy, K., & El Alami, M. (2023). Passive thermal management strategy for cooling multiple portable electronic components: Hybrid nanoparticles enhanced phase change materials as an innovative solution. *Journal of Energy Storage*, *70*(June). https://doi.org/10.1016/j.est.2023.108087

Laouer, A., Arıcı, M., Teggar, M., Bouabdallah, S., **Yıldız, Ç.**, Ismail, K. A. R., Ajarostaghi, S. S. M., & Mezaache, E. H. (2021). Effect of Magnetic Field and Nanoparticle Concentration on Melting of Cu-Ice in a Rectangular Cavity under Fluctuating Temperatures. *Journal of Energy Storage*, *36*(March), 102421. https://doi.org/10.1016/j.est.2021.102421

Li, Q., Ma, L., Li, D., Arıcı, M., **Yıldız, Ç.**, Wang, Z., & Liu, Y. (2021). Thermoeconomic analysis of a wall incorporating phase change material in a rural residence located in northeast China. *Sustainable Energy Technologies and Assessments*, *44*(January). https://doi.org/10.1016/j.seta.2021.101091

Li, Q., Wang, Y., Ma, L., Arıcı, M., Li, D., **Yıldız, Ç.**, & Zhu, Y. (2021). Effect of sunspace and PCM louver combination on the energy saving of rural residences: Case study in a severe cold region of China. *Sustainable Energy Technologies and Assessments*, *45*(March). https://doi.org/10.1016/j.seta.2021.101126

Ma, L., Zhang, X., Li, D., Arıcı, M., **Yıldız, Ç.**, Li, Q., Zhang, S., & Jiang, W. (2020). Influence of sunspace on energy consumption of rural residential buildings. *Solar Energy*, *211*, 336–344. https://doi.org/10.1016/j.solener.2020.09.043

Nedjem, K., Teggar, M., Hadibi, T., Arıcı, M., **Yıldız, Ç.**, & Ismail, K. A. R. (2021). Hybrid thermal performance enhancement of shell and tube latent heat thermal energy storage using nano-additives and metal foam. *Journal of Energy Storage*, *44*(September), 103347. https://doi.org/10.1016/j.est.2021.103347

Shahsavar, A., Farhadi, P., **Yıldız, Ç.**, Moradi, M., & Arici, M. (2022). Evaluation of entropy generation characteristics of boehmite-alumina nanofluid with different shapes of nanoparticles in a helical heat sink. *International Journal of Mechanical Sciences*, *225*(May). https://doi.org/10.1016/j.ijmecsci.2022.107338

Shahsavar, A., Heidarian, M., **Yıldız, Ç.**, & Arıcı, M. (2023). Effect of open-ring pin fin arrangement on the thermal performance and entropy generation of a heat sink cooled by biologically synthesized silver-water nanofluid. *Engineering Analysis with Boundary Elements*, *150*(February), 599–611. https://doi.org/10.1016/j.enganabound.2023.02.033

Shahsavar, A., Jafari, M., **Yıldız, Ç.**, Moradvandi, M., & Arıcı, M. (2023). On the cooling performance and entropy generation characteristics of a heat sink under ultrasonic vibration: Exploring the impact of porous medium. *International Journal of Heat and Mass Transfer*, *215*. https://doi.org/10.1016/j.ijheatmasstransfer.2023.124500

Shahsavar, A., Moradi, K., **Yıldız, Ç.**, Farhadi, P., & Arıcı, M. (2022). Effect of nanoparticle shape on cooling performance of boehmite-alumina nanofluid in a helical heat sink for laminar and turbulent flow regimes. *International Journal of Mechanical Sciences*, *217*(December 2021), 107045. https://doi.org/10.1016/j.ijmecsci.2021.107045

Shahsavar, A., Rashidi, M., **Yıldız, Ç.**, & Arıcı, M. (2021). Natural convection and entropy generation of Ag-water nanofluid in a finned horizontal annulus: A particular focus on the impact of fin numbers. *International Communications in Heat and Mass Transfer*, *125*. https://doi.org/10.1016/j.icheatmasstransfer.2021.105349

Shahsavar, A., Shaham, A., **Yıldız, Ç.**, & Arıcı, M. (2022). Entropy generation characteristics of phase change material in a variable wavy walled triplex tube latent heat storage unit for battery thermal management system. *Journal of Energy Storage*, *51*(January), 104374. https://doi.org/10.1016/j.est.2022.104374

Teggar, M., Ajarostaghi, S. S. M., **Yıldız, Ç.**, Arıcı, M., Ismail, K. A. R., Niyas, H., Lino, F. A. M., Mert, M. S., & Khalid, M. (2021). Performance enhancement of latent heat storage systems by using extended surfaces and porous materials: A state-of-the-art review. *Journal of Energy Storage*, *44*(September), 103340.

https://doi.org/10.1016/j.est.2021.103340

Tong, X., Li, D., Yang, R., Arıcı, M., Wu, Y., Liu, C., & **Yıldız, Ç.** (2023). Experimental investigation on photothermal properties of Zn–ZnO/paraffin hybrid nanofluids. *Journal of Thermal Analysis and Calorimetry*, *148*(20), 11029–11040. https://doi.org/10.1007/s10973-023-12310-1

Tunçbilek, E., **Yıldız, Ç.**, Arıcı, M., Ma, Z., & Awan, M. B. (2023). Thermal energy storage for enhanced building energy flexibility. In Z. Ma, M. Arıcı, & A. Shahsavar (Eds.), *Building Energy Flexibility and Demand Management* (1st ed., pp. 89–119). Elsevier. https://doi.org/10.1016/B978-0-323-99588-7.00004-3

Uludaş, M. Ç., Tunçbilek, E., **Yıldız, Ç.**, Arıcı, M., Li, D., & Krajčík, M. (2022). PCM-enhanced sunspace for energy efficiency and CO2 mitigation in a house in mediterranean climate. *Journal of Building Engineering*, *57*(April). https://doi.org/10.1016/j.jobe.2022.104856

Yang, R., Li, D., Arıcı, M., Salazar, S. L., Wu, Y., Liu, C., & **Yıldız, Ç.** (2023). Spectrally selective nanoparticle-enhanced phase change materials: A study on data-driven optical/thermal properties and application of energy-saving glazing under different climatic conditions. *Renewable and Sustainable Energy Reviews*, *186*(August). https://doi.org/10.1016/j.rser.2023.113646

Yıldız, Ç., Arıcı, M., & Karabay, H. (2019). Effect of inclination angle on natural convection of nanofluids in a U-shaped cavity. *International Journal of Environmental Science and Technology*, *16*(9), 5289–5294. https://doi.org/10.1007/s13762-019-02407-2

Yıldız, Ç., Arıcı, M., & Karabay, H. (2019). Comparison of a theoretical and experimental thermal conductivity model on the heat transfer performance of Al2O3-SiO2/water hybrid-nanofluid. *International Journal of Heat and Mass Transfer, 140,* 598–605. https://doi.org/10.1016/j.ijheatmasstransfer.2019.06.028

Yıldız, Ç., Arıcı, M., Karabay, H., & Bennacer, R. (2021). Natural convection of nanofluid in a U-shaped enclosure emphasizing on the effect of cold rib dimensions. *Journal of Thermal Analysis and Calorimetry*, *146*(2), 801–811. https://doi.org/10.1007/s10973-020-10023-3

Yıldız, Ç., Arıcı, M., & Nižetić, S. (2023). Heat transfer enhancement of phase change materials. In *Phase Change Materials for Heat Transfer*. https://doi.org/10.1016/B978-0-323-91905-0.00006-X

Yıldız, Ç., Arıcı, M., Nižetić, S., & Shahsavar, A. (2020). Numerical investigation of natural convection behavior of molten PCM in an enclosure having rectangular and tree-like branching fins. *Energy, 207*. https://doi.org/10.1016/j.energy.2020.118223

Yıldız, Ç., Kaptan, Ç., Arıcı, M., Baynal, K., & Karabay, H. (2022). Taguchi optimization of automotive radiator cooling with nanofluids. *The European*

Physical Journal Special Topics, *123*. https://doi.org/10.1140/epjs/s11734-022-00597-4

Yıldız, Ç., Seçilmiş, M., Arıcı, M., Krajčík, M., Shahsavar, A., Ye, W. B., & Karabay, H. (2024). Thermal interaction between water and liquid paraffin wax inside an intertwined enclosure: The role of natural convection in design of latent heat storage units. *Thermal Science and Engineering Progress*, *47*(December 2023). https://doi.org/10.1016/j.tsep.2023.102343

Yıldız, Ç., Seçilmiş, M., Arıcı, M., Mert, M. S., Nižetić, S., & Karabay, H. (2023). An experimental study on a solar-assisted heat pump incorporated with PCM based thermal energy storage unit. *Energy*, *278*(June), 128035. https://doi.org/10.1016/j.energy.2023.128035

Yıldız, Ç., Yıldız, A. E., Arıcı, M., Azmi, N. A., & Shahsavar, A. (2021). Influence of dome shape on flow structure, natural convection and entropy generation in enclosures at different inclinations: A comparative study. *International Journal of Mechanical Sciences*, *197*(January). https://doi.org/10.1016/j.ijmecsci.2021.106321

Zhang, S., Hu, W., Li, D., Zhang, C., Arıcı, M., **Yıldız, Ç.**, Zhang, X., & Ma, Y. (2021). Energy efficiency optimization of PCM and aerogel-filled multiple glazing windows. *Energy*, *222*. https://doi.org/10.1016/j.energy.2021.119916

Zheng, S., Fu, S., Pu, Y., Li, D., Arıcı, M., Wang, D., & **Yıldız, Ç.** (2023). Energy-saving microgrid system for underground in-situ heating of oil shale integrating renewable energy source: An analysis focusing on net present value. *Journal of the Taiwan Institute of Chemical Engineers*, 104717. https://doi.org/10.1016/j.jtice.2023.104717

Zhou, Y. ming, Wu, G. zhong, Li, D., Arici, M., Wang, Z. mei, Fu, S. bo, Yıldız, Ç., & Arici, A. A. (2021). Thermal stress investigation of glazing unit filled with paraffin in cold regions. Journal of Central South University, 28(11), 3599–3612. https://doi.org/10.1007/s11771-021-4878-4

BIOGRAPHY

Çağatay YILDIZ received his Bachelor's degrees in Mechanical Engineering and Automotive Engineering through a double major program at Çukurova University in 2014 and 2015, respectively. He went on to obtain his Master's degree in Mechanical Engineering from Kocaeli University in 2017. He also enrolled the PhD program in the same department at Kocaeli University in 2018. He has been working as a research assistant in the Mechanical Engineering Department at Kocaeli University since 2016.